

Co-funded by the



# DISCO

Grant Agreement: **755443**

***DELIVERABLE D1.20***

## **3<sup>rd</sup> Annual Meeting Proceedings**

Author(s)/Editor(s): **L.Z. Evins, A. Valls, L. Duro (SKB & Amphos 21)**

Date of issue of this report: **10/2020**

Report number of pages: **127 p**

Start date of project: **01/06/2017**

Duration: **48 Months**

Project co-funded by the European Commission under the Euratom Research and Training Programme on Nuclear Energy within the Horizon 2020 Framework Programme		
Dissemination Level		
<b>PU</b>	Public	X
<b>PP</b>	Restricted to other programme participants (including the Commission Services)	
<b>RE</b>	Restricted to a group specified by the partners of the Disco project	
<b>CO</b>	Confidential, only for partners of the Disco project	

## Foreword

The present document is the proceedings of the Third Annual Meeting of the EURATOM H2020 Collaborative Project DisCo (Modern Spent Fuel Dissolution and Chemistry in Failed Container Conditions). The electronic version of these proceedings is available on the webpage of the project (<https://disco-h2020.eu/>) The project started in June 2017 and will last for 48 months<sup>1</sup>. DisCo is implemented by a consortium with 16 Beneficiaries, advised by the so-called End User Group (EUG). EUG consists of Waste Management Organisations in 7 countries (Belgium, Finland, France, Spain, Sweden, Switzerland, and the UK) as well as Regulatory Authorities in 5 countries (Belgium, Germany, Spain, Sweden, and Switzerland). The inclusion of Waste Management Organisations (WMOs) and Regulatory Authorities in this group ensures that the research conducted in the proposed project will be relevant and useful for the ultimate goal of safe radioactive waste disposal.

These proceedings document the progress of the project by means of work-package summaries and individual Scientific and Technical contributions. The key purpose is to ensure dissemination of knowledge and creating the required awareness of the project achievements.

The progress shown corresponds to the work conducted during the 3<sup>rd</sup> year of the project and presented at the 3<sup>rd</sup> Annual Meeting organized as a virtual meeting (April 2020). Experiments are ongoing, data are collected and analysed, models are built and tested and improved. Overall, during our third year, all groups are producing good results.

The main technical outcome of the meeting are the Scientific and Technical contributions (S+T) explaining the progress of the research conducted by each partner. The contributions have been reviewed and validated by, at least, two members of the End User Group.

The proceedings give an overview of the project, its organization and planned activities. The project website (<https://disco-h2020.eu/>) provides all this information in detail. The reader could also contact the project Coordinator or its team for more information.

The editors are grateful to all consortium members and everyone involved who contributes to the smooth development of the project. We want to give special thanks to (i) work-package leaders for providing the summaries of their corresponding work-package, (ii) partners for their comprehensive and significant contributions, and to (iii) all members of the EUG for their reviews, providing constructive, relevant and interesting comments. These efforts reflect their commitment and dedication to the project and contribute to a high quality of research performed within DisCo.

---

<sup>1</sup> At least: due to the Covid-19 pandemic in 2020, an extension may be requested

# Contents

<b>Foreword</b> .....	<b>i</b>
<b>Contents</b> .....	<b>ii</b>
<b>The Project</b> .....	<b>1</b>
<b>The 3<sup>rd</sup> Annual Meeting</b> .....	<b>2</b>
<b>WP Overview</b> .....	<b>4</b>
WP1 Overview: Management, coordination and dissemination .....	5
WP2 Overview: Model systems dissolution experiments .....	7
WP3 Overview: Spent fuel dissolution experiments.....	8
WP4 Overview: Model material dissolution experiments.....	10
WP5 Overview: Chemical modelling.....	12
<b>Extended Abstracts</b> .....	<b>17</b>
Initial results of dissolution experiments with irradiated PWR MOX fuel (54 MWd/kg <sub>HM</sub> ) under anoxic conditions.....	18
Status of leaching experiments performed with irradiated MOX fuel in bicarbonate water under hydrogen overpressure at KIT-INE.....	26
High burnup spent nuclear fuel dissolution under reducing conditions .....	33
Aqueous leaching of ADOPT and standard UO <sub>2</sub> spent nuclear fuel under H <sub>2</sub> atmosphere .....	37
Chromium doped UO <sub>2</sub> -based model systems: Synthesis and characterization of model materials for the study of the matrix corrosion of spent modern nuclear fuels.....	44
Preliminary results of dissolution experiments with Cr-(Pu) doped UO <sub>2</sub> at SCK·CEN .....	54
Dissolution of alpha-doped UO <sub>2</sub> with and without Cr in the presence of corroding Fe, in synthetic and natural groundwater.....	65
Production and characterisation of (U <sub>1-x</sub> Th <sub>x</sub> )O <sub>2</sub> samples to model mixed oxide fuel dissolution.....	74
Production of unirradiated advanced doped UO <sub>2</sub> fuel for dissolution studies at repository conditions .....	79
Assessment of long-term durability of Cr <sub>2</sub> O <sub>3</sub> doped UO <sub>2</sub> .....	89
Spent fuel matrix alteration 1D model integrating water radiolysis and reactive solute transport – model calibration and validation .....	95
Full reactive transport model of U <sub>0.73</sub> Pu <sub>0.27</sub> O <sub>2</sub> experimental leaching in synthetic clay groundwater with metallic iron .....	109
Thermodynamic modelling of oxygen potential for Cr-doped and conventional UO <sub>2</sub> fuel as a function of temperature and burnup .....	117
<b>EUG Feedback</b> .....	<b>125</b>

## The Project

DisCo is a Collaborative Project funded by the European Commission under the Horizon 2020 Research and Training Programme of the European Atomic Energy Community (EURATOM) (H2020-NFRP-2016-2017-1), section B - Contribute to the Development of Solutions for the Management of Radioactive Waste. Topic NFRP 6: Addressing key priority R&I issues for the first-of-the-kind geological repositories.

DisCo is an acronym for “Modern Spent Fuel Dissolution and Chemistry in Failed Container Conditions.” It started on 1<sup>st</sup> June 2017 and it is planned to run for four years. The project is implemented by a consortium with 16 Beneficiaries.

The project is set up to answer the Euratom call of 2016-2017, which focused on high priority topics identified by the IGD- TP (Implementing Geological Disposal – Technology Platform: [www.igdt.eu](http://www.igdt.eu)). One of these areas is the disposal of new and unconventional fuels. DisCo started as a response to the need to test the hypothesis that dopants in the UO<sub>2</sub> fuel matrix do not significantly affect the dissolution rate of the spent fuel in a repository environment. Dopants in the UO<sub>2</sub> fuel matrix here considered are Cr, or Cr+Al, and Gd. In addition, the behaviour of Mixed-Oxide fuel (MOX) which contains Pu in addition to the UO<sub>2</sub> matrix is also investigated, leading to the study of the effect of an analogous mixed Th-U oxide for comparison. The DisCo project uses three paths to study these issues which mainly define the objectives of the technical work-packages (WP): dissolution experiments with real spent fuel (WP3), dissolution experiments with model materials (WP4) and modelling of the chemical system expected in the failed waste container (WP5). An additional technical work-package (WP2) is devoted to the preparation and characterization of the samples to be used in the experiments planned in WP3 and WP4.

The central part of the scientific investigation in this project concerns how elements other than uranium (metal, lanthanide, actinide) in the oxide matrix affect its redox chemistry and solubility. Any impurity in a solid phase will affect the crystal lattice and atomic bonds, so that parameters such that the solubility of the solid can be affected. In addition, the electronic configuration on an atomic scale affects the average oxidation state of the uranium in the solid. Since these aspects are fundamental to the spent fuel dissolution process, it is necessary to test whether these changes affect measured dissolution rates.

This DisCo project also contributes to knowledge management, dissemination and communication, through the efforts made in WP1. The involvement of an End User Group (EUG) representing waste management organisations and national regulators, as well as an Associate Group (AG) consisting mainly but not exclusively by organisations from countries with less advanced programs (LAPs), is central to the successful knowledge transfer and management foreseen in DisCo. Efforts are focused on communication and dissemination activities such as webinars and training events.

# The 3<sup>rd</sup> Annual Meeting

Due to the Covid-19 pandemic, the third annual meeting (3AM) of the DisCo project was held as a videoconference on 22-23 April 2020. The meeting was organized by Amphos 21. There were 61 attendees including representatives of the partners, the End User Group (EUG), the Associated Group (AG), the European Commission (EC) and some external organizations.

The meeting was organized to fit in two days, so that, partner presentations were reduced to 10 minutes and WP overviews were eliminated from the agenda. A summary of the progress achieved in each WP is presented in these Proceedings and is publicly available. The 3AM was scheduled in three blocks (see agenda in Figure 1): (i) individual talks where each partner presented the work conducted during the 3<sup>rd</sup> year of the project; (ii) separate WP sessions to discuss on the progress and organizing the work for the last project year; (iii) webinar as part of the training activities within the project.

Agenda (22 <sup>th</sup> - 23 <sup>th</sup> April 2020)	
	
<b>Restricted sessions</b> <i>These meetings can only be attended if you are a member of the corresponding group</i>	<b>Open sessions</b>
<b>Wednesday 22<sup>nd</sup> April 2020</b>	<b>Thursday 23<sup>rd</sup> April 2020</b>
10:00 <b>ExCom meeting</b> <i>(restricted to ExCom members)</i>	09:00 <b>Welcome &amp; meeting practicalities</b>
15:00 <b>Individual WP Session</b> <i>(restricted to WP partners)</i>	09:10 <b>Coordination Team Presentation</b>
15:00 <b>EUG Meeting</b> <i>(restricted to EUG members)</i>	09:45 <b>Individual talks (10'+ 5' each)</b> JRC / KIT-INE
	10:15 <b>Break</b>
	10:30 <b>Individual talks (10'+ 5' each)</b> CTM / Studsvik / JUELICH / SCK-CEN / CEA / VTT / UCAM
	12.15 <b>LUNCH time</b>
	13:00 <b>Individual talks (10'+ 5' each)</b> CIEMAT / USFD / NNL / A21 / Armines / PSI
	14.30 <b>Break</b>
	14:45 <b>Webinar – J. Bruno (A21) “Spent Fuel Model development and testing in Natural Analogue systems”</b>
	16:00 <b>Break</b>
	16:45 <b>EUG feedback</b>
	17:00 <b>End of the 3<sup>rd</sup> Annual Meeting</b>

Figure 1: General agenda of the 3<sup>rd</sup> Annual Meeting of DisCo.

In addition to the technical sessions, the meeting included the following sessions focused on the management and progress of the project.

- ▶ **ExCom meeting:** the Coordination Team (CT), WP leaders and the chair of the EUG discussed on the progress of the project, organizing future events (meetings, training...), identify deviations and providing/suggesting solutions.
- ▶ **EUG meeting** was restricted only to members of the End User Group. As Waste Management Organizations and Regulators, they ensure that the research conducted remains within the scope initially set and it is relevant and useful for the ultimate goal of safe radioactive waste disposal. At the end of each meeting they are providing their advice on the project status to all Consortium Members. Their feedback is included in the present Proceedings, Section “EUG Feedback”.

- ▶ The General Assembly is the forum where actions that must be approved by all partners take place. All decisions taken during that Assembly are compiled in the Meeting Minutes which are available at the project website.

One important goal of this meeting was the organization of the 3<sup>rd</sup> Webinar. The webinar was on “Spent Fuel Model development and testing in Natural Analogue systems” and was given by Jordi Bruno (Amphos 21). It was followed by 71 persons. The webinar was recorded, and it is available under demand (instructions given at the project webpage).

The Coordination Team want to thank all DisCo participants and Amphos 21 for a well-organized and productive meeting. It must be highlighted the effort of all partners to keep their time allocated for the presentations in this tight but very effective meeting. We are looking forward the next meeting that will be held in spring 2021 in Barcelona (Spain), hosted by Amphos 21. This meeting will be organized in conjunction with the Spent Fuel Workshop that will be held on the same week in Barcelona (Amphos 21 as host organization).



**Figure 2:** Group photo of the 3<sup>rd</sup> DisCo Annual Meeting.

---

# **WP Overview**

---

# WP1 Overview: Management, coordination and dissemination

*Lena Z. Evins, SKB (SE)*

---

The progress of the project is overseen and managed in Work Package 1, divided into two main tasks:

- 1) General management and coordination
- 2) Communication, dissemination and training

Task 1 involves maintaining all the general project management tasks including the financial and legal matters, while Task 2 involves setting up and maintaining all the communication tools used in the project, such as the webpage, meetings, webinars and other training events.

During the third year, data has been collected in the experimental work packages and analysed in conjunctions with the further development of the models. Several scientific articles have been written and are now published. 3 milestones have been reached: the 1<sup>st</sup> peer-reviewed paper was published, the third annual meeting has been held, and dissolution data have been delivered to modellers. The planned deliverables have been submitted, with one exception: The progress report outlining the WP3 dissolution data delivered to WP5, which is expected to be submitted in the early autumn 2020.

The 3<sup>rd</sup> annual meeting was held 22-23 April as a virtual meeting due to the COVID-19 pandemic. Overall, the project is following the work plan. Some delays have been encountered for some experiments, however, a significant amount of experimental data has still been delivered to work package 5 to be used in modelling during the final year. There are unfortunately major delays in some of the experiments at JRC-Karlsruhe and this may warrant a request for extension. Part of the reason for the delay is the outbreak of the COVID-19 pandemic which has limited the access to laboratories during several months.

The next annual meeting is planned to be held in Barcelona (Spain) in Spring 2021 (the exact date will be soon published at the project webpage). The meeting will be hosted by Amphos 21 and be held in conjunction with the Spent Fuel Workshop.

During the 3<sup>rd</sup> year, two individual training visits to JRC have been planned. Due to the pandemic, these will be hosted along the following year.

## Communication actions

During the third year, the general communication tools have been keep updated.

- The webpage (<https://www.disco-h2020.eu/>) is continuously updated with information relevant for the project, including published peer reviewed articles and presentations of results in international conferences. The home page contains a Twitter feed displaying all tweets tagged with #discoh2020. An example of the tweets displayed in the home page of the project webpage



is shown in Figure 1. 15 tweets have been published using the project hashtag during the third year.

## Modern Spent Fuel Dissolution and Chemistry in Failed Container Conditions


**DISCO** is a Collaborative Project funded by the European Commission under the Horizon 2020 Research and Training Programme of the European Atomic Energy Community (EURATOM) (H2020-NFRP-2016-2017-1), section B - Contribute to the Development of Solutions for the Management of Radioactive Waste. Topic NFRP 6: Addressing key priority R&I issues for the first-of-the-kind geological repositories. Funding scheme: RIA - Research and Innovation action. Project ID: 755443.

The project started on 1<sup>st</sup> of June 2017 and will last for 48 months. The project is implemented by a consortium with **16 Beneficiaries**. The consortium will be advised by a so-called **End User Group (EUG)**, consisting of Waste Management Organisations in 7 countries (**Belgium, Finland, France, Spain, Sweden, Switzerland, and the UK**) as well as regulatory authorities in 5 countries (**Belgium, Germany, Spain, Sweden, and Switzerland**). The inclusion of Waste Management Organisations (WMOs) as an EUG in the project ensures that the research conducted in the proposed project will be relevant and useful for the ultimate goal of safe radioactive waste disposal.

The total budget is 4.69 million Euros. The European Commission contributes with 3.99 million Euros to the project.

### COUNTRIES INVOLVED IN DISCO

(n° of beneficiaries)



**Lara Duro** @laraduro1  
A great success #discoh2020. I only missed the "get together drinks" part of the workshop. Next time...double glass!! 🍷🍷  
twitter.com/amphos\_21/stat...

**AMPHOS 21** @amphos\_21  
Thanks to all participants of the 3 Annual meeting of #discoh2020. Fully virtual to learn that things can be done in al alternative way, and not necessarily worse! twitter.com/lenazevins/sta...

**AMPHOS 21** @amphos\_21  
Thanks to all participants of the 3 Annual meeting of #discoh2020. Fully virtual to learn that things can be done in al alternative way, and not necessarily worse! twitter.com/lenazevins/sta...

**Lena Z Evins** @lenazevins  
3rd Annual Meeting of DisCo was a success! Great contributions from partners, interesting Webinar and fantastic organisation by @albanitavp and @amphos\_21 Thanks everyone! #discoh2020

**Lena Z Evins** @lenazevins  
3rd Annual Meeting of DisCo was a success! Great contributions from partners, interesting Webinar and fantastic organisation by @albanitavp and @amphos\_21 Thanks everyone! #discoh2020

**Figure 1:** Home page of the DisCo project.

- The LinkedIn Group, also active since September 2017, has now 37 members, representing most of the project participants and some project external members.
- A newsletter was distributed in July 2020 after the 3<sup>rd</sup> Annual meeting. It contains a summary of the project status reported during this meeting, and it is available in the project website
- The third Webinar, featuring Dr. Jordi Bruno (Amphos 21, Spain) dealt with Spent Fuel Model development and testing in Natural Analogue systems and it was followed on-line by 71 people.
- The Mobility Grants to attend the 3<sup>rd</sup> Annual Meeting were not available as the meeting was held as a videoconference. The budget will be used to be able to have more Mobility Grants for the Final Project Meeting to be held in Barcelona (Spring 2021).
- The group training to be held in JRC-Karlsruhe has been also postponed due to the COVID-19 pandemic and a new date will be published soon.

## WP2 Overview: Model systems dissolution experiments

*Ian Farnan, UCAM (UK)*

---

This work-package was intended to coordinate the preparation and characterisation of a range of spent fuel related samples, before dissolution tests, from real spent MOx and Cr-doped fuels handled in hot cells, synthetic UO<sub>2</sub> and Cr-doped UO<sub>2</sub> samples containing <sup>238</sup>Pu and <sup>233</sup>U with high alpha activities handled in alpha glove-boxes to university and research institute laboratory based model systems working with U and Th. The work package is almost complete and dissolution experiments have begun in WP4 for the vast majority of samples prepared and characterised in WP2.

In Task 2.1, which deals with the highest activity materials handled in hot cells, spent MOx fuel originally prepared by the optimised co-milling process (OCOM) burnt up to 38 GWd/t<sub>HM</sub> has been cut into two samples and characterised by optical microscopy and Raman spectroscopy before being submitted to leaching experiments by KIT-INE. Likewise, at JRC a 54 GWd/t<sub>HM</sub> burn-up MOx fuel fabricated by the short-binderless route (SBR) was prepared and observed by optical microscopy before being submitted to dissolution experiments. A further MOx sample (cut from the same 54 GWd/t<sub>HM</sub> rod) and a Cr doped, high burn-up (58 GWd/t<sub>HM</sub>) UOx fuel sample have been prepared and characterised by optical microscopy and are awaiting dissolution experiments that are delayed due to COVID-19 measures (laboratory closure). Detailed work in WP2 Task 3 at FZJ involved varying the amount and form of chromate additions and sintering times to established a method to produce Cr-doped UO<sub>2</sub> fuels with a particular grain-size (similar to commercial fuel, where the process is proprietary). This knowledge was transferred to WP2 Task 2 to allow UO<sub>2</sub> and Cr-doped UO<sub>2</sub> samples to be prepared in plutonium gloveboxes at SCK CEN with a <sup>238</sup>Pu doping to provide equivalent alpha-activity to 10,000 year-old fuel. Some of these materials were retained onsite for dissolution tests in WP4 and a set was recently shipped to Finland (VTT) for dissolution testing and comparison with reconstituted <sup>233</sup>U doped UO<sub>2</sub> samples that also exhibit alpha-activities equivalent to 3000 and 10,000 years out of reactor. Further work in Task 3 has completed the preparation, by cold-press and sinter, of Cr-doped fuels with a range of chromium levels (100-2400 ppm) to test the influence of Cr content on U release directly and as a function of grain-size imposed by Cr content (USFD); methods based on PUREX to dissolve existing UO<sub>2</sub> ceramics in nitric acid to remove impurities and increase the crystallinity of the final sintered material (CIEMAT). These samples and a reference UO<sub>2</sub> material produced by hot-isostatic pressing (HIP) are going forward to dissolution tests in WP4. Samples of U/Th inhomogeneous MOx pellets with a nominal Th content of 25 wt.% have been prepared and analysed by SEM, electron back-scatter diffraction and X-ray diffraction. A homogeneous U/Th MOx sample will be created by extended high temperature anoxic annealing as soon as the COVID-19 closure is lifted. Homogeneous plutonium-uranium mixed oxide samples, with Pu content of 27 wt.%, have been prepared in Task 2 by CEA through re sintering to remove accumulated damage and have been characterised before dissolution by X-ray diffraction, Raman spectroscopy and scanning electron microscopy. The Pu/U MOx dissolution experiments have been completed and are closely coupled with the U/Th MOx dissolution and both will be modelled with the same code in WP5 (ARMINES).

# WP3 Overview: Spent fuel dissolution experiments

*Volker Metz, KIT-INE (DE)*

---

## Introduction

The main goal of Work Package 3 of the H2020-project DisCo is to study experimentally the dissolution of spent  $\text{UO}_x$  fuels containing dopants as well as the dissolution of spent MOX fuels under relevant disposal conditions. The research groups that contribute with experiments to WP3 are Fundacio Eurecat (EURECAT) in conjunction with Universitat Politècnica de Catalunya (UPC), Joint Research Centre (JRC-KA), Karlsruhe Institut für Technologie (KIT-INE) and Studsvik Nuclear AB (STUDSVIK).

All partners of WP3 dealt with spent nuclear fuel, which had been irradiated in light water nuclear reactors. Current experiments are performed with two BWR  $\text{UO}_x$  fuels having burnups of 57 and 59  $\text{MWd/kg}_{\text{HM}}$  as well as with two PWR MOX fuels having burnups of 38 and 54  $\text{MWd/kg}_{\text{HM}}$  (average burnups). In several autoclave experiments, fragments and clad segments of these irradiated fuel samples were exposed diluted NaCl solution with 1 to 2 mM  $\text{NaHCO}_3$  (pH ~ 8, denoted as NaCl-BIC) under strongly reducing conditions. Moreover, a dissolution experiment with a PWR  $\text{UO}_x$  fuel, having a burnup of 73  $\text{MWd/kg}_{\text{HM}}$ , had been conducted under oxic conditions in so-called “Young Cement Water with Calcium” (YCWCa), which is a hyper-alkaline diluted NaOH,  $\text{Ca}(\text{OH})_2$  solution, containing 77 mM  $\text{Na}_2\text{CO}_3$  and other minor constituents.

Results of experiments with irradiated  $\text{UO}_x$  and MOX fuels performed by JRC-KA, KIT-INE and STUDSVIK under strongly reducing conditions are presented in the Proceedings of the 3<sup>rd</sup> Annual Workshop (this document). Since there were delays in the sample preparation of the fuel samples and technical problems with the experimental set-ups of EURECAT and JRC-KA, start of some of their experiments is expected in the second half-year of 2020.

## Achievements

Within WP3, EURECAT in conjunction with UPC contributed with a dissolution experiment on a PWR  $\text{UO}_x$  fuel with a local burnup of 73  $\text{MWd/kg}_{\text{HM}}$  under oxic conditions. In their paper, Kokinda et al. [1] reports on activities related to preparation of future experiments with sub-samples of a PWR  $\text{UO}_x$  fuel (73  $\text{MWd/kg}_{\text{HM}}$ ), to be exposed to NaCl-BIC and YCWCa type solutions.

JRC-KA is contributing to WP3 with an experimental study of the long-term stability of a spent MOX fuel (54  $\text{MWd/kg}_{\text{HM}}$ ) in NaCl-BIC type solution. Serrano-Purroy et al. [2] present initial results on the release of U, Pu, Cs, Tc and Mo in the dissolution experiments for 160 days of leaching under hydrogen overpressure.

KIT-INE investigates matrix dissolution and the Instant Release Fraction in two dissolution experiments with a clad segment and fragments of an irradiated PWR MOX fuel (73  $\text{MWd/kg}_{\text{HM}}$ ). Herm et al. [3] present data on radionuclide release in the two experiments for 370 days of leaching in NaCl-BIC type solution under hydrogen overpressure. In both experiments, a continuous release of the fission products

$^{90}\text{Sr}$  and  $^{137}\text{Cs}$  is seen. Within an initial period of 158 days, aqueous concentrations of actinides in solution are constant except for neptunium and uranium.

STUDSVIK performs two autoclave experiments with a standard BWR  $\text{UO}_x$  fuel (57 MWd/kg<sub>HM</sub>) and with an Al-Cr-doped BWR  $\text{UO}_x$  fuel (59 MWd/kg<sub>HM</sub>). Fragments of both SNF samples are exposed to NaCl-BIC type solution under hydrogen overpressure. Results of the two dissolution experiments are reported by Barreiro-Fidalgo et al. [4]. After more than 640 days of exposure, aqueous concentrations of  $^{129}\text{I}$ ,  $^{137}\text{Cs}$ ,  $^{100}\text{Mo}$ ,  $^{90}\text{Sr}$  and  $^{90}\text{Tc}$  reached a relative constant level. Differences in  $^{129}\text{I}$  release are observed between standard BWR  $\text{UO}_x$  fuel and Al-Cr-doped BWR  $\text{UO}_x$  fuel. As discussed by Barreiro-Fidalgo et al. [4], measured actinide concentrations are higher than expected.

## References

- [1] Kokinda J., Serrano-Purroy, D., Clarens, F., de Pablo, J., High burnup spent nuclear fuel dissolution under reducing conditions. Proceedings of the 3rd Annual Workshop, H2020-project DisCo, April 22nd-23rd, 2020.
- [2] Serrano-Purroy, D., Carbol P., Van Winckel, S., Initial results of dissolution experiments with irradiated PWR MOX fuel (54 MWd/kg(HM)) under anoxic condition. Proceedings of the 3rd Annual Workshop, H2020-project DisCo, April 22nd-23rd, 2020.
- [3] Herm, M., González-Robles, E., Walschburger, A., Müller, N., Bohnert, E., Böttle, M., Geyer, F., Fuss, M., Metz, V., Status of leaching experiments performed with irradiated MOX fuel in bicarbonate water under hydrogen overpressure at KIT-INE. Proceedings of the 3rd Annual Workshop, H2020-project DisCo, April 22nd-23rd, 2020.
- [4] Barreiro-Fidalgo, A., Roth, O., Puranen, A., Evins, L.Z., Spahiu, K., Aqueous leaching of ADOPT and standard  $\text{UO}_2$  spent nuclear fuel under  $\text{H}_2$  atmosphere. Proceedings of the 3rd Annual Workshop, H2020-project DisCo, April 22nd-23rd, 2020.

# WP4 Overview: Model material dissolution experiments

*Dirk Bosbach, FZJ (DE)*

---

## Introduction

The main objectives of workpackage (WP) 4 of DisCo are: (1) Understanding matrix corrosion of modern LWR fuels under deep geological repository relevant conditions, and (2) Systematic corrosion studies on Cr/Al/Gd-doped-UO<sub>2</sub>-based and MOX model systems (prepared and characterized in WP2) complementary to SNF corrosion studies in WP3. Special focus will be on the long-term (> 1000 years) SNF matrix corrosion by using alpha-doped model systems. The experimental programme is intended to overcome the inherent complexity of SNF corrosion and to identify the separate effects of microstructure, doping level, and surface area in support of the spent fuel corrosion studies in WP3. The results will allow for improving the predictive capability of SF corrosion models and reduction of associated uncertainties.

Since the formal start of WP4 in February 2018 a broad range of samples has been studied in a range of experimental conditions. In general, a set of experimental conditions has been defined in close communication with WP3 in order to allow for an easier comparison between the dissolution experiments performed in WP3 and WP4. Five different chemical compositions for the aqueous solution have been defined: (1) a bicarbonate solution similar to the one used in the First Nuclides project in combination with H<sub>2</sub> atmosphere (reducing, anoxic), (2) young cementitious water in combination with H<sub>2</sub> atmosphere (YCWCa, reducing, anoxic), (3) synthetic CO<sub>x</sub> water, (4) natural ground water (with Fe(0)), and (5) bicarbonate and cementitious waters containing H<sub>2</sub>O<sub>2</sub> (for accelerated dissolution experiments).

The dissolution behaviour of the model systems has been studied on respective pellets, which were prepared (and characterized) in WP2. One focus was on Cr-doped UO<sub>2</sub> pellets. The preparation of these materials by different groups has provided a variety of samples, which cover a broad range in dopant levels and grain sizes. Since these parameters are not known for irradiated modern fuel pellets, the approach followed here ensures that the envelope of these parameters covers most likely those in “real” SNF.

## Achievements

In this first phase of the leaching experiments of model UO<sub>2</sub> by SCK CEN, static leaching tests with depleted UO<sub>2</sub> and Cr-doped UO<sub>2</sub> pellet were performed in autoclaves in the two reference solutions YCWCa-L and FIN under 10 bar H<sub>2</sub> pressure and in presence of Pt/Pd catalyst to scavenge the oxygen in solution. After a fast initial release independent on type of solution, the results demonstrated a promoted U released in cementitious solution compared to bicarbonate water for both kind of fuels. However, while a reducing effect of Cr on U release is observed in cementitious conditions, this effect seems to be temporary in bicarbonate conditions. Several hypotheses are forwarded to explain these observations, but they need to be supported by future surface analyses and modelling calculations.

In JUELICH, a broad range of accelerated dissolution experiments in degassed bicarbonate  $\text{H}_2\text{O}_2$  aqueous solution have been performed to mimic radiolytic oxidation processes evoked from the alpha-irradiation of water in long-term disposal scenarios for spent nuclear fuel. Pure  $\text{UO}_2$  and Cr-doped  $\text{UO}_2$  pellets were used for these experiments, focusing systematically on the effect of density, method of Cr-doping, Cr concentration and particle size. Initial dissolution rates indicate a strong dependence on the theoretical densities of the pellets but no or only minor dependence between different Cr-doped  $\text{UO}_2$  pellets, independent of doping method, doping level, and oxygen potential during sintering (i.e. grain size).

In CIEMAT, specimens of  $\text{UO}_2$  doped with Cr, Cr/Al and Gd were tested in three representative aqueous systems: inert water (PC, pH 7.2), high bicarbonated solution (BC, pH 8.5) and Young Cementitious Water (YCW-6, pH 13.5). Based on the data from the first series of tests,  $\text{H}_2$  atmosphere ( $p_{\text{H}_2} = 0.37 \pm 1$  bar) was not capable to maintain the system under reducing conditions. The U concentration in the solutions reached plateau levels in PC and YCW-6, but not in BC system. As the obtained U concentration were unexpectedly high and, in light of the redox measurements (ex-situ) that were close to zero, one can hypothesize that in such case, the potential role of dissolved oxygen in the aqueous phase of a readily accessible glovebox during its storage, could contribute to promoting an oxidative dissolution even though the hydrogen gas in equilibria was maintained inside the autoclaves. However, in order to give an explanation about this behaviour, surface analyses (SEM, XRD and Raman) on the post-leached samples should be performed.

VTT has conducted 200 days leaching experiments with existing  $\text{UO}_2$  materials with 5% or 10%  $^{233}\text{U}$  alpha doping, simulating the alpha dose of 10,000 years old and 3000 years old spent nuclear fuel, respectively. These experiments were run in OL-KR6 groundwater in the presence of metallic iron foil under anaerobic conditions of Ar glove box. In all experiments the solubility of uranium settles between  $2 \cdot 10^{-11}$  and  $5 \cdot 10^{-11}$  mol/L. However, the cumulative release, calculated from isotopic dilution, indicates total release has increased above  $1 \cdot 10^{-7}$  mol/L during 200 days. Clear indication of the effect of doping level could not be observed in OL-KR6 groundwater.

Initial results reported by USFD concerning the dissolution behaviour of  $\text{Cr}_2\text{O}_3$  doped  $\text{UO}_2$  show increased durability with  $\text{Cr}_2\text{O}_3$  content. Potential influence of oxygen vacancy formation has been suggested from relating the dissolution results to studies of grain size, defect concentration and Cr oxidation state.

The long-term leaching experiment of CEA on a homogeneous MOX under environmental conditions (synthetic COX groundwater and corroded iron foil) is over. All analyzes both on the solution and on the solids were carried out. All of these data provide a fairly clear vision of the mechanisms involved. The presence of iron inhibits the oxidative dissolution of the MOX fuel under alpha radiolysis of water. The consumption of oxidizing species leads to the precipitation of magnetite on the surface of the fuel. The slightly basic pH value and the production of oxidants at the extreme surface of the fuel explain these observations. In parallel, the precipitation of calcium carbonates and corrosion products with Fe II is observed on the iron foil. The presence of a redox front at the extreme surface of the fuel pellet is confirmed for this system. This fuel has a strong similarity in behavior with UOX fuels.

UCAM has, in preparation for upcoming dissolution experiments, been investigating the earlier observations of stability of hydrogen peroxide in Callovo-Oxfordian groundwaters. A methodology to conduct UV/vis spectroscopy of hydrogen peroxide and to carry out direct spectroscopic tests using nuclear magnetic resonance on the same samples is being developed.

## WP5 Overview: Chemical modelling

Lara Duro, Olga Riba, Amphos 21 (ES)

---

### Introduction

WP5 focuses on the development of conceptual and numerical models to better understand the spent fuel matrix dissolution, of both regular and modern types of spent fuel, under conditions representative of failed containers in reducing repository environments.

The work package is divided into the following major tasks:

1. Thermodynamic equilibrium calculations, targeting (a) the effect of dopants in the dry matrix in terms of oxygen potential and (b) dissolution/precipitation reactions inside the water-saturated canister.
2. Matrix dissolution model, incorporating redox and electron transfer reactions involving matrix, separate phases (e.g. metallic fission products), radiolysis and hydrogen in the system.
3. MOX-matrix dissolution model, focusing on i) the effect of Pu content on the alpha-radiolytic dissolution kinetics of the matrix and ii) the interplay with Fe(II) species released from iron-based canister in clayey groundwater under anoxic conditions.

Four partners are participating in this WP: Amphos 21 (ES), PSI (CH), NNL(UK) and Armines (FR). Task 1 is developed by Amphos 21, PSI and NNL; Task 2 is developed by Amphos 21 and NNL, and Task 3 is developed by Armines.

### Achievements

At the end of the third year of the project, all the institutions have developed, calibrated and performed validation exercises of their models, which have been presented in Scientific and Technical contributions to the proceedings and Deliverables [1-4].

**Amphos** has developed a 1D reactive transport model implemented in iCP (interface COMSOL Multiphysics - PhreeqC) [5] to assess the corrosion of Spent Fuel (SF) matrix, considered as  $\text{UO}_2(\text{am,hyd})$  with Pd as representative element of the epsilon particles, and assumed to be a homogeneous material. The model couples: i) the generation of water radiolysis species by alpha and beta radiation considering a complete radiolysis system with kinetic reactions involving:  $\text{H}^+$ ,  $\text{OH}^-$ ,  $\text{O}_2$ ,  $\text{H}_2\text{O}_2$ ,  $\text{H}_2$ ,  $\text{HO}_2^-$ ,  $\text{HO}_2^\cdot$ ,  $\text{O}^\cdot$ ,  $\text{O}^-$ ,  $\text{O}_2^-$ ,  $\text{H}^\cdot$ ,  $\cdot\text{OH}$  and  $e^-$ , ii) the processes occurring at the SF surface: oxidation of  $\text{UO}_2(\text{am,hyd})$  and subsequent dissolution or reduction of the oxidized fuel by activated  $\text{H}_2$ , and iii) corrosion of Fe(s) in oxic and anoxic conditions. Processes i) were implemented in COMSOL and processes ii) and iii) were implemented in PHREEQC using ThermoChimie v.9.0 database (<https://www.thermochimie-tdb.com/>) [6] with their kinetic constants being calibrated with existing experimental data from Cera et al. (2006) [7] and from REDUPP European project [8].

After calibrating the kinetic constants, a 1D reactive transport model was implemented under reducing conditions considering a SF matrix with a homogeneous chemical composition of  $\text{UO}_2$  ( $\text{UO}_2$  containing 1 atom % of Pd, as representative element of the epsilon particles, behaving as catalyst for the activation of  $\text{H}_2$ ). The results of the 1D simulations allow us to quantify i) the effect of metallic Fe corrosion on the spent fuel matrix dissolution, and ii) the effect of considering SF as a porous medium.

The model was compared to new experimental data generated in the WP3 of DisCo project demonstrating its ability to reproduce independent data not used in its calibration. This promoted the collaboration between modellers and experimentalists of the DisCo project.

Two activities are planned for the last year of the project:

1. extending the reactive transport model to a 1D axi-symmetrical geometry for the spent fuel domain.
2. simulation of different sets of experimental data generated in the DisCo project

PSI carried out thermodynamic calculations in order to assess the influence of Cr-doping on the fuel oxygen potential. Exceedingly high oxygen potentials could lead to detrimental effects under repository conditions, such as enhanced  $\text{UO}_2$  matrix dissolution and increased solubility of redox sensitive nuclides (e.g. Pu, Np, Mo). The model was implemented in the chemical equilibrium code GEM-Selektor (<http://gems.web.psi.ch>) [9] with the in-house database HERACLES (<https://www.psi.ch/heracles/>) [10] applied both to non-doped and Cr-doped model  $\text{UO}_2$  fuel compositions.

During the first two years of the project the efforts were directed to develop a ternary three-sites solid solution model for Cr-doped hyperstoichiometric urania. In the past year, efforts were focused on expanding the  $\text{UO}_2$  solid solution model by including end-members of soluble radionuclides (lanthanides, minor actinides and Pu). As far as possible, mixing parameters were determined by fitting experimental data. Moreover, two new ideal solid solutions were introduced: a binary (Ba,Sr) $\text{ZrO}_3$  phase (grey phase) and a quinary (Mo, Ru, Pd, Tc, Rh) metallic phase ( $\epsilon$ -particles). These implementations revealed that the fuel oxygen potential is sensitive to the activity of Mo in the metallic inclusions ( $\epsilon$ -particles). With increasing molybdenum dilution in the  $\epsilon$ -particle phase, higher oxygen potentials result, but still identical for Cr-doped and non-doped fuels and within the range of experimental values.

Zircaloy oxidation at the inner side of the cladding was estimated to potentially reduce oxygen potentials by up to 40-60 kJ/mol. Finally, the evolution of oxygen potential as a function of burnup was computed. The results indicate initially low, rapidly increasing oxygen potentials, reaching a limiting curve in the Ellingham diagram at burnups  $\geq 42$  GWd/tiHM. The oxygen potentials calculated for Cr-doped fuel were found to be higher than for conventional fuel only in the very initial burning stages, otherwise no or negligible differences are found.

The major conclusion from this modelling study is that Cr-doping should have no significant effect on oxygen potential and stoichiometry of  $\text{UO}_2$  fuels irradiated in light water reactors. Therefore, undesired in-pile effects such as enhanced diffusivity of radionuclides, a reduction of fuel thermal conductivity during neutron irradiation, or increased Zircaloy oxidation at the inner side of the cladding, are unlikely.

Armines worked in a 2D reactive transport model to assess the alteration of  $\text{U}_{0.73}\text{Pu}_{0.27}\text{O}_2$  under self  $\alpha$ -radiolysis, considering  $\text{H}_2\text{O}_2$  as the most important species regarding MOX dissolution. The model is implemented in HYTEC code, dealing with diffusive transport of a reactive species coupled to chemistry



and using CHESS as a geochemical code for thermodynamic equilibrium and kinetic controls. The thermodynamic database ThermoChimie [5] was used for all the simulations.

During the first two years of the DisCo project, two consistent models were developed: MOx leaching in carbonate water and MOx leaching in clay porewater in presence of an iron foil [11].

During the third year of the DISCO project, the following tasks were undertaken:

- Publication of a peer-reviewed paper in collaboration with CEA, ANDRA and EDF [12].
- Completion of the reactive transport model of  $U_{0.73}Pu_{0.27}O_2$  experimental leaching in synthetic clay groundwater with metallic iron, thanks to the new results acquired by CEA in WP4 over more than one year (see the extended abstract of Jegou et al., this volume).
- Simulation grid and the input file of HYTEC have been adapted as a preliminary step to apply the model to the configuration of a disposal cell of MOX fuels

The concluding remarks of the work undertaken by Armines are:

1. The present reactive transport model fully couples the interconnected key geochemical reactions and simulates reasonably well – over more than 1 year – the experimental evolution of the aqueous chemistry, the degree of alteration of the homogeneous MOx matrix, the corrosion of the iron, the location of the redox front and the subsequent precipitation of magnetite.
2. The coupled geochemical scheme, the mineralogical secondary products, the kinetics, as well as the actinide concentrations, are very close to the results already obtained for alpha-doped  $UO_2$  (a proxy for  $UOx$  fuel matrix).
3. Under oxidative conditions, the higher content of Pu decreases the alteration of the matrix compared to  $UO_2$ . Under strongly reducing conditions, the possibility of promoting the alteration of the MOx matrix by reducing Pu(IV) into the more soluble Pu(III) state should be further investigated.

In the last year of the DisCo project, the knowledge gained from this reactive transport modeling at the laboratory scale will serve as a basis for a simplified mass balance simulation (e.g. between radiolytic  $H_2O_2$  and iron scavenging) at the scale of a disposal cell of spent MOX fuel.

NNL has built a mixed-potential model of matrix dissolution based on previous work by Canadian and American national laboratories. The model, implemented in gPROMS V5.1.1, has been compared to observations made of pond-stored WAGR fuel pins. For these fuel pins, no notable fuel dissolution occurred during their storage. Contrary to this the model predicted some dissolution – however the extent of this was minor. Thus, the model can be said to agree somewhat with observations made on real fuel pins, if not perfectly.

The model accounts for the effects of: oxidative and chemical dissolution, diffusion, reaction, radiolysis, precipitation on the fuel surface and the presence of small noble metal particles on the fuel surface.

Work was also undertaken to evaluate the applicability of data for higher pH pond systems used at Sellafield. One method considered to improve the way in which solution chemistry effects are accounted for was to interface the model with PHREEQ-C.

The dissolution model has also been coupled with key elements of a pond storage model developed for Sellafield Limited to allow comparison of the model predictions with observations of the condition of cut oxide fuel which has been pond stored for over 40 years, to assess the model's predictive capabilities.

Through the development of the NNL model, a wide range of uncertainties in the approach, parameters and implementation of the model have been identified. These range from fundamental questions about some of the assumptions made in the literature on which the model is based, to issues surrounding the applicability of the model to a range of conditions and a lack of fundamental input data. These uncertainties are set out in detail in the report [4] so that future researchers would be able to address them. It should be noted that to address these concerns a significant experimental programme would need to be undertaken. This would need experimental work to require (but not be limited to).

## References

- [1] Riba, O., Coene, E., Silva, O., Duro, L. (2020). Spent fuel matrix alteration 1D model integrating water radiolysis and reactive solute transport – model calibration and validation. *This volume*.
- [2] Curti, E. and Kulik, D.A. (2020). Thermodynamic modelling of oxygen potential for Cr-doped and conventional UO<sub>2</sub> fuel as a function of temperature and burnup. *This volume*.
- [3] De Windt, L., Kerleguer, V., Jégou, C., Goblet, P., Martin, C., Tocino, F. (2020). Full reactive transport model of U<sub>0.73</sub>Pu<sub>0.27</sub>O<sub>2</sub> experimental leaching in synthetic clay groundwater with metallic iron. *This volume*.
- [4] Hughes, R.J., Hambley, D.I., Bankhead, M. (2020). Deliverable 5.4. EU DisCo Model Description, Uncertainties and Results. DisCo project (Grant Agreement: 755443).
- [5] ThermoChimie Database. Andra thermodynamic database for performance assessment. <https://www.thermochimie-tdb.com/pages/version.php>.
- [6] Nardi, A., Idiart, A., Trincherro, P., de Vries, L.M., Molinero, J. (2014). Interface COMSOL-PHREEQC (iCP), an efficient numerical framework for the solution of coupled multiphysics and geochemistry. *Comput. Geosci.*, 69, 10-21.
- [7] Cera, E., Bruno, J., Duro, L., Eriksen, T. (2006). Experimental determination and chemical modelling of radiolytic processes at the spent fuel/water interface. SKB Technical Report, TR 06-07.
- [8] Evins, L.Z., Juhola, P., Vähänen, M. (Eds.) (2014). REDUPP Final Report. POSIVA Report, 2014-12.1.
- [9] Wagner, Th., Kulik, D.A., Hingerl, F.F., Dmytrieva, S.V. (2012). GEM-Selektor geochemical modeling package: TSolMod library and data interface for multicomponent phase models, *Can. Mineral.*, 50, 1173-1195.
- [10] GEMS specific HERACLES v.0.2. database for U, TRU and FP speciation, <https://www.psi.ch/en/heracles/gems-specific-heracles-database> (accessed 30 January 2020).
- [11] De Windt, L., Goblet, P., Kerleguer, V., Jégou, C. (2019). Deliverable D5.3. Progress on the modeling of the homogeneous U<sub>0.73</sub>Pu<sub>0.27</sub>O<sub>2</sub> alteration as a simulant of MOX fuel matrices in an underground disposal cell. DisCo project (Grant Agreement: 755443).
- [12] Kerleguer, V., Jégou, C., De Windt, L., Broudic, V., Jouan, G., Miro, S., Tocino, F., Martin, C. (2020). The mechanisms of alteration of a homogeneous U<sub>0.73</sub>Pu<sub>0.27</sub>O<sub>2</sub> MOX fuel under alpha radiolysis of water. *J. Nucl. Mater.*, 529, 151920.



---

# **Extended Abstracts**

---

# Initial results of dissolution experiments with irradiated PWR MOX fuel (54 MWd/kg<sub>HM</sub>) under anoxic conditions

Serrano-Purroy, D., Carbol, P. and Van Winckel, S.

EC-JRC (BE)

---

## 1. Introduction

JRC-Karlsruhe is contributing to the DisCo project in WP2 and WP3 with experimental studies of the long-term stability of a spent MOX fuel (54 MWd/kg<sub>HM</sub>) and an irradiated Cr<sub>2</sub>O<sub>3</sub>-doped UO<sub>x</sub> fuel (58 MWd/kg<sub>HM</sub>) in simplified groundwater (diluted NaCl solution with NaHCO<sub>3</sub>) under anoxic and reducing conditions respectively. Not only leachates and solids after leaching, but also the gas phase will be analysed in order to obtain a complete description of the redox conditions.

The first experiment with a MOX sample (under Ar atmosphere) has already started and is ongoing since the 8<sup>th</sup> of October 2019. Although the two autoclaves for the remaining MOX and Cr<sub>2</sub>O<sub>3</sub>-doped samples are ready and experiments were supposed to be started at the end of February-beginning of March, the present situation of the SARS-CoV-2 pandemic and the consequent temporary closure of the laboratories at JRC-Karlsruhe forced us to postpone the start of the remaining experiments until the hot cells functionality is back to normality.

This report focuses on the initial dissolution results of the first autoclave experiment.

## 2. Methods

### 2.1 Sample preparation

The fuel selected is a Short Binderless Route (SBR) MOX, labelled M502, which was irradiated in Beznau-1 (PWR) in the 90's. From two selected sampling positions, and according to the available gamma scanning, the sample corresponding to the section with higher local burnup was selected for the first autoclave. The main characteristics of the cladded segment are summarized in Table 1.

**Table 1:** Parameters of SNF cladded segment used in the described leaching experiment.

Sample	MOX-H
Length (mm)	2.1 ± 0.1
Weight	1.538 ± 0.001
Estimated local burn-up (MWd/kg <sub>HM</sub> )	56
Fabrication process	SBR
Pu enrichment (weight%)	5.54
Fission Gas Release (%)	2.5

The samples were cut by a diamond saw with a slow rotation speed (described in [1]) in a N<sub>2</sub> purged hot-cell and were stored under vacuum to minimise potential oxidation until the start of the experiment.

## 2.2 Autoclaves

Studies of spent fuel dissolution experiments under anoxic or reducing conditions can only be performed in an autoclave. Anoxic and reducing condition requires a very tight autoclave to reduce oxygen intrusion and thereby fuel oxidation. At JRC-Karlsruhe hot-cells the requirement of autoclave tightness is also related to hot-cell safety conditions. The construction, manufacturing and testing of the autoclave design for hot-cell use and dissolution experiments mimicking repository conditions must fulfil strict requirements, i.e. be manufactured from non-reductive materials (mainly Ti and PEEK), have a pressure tightness up to 50 bar H<sub>2</sub> or Ar, have a solution volume sufficient for 10 samplings, allow gas purging during loading and start-up of experiment, consist of materials withstanding high radiation doses (especially gaskets and valve seats), allow remote handling and most importantly, fulfil the high safety standards related to the operation of hot-cells.

In respect to the strict safety requirements described in the text above, three autoclaves for the dissolution tests of MOX and Cr<sub>2</sub>O<sub>3</sub>-doped UO<sub>2</sub> (JRC-Karlsruhe contribution) and two for the dissolution tests of high burn-up UO<sub>2</sub> (Eurecat contribution) have been thoroughly tested for H<sub>2</sub> tightness, which has been confirmed being less than 0.3 bar per annum at a He gas pressure of 50 bar. The autoclave set-up adapted for the experiment and gas sampling, has been extensively tested and the first experiment started in October 2019.

The system consists of an ‘experiment autoclave’, located inside a hot-cell, and a ‘refill autoclave’ located in a glovebox outside of the hot-cell from which solution can be transferred via gas tubes into the ‘experiment autoclave’. Filling and refilling of solution and gas in the ‘experiment autoclave’ is driven by difference in gas pressure between the ‘refill autoclave’ and the ‘experiment autoclave’. For refilling solution from the ‘refill autoclave’ to the ‘experiment autoclave’ a 5-10 bar higher pressure is needed in the ‘refill autoclave’. The pressure of the gas can vary in the range of 1 bar to a maximum of 50 bar at 25°C. The autoclaves are foreseen to be operated in the temperature range 10-80°C (Figure 1a). A polyether ether ketone (PEEK) container including a sample holder (Figure 1b) and PEEK lid is placed inside the autoclave vessel. In total, seven bellow valves control the liquid and gas in and out flows. A manometer controls the pressure inside the vessel. Solution and gas can be sampled from the ‘experiment autoclave’ during the experiment.

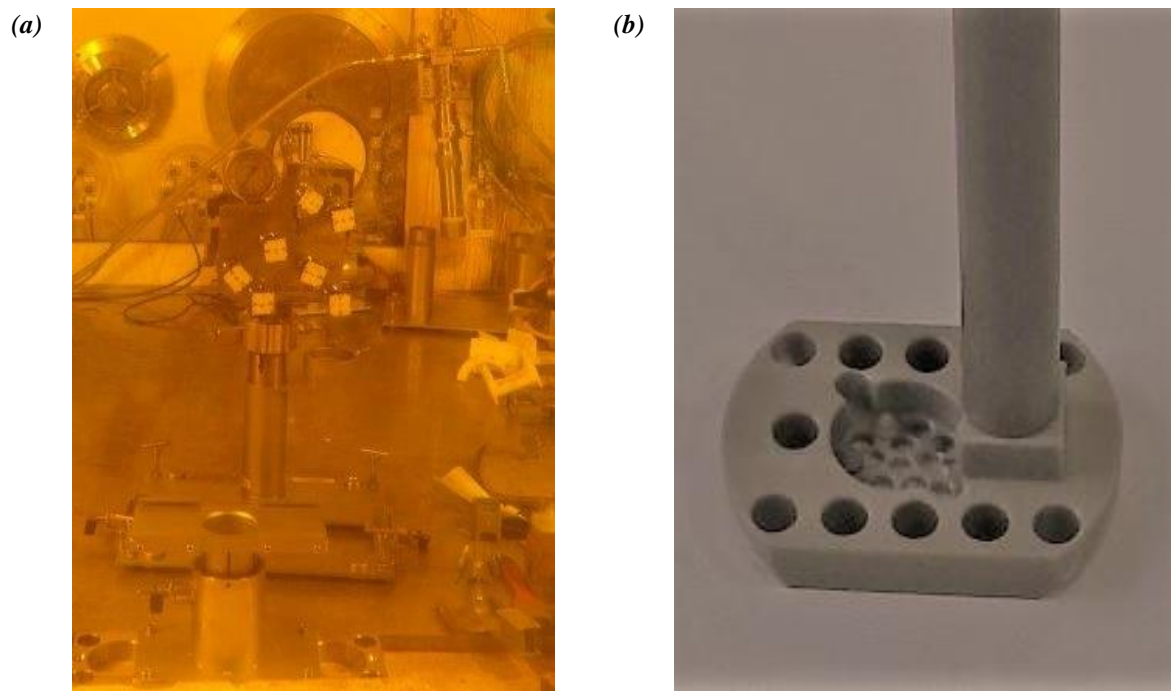


**Figure 1:** (a) 'Experiment autoclave' inside the hot-cell and (b) PEEK sample holder.

### 2.3 Experimental

The experiment was performed at an initial pressure of 32 bars under anoxic conditions (Ar / 0.003% CO<sub>2</sub>) using approximately 110-120 mL of the selected simulated simplified groundwater (BIC: 1 mM NaHCO<sub>3</sub> and 19 mM NaCl). The experimental temperature corresponds to standard hot-cells working conditions:  $25 \pm 5^\circ\text{C}$ .

At the beginning of the experiment, two complete solution replenishments were carried out over two consecutive days. This was done to minimize contribution from existing pre-oxidized phases. After the second replenishment, the solution was not any more renewed after the samplings to minimize introduction of oxygen into the system. Sample were taken at regular intervals. Sampling will continue up to one year after the start of the experiments. In all samplings, at the initial complete replenishments or later under static conditions, both acidified and non-acidified samples were taken. Each complete set of sampling corresponds to a reduction in volume and pressure inside the autoclave of approximately 6-8 mL and 3-4 bar respectively. After the first complete replenishment a gas sample was recovered in order to determine the O<sub>2</sub> intrusion and the initial release of fission gases by Gas Mass Spectrometry. A second gas sample will be taken at the end of the experiment. The solutions taken were further diluted in 1 mol/L nitric acid according to the levels of concentration and dose rate required for subsequent analysis by ICP-MS using a Thermo ELEMENT 2 instrument (Thermo Electron Corporation, Germany). They were measured with the addition of In, Ho, Co and Th as internal standards and calibration curves were produced using a series of dilutions of certified multi-element standard solutions in the concentration range of the major elements in solution.

Until now, 6 samples have been taken corresponding to the two replenishments (R1 and R2 corresponding to 0.15 and 1 day of experimental time) and four samples, S1 to S4, taken at days 3, 13, 48 and 150.

Table 2 summarises the main characteristics of the experiment.

**Table 2:** Main characteristics of experiments.

Experiment	Sample Weight (g)	Initial leachate volume* (mL)	Solution	Initial gas pressure* (bar)	Gas atmosphere composition
MOX-H	1.538	112	BIC	32	Ar + 0.003% CO <sub>2</sub>

\* Those numbers correspond to the conditions after the second replenishment. Conditions for the first two replenishments were similar.

Based on previous experience [2] some radionuclides (U, Rb, Sr, Mo, Tc, Cs and I) have been selected to be analysed. Fraction of Inventory in Aqueous Phase (FIAP) results will be determined.

Five out of the six samples (both acidified and non-acidified) have been analysed by ICP-MS before the 3<sup>rd</sup> Annual DisCo meeting. Gamma-spectroscopy and iodine analysis were not finished and cannot be reported yet.

## 2.4 Data treatment

Two complete solution replenishments were made at the beginning of the experiment to minimise the effect of pre-oxidised layers and avoid precipitation of secondary phases. The total moles in solution should be the moles measured in solution at a given time plus the moles released in the previous replenishments. The cumulative concentration is then calculated dividing the cumulative moles by the volume of solution.

The cumulative concentration in solution gives information about the absolute release of an element but it is not suitable to compare the release between elements since the cladded segment inventory of each element will be different. To compare the release between elements of the same cladded segment the Fraction of Inventory in the Aqueous Phase can be calculated (FIAP):

$$FIAP_i = \frac{m_{i, aq}}{m_{i, SNF}} \quad \text{Eq. 1}$$

where  $m_{i, aq}$  is the mass of element  $i$  in the aqueous phase (g);  $m_{i, SNF}$  the mass of element  $i$  in the SNF sample (g). The FIAP is given as a percentage. The total FIAP in the experiment is corrected by including the FIAP of the first two replenishments.

The elements that present a FIAP higher than the FIAP of uranium can be considered as part of the IRF, since the dissolution of uranium, in the absence of secondary precipitation reactions, is considered to correspond to the dissolution of the matrix. A way to determine if an element belongs to the IRF is to normalise the FIAP of this element to the FIAP of uranium (FNU<sub>*i*</sub>):

$$FNU_i = \frac{FIAP_i}{FIAP_U} \quad \text{Eq. 2}$$

where  $FIAP_i$  and  $FIAP_U$  are the cumulative FIAP of element  $i$  and uranium, respectively.



If the FNU of an element is higher than 1, then this radionuclide belongs to the IRF. The FIAP of an element contains the fraction of this element belonging to the IRF but also the fraction of this element that was trapped in the matrix. The fraction trapped in the matrix will be released as the matrix is dissolved and releases the elements trapped within. Therefore, the FIAP is the sum of the  $FIAP_{IRF}$  and the  $FIAP_{matrix}$ . The  $FIAP_{matrix}$  would have the same values as the FIAP of uranium ( $FIAP_U$ ) taking uranium, as described above, as a reference for the matrix. Then the  $FIAP_{IRF}$  or simply the IRF of an element can be calculated as:

$$IRF_i = FIAP_i - FIAP_U \quad \text{Eq. 3}$$

where  $FIAP_i$  and  $FIAP_U$  are the cumulative FIAP of element  $i$  and uranium respectively.

### 2.5 Uncertainty calculation

The uncertainties of each value were obtained combining the uncertainty of the dilutions, experimental uncertainty and ICP-MS measurement uncertainties, and propagating the uncertainties through all the calculations made, using the following equation:

$$e_F = \sqrt{\left(\frac{\partial F}{\partial x}\right)^2 e_x^2 + \left(\frac{\partial F}{\partial y}\right)^2 e_y^2 + \left(\frac{\partial F}{\partial z}\right)^2 e_z^2 + \dots} \quad \text{Eq. 4}$$

where  $F$  is the equation used to find the value for which an uncertainty is required;  $x, y, z, \dots$  are the parameters of this equation and  $e_i$  is the uncertainty of each parameter [3].

### 2.6 Theoretical inventory

The theoretical inventory was calculated using the ORIGEN code [4]. The most relevant inventory results are summarised in Table 3.

**Table 3:** Theoretical radionuclide inventory of the MOX-H fuel.

Radionuclide	Calculated inventory ( $\mu\text{g/g fuel}$ )	Radionuclide	Calculated inventory ( $\mu\text{g/g fuel}$ )
<b>Rb</b>	282.1	<b>Cs</b>	3790
<b>Sr</b>	484.8	<b>Ba</b>	2644
<b>Y</b>	326.1	<b>La</b>	1498
<b>Zr</b>	3702	<b>Ce</b>	3085
<b>Mo</b>	4407	<b>Pr</b>	1498
<b>Tc</b>	1057	<b>Nd</b>	4672
<b>Ru</b>	3526	<b>Pm</b>	2.1
<b>Rh</b>	1058	<b>Sm</b>	1234.1
<b>Pd</b>	3790	<b>U</b>	793,333
<b>Ag</b>	149.9	<b>Np</b>	290.9

Radionuclide	Calculated inventory (µg/g fuel)	Radionuclide	Calculated inventory (µg/g fuel)
<b>Cd</b>	211.6	<b>Pu</b>	37,903
<b>Te</b>	511.3	<b>Am</b>	6082
<b>I</b>	405.5	<b>Cm</b>	167.5

### 3. Results and discussion

Due to an unforeseen contamination of the water used for leachant preparation (from the de-ionised water preparation unit), the concentration of Rb, Sr and Ba released from the fuel could not be determined (natural background too high). Trustful results of leachate concentrations of U, Pu, Cs, Mo and Tc are reported. Further analysis and evaluations will be made in order to extend the list of reported radionuclides. Special effort will be dedicated to the analysis of iodine.

#### 3.1 FIAP

The FIAP including the released fraction in both replenishments from the MOX-H clad segment are presented against time in Figure 2.

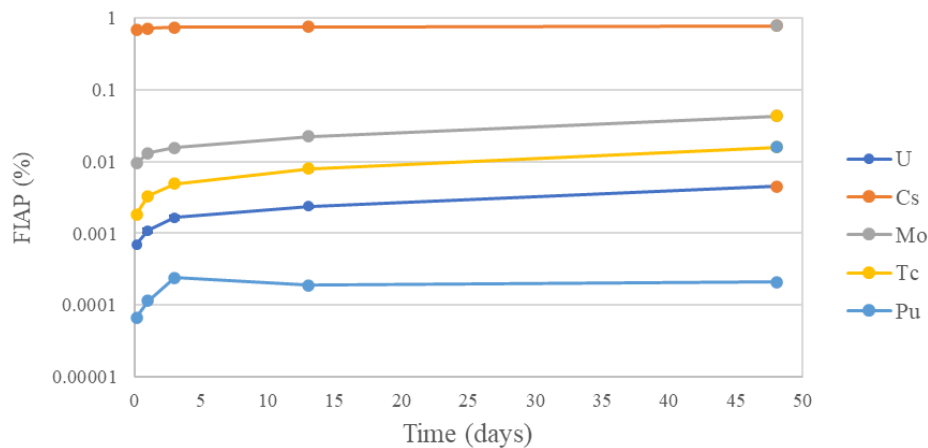


**Figure 2:** FIAP (%) including the first two replenishments.

It is possible to observe different trends at the beginning and during the rest of the experiment. In case of uranium and plutonium the initial fast release might be due to the presence of pre-oxidised layers, which is still significant after the second replenishment. The second, slower release is assumed to come from the matrix. Uranium release, even after 50 days, is still increasing. However, Plutonium after an initial higher release seems to remain stable, which might indicate no further release or equilibrium with Pu secondary phases.

In contrast, for IRF elements this initial release can come from the gap and open voids such as fractures and cracks in the surface of the sample. Tc and Mo, both redox sensitive elements, present a continuous increase during the experiment. In the case of Cs the initial release is significantly higher than the others but immediately after, the release tends to moderate, even to lower values than uranium.

### 3.2 FNU and IRF

The fraction in aqueous phase of Mo, Tc and Cs in relation to the FIAP of uranium together with their calculated uncertainties in the different sampling occasions are given in Table 4. The table also includes the instant release fraction for the three elements up to the last sampling.

**Table 4:** FNU and IRF determined for the MOX-H fuel.

Sample (experimental time in d)	R1 (1)	R2 (1)	S1 (3)	S2 (13)	S3 (48)	IRF (%)
Mo	13.6 ± 0.1	9.1 ± 0.1	4.5 ± 0.1	7.2 ± 0.1	8.9 ± 0.1	0.0390 ± 0.0004
Tc	2.6 ± 0.1	3.9 ± 0.1	2.8 ± 0.1	3.5 ± 0.1	3.7 ± 0.1	0.0114 ± 0.004
Cs	960 ± 1	108 ± 1	36 ± 1	32 ± 1	19 ± 1	0.775 ± 0.008

As expected, the contribution to the IRF is higher at the beginning of the experiments, especially for Cs with an initial FNU of approximately 1000. Even after 50 days, the FNU for both Tc and Mo still show an increasing trend, while for Cs after the initial significant release this trend seems to decrease which will eventually finish reaching a similar release as the matrix.

### Conclusions

Corrosion experiments on spent PWR MOX fuel under anoxic conditions (in 32 bar Ar / 0.003 vol.% CO<sub>2</sub>) were started in October 2019.

The initial release of uranium, plutonium, caesium, technetium und molybdenum has been analysed and reported. An initial high release rate was observed for all analysed elements, which was followed by a significant lower release rate. The initial fast release can for uranium and plutonium be attributed to pre-oxidised phases and in the case of the IRF elements to segregated phases in open fuel voids. Further samplings and analysis are needed in order to fully understand the behaviour of some elements like Cs and Pu.

The start of the second and third experiment, as well as some sampling and analysis from the first experiments had to be postponed after 3<sup>rd</sup> DisCo Annual Meeting.

### Acknowledgement

*The research leading to these results has received funding from the European Commission Horizon 2020 Research and Training Programme of the European Atomic Energy Community (EURATOM) (H2020-NFRP-2016-2017-1) under grant agreement n° 755443 (DisCo project).*

### References

- [1] Farnan, I., Bosbach, D., Wegen, D., Gonzales-Robles Corrales, E., Jegou, C., Corkhill, C., Hambley, D.I., Cobos Sabate, J. (2018). Deliverable D2.1: Initial state report: sample characterisation and experimental set-up. DisCo project (Grant Agreement: 755443).

- [2] Martínez-Torrents, A., Serrano-Purroy, D., Sureda, R., Casas, I., de Pablo, J. (2017). Instant release fraction corrosion studies of commercial UO<sub>2</sub> BWR spent nuclear fuel. *J. Nucl. Mater.*, 488, 302-313.
- [3] Ellison, S.L.R. and Williams, A. (Eds) (2012). *Eurachem/CITAC guide: Quantifying uncertainty in analytical measurement*. Third edition, ISBN 978-0-948926-30-3. Available from: [www.eurachem.org](http://www.eurachem.org).
- [4] WebKORIGEN++, [www.nucleonica.com](http://www.nucleonica.com)

# Status of leaching experiments performed with irradiated MOX fuel in bicarbonate water under hydrogen overpressure at KIT-INE

*Herm, M., González-Robles, E., Walschburger, A., Müller, N., Bohnert, E., Böttle, M., Geyer, F., Fuss, M. and Metz, V.*

KIT, Eggenstein-Leopoldshafen (DE)

---

## Abstract

In this Scientific and Technical (S+T) contribution, results of two leaching experiments performed with irradiated MOX fuel after 370 days of leaching in bicarbonate water (containing 19 mM NaCl and 1 mM NaHCO<sub>3</sub>) under strongly reducing conditions are shown. A continuous release of <sup>90</sup>Sr, <sup>99</sup>Tc, <sup>129</sup>I, <sup>137</sup>Cs and fission gases is observed in both experiments conducted with a cladded MOX pellet and fragments of a MOX pellet without cladding. This trend is slightly more pronounced in the experiment with fragments without cladding.

## 1. Introduction

Disposal in deep bedrock repositories is considered as the preferred option for the management of spent nuclear fuel (SNF) in many countries [1-3]. The aim is a permanent and safe disposal of this type of highly active waste so that its radionuclide inventory is isolated from the biosphere for an appropriate length of time. A multi-barrier system is interposed between the SNF and the environment considering the SNF matrix as the first technical barrier. In safety assessments for disposal of SNF in a deep underground repository, water access, consecutive failure of canisters and loss of integrity of fuel cladding is considered in the long-term. Assessing the performance of SNF in a potential geological disposal system requires the mechanistic understanding and quantification of the radionuclide release from SNF under reducing conditions of a breached container.

Up to now, many studies have been performed on dissolution of initially <sup>235</sup>U-enriched UO<sub>2</sub> fuels and CANDU fuels under oxidizing conditions and, in a lesser extent, studies on SNF dissolution under reducing conditions. Moreover, regarding the dissolution of irradiated mixed Pu/U oxide (MOX) fuels, there is a lack of studies, especially, under reducing conditions.

Present studies performed at KIT-INE provide experimental data concerning the matrix dissolution of irradiated MOX fuel under reducing conditions. Moreover, the instant release fraction of safety relevant radionuclides is determined. For this purpose, two leaching experiments with spent MOX fuel (a cladded pellet and fragments of a pellet without cladding) are currently conducted in the shielded box-line of KIT-INE with periodical sampling campaigns of the gaseous and the aqueous phase. In this communication, results of fission products and gases released into the aqueous and gaseous phases up to 370 days of leaching are shown.

## 2. Materials and methods

### 2.1 Spent nuclear fuel characteristics, irradiation history and experimental details

Irradiated fuel specimens were sampled from a MOX fuel rod that was irradiated in the pressurized water reactor of the Obrigheim nuclear power plant (KKO) in Germany. The irradiation was conducted in four cycles for a period of 1157 effective full power days with an average linear heat generation rate of 200 W/cm, achieving an average burn-up of 38 GWd/t<sub>HM</sub>. The fuel rod was discharged in 1984, which implies a cooling time of 32 years before characterisation and cutting of the MOX samples. Initially, the fuel consisted of natural UO<sub>2</sub> enriched by 3.2% Pu and was fabricated following the optimised co-milling (OCOM) process.

The leaching experiments are performed in two stainless steel autoclaves with titanium inserts and lid under Ar/H<sub>2</sub> atmosphere. In both autoclaves, a total gas pressure of 40 bar is maintained using a certified Ar/H<sub>2</sub> gas mixture (with volume fractions of 92% of Ar and 8% of H<sub>2</sub>, Basi and Schöberl GmbH) to create strongly reducing conditions (H<sub>2</sub> partial pressure: 3.2 bar). As leachant bicarbonate water, containing 19 mM NaCl and 1 mM NaHCO<sub>3</sub> (pH 7.9 ± 0.1) is used.

### 2.2 Analytical methods

Concentrations of technetium in aqueous solutions were determined using high-resolution inductively coupled plasma mass spectrometry (HR-ICP-MS) A sector field device (ELEMENT XR, ThermoFisher Scientific) was used to quantify <sup>99</sup>Tc.

Liquid scintillation counting (LSC, Quantulus 1220, Wallac Oy, PerkinElmer) was used to quantify aqueous concentration of <sup>90</sup>Sr. Firstly, <sup>90</sup>Sr was extracted from the liquid sample aliquots by chromatography using a Sr-Resin crown ether (4,4'(5')-di-t-butylcyclohexano-18-crown-6). Then, solution aliquots were homogenized in Polyvials (HDPE, Zinsser Analytic) with LSC-Cocktail (Ultima Gold LLT, Perkin Elmer) for the measurements.

Aqueous concentrations of <sup>137</sup>Cs and <sup>129</sup>I were quantified using  $\gamma$ -spectroscopy. Measurements were performed by means of an extended range coaxial Ge detector (GX3018, Canberra Industries Inc.) with a relative efficiency of  $\geq 30\%$ . Energy and efficiency calibration of the detector was done using a certified multi-nuclide standard solution (Mixed Gamma 7600, Eckert & Ziegler Strahlen- und Medizintechnik AG). Data evaluation was performed using the Genie 2000 software (Canberra Industries Inc.). APEX screw-cap microcentrifuge tubes (2 mL, polypropylene, Alpha Laboratories Ltd.) were used as sample vessels during the measurements.

Gas phase composition and concentration of fission gases Kr and Xe released during dissolution of SNF into the gas phase were analysed by means of a multipurpose mass spectrometer with customized gas inlet system (GAM 400, InProcess Instruments). The system was equipped with a quadrupole mass analyser and a secondary electron multiplier (SEM) detector. The total gas pressure was monitored at four successive positions within the inlet system. Ten scans of each gas sample were measured, using the SEM detector, and the mean value was taken. Calibration of the instrument was performed in the same pressure range as the respective range for analysis of the sample aliquots. For calibration, standard gases containing He, N<sub>2</sub>, O<sub>2</sub>, Ne, Ar, Kr, Xe, and CO<sub>2</sub> were used. Additionally, the Kr and Xe background of the Ar/H<sub>2</sub> gas mixture, used in the leaching experiments, was periodically analysed and taken into account for background correction of the fission gas results.

### 3. Results and discussion

Aqueous concentrations of fission products  $^{90}\text{Sr}$ ,  $^{99}\text{Tc}$ ,  $^{129}\text{I}$  and  $^{137}\text{Cs}$  as a function of leaching time are shown in Figure 1. After about 370 days of leaching, concentrations of the studied fission products are still slightly increasing except for  $^{99}\text{Tc}$ . In the first two samplings, aqueous concentrations of  $^{99}\text{Tc}$  and  $^{129}\text{I}$  were below detection limit. Aqueous concentrations of the volatile fission products  $^{129}\text{I}$  and  $^{137}\text{Cs}$  are similar, and those of the predominantly matrix bound fission products  $^{90}\text{Sr}$  and  $^{99}\text{Tc}$  are similar, respectively.

The fraction of the radionuclide inventory released into the aqueous phase is calculated to compare the release behaviour of the different radionuclides and to assess the corrosion of the spent MOX fuel. The fraction of inventory of a radionuclide  $i$  released in the aqueous phase (FIAP<sub>*i*</sub>) [4] is given by Eq. 1.

$$FIAP_i = \frac{m_{i,aq}}{m_{i,SNF}} = \frac{C_{(i,n)} \cdot V_{aq}}{m_{SNF} \cdot H_i} \quad \text{Eq. 1}$$

where  $m_{i,aq}$  is the mass of radionuclide  $i$  in the aqueous phase (g),  $m_{i,SNF}$  the mass of radionuclide  $i$  in the spent nuclear fuel sample (g),  $m_{SNF}$  is the mass of SNF sample used in the experiment (g),  $C_i$  is the concentration of element  $i$  in solution (g/mL), and  $V_{aq}$  is the volume of solution (mL).  $H_i$  corresponds to the fraction of inventory for the radionuclide  $i$  (g/g<sub>SNF</sub>) based on inventory calculations by means of the webKORIGEN [5] code using above mentioned irradiation characteristics and a cooling time of 32 years until start of experiments as input for the calculation. The calculated fission products inventories are shown in Table 1.

FIAP data is shown in Figure 2 for  $^{90}\text{Sr}$ ,  $^{99}\text{Tc}$ ,  $^{129}\text{I}$  and  $^{137}\text{Cs}$ . Qualitatively, the temporal evolution of FIAP values of the studied fission products are similar to the evolution of the aqueous concentrations of the respective radionuclides. Quantitatively, it is obvious from the FIAP data that  $^{129}\text{I}$  and  $^{137}\text{Cs}$  release is significantly incongruent, and two to four orders of magnitude higher than FIAP values of  $^{90}\text{Sr}$  and  $^{99}\text{Tc}$ . The considerable  $^{129}\text{I}$  and  $^{137}\text{Cs}$  release is related to a fast dissolving  $^{129}\text{I}$  and  $^{137}\text{Cs}$  fraction in the SNF samples.

Moles of krypton and xenon released into the gas phase of the two leaching experiments are shown in Figure 3. Fission gas release is increasing up to about 160 days of leaching. Thereafter, fission gas release is decreasing in both experiments. A higher release of fission gases is seen from the fragments without cladding compared to the pellet with cladding (see also Table 4).

The fraction of inventory released into the gas phase of a fission gas  $i$ , FIG<sub>*i*</sub>, is calculated for each sample aliquot according to Eq. 2:

$$FIG_i = \frac{n_i}{m_{UO_2} \times H_i} \quad \text{Eq. 2}$$

where  $n_i$  denotes the amount of moles of element  $i$  released into the gas phase of the autoclave,  $m_{UO_2}$  denotes the initial oxide mass in the fuel sample (g) and  $H_i$  denotes the fraction of inventory of element  $i$  in the fuel (mol/g<sub>UO<sub>2</sub></sub>). In the leaching experiments, the fraction of inventory is corrected by the amount of fission gases that were already released into the plenum (6%). The calculated fission gas inventories are shown in Table 1.

**Table 1:** Calculated inventory of the MOX fuel used in the present study.

<b>calculated inventory (mol/g<sub>UO2</sub>)</b>	
Kr	$1.9 \cdot 10^{-6}$
Xe	$3.4 \cdot 10^{-5}$
Kr + Xe	$3.6 \cdot 10^{-5}$
<sup>90</sup> Sr	$1.2 \cdot 10^{-6}$
<sup>99</sup> Tc	$7.8 \cdot 10^{-6}$
<sup>129</sup> I	$1.6 \cdot 10^{-6}$
<sup>137</sup> Cs	$4.1 \cdot 10^{-6}$

The fraction of inventory released into the gaseous phase (FIG<sub>i</sub>) for Kr, Xe and Kr + Xe is shown in Table 2 and Table 3.

**Table 2:** Fraction of released inventory of Kr, Xe and (Kr + Xe) obtained from experiment performed with a clad pellet of irradiated MOX fuel.

<b>Leaching time (days)</b>	<b>Kr</b>	<b>Xe</b>	<b>Kr + Xe</b>
1	$(6.77 \pm 25) \cdot 10^{-3}$	$(3.74 \pm 0.61) \cdot 10^{-3}$	$(3.90 \pm 1.50) \cdot 10^{-3}$
2	–	$(3.47 \pm 0.96) \cdot 10^{-4}$	–
160	$(6.84 \pm 1.23) \cdot 10^{-2}$	$(5.19 \pm 0.81) \cdot 10^{-2}$	$(5.28 \pm 0.82) \cdot 10^{-2}$
370	$(4.75 \pm 0.93) \cdot 10^{-2}$	$(7.81 \pm 1.23) \cdot 10^{-3}$	$(9.98 \pm 0.16) \cdot 10^{-3}$
727	$(3.32 \pm 0.78) \cdot 10^{-2}$	$(3.30 \pm 0.56) \cdot 10^{-3}$	$(4.93 \pm 0.85) \cdot 10^{-3}$

**Table 3:** Fraction of released inventory of Kr, Xe and (Kr + Xe) obtained from experiment performed with fragments without cladding of irradiated MOX fuel.

<b>Leaching time (days)</b>	<b>Kr</b>	<b>Xe</b>	<b>Kr + Xe</b>
1	$(6.23 \pm 4.68) \cdot 10^{-3}$	$(3.29 \pm 0.55) \cdot 10^{-3}$	$(3.46 \pm 0.62) \cdot 10^{-3}$
2	$(7.38 \pm 4.69) \cdot 10^{-3}$	$(3.49 \pm 0.58) \cdot 10^{-3}$	$(3.70 \pm 0.65) \cdot 10^{-3}$
154	$(1.38 \pm 0.24) \cdot 10^{-1}$	$(9.66 \pm 1.50) \cdot 10^{-2}$	$(9.88 \pm 1.53) \cdot 10^{-2}$
365	$(1.18 \pm 0.20) \cdot 10^{-1}$	$(2.88 \pm 0.45) \cdot 10^{-2}$	$(3.37 \pm 0.52) \cdot 10^{-2}$
721	$(9.23 \pm 1.90) \cdot 10^{-2}$	$(1.93 \pm 0.30) \cdot 10^{-2}$	$(2.33 \pm 0.37) \cdot 10^{-2}$



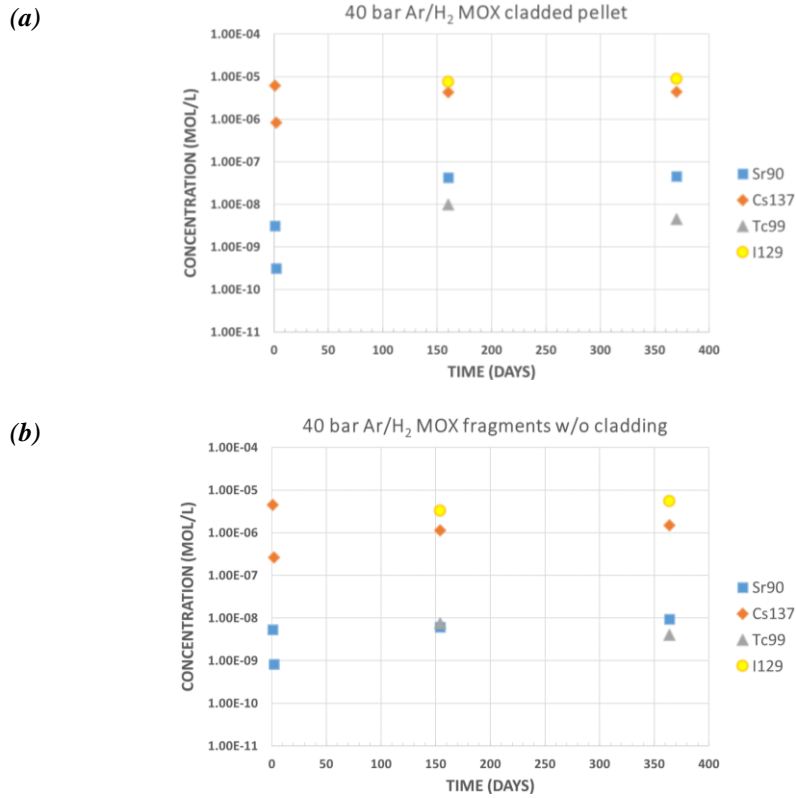


**Figure 1:** Aqueous concentrations of <sup>90</sup>Sr, <sup>99</sup>Tc, <sup>129</sup>I and <sup>137</sup>Cs as a function of leaching time in experiments performed with a cladded SNF pellet (a) and SNF fragments of irradiated MOX fuel (b).

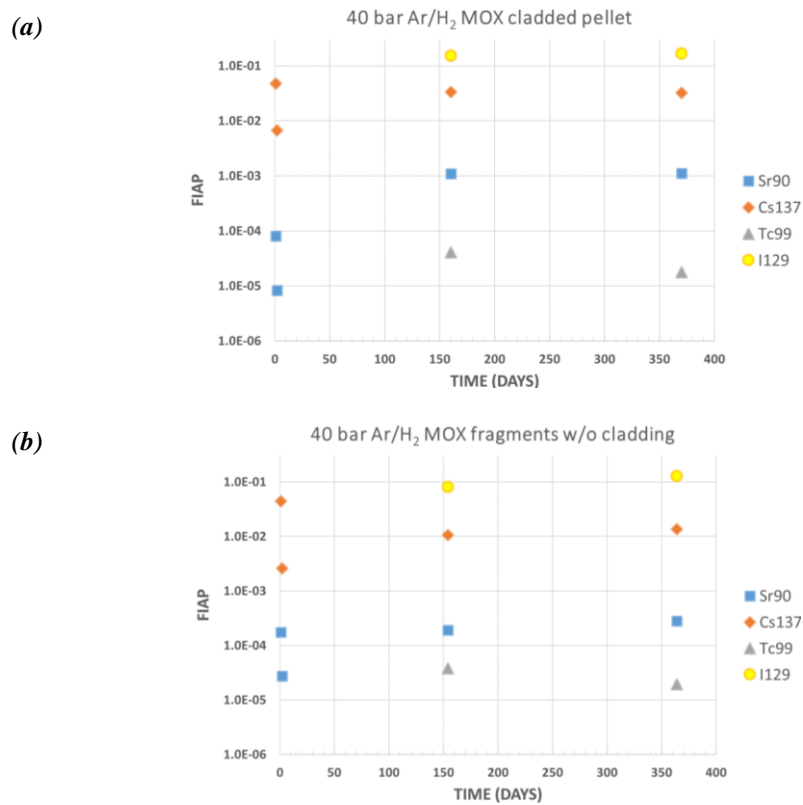


**Figure 2:** FIAP of <sup>90</sup>Sr, <sup>99</sup>Tc, <sup>129</sup>I and <sup>137</sup>Cs as a function of leaching time in experiments performed with a cladded pellet (a) and fragments of irradiated MOX fuel (b).

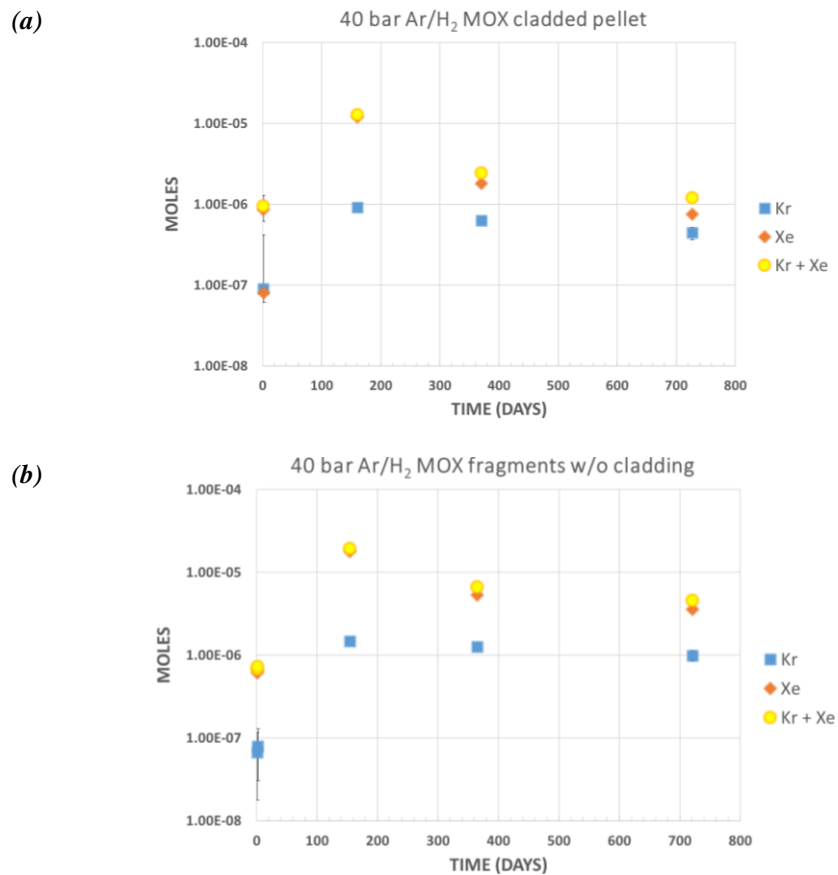


**Figure 3:** Measured moles of fission gases as a function of leaching time in experiments performed with a cladded pellet (a) and fragments of irradiated MOX fuel (b).

To assess the temporal evolution of the fission gas release during the leaching experiments, the cumulative fraction of the inventory released into the gas phase,  $FIG_{ci}$ , is calculated as the sum of the release for each contact period according to Eq. 3:

$$FIG_{ci} = \sum FIG_i \quad \text{Eq. 3}$$

A summary of the cumulative fission gas release values obtained until the last sampling is given, as percentage, in Table 4.

**Table 4:** Cumulative fraction of released inventory of Kr, Xe, and (Kr + Xe) until the last sampling.

Experiment	Leaching time (days)	Kr (%)	Xe (%)	Kr + Xe (%)
Pellet w cladding	727	15.6 ± 3.0	6.7 ± 0.8	7.2 ± 0.9
Fragments w/o cladding	721	36.1 ± 3.7	15.2 ± 1.6	16.3 ± 1.7

## Summary and outlook

Two leaching experiments in autoclaves are currently performed using irradiated MOX fuel in bicarbonate water and hydrogen overpressure. Experiments will be terminated at the end of 2020 or beginning of 2021. Four of seven sampling campaigns are completed including sampling of aqueous and gaseous phases. Analysis of the fifth sampling campaign is currently ongoing.

Once, more results of radionuclide release into aqueous (and gaseous) phases become available a thorough discussion will be performed. Additionally, the data obtained in this study, using spent MOX fuel, will be compared to previous studies performed under similar conditions but with spent UO<sub>2</sub> fuel [6-8].

## Acknowledgement

*The research leading to these results has received funding from the European Commission Horizon 2020 Research and Training Programme of the European Atomic Energy Community (EURATOM) (H2020-NFRP-2016-2017-1) under grant agreement n° 755443 (DisCo project).*

## References

- [1] Ewing, R.C. (2015). Long-term storage of spent nuclear fuel. *Nat. Mater.*, 14, 252-257.
- [2] Bruno, J. and Ewing, R.C. (2006). Spent nuclear fuel. *Elements*, 2, 343-349.
- [3] Shoesmith, D.W. (2000). Fuel corrosion process under waste disposals. *J. Nucl. Mater.*, 282, 1-31.
- [4] Hanson, B.D. and Stout, R.B. (2004). Reexamining the dissolution of spent fuel: A comparison of different methods for calculating rates. *MRS Proceedings*, 824, 89-94.
- [5] Nucleonica GmbH (2011). Nucleonica Nuclear Science Portal ([www.nucleonica.com](http://www.nucleonica.com)). Version 3.0.11. KORIGEN code. <http://www.nucleonica.net/Application/Korigen.aspx>
- [6] Gonzalez-Robles, E., Metz, V., Wegen, D.H., Herm, M., Papaioannou, D., Bohnert, E., Gretter, R., Müller, N., Nasyrow, R., De Weerd, W., Wiss, T., Kienzler, B. (2016). Determination of fission gas release of spent nuclear fuel in puncturing test and leaching experiments under anoxic conditions. *J. Nucl. Mater.*, 479, 67-75.
- [7] Kienzler, B., Duro, L., Lemmens, K., Metz, V., de Pablo, J., Valls, A., Wegen, D.H., Johnson, L., Spahiu, K. (2017). Summary of the Euratom Collaborative project FIRST-Nuclides and conclusions for the safety case. *Nucl. Technol.*, 198(3), 260-276.
- [8] Lemmens, K., Gonzalez-Robles, E., Kienzler, B., Curti, E., Serrano-Purroy, D., Sureda, R., Martinez-Torrents, A., Roth, O., Slonszki, E., Menecart, T., Günther-Leopold, I., Hozer, Z. (2017). Instant release of fission products in leaching experiments with high burn-up nuclear fuels in the framework of the Euratom project FIRST-Nuclides. *J. Nucl. Mater.*, 484, 307-323.

# High burnup spent nuclear fuel dissolution under reducing conditions

*Kokinda, J.<sup>1</sup>, Serrano-Purroy, D.<sup>2</sup>, Clarens, F.<sup>1</sup> and de Pablo, J.<sup>3</sup>*

<sup>1</sup> Eurecat, Centre Tecnològic de Catalunya, Waste, Energy and Environmental Impact Unit (ES)

<sup>2</sup> Joint Research Center Karlsruhe (EU)

<sup>3</sup> UPC - Barcelona Tech, Dept. of Chemical Engineering (ES)

---

## 1. Introduction

Within WP3 of DisCo European project, EURECAT in conjunction with UPC and JRC collaboration, is contributing with three dissolution experiments on a high burn-up (73 MWd/kg<sub>HM</sub>) PWR UO<sub>2</sub> spent nuclear fuel under different leaching conditions. One experiment performed with high pH (YCWCa) solution under oxidizing conditions was already reported previously, while this report focusses on the remaining two experiments under reducing conditions in simplified bicarbonate (BIC) and YCWCa waters. Since both dissolution studies are going to be performed in presence of hydrogen under pressure, autoclaves will be used as reaction vessels in these experiments. The sample preparation methods, leachant composition and analytical methods have been discussed between the participating institutes, to come to an optimal set-up.

## 2. Spent Fuel samples characteristics

Samples were prepared at the JRC laboratories in Karlsruhe from the same fuel rod previously reported [1]. The samples were selected from a UO<sub>2</sub> spent nuclear fuel irradiated in a PWR for five cycles to an average burnup of ~ 60 MWd/kg<sub>HM</sub> and an average linear power density of 255 W/cm. Sampling section was selected according to the rod axial gamma scan, see Figure 1, and in neighbouring positions to those used in the experiments under oxidising conditions. The main characteristics of the cladded segments, this means, fuel segments with their Zircaloy claddings, are summarised in Table 1.

**Table 1:** Parameters of SNF cladded segment used in the described leaching experiment.

Sample	YCWCa	BIC
Length (mm)	1.7 ± 0.1	1.9 ± 0.1
Diameter without cladding (mm)	9.1 ± 0.1	9.1 ± 0.1
Expected local burn-up (MWd/kg)	73	73
Surface area (mm <sup>2</sup> )	460 ± 10	460 ± 10
<sup>235</sup> U enrichment (weight%)	3.95	3.95
Grain size (µm)	6.4	6.4
Fission gas release (%)	13.6	13.6
Average Linear Power Density (W/cm)	255	255

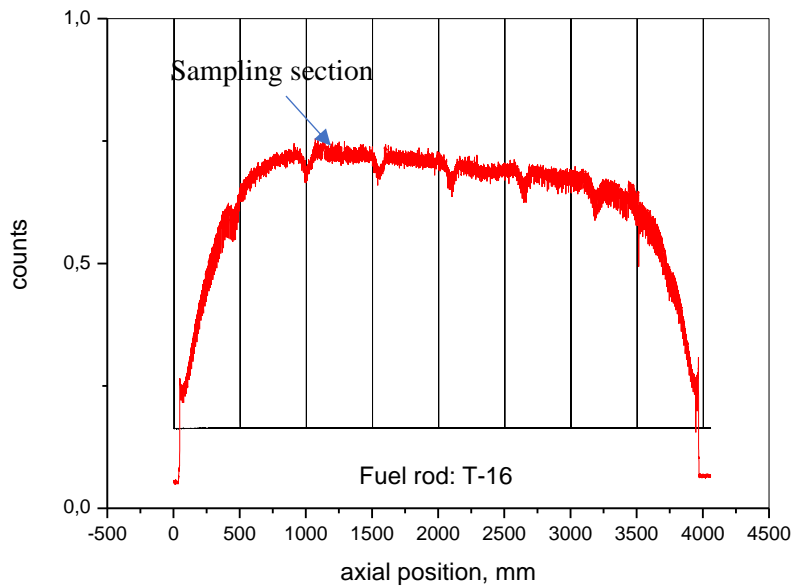


**Figure 1:** UO<sub>2</sub> sample rod gamma scanning. Sampling Section.

The samples were cut using a Bühler cutting machine adapted for use with manipulators. Dry cutting was carried out using a diamond wheel of thickness ~ 0.4 mm. Heating of the samples was avoided by using a slow rotation speed of less than 1000 rpm. In addition, minimum pressure was applied to the cutting wheel throughout. No washing of the samples was made during and after removal from the rod. At the selected location, three adjacent clad segments of range 1.4-1.9 mm, without dishing, were cut through a pellet to obtain samples without the interface between pellets. Two samples will be used in the experiments under reducing conditions while the third one will be used for chemical inventory and burn-up determination. Samples are presently stored under vacuum to avoid pre-oxidation.

### 3. Methods

#### 3.1 Autoclaves

Experiments will be carried out using the same type of titanium autoclaves as those reported by JRC-Karlsruhe. The autoclave system is designed for corrosion studies of spent nuclear fuel under different gas and leachant conditions. The system consists of an experiment autoclave, located inside a hot cell, and a refill autoclave located in a glovebox from which solution can be introduced via pipes into the experiment autoclave. Filling and refilling of solution, and gas in the experiment autoclave is driven by difference in gas pressure between the refill autoclave and the experimental autoclave. For refilling solution from the refill autoclave to the experimental autoclave a 5-10 bar higher pressure is needed in the refill autoclave. The pressure of the gas can vary in the range of 1 bar to a maximum of 50 bar at 25°C. The autoclaves are foreseen to be operated in the temperature range 10-80°C (Figure 2). A polyether ether ketone (PEEK) container including a sample holder (Figure 3) is placed inside the autoclave vessel. In total, seven needle valves control the liquid and gas in and out flows. A manometer controls the pressure inside the vessel. Solution can be sampled from the experimental autoclave during the experiment.



**Figure 2:** Experimental autoclave inside the hot cell.



**Figure 3:** PEEK sample holder.

### 3.2 Experimental procedure and conditions

The experiments will be performed at high pressure (initially 30-35 bars) under reducing conditions (Ar / 5% H<sub>2</sub> / 0.003% CO<sub>2</sub>) using approximately 130 mL of the selected leaching solutions, BIC and YCWCa, see Table 2. The expected experimental temperature corresponds to standard hot cells working conditions: 25 ± 5°C.

**Table 2:** Composition of major ions present in the selected leaching solutions: YCWCa and BIC.

Solution	pH	Na <sup>+</sup> (mmol/L)	Ca <sup>2+</sup> (mmol/L)	Cl <sup>-</sup> (mmol/L)	SiO <sub>3</sub> <sup>2-</sup> (mmol/L)	CO <sub>3</sub> <sup>2-</sup> (mmol/L)	OH <sup>-</sup> (mmol/L)
73YCWCa	13.4	5.0·10 <sup>2</sup>	9.8·10 <sup>-1</sup>	–	2.0·10 <sup>2</sup>	2.5·10 <sup>0</sup>	2.5·10 <sup>2</sup>
73BIC	7.4	2.0·10 <sup>1</sup>	–	1.9·10 <sup>1</sup>	–	1.0·10 <sup>0</sup>	2.5·10 <sup>-7</sup>

At least two full replenishments are foreseen at the beginning of the experiments in order to remove as much as possible contributions from possible pre-oxidized phases. Analysis of the replenished solutions will be carried out to recover information about the IRF.

After those full replenishments will be completed samples and will be taken at regular intervals for a period up to one year.

At each sampling time, samples will be extracted from the autoclave and both acidified and un-acidified samples will be analysed by ICP-MS and  $\gamma$ -spectrometry after proper dilution.

Table 3 summarises the main characteristics of the planned experiments.

**Table 3:** Main characteristics of planned experiments.

Experiment	Sample	Reactor type	Expected burn-up (MWd/kg <sub>HM</sub> )	Solution	Initial gas pressure (bar)	Gas atmosphere composition
73BIC-H <sub>2</sub> (to be started)	Cladded UO <sub>2</sub>	PWR	73	BIC	30-35	Ar + 5% H <sub>2</sub> + 0.003% CO <sub>2</sub>
73YCWCa-H <sub>2</sub> (to be started)				YCWCa		

Based on previous experience [3], some radionuclides (U, Rb, Sr, Mo, Tc, Cs, I) have been selected to be analysed. Cumulative Fraction of Inventory in Aqueous Phase (CFIAP) results will be determined.

#### 4. Final remark and outlook

Start of the experiments was foreseen for the month of March 2020. However, due to the present situation with the JRC laboratories closed until further notice both experiments are postponed. Autoclaves are ready and tested, samples cut and solutions prepared. Once the situation becomes normal an optimised experimental set-up in combination with the remaining experiments from JRC will be provided.

#### Acknowledgement

*The research leading to these results has received funding from the European Commission Horizon 2020 Research and Training Programme of the European Atomic Energy Community (EURATOM) (H2020-NFRP-2016-2017-1) under grant agreement n° 755443 (DisCo project).*

*The authors especially acknowledge the fuel owners for the permission to use their fuel to perform the experiments and would like to acknowledge ENRESA for its interest in this work.*

#### References

- [1] Herm, M., González-Robles, E., Iglesias, L., Carbol, P., Serrano-Purroy, D., Barreiro, A., Roth, O., Casas, I. (2019). Deliverable D3.1: Spent fuel experiments: First dissolution results. DisCo project (Grant Agreement: 755443).
- [3] González-Robles, E., Serrano-Purroy, D., Sureda, R., Casas, I., de Pablo, J. (2015). Dissolution experiments of commercial PWR (52 MWd/kg<sub>U</sub>) and BWR (53 MWd/kg<sub>U</sub>) spent nuclear fuel cladded segments in bicarbonate water under oxidizing conditions. experimental determination of matrix and instant release fraction. J. Nucl. Mater., 465, 63-70.

# Aqueous leaching of ADOPT and standard UO<sub>2</sub> spent nuclear fuel under H<sub>2</sub> atmosphere

*Barreiro-Fidalgo, A.<sup>1</sup>, Roth, O.<sup>1</sup>, Puranen, A.<sup>1</sup>, Evins, L.Z.<sup>2</sup> and Spahiu, K.<sup>2</sup>*

<sup>1</sup> Studsvik Nuclear AB, Nyköping (SE)

<sup>2</sup> SKB, Stockholm (SE)

---

## 1. Introduction

Within the EURATOM collaborative project “Modern Spent Fuel Dissolution and Chemistry in Failed Container Conditions – DisCo”, Studsvik is contributing with two experiments on different fuel types.

Improving reactor performance and reliability, reducing fuel cycle cost and the consequences of fuel failure are constant challenges for the nuclear industry. For this reason, new types of fuel have been developed in recent years. One example is the ADOPT fuel (Advanced Doped Pellet Technology), developed by Westinghouse Electric, which consists of a UO<sub>2</sub>-based fuel containing additions of chromium and aluminium oxides. One of the main characteristics of this fuel is the enlarged grain size which results in lower Fission Gas Release (FGR) and increased density [1].

From the safety perspective of a deep geological repository for spent nuclear fuel (SNF), the new type of fuels must fulfil the acceptance criteria of low solubility under relevant repository conditions. Minor modifications on the UO<sub>2</sub> matrix resulting in property changes might affect the leaching behaviour of the fuel. The Instant Release Fraction (IRF) and matrix dissolution were investigated for both standard UO<sub>2</sub> and ADOPT in a previous study [2]. The results showed that the doping effect had little to no effect on the matrix dissolution, while some differences were observed in the release of some elements with low solubility in UO<sub>2</sub>. For this reason, it is important to gather further data on the dissolution behaviour of a new type of fuel with additives under reducing conditions in presence of hydrogen. In this study, the behaviour of the doped fuel (ADOPT) will be compared to the performance of standard UO<sub>2</sub> fuel under identical conditions.

The objective of this study is to gather data that will be used to support or refute the hypothesis that there is no significant difference in leaching behaviour between the two fuels. In addition, thermodynamic and kinetic models will be developed in WP5 using the experimental data.

## 2. Experimental method

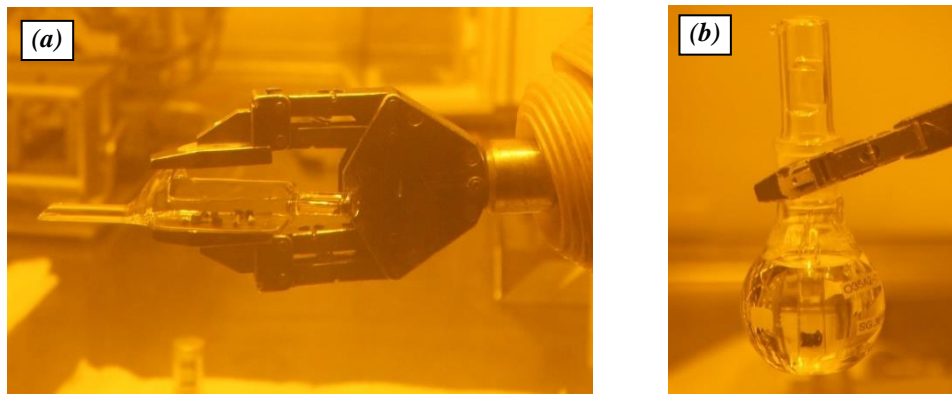
The experiments are being performed on fuel fragments without cladding. The selected fragments are the same samples leached in a previous EURATOM project, FIRST-Nuclides, which were used to establish the instant release fraction and the matrix dissolution behaviour under aerated conditions [2]. The fuels are listed in Table 1. The two fuels have very similar power histories since they have been irradiated in the same fuel assembly.



**Table 1:** Fuels selected for the experiments performed at Studsvik.

Sample name	Reactor type	Fuel type	FGR (%)	Calculated BU (rod average) (MWd/kgU)
O35A2	BWR	Std. UO <sub>2</sub>	2.4	57.1
O3C1	BWR	ADOPT (Al/Cr doped UO <sub>2</sub> )	1.4	59.1

The fuel fragments (2 g from each fuel type) were exposed to an initial leaching period (pre-wash) under aerated conditions in 200 mL 10:10 mM NaCl:NaHCO<sub>3</sub> solutions in the Hot Cell Laboratory at Studsvik. The main objective of this initial step is to attempt to wash away any pre-oxidized phases that were presumably formed during air storage in the hot cell (approx. 3 years) by exposing them to relatively high NaHCO<sub>3</sub> concentrations. Figure 1a and Figure 1b show the collected fuel fragments and a leaching flask with the fuel immersed in the leaching solution.

**Figure 1:** (a) One batch of fuel fragments and (b) leaching flask containing fuel samples.

The washing step was divided into a total of 5 contact periods as shown in Table 2. At the end of each contact period the glass baskets containing the fuel were transferred into a new flask containing fresh leaching solution.

**Table 2:** Contact periods for the washing step.

Contact period	Duration (days)	Cumulative duration (days)
1	1	1
2	5	6
3	8	14
4	20	54
5	71	105

Samples of the leaching solution were centrifuged for 1 h at 74,000 g at the end of each contact period to try to separate colloids from the solution.

Thereafter the samples were preserved in either 1% HNO<sub>3</sub> or 0.5% TMAH for analysis by Inductively Coupled Plasma Mass Spectrometry (ICP-MS) for masses 82-254 and <sup>129</sup>I respectively and gamma spectrometric analysis for <sup>137</sup>Cs determination. <sup>115</sup>In and <sup>209</sup>Bi are used as internal standards for the ICP-MS analysis.

After the initial leaching period, both fuels were introduced in stainless-steel autoclaves with an inner quartz vessel that contains the leaching solution and PEEK internals. The sampling system consists of an internal PEEK line with a quartz filter (P4 10-16 μm pore size). The external line is made of stainless steel with two valves in series. Figure 2a and Figure 2b show an example of the internal and external parts of the autoclaves.

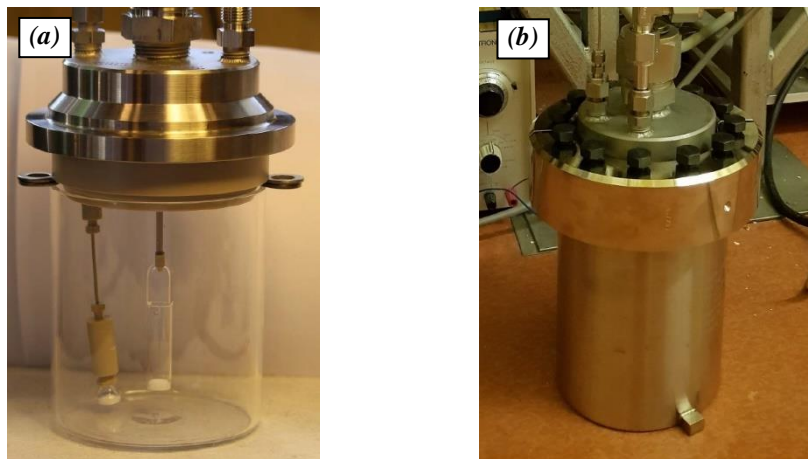


**Figure 2:** (a) Autoclave internals and (b) exterior of the autoclave.

Prior to assembling the autoclaves, the free internal volume was determined for gas phase calculations obtaining a value of 950 cm<sup>3</sup>. Leak tests were also performed by pressurizing the autoclaves with 50 bar of He and monitoring the pressure through 1 month. The pressure drop rate found was ~ 0.16 bar/month.

The autoclave vessels were filled with 680 mL of simplified groundwater, consisting of 10 mM NaCl and 2 mM NaHCO<sub>3</sub>. Prior to loading, the autoclaves were sparged during 30 min with argon to minimize the air content. After loading the quartz baskets containing the fuel, the autoclaves were closed and sparged for another hour before the argon flow was stopped. Thereafter, the autoclaves were pressurized up to the target pressure of 55 bar of H<sub>2</sub>. No replenishment of gas due to pressure loss during the experiment is planned. This is done to avoid air intrusion in the system during the re-pressurization procedure and to facilitate the gas phase composition calculations.

The concentration of fission products and actinides in the autoclave solution will be followed by sampling 9 times over two years (liquid and gas sampling). The sample solutions are analysed in the same way as the solutions from the washing experiments. In addition, the composition of the gas phase is analysed by Gas-MS to detect air intrusion or release of fission gas from the fuel samples. The status of the planned sampling points is presented in Table 3.

**Table 3:** Autoclave sampling points. Samples already taken and analysed are marked with an “✓”.

Sampling point	Leaching time (days)	Liquid sample	Gas sample
1	0.1	✓	x
2	1	✓	✓
3	7	✓	✓
4	28	✓	✓
5	91	✓	✓
6	203	✓	✓
7	432	✓	✓
8	640	March 2020	March 2020
9	730	June 2020	June 2020

Each sample point is taken in triplicate. The first sample (A) is used to rinse the sampling system and it is not analysed. Samples B and C (8 mL each) are centrifuged at 74,000 g during one hour and thereafter the supernatant is removed and preserved as described above for the samples taking during the pre-wash.

### 3. Preliminary results and discussion

It must be noted that the results presented here are preliminary and may therefore be subjected to changes or adjustments in the future.

#### 3.1 Washing step

The uranium release rate is plotted against cumulative time in Figure 3. It can clearly be seen how the uranium release rate decreases markedly with washing time. After ~ 3 months both fuels exhibit considerably low and identical uranium release rates.

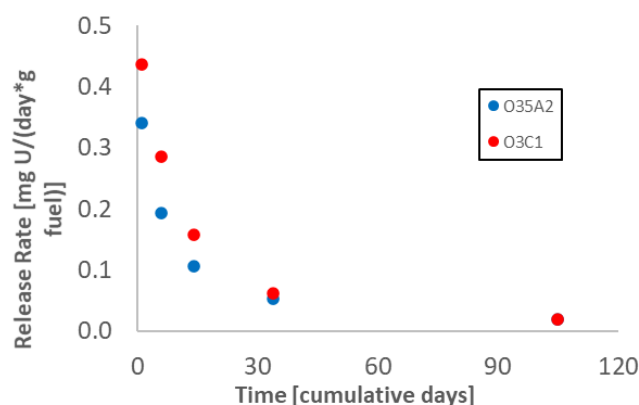


**Figure 3:** Uranium release rate as a function of time during the pre-wash. O35A2 corresponds to the standard UO<sub>2</sub> fuel and O3C1 to ADOPT.

### 3.2 Leaching under $H_2$ atmosphere

The initial pH and carbonate concentration were measured obtaining 8.2 and 2.0 mM respectively.

#### 3.2.1 Gas phase analysis

Table 4 and Table 5 summarize the evolution of the composition of the gas phase in the two autoclaves.

**Table 4:** Pressure and gas composition autoclave O35A2 (Std.  $UO_2$ ).

O35A2	Gas	G1	G2	G3	G4	G5	G6
(Std. $UO_2$ )	Kr (%)	< 0.001	< 0.001	< 0.001	< 0.001	< 0.001	0.001
	Xe (%)	< 0.001	< 0.001	0.001	0.001	0.002	0.002
	$H_2$ (%)	98.071	97.605	97.040	97.031	96.995	96.971
	He (%)	0.113	0.522	1.015	1.029	1.0584	1.065
	$N_2$ (%)	0.010	0.011	0.016	0.023	0.033	0.042
	$O_2$ (%)	0.006	0.006	0.006	0.007	0.007	0.007
	Ar (%)	1.800	1.856	1.920	1.909	1.904	1.912
<b>Autoclave Pressure</b>	(bar)	50.23	43.54	35.19	31.28	27.57	25.12
<b>Duration</b>	(days)	1	6	34	91	211	432

**Table 5:** Pressure and gas composition autoclave O3C1 (ADOPT).

O3C1	Gas	G1	G2	G3	G4	G5	G6
(ADOPT)	Kr (%)	< 0.001	< 0.001	< 0.001	< 0.001	< 0.001	0.001
	Xe (%)	< 0.001	< 0.001	0.001	0.001	0.001	0.002
	$H_2$ (%)	98.901	98.228	98.695	97.562	97.435	97.319
	He (%)	0.056	0.274	0.724	0.847	0.934	0.977
	$N_2$ (%)	0.010	0.011	0.014	0.017	0.023	0.025
	$O_2$ (%)	0.006	0.006	0.006	0.006	0.008	0.008
	Ar (%)	1.027	1.481	1.560	1.567	1.598	1.668
<b>Autoclave Pressure</b>	(bar)	49.02	43.77	37.72	34.41	31.98	30.07
<b>Duration</b>	(days)	1	6	34	91	211	432

The Kr and Xe results were close or below the limit of quantification, making it difficult to obtain reliable values. However, from the first leaching month, the isotopic composition of Xe in the gas phase matched fairly well the Xe inventory in the fuel. For Kr, the levels detected were clearly below

quantification limit. This implies that fission gas is released to some extent from both samples. In addition, no significant air intrusion or leakage in the system is observed as indicated by the  $N_2$  levels.

Preliminary results of a number of radionuclides of interest from the aqueous phase of both autoclaves are summarized in Figure 4.

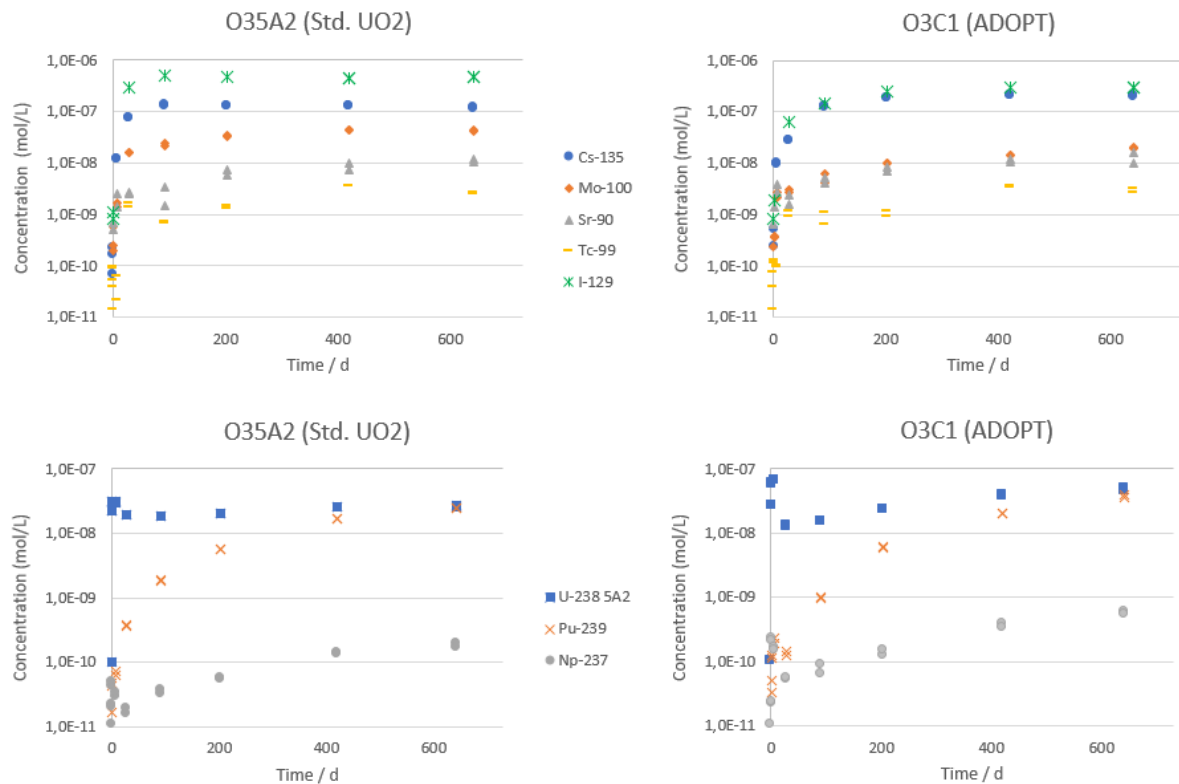


**Figure 4:** Aqueous concentrations of  $^{238}\text{U}$ ,  $^{239}\text{Pu}$  and  $^{237}\text{Np}$ ,  $^{129}\text{I}$ ,  $^{135}\text{Cs}$ ,  $^{100}\text{Mo}$ ,  $^{90}\text{Sr}$  and  $^{99}\text{Tc}$ . The plots to the left belong to sample O35A2 (standard  $\text{UO}_2$ ) and to the right to sample O3C1 (ADOPT).

As can be seen in Figure 4, the initial rise of  $^{238}\text{U}$  concentration in both autoclaves (presumably due to dissolution of oxidized fuel layers as a result of air exposure during the transfer from the pre-wash to the autoclaves) is followed by a slow decrease attributable to reduction by  $\text{H}_2$ . Interestingly, this effect seems to vanish with time. For both autoclaves, the  $^{238}\text{U}$  concentration increases at a slow rate reaching a concentration of  $3\text{-}4 \cdot 10^{-8}$  M after 421 days, an order of magnitude higher than the solubility of amorphous  $\text{UO}_2$  ( $2\text{-}5 \cdot 10^{-9}$  M) [3]. The  $^{239}\text{Pu}$  concentrations are also surprisingly high reaching a concentration of  $2 \cdot 10^{-8}$  M, while relative low concentrations for  $^{237}\text{Np}$  are observed in both cases ( $2 \cdot 10^{-10}$  M), although one order or two orders of magnitude higher than values reported by a previous study on high burnup standard  $\text{UO}_2$  fuel under hydrogen conditions [4].

Highly soluble nuclides such as  $^{129}\text{I}$  and  $^{137}\text{Cs}$  increased steadily during the first month reaching a relative constant level for both the standard  $\text{UO}_2$  and ADOPT specimens. The major release of other elements of interest such as  $^{100}\text{Mo}$ ,  $^{90}\text{Sr}$  and  $^{99}\text{Tc}$  occurs within a few days, yet their concentrations continue to slowly increase with time in both autoclaves.

The largest difference between both fuels can be observed in the leaching behaviour of  $^{129}\text{I}$ . The FIAP of an element (Fraction of Inventory in Aqueous Phase) is calculated by dividing the mass of the element

present in the aqueous phase by the mass of the element in the spent nuclear fuel at the end of irradiation in the nuclear reactor. After 1 year and 2 months, the FIAP for  $^{129}\text{I}$  for the standard  $\text{UO}_2$  fuel is 7.0% while for ADOPT it is 4.6%. This difference could be explained given the larger grain size in ADOPT fuel, decreasing fission gas diffusion through the fuel.

The fraction of Xe inventory in the gas phase after 421 days was also calculated for both fuels, resulting in 6.5% for the standard  $\text{UO}_2$  fuel and 8.0% for ADOPT. Contrary to what it could be expected, the release of Xe became larger for ADOPT than for the standard  $\text{UO}_2$  fuel in the last sampling point. This trend will be further investigated by taking two additional samples from the gas phase.

At this point in the experiment, radionuclide concentrations remain fairly low compared to dissolution under oxidizing conditions but considerably higher than previous leaching studies under hydrogen atmosphere [4-7]. In addition, the overall doping effect on the leaching behaviour seem to be small.

## Future work

As previously mentioned, the preliminary results presented so far support the hypothesis that there is no major difference in leaching behaviour between the two fuels. To further support this hypothesis, 2 additional sampling points (both liquid and gas) are planned in the next three months as summarized in Table 3.

## Acknowledgement

*The research leading to these results has received funding from the European Commission Horizon 2020 Research and Training Programme of the European Atomic Energy Community (EURATOM) (H2020-NFRP-2016-2017-1) under grant agreement n° 755443 (DisCo project).*

## References

- [1] Arborelius, J., Backman, K., Hallstadius, L., Limbaeck, M., Nilsson, J., Rebensdorff, B., Zhou, G., Kitano, K., Loeffstroem, R., Roennberg, G. (2006). Advanced doped  $\text{UO}_2$  pellets in LWR applications. *J. Nucl. Sci. Technol.*, 43, 967-976.
- [2] Kienzler, B., Metz, V., Duro, L., Valls, A. (2014). Final (3<sup>rd</sup>) Annual Workshop Proceedings of the 7<sup>th</sup> EC FP CP FIRST-Nuclides project.
- [3] Guillaumont, R., Fanghänel, Th., Neck, V., Fuger, J., Palmer, D.A., Grenthe, I., Rand, M.H. (2003). Update on the chemical thermodynamics of U, Np, Pu, Am and Tc. OECD NEA, Elsevier
- [4] Puranen, A., Roth, O., Evins, L.Z., Spahiu, K. (2018). Aqueous leaching of high burnup  $\text{UO}_2$  fuel under hydrogen conditions. *MRS Advances*, 3(19), 1013-1018.
- [5] Fors, P., Carbol, P., Van Winkel, S., Spahiu, K. (2009). Corrosion of high burn-up structured  $\text{UO}_2$  fuel in presence of dissolved  $\text{H}_2$ . *J. Nucl. Mater.*, 394, 1-8.
- [6] Loida, A., Metz, V., Kienzler, B., Geckeis, H. (2005). Radionuclide release from high burnup spent fuel during corrosion in salt brine in the presence of hydrogen overpressure. *J. Nucl. Mater.*, 346, 24-31.
- [7] Spahiu, K., Cui, D., Lundström, M. (2004). The reduction of U(VI) by near field hydrogen in the presence of  $\text{UO}_2(\text{s})$ . *Radiochim. Acta*, 92, 625-629.

# Chromium doped UO<sub>2</sub>-based model systems: Synthesis and characterization of model materials for the study of the matrix corrosion of spent modern nuclear fuels

*Kegler, P., Klinkenberg, M., Bukaemskiy, A., Brandt, F., Deissmann, G. and Bosbach, D.*

Forschungszentrum Jülich GmbH, Institute of Energy and Climate Research Nuclear Waste Management and Reactor Safety (IEK-6), Jülich, (DE)

---

## Abstract

Up to now it is not known if the behaviour of modern doped LWR fuels under post-closure conditions expected in a deep geological repository is similar to conventional spent nuclear fuel. Studies on tailor-made UO<sub>2</sub> model materials can provide additional insights on the influence of doping on the dissolution behaviour. In this study we present recent improvements of the wet chemical synthesis route developed for the synthesis of pure UO<sub>2</sub> reference as well as Cr-doped UO<sub>2</sub> model materials. The systematic investigation of process parameters like oxygen partial pressure and Cr-doping level was extended and compared to the works described in the second annual meeting proceedings. It was shown, that both the increase of the oxygen partial pressure as well as the increase of the doping level results in an increase of the grain size. Dissolution experiments are presented, using H<sub>2</sub>O<sub>2</sub> to mimic radiolytic oxidation processes evoked from the alpha-irradiation of water in long-term disposal scenarios for spent nuclear fuel. Pure UO<sub>2</sub>, Nd-doped and materials which were produced with varying Cr-doping methods and doping-levels are used in these experiments. These experiments allowed for the determination of further initial dissolution rates for pure UO<sub>2</sub> reference, Nd-doped as well as for Cr-doped pellets. Three different initial dissolution rates could be determined for the three different groups: pure UO<sub>2</sub>:  $(1.3 \pm 0.1) \cdot 10^{-6}$  mol/m<sup>2</sup>·s; Cr-doped UO<sub>2</sub>:  $(0.65 \pm 0.2) \cdot 10^{-6}$  mol/m<sup>2</sup>·s; Nd-doped UO<sub>2</sub>:  $(1.63 \pm 0.7) \cdot 10^{-7}$  mol/m<sup>2</sup>·s

## 1. Introduction

During the last decades, a variety of new types of light-water reactor (LWR) fuels including Cr-, Al-, and Si-doped fuels have been developed to improve fuel performance under radiation [1-3]. While the improved in-reactor performance of these fuels has already been shown, uncertainties remain, whether their corrosion/dissolution behaviour in a deep geological disposal facility (GDF) will be similar to conventional spent LWR-fuels. However, experiments with spent nuclear fuel (SNF) cannot unravel all concurring dissolution mechanisms in aqueous media, due to the chemical and structural complexity of SNF. In addition, “young” SNF is associated with a high beta- and gamma radiation field, whereas at the time SNF in a GDF will come into contact with water, the radiation field and thus water radiolysis will be dominated by alpha radiation. Thus within the EU-DisCo project ([www.disco-h2020.eu](http://www.disco-h2020.eu)), experiments on doped SNF are complemented with dedicated dissolution studies using systematically produced and carefully characterised UO<sub>2</sub>-based model materials to understand the effects of the addition of Cr- or Al-oxide into the fuel matrix on SNF dissolution behaviour under conditions expected in a GDF post-closure. These model materials comprise (i) UO<sub>2</sub> reference materials, and

(ii) Cr-/Al-doped  $\text{UO}_2$ , both, with and without alpha-emitting nuclides such as  $^{238}\text{Pu}$ . The alpha doped materials should address the effects of alpha-radiolysis on the oxidative dissolution of aged SNF after recession of the beta/gamma radiation field in the long-term. Single-effect studies on the dissolution behaviour of the model materials will provide complementary insights and supporting process understanding regarding the performance of modern doped fuels in the repository environment, which cannot be directly obtained from dissolution studies on SNF.

In this contribution, we provide an overview on:

- (i) The optimisation of the synthesis route for the production of the  $\text{UO}_2$  reference material and Cr-doped  $\text{UO}_2$  materials. The focus is on the effect of Cr-doping and oxygen partial pressure during the sintering of the pellets on grain growth and distribution of Cr in the  $\text{UO}_2$  matrix.
- (ii) New results from accelerated dissolution experiments using pure, Cr-doped and Nd-doped  $\text{UO}_2$  pellets. In these experiments,  $\text{H}_2\text{O}_2$  was used to mimic the radiolytic oxidation due to alpha-radiolysis that is relevant for SNF dissolution in the repository environment in the long-term. To provide insights into the effects of the material's microstructure on the dissolution behaviour (e.g. regarding the larger grain size in doped fuels and contributions from grain boundaries) as well as for comparability to SNF experiments, the model materials were produced in form of sintered pellets.

## 2. Development and optimisation of synthesis route

Within the framework of WP2 of the DisCo-project, a wet chemical synthesis route for the production of Cr-doped  $\text{UO}_2$  pellets and undoped  $\text{UO}_2$  reference pellets was developed and optimised. In addition, a careful structural characterisation of the produced pellets was performed. The following challenges had to be met during the optimisation of the synthesis route:

- (i) The procedures had to be robust and easily reproducible in different laboratories (i.e. in Jülich and in Mol) with different equipment.
- (ii) In order to obtain a homogeneous distribution of Cr and, in particular, of  $^{238}\text{Pu}$  present only in trace amounts (< 50 ppm) in the pellets, a wet chemical synthesis was favoured.
- (iii) Milling/grinding steps should be avoided to minimise dust generation and carry-over of Pu.
- (iv) No lubricants such as Zn-stearate or sintering aids should be used during pelletising and sintering.
- (v) Moreover, all process steps, tested and optimised in Jülich without alpha-doping, had to be designed in a way to be accomplished also in a glove-box line at SCK·CEN in Mol, to produce  $^{238}\text{Pu}$ -doped pellets with similar characteristics.

A two-stage synthesis route was developed and an extensive study was performed to identify the influence of the following parameters on the final density and grain size of the pellets produced (see [4-5]):

- Temperature of denitration step.
- Temperature of reduction step.



- Pressure during production of the green body of the pellet.
- Way of Cr-doping (co-precipitation or wet-coating method).

Target densities of the Cr-doped pellets of above 95% relative density (relative density =  $100 \times \text{experimental density} / \text{theoretical density}$ ) were achieved with a first calcination / denitration step at 800°C and a second reductive calcination step at 600°C (reduction from  $\text{U}_3\text{O}_8$  to  $\text{UO}_2$ ), respectively. We worked out that the optimal density of the sintered pellets can be achieved using a pressure of 650 MPa for the pelletisation step. Higher pressures lead to the formation of cracks due to elastic response of the green body. After pressing of the green body, the pellets were sintered for 10 h at 1700°C. As shown in Figure 1 the doping method has an effect on the grain size. The co-precipitation of Cr (here 1000 weight ppm Cr) only has a minor influence on grain size compared to pure  $\text{UO}_2$  pellets and it is surmised that most of the Cr is dissolved within the  $\text{UO}_2$  grains. In contrast, Cr-doping using the wet-coating method leads to an increase in the materials' density and grain size.

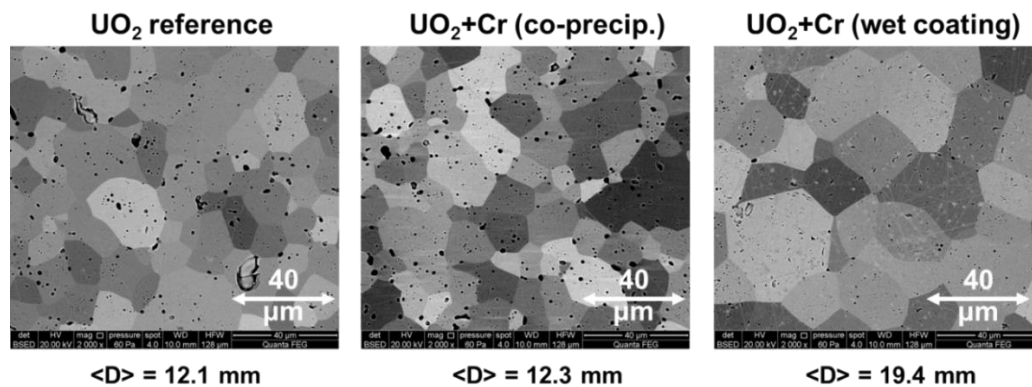


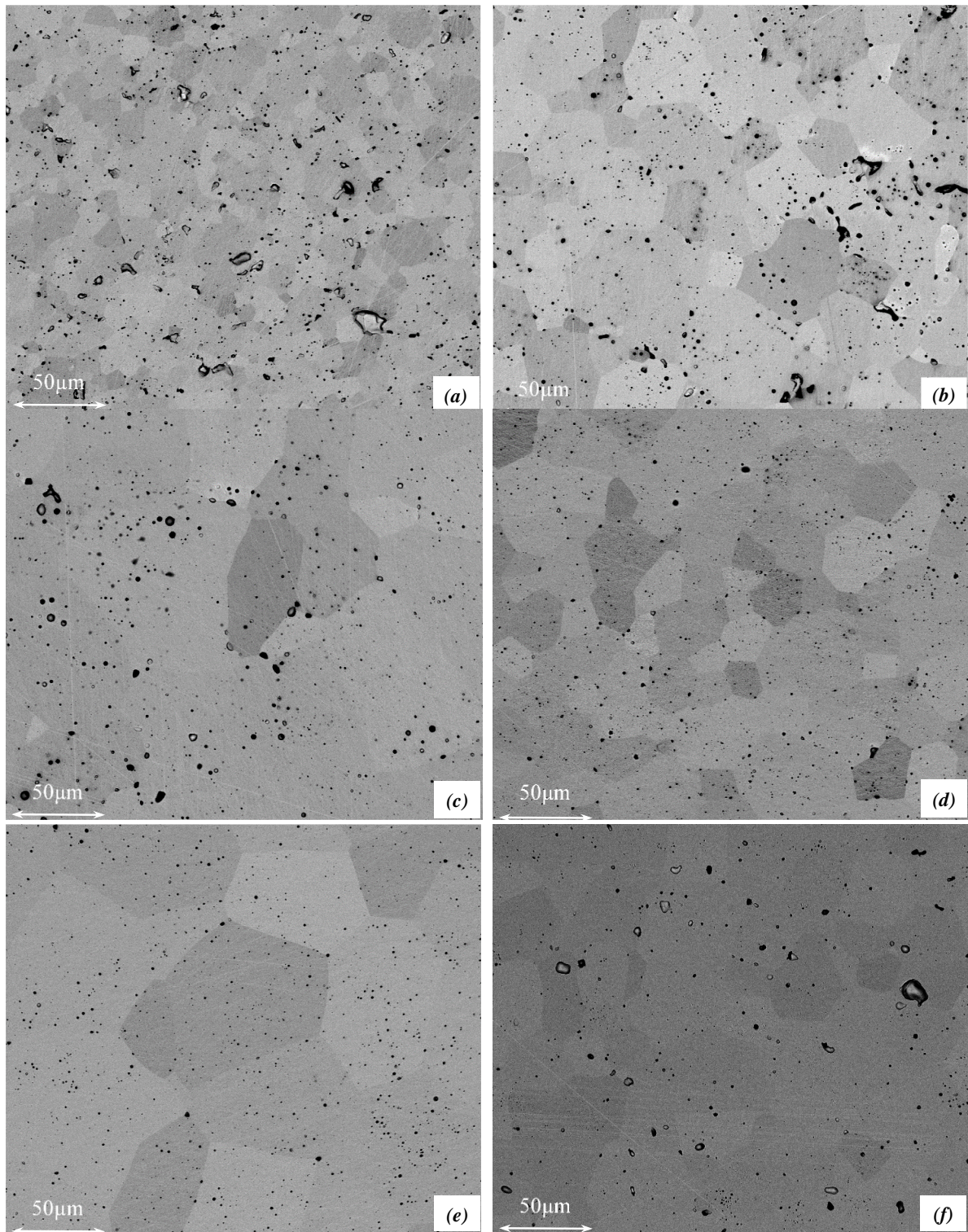
**Figure 1:** Microstructure of pure  $\text{UO}_2$  and Cr-doped pellets depending on the doping method. The doping level was 1000 weight ppm Cr, the oxygen potential during sintering was  $-510 \text{ kJ/mol O}_2$ .

Previous studies have shown that the grain growth of  $\text{UO}_2$  in sintered pellets [6] and Cr incorporation into the lattice of  $\text{UO}_2$  [7] is strongly dependent on the Cr-doping level and the oxygen partial pressure (in the following expressed as oxygen potential,  $\Delta G = RT \ln P_{\text{O}_2} / \text{kJ} \cdot \text{mol}^{-1} \text{O}_2$ , with  $P_{\text{O}_2} = p_{\text{O}_2} / p^\circ$ ) during the sinter process. Therefore, an extensive study on the influence of  $f_{\text{O}_2}$  and Cr-doping level on the microstructure of pure and Cr-doped  $\text{UO}_2$  pellets was performed.

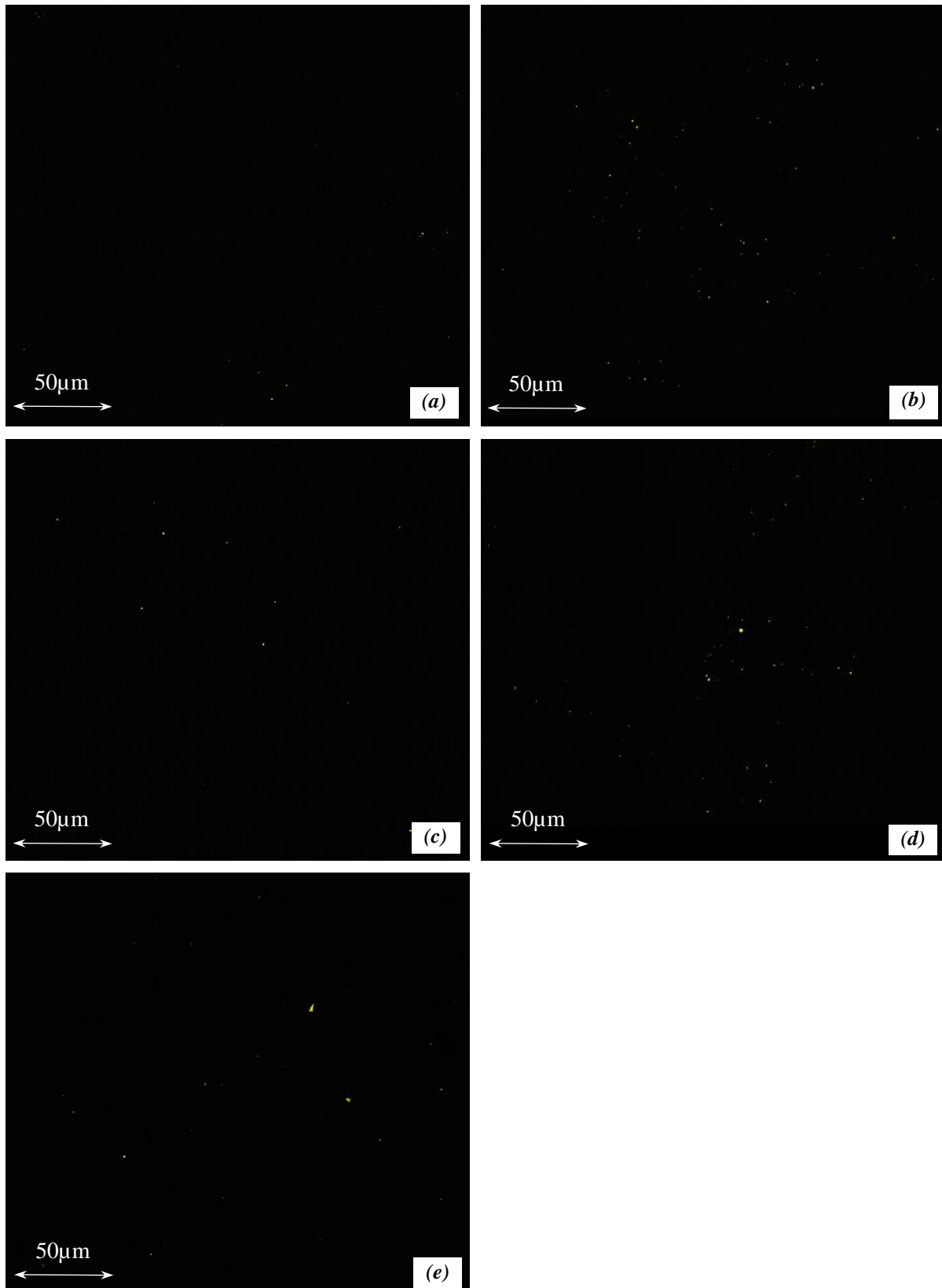
The structural difference between pure  $\text{UO}_2$  pellets sintered at oxygen potential of  $-510 \text{ kJ/mol O}_2$  (Figure 1, left) and  $-420 \text{ kJ/mol O}_2$  (Figure 2a) seems to be insignificant. But further investigations show that Cr-doping level (1000 and 2500 weight ppm) together with the change of the oxygen potential during the sintering step have a strong impact on the size of the  $\text{UO}_2$  grains in the pellets, but only minor effects on the final density of the pellets. Both, the increase of the doping level from 1000 weight ppm to 2500 weight ppm and the increase of the oxygen potential from  $-510 \text{ kJ/mol O}_2$  to  $-420 \text{ kJ/mol O}_2$  during the sintering of the pellets lead to an increase of the grain size.

Figure 2 shows the micro structure and Figure 3 the Cr-distribution of  $\text{UO}_2$  pellets doped with different Cr-levels (1000 and 2500 weight ppm) and using different doping methods (co-precipitation and wet coating method) sintered at an oxygen potential of  $-420 \text{ kJ/mol O}_2$ .

Compared to the micro structure of a pellet doped with 1000 weight ppm Cr via the co-precipitation method and sintered at an oxygen potential of  $-510 \text{ kJ/mol O}_2$  (Figure 1, middle), the increase of the oxygen potential to  $-420 \text{ kJ/mol O}_2$  lead to an considerable increase of the average grain size from  $12.3 \text{ }\mu\text{m}$  (Figure 1, middle) to  $20 \text{ }\mu\text{m}$  (Figure 2b). The EDX-mapping shows the appearance of only some small isolated Cr-bearing grains (very likely  $\text{Cr}_2\text{O}_3$ ) (Figure 3a). An increase of the Cr-doping level from 1000 weight ppm to 2500 weight ppm via co-precipitation method results in a significant increase of the average grain size to  $56 \text{ }\mu\text{m}$  (Figure 2c). At the same time the number of small Cr-bearing particles in the matrix of the pellets increased at higher doping level (Figure 3b). This is to be expected since the solubility limit of Cr in  $\text{UO}_2$  is around 1500 weight ppm [8]. An increase of the oxygen potential and the doping level had the same effect for samples doped by the wet coating method. Compared to samples doped by wet coating and sinter conditions of  $-510 \text{ kJ/mol O}_2$  (see Figure 1, left) an increase of the oxygen potential to  $-420 \text{ kJ/mol O}_2$  results in the change of the average grain size from  $19.4 \text{ }\mu\text{m}$  to  $24 \text{ }\mu\text{m}$  (Figure 2d). Compared to the samples doped with 1000 weight ppm Cr with the co-precipitation method (Figure 3a) a higher number of Cr-bearing grains occur (Figure 3c). Figure 2e and Figure 3d show the effect of the increase of the Cr-doping level to 2500 weight ppm. The average grain size in these pellets is  $69 \text{ }\mu\text{m}$  (Figure 2e). In addition, a larger number and even bigger Cr-bearing grains are clearly visible (Figure 3d). Figure 2f shows the microstructure and Cr-grain distribution (Figure 3e) of a commercially available Cr doped  $\text{UO}_2$  pellet (AREVA). With an average grain size of  $37 \text{ }\mu\text{m}$  and the number and size of Cr-bearing grains, the microstructure is similar to the pellets produced in the frame of this work doped with 2500 weight ppm Cr using the wet-coating method and sintered at an oxygen potential of  $-420 \text{ kJ/mol O}_2$ . The structural similarities are very promising as it is very likely that the production routes from the commercial Cr-doped pellets and the pellets produced in this study are very different.



**Figure 2:** Backscattered electron (BSE) images of (a) pure  $\text{UO}_2$  sample SL-DC 35-2. Average grainsize is  $12\ \mu\text{m}$ ; (b) sample SL-DC 33-1 doped by co-precipitation with 1000 weight ppm Cr. Average grainsize is  $20\ \mu\text{m}$ ; (c) sample SL-DC 34-1 doped by co-precipitation with 2500 weight ppm Cr. Average grainsize is  $56\ \mu\text{m}$ ; (d) sample SL-DC 36-1 doped by wet coating method with 1000 weight ppm Cr. Average grainsize is  $24\ \mu\text{m}$ ; (e) sample SL-DC 37-1 doped by wet coating method with 2500 weight ppm Cr. Average grainsize is  $69\ \mu\text{m}$ . All pellets from (a) to (e) are sintered at the following conditions:  $1700^\circ\text{C}$  for 10 h under an oxygen potential of  $-420\ \text{kJ/mol O}_2$ ; (f) industrial Cr-doped  $\text{UO}_2$  sample containing 1500 weight ppm Cr. Sintering conditions are unknown. Average grainsize is  $37\ \mu\text{m}$ .



**Figure 3:** EDX-mapping of Cr distribution in (a) sample SL-DC 33-1 doped by co-precipitation with 1000 weight ppm; (b) sample SL-DC 34-1 doped by co-precipitation with 2500 weight ppm Cr; (c) sample SL-DC 36-1 doped by wet coating method with 1000 weight ppm Cr; (d) sample SL-DC 37-1 doped by wet coating method with 2500 weight ppm Cr; (e) industrial Cr-doped sample.



### 3. Accelerated dissolution experiments

New accelerated dissolution experiments with  $\text{UO}_2$  model materials with and without Cr doping synthesised in the framework of WP2 were carried out in previously degassed bicarbonate solutions ( $\text{NaHCO}_3$ , 10 mmol/L), using hydrogen peroxide ( $\text{H}_2\text{O}_2$ , 2.25 mmol/L) to mimic the oxidative radiolytic dissolution of  $\text{UO}_2$ . To achieve anoxic conditions the solutions were flushed with argon during the complete experimental run time. The experimental setup, developed at JUELICH for these dissolution experiments and shown in Figure 4, aimed in particular at:

- maintaining the pellets completely covered with test solution throughout the whole dissolution experiments,
- allowing easy sampling of test solution and permanent flushing of the vessels with argon,
- providing constant conditions regarding  $\text{H}_2\text{O}_2$  degradation during the experiments, and
- controlling the experimental temperature.

The setup allowed for the accomplishment of 11 dissolution experiments in parallel. The sample vessels were placed in a massive aluminium block equipped with a water conduit connected to a thermostat for temperature control. Plasticine gaskets were used to close the contact between the vessels and aluminium block and to ensure the light tightness of the vessels. In all experimental runs performed to date, 8 vessels were used for dissolution tests (Figure 4a, blue gaskets) with  $\text{UO}_2$  based pellets, while 3 vessels were used as blanks to monitor the bulk degradation of  $\text{H}_2\text{O}_2$  (Figure 4a, red gaskets). For all dissolution experiments pellets with one side polished to mirror finish and the other side only slightly grinded are used.

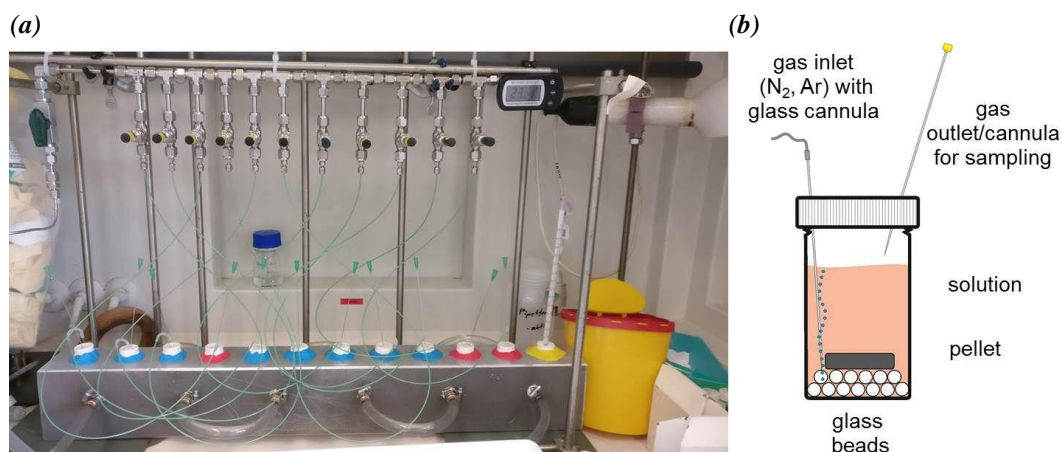


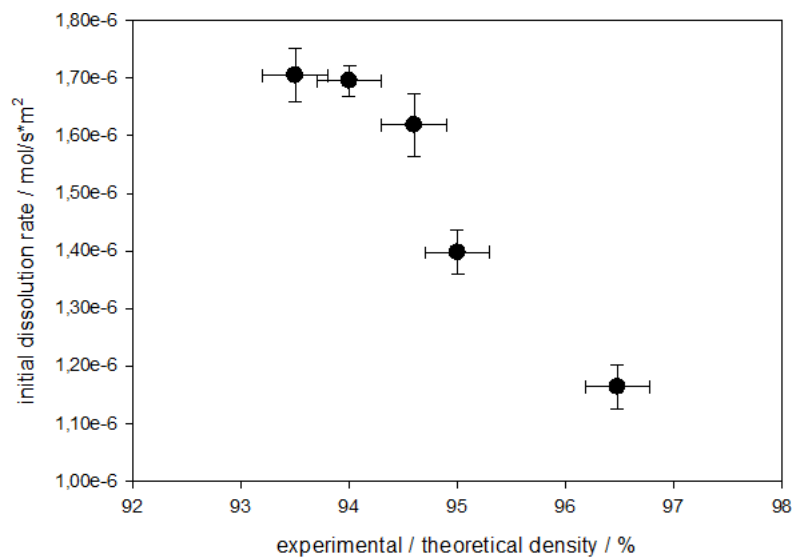
**Figure 4:** (a) Experimental setup of the dissolution experiments. (b) Schematic drawing of the experimental vessels for the accelerated dissolution experiments.

The driving force for the  $\text{UO}_2$  dissolution in this kind of accelerated dissolution experiment is the oxidative potential of  $\text{H}_2\text{O}_2$  which is proportional to its concentration in solution. The  $\text{NaHCO}_3$  in the solution represents the bicarbonate contained in groundwater. It additionally serves the purpose to prevent the precipitation of U(VI) phases and therefore to ensure a reliable measurement of the uranium concentration in the solution. Bicarbonate does not intervene directly in the oxidation process, but - with oxidative dissolution - complexes the U(VI) and thus influences the kinetics / driving force, so that the

dissolution rate increases with the bicarbonate content [9]. As stated before, this plateau is not due to the limit of U(VI) solubility, but due to the complete consumption of  $\text{H}_2\text{O}_2$  in the solution.

In the last reporting period [2], a surface passivation effect was described, which leads to a decreased dissolution of uranium from one run to the next in experiments where the same pellets were used several times [10]. Due to this effect, only results from dissolution experiments using pristine pellets are presented in this report.

Figure 5 shows the initial dissolution rates of pure  $\text{UO}_2$  pellets, normalised to their geometrical surface area, in dependence of their relative density. The (initial) dissolution rates of the pellets were determined from the concentrations of dissolved U(VI) obtained within the first 24 hours of the experiments. A clear dependence of the initial dissolution rates on the density of the pellets is visible with higher initial dissolution rates at lower densities. This is obvious since the initial dissolution rates are normalised to the geometrical surface area and not to the real available reactive surface area of the pellets. As lower density means higher porosity, the less dense pellets offer more surface area for the dissolution of uranium.



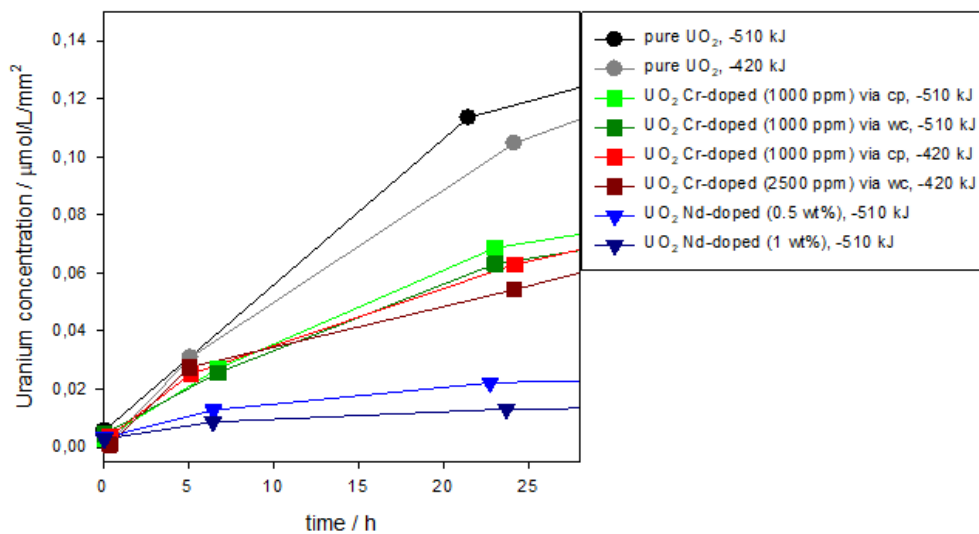
**Figure 5:** Initial dissolution rates of pure  $\text{UO}_2$  pellets, normalised to the geometrical surface area in dependence of relative density ( $100 \times$  experimental / theoretical density).

Figure 6 shows the uranium concentration in solution normalised to the geometrical surface area during the first 24 hours of dissolution experiments using pellets with different composition. Circles represent experiments with pure  $\text{UO}_2$ , squares experiments with Cr-doped samples and triangles experiments with Nd-doped pellets. It has to be noted that the Nd-doped pellets were not produced within the frame of the DisCo-project but within the context of another project concerning the use of  $\text{UO}_2$ -based model materials for addressing specific aspects of SNF corrosion.

The results shown in Figure 6 can be arranged in three groups: i) pure  $\text{UO}_2$  pellets with the highest dissolution rate, independent of the oxygen potential during sintering (and therefore the grain size), ii) Cr-doped  $\text{UO}_2$  pellets, independent of doping method, doping level, and oxygen potential during sintering (grain size), and iii) Nd-doped  $\text{UO}_2$  pellets with the lowest dissolution rate. The following initial dissolution rates can be calculated for the different groups:

- pure UO<sub>2</sub>:  $(1.3 \pm 0.1) \cdot 10^{-6}$  mol/m<sup>2</sup>·s
- Cr-doped UO<sub>2</sub>:  $(0.65 \pm 0.2) \cdot 10^{-6}$  mol/m<sup>2</sup>·s
- Nd-doped UO<sub>2</sub>:  $(1.63 \pm 0.7) \cdot 10^{-7}$  mol/m<sup>2</sup>·s

The difference between pure UO<sub>2</sub> and Cr-doped UO<sub>2</sub> pellets can partly be explained by the slightly lower density of pure UO<sub>2</sub> pellets compared to Cr-doped UO<sub>2</sub> pellets. A very strong influence of Nd on the dissolution of the pellet in this type of experiments is clearly visible. Although the density of the Nd-doped UO<sub>2</sub> pellets is in the same range of the Cr-doped pellets (96-98% relative density), the initial dissolution rate is more than half an order of magnitude lower than that for Cr-doped pellets.



**Figure 6:** Concentration of uranium in solution normalised to geometrical surface area of pure UO<sub>2</sub> pellets (circles), Cr-doped UO<sub>2</sub> pellets (squares), and Nd-doped UO<sub>2</sub> pellets (triangles, not in the scope of the DisCo project). cp = coprecipitation; wc = wet coating; -510 kJ= sinter atmosphere was Ar / 4% H<sub>2</sub> with an oxygen potential ( $\Delta G^\circ = -RT \ln p_{O_2}$ ) of -510 kJ/mol O<sub>2</sub>; -420 kJ = sinter atmosphere was Ar / 4% H<sub>2</sub> + Ar / 1% O<sub>2</sub> atmosphere with an oxygen potential of -420 kJ/mol O<sub>2</sub>.

## Outlook

Further experiments have to be carried out to evaluate the systematic uncertainties of the dissolution experiments (up to now only analytical errors are used). As mentioned in the roadmap of the DisCo project, further dissolution experiments using a young cementitious water (YCWCa) with a pH of ~ 13.5 will be performed. These dissolution experiments require a redesign of the experimental setup as solutions with high pH would etch the surface of glass, thus PTFE vessels will be tested as reactor vessels. As Ca rich YCW can react with CO<sub>2</sub> from the surrounding air, it has to be tested, if it is necessary to use an additional Ar flushing to prevent the formation of CaCO<sub>3</sub>, due to the reaction with CO<sub>2</sub> from air which would result in a decrease of the solution pH. A transfer of the complete experimental setup into an inert gas glovebox might be an alternative procedure.

## Acknowledgement

*The research leading to these results has received funding from the European Commission Horizon 2020 Research and Training Programme of the European Atomic Energy Community (EURATOM) (H2020-NFRP-2016-2017-1) under grant agreement n° 755443 (DisCo project).*

## References

- [1] Commissariat à l'Énergie Atomique (CEA) (2009). Nuclear fuels. A Nuclear Energy Division Monograph. Gif-sur-Yvette.
- [2] Arborelius, J., Backman, K., Hallstadius, L., Limbäck, M., Nilsson, J., Rebensdorff, B., Zhou, G., Kitano, K., Löfström, R., Rönnerberg, G. (2006). Advanced doped UO<sub>2</sub> pellets in LWR applications. *J. Nucl. Sci. Technol.*, 43, 967-976.
- [3] Massih, A.R. (2014). Effects of additives on uranium dioxide fuel behavior. SSM Report, 2014:21, 62 pp.
- [4] Evins, L.Z., Valls, A., Duro, L. (2018). Deliverable D1.10: 1<sup>st</sup> Annual Proceedings. DisCo project (Grant Agreement: 755443).
- [5] Evins, L.Z., Valls, A., Duro, L. (2019). Deliverable D1.15: 2<sup>nd</sup> Annual Proceedings. DisCo project (Grant Agreement: 755443).
- [6] Bourgeois, L., Dehaut, P., Lemaignan, C., Hammou, A. (2001). Factors governing microstructure development of Cr<sub>2</sub>O<sub>3</sub>-doped UO<sub>2</sub> during sintering. *J. Nucl. Mater.*, 297, 313-326.
- [7] Riglet-Martial, C., Martin, P., Testemale, D., Sabathier-Devals, C., Carlot, G., Matheron, P., Iltis, X., Pasquet, U., Valot, C., Delafoy, C., Largenton, R. (2014). Thermodynamics of chromium in UO<sub>2</sub> fuel: A solubility model. *J. Nucl. Mater.*, 447, 63-72.
- [8] Leenaers, A., de Tollenaere, L., Delafoy, Ch., Van den Berghe, S. (2003). On the solubility of chromium sesquioxide in uranium dioxide fuel. *J. Nucl. Mater.*, 317, 62-68.
- [9] Ekeröth, E. and Jonsson, M. (2003). Oxidation of UO<sub>2</sub> by radiolytic oxidants. *J. Nucl. Mater.*, 322, 242-248.
- [10] Maier, A.C., Kegler, P., Klinkenberg, M., Baena, A., Finkeldei, S., Brandt, F., Jonsson, M. (2020). On the change in UO<sub>2</sub> redox reactivity as a function of H<sub>2</sub>O<sub>2</sub> exposure. *Dalton Trans.*, 49, 1241-1248.



# Preliminary results of dissolution experiments with Cr-(Pu) doped UO<sub>2</sub> at SCK·CEN

*Cachoir, C., Mennecart, T. and Lemmens, K.*

SCK·CEN, Waste and Disposal Unit, Belgium (BE)

---

## 1. Introduction

The development of robust safety cases for geological disposal of spent fuel requires a solid understanding of its dissolution over very long-time scale (up to a million years). While the dissolution of standard spent fuel has reached a good level of comprehension, the development of modern LWR fuels (Cr/Al-doped UO<sub>2</sub> or MOX fuels) raises the question whether these fuels will behave similarly to standard fuels in geological repository conditions. The EU-DisCo project aims at understanding the matrix dissolution of these modern LWR fuels, under deep geological repository relevant conditions. Experiments on irradiated fuels (WP3) are thus complemented with systematic dissolution studies (WP4) carried out with carefully prepared and characterized, simplified UO<sub>2</sub>-based model materials, prepared in WP2. A special focus is given on the long-term matrix dissolution by using alpha doped UO<sub>2</sub>. Therefore Pu/Cr-doped materials, representative for 10,000 years old spent fuel, are prepared, next to Cr doped materials. These model materials are further exposed to two reference waters (young cementitious water at pH 13.5 and bicarbonate water at pH 9) in reducing/anoxic conditions, relevant for geological disposal. This paper describes the results of the leaching experiments, started in October 2019 and performed with inactive materials (depleted UO<sub>2</sub> and Cr-doped depleted UO<sub>2</sub>) for the two reference solutions. Similar tests are planned with Pu-doped UO<sub>2</sub> and Pu/Cr-doped UO<sub>2</sub> in the first semester of 2020. The production method of the Pu doped pellets is briefly explained, but as the leach tests with these materials have not yet been started, the results of the leach tests with the Pu- and Pu/Cr-doped UO<sub>2</sub> will be presented in a future publication.

## 2. Experimental

Static dissolution experiments were performed with depleted UO<sub>2</sub> and Cr-doped UO<sub>2</sub> pellets, either in Young Cementitious Water Light at pH 13.5 (YCWCa-L = cementitious water at pH 13.5 with a Ca concentration lower than the concentration at equilibrium [1]) or in bicarbonate solution at pH 9 (= the solution used also in the project First Nuclides, hence denominated as FIN solution). Table 1 gives the composition of the reference waters. The reference solutions contain a non-negligible concentration of Cr and Zn, especially for the YCWCa-L solution.

All tests are performed in an Ar glove box with pO<sub>2</sub> below 10 ppm and pCO<sub>2</sub> below the detection limits. All experimental details (materials, water composition, set-up and conditions) are described in the next paragraphs.

## 2.1 Materials

Four model materials are tested: (depleted)  $\text{UO}_2$ , Cr-doped (depleted)  $\text{UO}_2$ , Pu-doped  $\text{UO}_2$  and Pu/Cr doped  $\text{UO}_2$ . These model materials are synthesised at SCK·CEN in collaboration with FZ Juelich within WP2 of this project [2]. Even if the Pu-doped  $\text{UO}_2$  production is well known, the production of Cr-doped  $\text{UO}_2$  required some development in order to obtain pellets with a density of 95% of the theoretical density, with sufficiently large grains, and with the same specifications as standard fuel ( $\text{UO}_2$  reference), i.e. defects, porosity and impurities. The two first years of the project were thus focussed on the development of a production method of the model materials (and on the testing of various methods to control the redox conditions in the experiment). It was concluded that, when the Cr-doped  $\text{UO}_2$  is prepared by dry mixing of  $\text{UO}_2$  and  $\text{Cr}_2\text{O}_3$  powders, it is possible to get a grain size close to  $50\ \mu\text{m}$  and a more or less homogeneous Cr distribution within the  $\text{UO}_2$  matrix (in the grain and at grain boundary). The Pu-doped  $\text{UO}_2$  is obtained by a co-precipitation method to achieve a homogeneous distribution of Pu in the  $\text{UO}_2$  matrix. The doping level is representative for a fuel age of 10,000 years ( $\sim 18\ \text{MBq/g}_{\text{UO}_2}$ ). The Pu/Cr-doped  $\text{UO}_2$  is then synthesised by combining the two previous methods, with first the co-precipitation of Pu in  $\text{UO}_2$ , followed by dry mixing of  $\text{Cr}_2\text{O}_3$  and the Pu-doped  $\text{UO}_2$  powders. Although FZJ does not recommend the addition of lubricant for the preparation of Cr-doped samples, 0.3 wt.% of zinc stearate had to be added at SCK·CEN to limit the formation of cracks in the pellets as a result of differences in the press characteristics used at FZJ and at SCK·CEN. However, this additive is used also in the industry for the preparation of fuels, so the pellets should be representative of commercial fuel. Even if most of this zinc is volatilised during the sintering process, some traces can be still present within the pellet structure. Therefore, the Zn concentration in solution is also measured during the leaching experiments (see section 2.2).

Based on a series of preliminary production tests, a  $1600\ \mu\text{g/g}\ \text{Cr}_2\text{O}_3$  doping was found to be optimal to reach the requirements [3]. A first set of materials was produced with the characteristics given in Table 2.

These depleted  $\text{UO}_2$  and Cr-doped  $\text{UO}_2$  pellets (Figure 1) were used to start the leaching experiments (see section 3), although the grain size of the Cr-doped  $\text{UO}_2$  ( $35\text{-}50\ \mu\text{m}$ ) was slightly less than the target  $50\ \mu\text{m}$ . Further optimisation of the speed of the sintering process, the sieving/crushing and granulometry of the different powders ( $\text{Cr}_2\text{O}_3$ ,  $\text{UO}_2$ ) were attempted to reach a grain size of  $50\ \mu\text{m}$ . This optimised procedure will be applied for the preparation of the Pu-doped  $\text{UO}_2$  and the Pu/Cr doped  $\text{UO}_2$ . In Figure 1b, no agglomerates of Cr in the matrix are detected. It was observed, however, that the grain size is smaller near the surface of the Cr-doped  $\text{UO}_2$ .

**Table 1:** Composition of the reference leaching solutions (YCWCa-L and FIN).

mol/L	YCWCa-L	FIN
Na	$1.28 \cdot 10^{-1}$	$2.07 \cdot 10^{-2}$
K	$3.67 \cdot 10^{-1}$	$2.33 \cdot 10^{-5}$
Ca	$4.43 \cdot 10^{-4}$	$5.00 \cdot 10^{-6}$
C	$5.08 \cdot 10^{-4}$	$9.83 \cdot 10^{-4}$
$\text{SO}_4^{2-}$	$1.86 \cdot 10^{-3}$	$5.21 \cdot 10^{-6}$
Si	$4.32 \cdot 10^{-5}$	$3.71 \cdot 10^{-5}$

mol/L	YCWCa-L	FIN
Cl	$< 8.45 \cdot 10^{-6}$	$1.81 \cdot 10^{-2}$
U	$< 8.40 \cdot 10^{-10}$	$< 8.40 \cdot 10^{-10}$
Cr	$4.93 \cdot 10^{-8}$	$< 1.35 \cdot 10^{-8}$
Zn	$2.29 \cdot 10^{-7}$	$1.17 \cdot 10^{-7}$
pH	13.6	9.1
Eh (MV <sub>SHE</sub> )	177	202

**Table 2:** Specifications of the depleted UO<sub>2</sub> and Cr-doped UO<sub>2</sub>.

Type of model material	Depl. UO <sub>2</sub>	Cr-doped UO <sub>2</sub>
Pellet ( $\phi$ mm/h mm)	5.8 / 6	5.8 / 6
TD %	$95 \pm 1$ (95)	$95 \pm 1$ (95)
Cr <sub>2</sub> O <sub>3</sub> added ( $\mu$ g/g)	0	1600
Grain size ( $\mu$ m)	10 (10)	35- 50 (50)
Geometric Surface area (cm <sup>2</sup> )	1.696	1.696
Lubricant*	0.3 wt.%	0.3 wt.%

Value in brackets corresponds to the target characteristics; \* zinc stearate

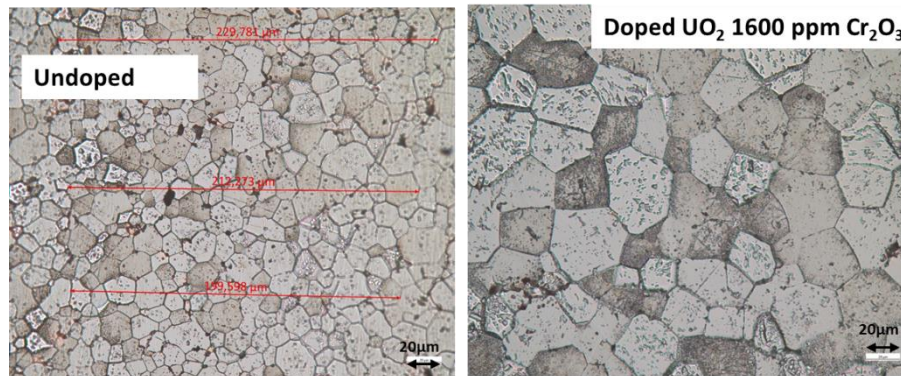


**Figure 1:** (a) depleted UO<sub>2</sub> (grain size 10  $\mu$ m), (b) Cr-doped UO<sub>2</sub> (grain size 35-50  $\mu$ m).

## 2.2 Experimental set-up and procedure

Static leaching experiments are carried out in autoclaves with 10 bar H<sub>2</sub> gas in presence of Pt/Pd catalyst to scavenge the oxygen traces inside the autoclaves. The catalyst is placed in the headspace of the autoclaves (and not immersed in the solution), because it should remove traces of atmospheric O<sub>2</sub> without perturbation of the formation of oxidizing species in solution through radiolysis (Figure 2a). The reaction of dissolved H<sub>2</sub> with oxidized species in solution may still be activated by the catalytic properties of the UO<sub>2</sub> surface. No other reducing agent was added to the solution, as preliminary tests showed that this did not improve the redox control [4-5].

The set-up consists of stainless steel autoclaves with a PEEK insert of 50 mL (Figure 2). The cover of the autoclaves is equipped with two outlet valves. One outlet consists of a short tube stopping immediately under the cover. This is used for gas sampling. The other outlet has a longer tube for the sampling of the solution near the bottom of the solution. A manometer is placed on top of the autoclave to monitor the gas pressure ( $H_2$ ) during the experiment. Each cell is filled with 30 mL of solution and one pellet of (doped)  $UO_2$  (Table 1), previously washed in 0.01 M NaCl for three weeks (see further).

Based on the optimisation of the leaching procedure [4-5], the experiments are divided in two consecutive steps. A first step consists of a washing period of three to four weeks in 0.01 M NaCl. This washing step is carried out in PE bottles with one pellet per bottle. During the first week the solution is renewed daily while a weekly renewal is done for the weeks thereafter. When the measured U concentration is in the range of the U(IV) solubility ( $10^{-8.5 \pm 1}$  M) [6], the leaching experiment is started in one of the reference waters for a period of at least one month. In this period, samples of 2 mL are taken regularly without replenishment, while the autoclaves are put again at 10 bar  $H_2$  pressure.

No annealing of the  $UO_2$  pellets nor pre-leaching in KOH or  $NaHCO_3$  solution is done, as the added-value of these extra treatments was not clearly demonstrated [4-5]. In order to reduce possible traces of oxygen in the reference solutions, the autoclaves are filled already before the start of the leaching experiment with 30 mL of solution in presence of the Pd/Pt catalyst and placed under 5 bar  $H_2$  pressure during at least one week.

The not-filtered U concentrations are measured during the washing and the leaching period while the ultrafiltered U concentrations ( $< 3.5$  nm), corresponding to the dissolved U concentration, are only determined in the leaching step at pH 9 or pH 13.5. We have also determined the not-filtered and ultrafiltered ( $< 3.5$  nm) concentrations of Cr and Zn to assess the potential influence of their release (section 2.1) on the U behaviour. The Cr concentration is followed as a function of leaching time, while the Zn concentration is measured at the start and at the end of the experiments. All three elements (U, Cr and Zn) are determined by ICP-MS.

Sampling was performed after 1, 3, 10, 30 and 72 days of leaching, this corresponds to 22, 24, 31, 51 and 93 days, respectively, including the 21 days of the washing period.

The experiments with depleted  $UO_2$  and Cr-doped  $UO_2$  have been started in October 2019.

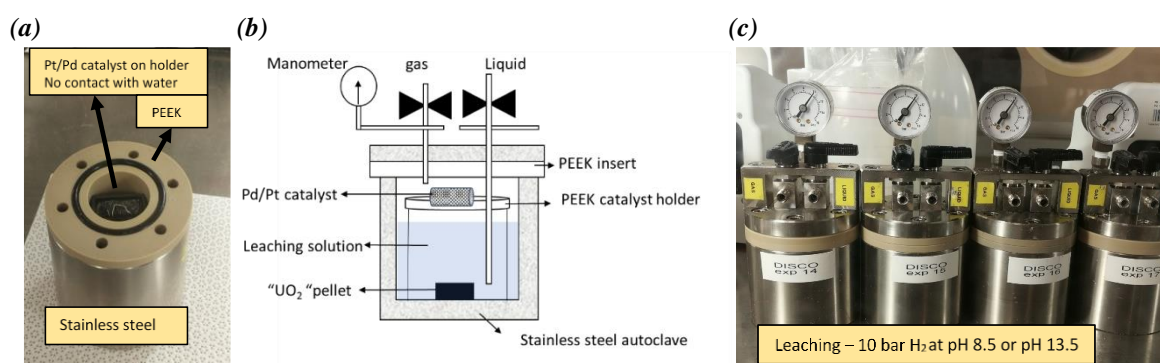


**Figure 2:** Experimental set-up (a) inside the cell, (b) schematic drawing and (c) autoclaves under 10 bar pressure.

### 3. Results and discussion

#### 3.1 pH and redox potential

In the YCWCa-L the pH of the solution remains close to  $13.4 \pm 0.1$  over the leaching period for both depleted  $\text{UO}_2$  and Cr-doped  $\text{UO}_2$ , while the redox potential is decreasing from -190 to -440 mV<sub>SHE</sub>. In the FIN solution, the pH of the leaching solution is more fluctuating and slightly higher (between  $9.4 \pm 0.3$  and  $9.8 \pm 0.4$  for depleted  $\text{UO}_2$  and Cr-doped  $\text{UO}_2$ , respectively) than the target value of 9. On the contrary, the redox potential behaves similarly as in the YCWCa-L with a decrease from -110 to -350 mV<sub>SHE</sub> for whichever the type of  $\text{UO}_2$ . The low values of the redox potential in both media suggest that the Pt/Pd catalyst coupled to the  $\text{H}_2$  pressure allowed a good scavenging of atmospheric oxygen.

#### 3.2 Uranium concentration

Figure 3 shows the U concentration as a function of time for the depleted  $\text{UO}_2$  and the Cr-doped  $\text{UO}_2$  during the washing period (0-21 days) in 0.01 M NaCl and the leaching period (22-93 days) in YCWCa-L and in FIN solutions. Table 3 and Table 4 give the measured U concentrations as a function of leaching time for the different experiments.

##### Uranium concentration during washing period (0-21 days)

During the washing in NaCl solution, the U concentration first decreased from  $10^{-8}$  mol/L to less than  $5.7 \cdot 10^{-10}$  mol/L, this is the detection limit, indicated by the dotted line in Figure 3. In the last samples taken from the NaCl solution (after 21 days), the U concentration slightly increased. It increases somewhat more for the Cr-doped  $\text{UO}_2$  ( $3.4 \cdot 10^{-9}$  mol/L) than for the depleted  $\text{UO}_2$  ( $7.5 \cdot 10^{-10}$  -  $1.5 \cdot 10^{-9}$  mol/L). Although all experimental parameters remained constant (i.e. oxygen in the glove box, temperature), we cannot exclude that oxygen traces in the glove box were responsible for the observed U increase, as the washing step was done in PE bottles that were possibly not fully tight. After 21 days of washing (vertical dotted line in Figure 3), the leaching experiments in the two reference solutions were nevertheless started, as the U concentration was in the range of the U(IV) solubility ( $10^{-8.5 \pm 1}$  M; red dotted line in Figure 3).

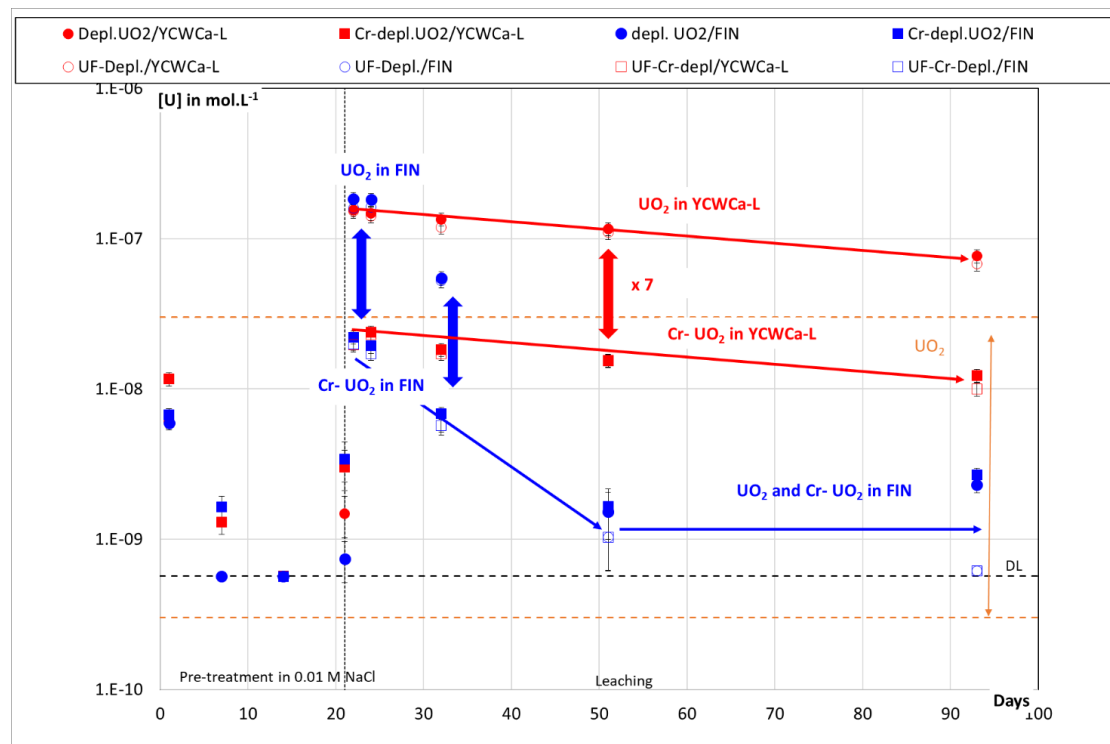


**Figure 3:** U concentrations as a function of time for experiments with depleted  $\text{UO}_2$  and Cr-doped  $\text{UO}_2$  pellets in Young Cementitious water (pH 13.5 - red symbols) and in FIN solution (pH 9 - blue symbols) under 10 bar  $\text{H}_2$ . Filled symbols correspond to not-filtered total U concentrations, while open symbols are the ultrafiltered soluble concentrations.

#### Uranium concentration during leaching period (21-93 days)

At pH 13.5 (YCWCa-L), after a high initial U release, respectively up to  $1.6 \cdot 10^{-7}$  and  $2.2 \cdot 10^{-8}$  mol/L for depleted  $\text{UO}_2$  and Cr-doped  $\text{UO}_2$ , the U concentration slightly decreases as a function of time. After 93 days, the U concentration is not yet stabilised and is  $7.7 \cdot 10^{-8}$  and  $1.2 \cdot 10^{-8}$  mol/L for depleted  $\text{UO}_2$  and Cr-doped  $\text{UO}_2$ , respectively. As reflected by the U concentrations, the presence of Cr reduces by a factor around 7 the U release for the Cr-doped  $\text{UO}_2$  over the entire leaching duration. The ratio colloidal U / total U is small, as shown by the small difference between the total and the ultrafiltered U concentration for both depleted and Cr-doped  $\text{UO}_2$ . This difference is mostly < 10% and corresponds to the uncertainty of the ICP-MS measurements.

A high initial U release is also measured at pH 9 (FIN), respectively  $1.8 \cdot 10^{-7}$  and  $2.2 \cdot 10^{-8}$  mol/L for depleted  $\text{UO}_2$  and Cr-doped  $\text{UO}_2$ . The U concentration then considerably decreased to stabilize after 51 days around  $2.5 \cdot 10^{-9}$  mol/L with the a higher ratio of colloidal U / total U, possibly reflecting the over-saturation with a U secondary phase, but the concentration of colloidal U is still small (about  $10^{-9}$  M). Modelling of the experiments will be performed to confirm this hypothesis. Even if during the first 10 days of leaching (up to 31 days in Figure 3), the presence of Cr seems to have a reducing effect on U release similarly as reported in YCWCa-L, this effect disappears with time. After 93 days, the total U concentration close to  $2.5 \cdot 10^{-9}$  mol/L and the soluble U concentration  $< 6.2 \cdot 10^{-10}$  mol/L are identical for the depleted and Cr-doped  $\text{UO}_2$ .

**Table 3:** U concentration in mol/L measured after 22, 24, 31, 51 and 93 days for the experiments with depleted UO<sub>2</sub> and Cr-doped UO<sub>2</sub> pellets in Young Cementitious water (pH 13.5) under 10 bar H<sub>2</sub>.

YCWCa-L				
Day	Depleted UO <sub>2</sub>		Cr-doped UO <sub>2</sub>	
	[U] <sub>Total</sub> (mol/L)	[U] <sub>soluble</sub> (mol/L)	[U] <sub>Total</sub> (mol/L)	[U] <sub>soluble</sub> (mol/L)
22	$(1.6 \pm 0.2) \cdot 10^{-7}$	$(1.5 \pm 0.2) \cdot 10^{-7}$	$(2.2 \pm 0.2) \cdot 10^{-8}$	$(2 \pm 0.2) \cdot 10^{-8}$
24	$(1.5 \pm 0.2) \cdot 10^{-7}$	$(1.4 \pm 0.1) \cdot 10^{-7}$	$(2.4 \pm 0.2) \cdot 10^{-8}$	$(2.3 \pm 0.2) \cdot 10^{-8}$
31	$(1.3 \pm 0.1) \cdot 10^{-7}$	$(1.2 \pm 0.1) \cdot 10^{-7}$	$(1.8 \pm 0.2) \cdot 10^{-8}$	$(1.7 \pm 0.2) \cdot 10^{-8}$
51	$(1.2 \pm 0.1) \cdot 10^{-7}$	$(1.1 \pm 0.1) \cdot 10^{-7}$	$(1.6 \pm 0.1) \cdot 10^{-8}$	$(1.5 \pm 0.1) \cdot 10^{-8}$
93	$(7.7 \pm 0.8) \cdot 10^{-8}$	$(6.8 \pm 0.7) \cdot 10^{-8}$	$(1.2 \pm 0.1) \cdot 10^{-8}$	$(1 \pm 0.1) \cdot 10^{-8}$

**Table 4:** U concentration in mol/L measured after 22, 24, 31, 51 and 93 days for the experiments with depleted UO<sub>2</sub> and Cr-doped UO<sub>2</sub> pellets in FIN solution (pH 9) under 10 bar H<sub>2</sub>.

FIN				
Day	Depleted UO <sub>2</sub>		Cr-doped UO <sub>2</sub>	
	[U] <sub>Total</sub> (mol/L)	[U] <sub>soluble</sub> (mol/L)	[U] <sub>Total</sub> (mol/L)	[U] <sub>soluble</sub> (mol/L)
22	$(1.8 \pm 0.2) \cdot 10^{-7}$	$(1.6 \pm 0.2) \cdot 10^{-7}$	$(2.2 \pm 0.2) \cdot 10^{-8}$	$(2 \pm 0.2) \cdot 10^{-8}$
24	$(1.8 \pm 0.2) \cdot 10^{-7}$	$(1.6 \pm 0.2) \cdot 10^{-7}$	$(1.9 \pm 0.2) \cdot 10^{-8}$	$(1.7 \pm 0.2) \cdot 10^{-8}$
31	$(5.4 \pm 0.6) \cdot 10^{-8}$	$(5.2 \pm 0.6) \cdot 10^{-8}$	$(6.8 \pm 0.7) \cdot 10^{-9}$	$(5.7 \pm 0.6) \cdot 10^{-9}$
51	$(1.5 \pm 0.5) \cdot 10^{-9}$	$(1 \pm 0.4) \cdot 10^{-9}$	$(1.6 \pm 0.5) \cdot 10^{-9}$	$(1 \pm 0.4) \cdot 10^{-9}$
93	$(2.3 \pm 0.3) \cdot 10^{-9}$	$< 6.1 \cdot 10^{-10}$	$(2.7 \pm 0.3) \cdot 10^{-9}$	$< 6.2 \cdot 10^{-10}$

Between 1 and 3 days of leaching (21-24 days in Figure 3), the U concentration seems constant and equivalent for the two reference solutions. In this stage, there is no clear effect of pH or the complexing agent (OH<sup>-</sup> or CO<sub>3</sub><sup>2-</sup>) on the U release. The U concentrations are, however, much lower for the Cr-doped UO<sub>2</sub> than for the depleted UO<sub>2</sub>: we can clearly distinguish a reducing effect of Cr on the U concentration by a factor 7-8.

A fast initial dissolution rate has been determined for the depleted UO<sub>2</sub> at  $4.6 \pm 0.5$  (YCWCa-L) and  $5.4 \pm 0.5$  mg/m<sup>2</sup>·d (FIN), while somewhat lower initial dissolution rates were determined for the Cr-doped UO<sub>2</sub> at  $0.7 \pm 0.1$  (YCWCa-L) and  $0.6 \pm 0.1$  mg/m<sup>2</sup>·d (FIN). These values support the lowering effect of Cr on the UO<sub>2</sub> dissolution rate. The nature of the complexing agent does not play any role on this initial release.

After this short initial period (after 24 days in Figure 3), no meaningful dissolution rate can be determined as the U concentrations are decreasing for all experiments. However, depending on the type of solution, the U release has different behaviours. In YCWCa-L, even if the U concentrations are slightly decreasing by a factor of about 2 between 24 and 93 days for the depleted and Cr-doped UO<sub>2</sub>,

the Cr effect on U release (the factor 7 difference between depleted and Cr-doped  $\text{UO}_2$ ) remains constant over time. This suggests a continuous driving effect of the  $\text{OH}^-$  on the Cr and U release. In FIN solution, the U concentrations decrease much faster. Moreover, they decrease faster for the depleted  $\text{UO}_2$  than for the Cr-doped  $\text{UO}_2$ . Whereas the Cr-doping decreased the U concentration by a factor 7 to 3 in the first 12 days of leaching (21-32 days in Figure 3), the longer term concentrations are thus the same with and without Cr, suggesting a temporary effect of Cr in FIN solution, in the tested reducing conditions.

Several hypotheses can be proposed to explain the lower U concentrations for the Cr-doped  $\text{UO}_2$  in YCWCa-L (over the entire test duration) and in FIN (before 51 days). The Cr-doped  $\text{UO}_2$  could be less sensitive to oxidation by the exposure to traces of oxygen at the start of the leach test. Secondly, the catalytic properties of the  $\text{UO}_2$  surface could be enhanced by the Cr in the  $\text{UO}_2$ , thus making the  $\text{H}_2$  more reactive towards oxidizing or oxidized species. Thirdly, the surface of the  $\text{UO}_2$  might get covered by precipitating Cr (see next section 3.3). This would lower the further U release as observed for the Cr-doped  $\text{UO}_2$  in both media (Figure 3). Before drawing robust conclusions, these hypotheses need to be confirmed by the surface analysis of the leached materials and also tested by modelling calculations.

### 3.3 Cr concentration

The Cr concentrations are mostly close to the detection limit of the ICP-MS (from 1 to  $8 \cdot 10^{-8}$  mol/L) and close to the background concentration of the reference solutions of  $5 \cdot 10^{-8}$  and  $< 1.4 \cdot 10^{-8}$  mol/L for YCWCa-L and FIN solutions, respectively. Taking into account the uncertainties on the concentration and the fluctuations of the detection limit of the ICP-MS, a small Cr release can nevertheless be discerned for the Cr-doped  $\text{UO}_2$ , especially for the YCWCa-L while no Cr release is observed for the undoped  $\text{UO}_2$ , as expected (Figure 4). We focus the further discussion on the Cr-doped  $\text{UO}_2$ .

At pH 13.5 (YCWCa-L), the total Cr concentration is in the range  $5 \cdot 10^{-8}$  -  $1.9 \cdot 10^{-7}$  mol/L, whereas the soluble Cr concentration is close to  $5 \cdot 10^{-8}$  mol/L, which also corresponds to the background concentration of the reference solution.

At pH 9 (FIN), the Cr concentrations are lower than at pH 13.5. The total Cr concentration is in the range  $8 \cdot 10^{-8}$  to  $3 \cdot 10^{-8}$  mol/L, while the soluble Cr concentration is around  $3 \cdot 10^{-8}$  mol/L.

The doping level of 1600 ppm  $\text{Cr}_2\text{O}_3$  for the Cr-doped  $\text{UO}_2$  would correspond to a Cr concentration in solution close to  $4 \cdot 10^{-5}$  mol/L if all Cr in the pellets would be dissolved. Based on the measured concentrations, we can thus conclude that a very small Cr fraction of 0.2 and 0.5% is released in FIN and YCWCa-L, respectively. We can nevertheless notice that this Cr release fraction is much higher than the released U fraction of 0.0003% for the both solutions, suggesting that Cr could be present in the accessible part of the materials and that the release is promoted at high pH. Furthermore, the constant soluble concentration suggests a Cr phase(s) controlling the concentrations in solution. This assumption is also supported by the presence of colloids highlighted by the difference between the soluble and total Cr concentrations. This observation is valid for both of the reference solutions. Modelling of the experiments might support this hypothesis. The slightly higher soluble concentration in YCWCa-L than in FIN suggests that the Cr release is (slightly) enhanced at high pH.



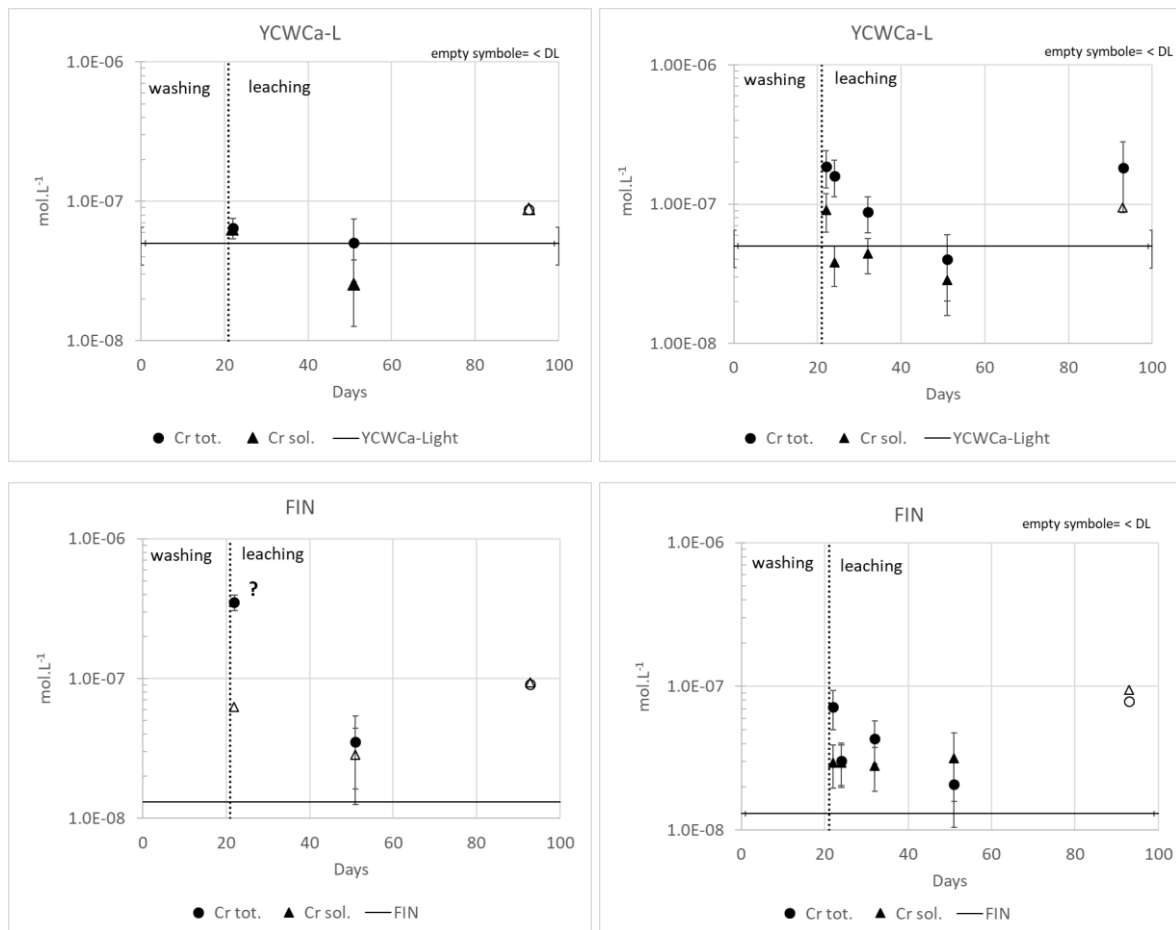


**Figure 4:** Cr concentrations as function of time for experiments under 10 bar H<sub>2</sub> with depleted UO<sub>2</sub> pellet (left column) and Cr-doped UO<sub>2</sub> pellet (right column) in Young Cementitious water (pH 13.5 - upper graphs) and in FIN water (pH 9 - lower graphs). The horizontal line shows the background concentration. The open symbols are for concentrations below detection limit.

### 3.4 Zn concentration

A clear increase of Zn concentration compared to the background in the reference solutions (Table 1) is observed for both depleted UO<sub>2</sub> and Cr-doped UO<sub>2</sub> in both solutions (Figure 5). The measured concentration appears more or less constant and seems equivalent for the undoped and doped UO<sub>2</sub> leached in the same reference solution. This shows that the Zn stearate, used as lubricant, was not fully volatilized during the sintering process of the pellets and can thus be released during the leaching experiment. However, no interaction of Zn with U and Cr is expected.

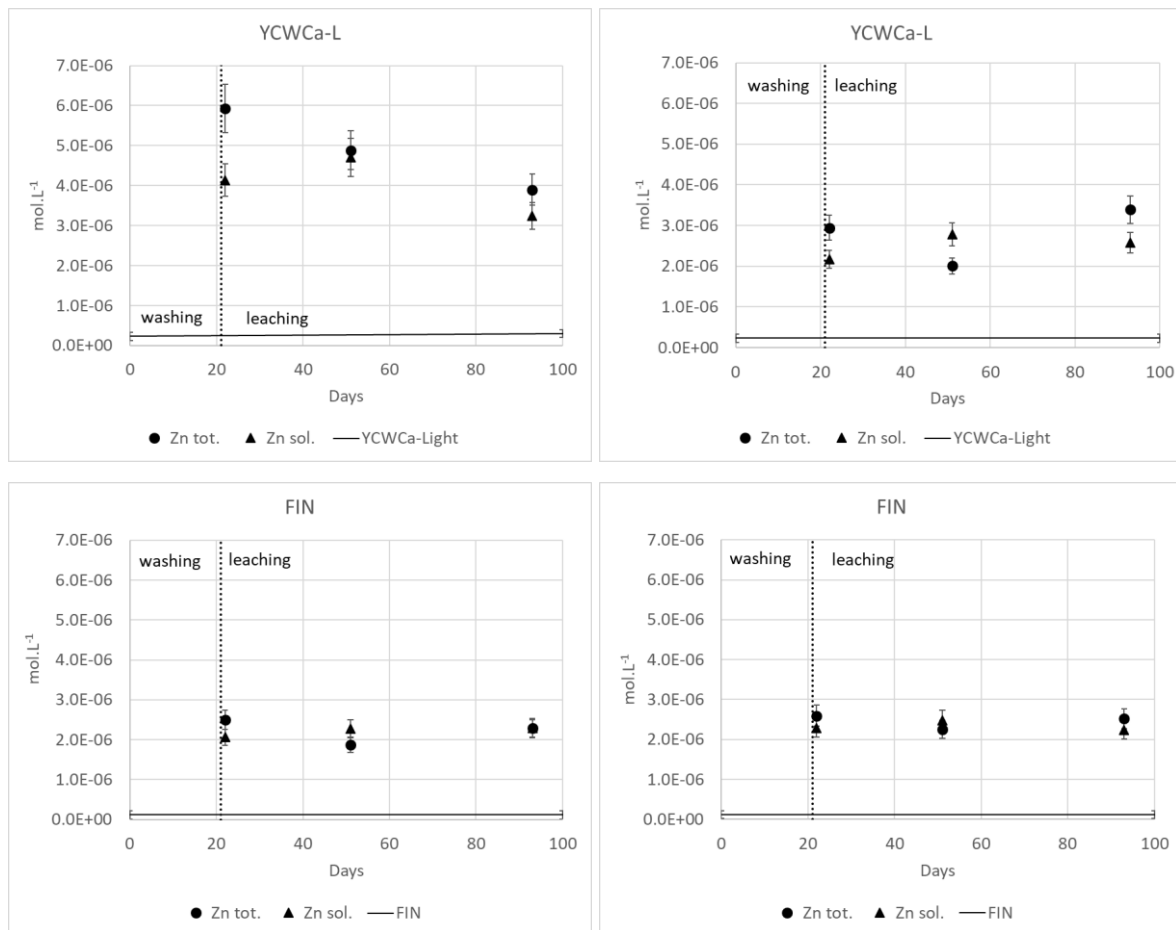


**Figure 5:** Zn concentrations as function of time for experiments under 10 bar  $H_2$  with depleted  $UO_2$  pellet (left column) and Cr-doped  $UO_2$  pellet (right column) in Young Cementitious water (pH 13.5 - upper graphs) and in FIN water (pH 9 - lower graphs). The horizontal line shows the background concentration.

## Conclusions

In this first phase of the leaching experiments of model  $UO_2$  by SCK·CEN in the framework of the DisCo project, static leaching tests with depleted  $UO_2$  and Cr-doped  $UO_2$  pellet were performed in autoclaves in the two reference solutions YCWCa-L and FIN under 10 bar  $H_2$  pressure and in presence of Pt/Pd catalyst to scavenge the oxygen present in the autoclave atmosphere. After a fast initial release independent on type of solution, the results demonstrated a promoted U release in cementitious solution compared to bicarbonate water for both kind of fuels. However, while a reducing effect of Cr on U release is observed continuously in cementitious conditions, this effect seems to be temporary in bicarbonate conditions. Several hypotheses are forwarded to explain these observations, but they need to be supported by future surface analyses and modelling calculations.

## Acknowledgement

*The research leading to these results has received funding from the European Commission Horizon 2020 Research and Training Programme of the European Atomic Energy Community (EURATOM) (H2020-NFRP-2016-2017-1) under grant agreement n° 755443 (DisCo project).*

## References

- [1] Cachoir, C. (2019). Preparation of Evolved Cement Water (ECW, ECW-light), Young Cement Waters (YCW, YCWCa and YCWCa-light) and Old Cement Water (OCW) for the supercontainer experiments. 176-INS-0001, SCK·CEN restricted report, SCK·CEN/12272337.
- [2] Farnan, I., Bosbach, D., Wegen, D., Gonzales-Robles Corrales, E., Jegou, C., Corkhill, C., Hambley, D.I., Cobos Sabate, J. (2018). Deliverable D2.1: Initial state report: sample characterisation and experimental set-up. DisCo project (Grant Agreement: 755443).
- [3] Delville, R. (2019). Investigation of fabrication routes of model fuels with tailored microstructures for leaching studies. Oral communication at the 30<sup>th</sup> Spent Fuel Workshop. Ghent (Belgium), November 14-15.
- [4] Cachoir, C., Mennecart, T., Lemmens, K. (2019). Dissolution experiments with Cr-(Pu) doped UO<sub>2</sub> at FZJ and SCK·CEN: Preparatory tests with depleted and low alpha-doped UO<sub>2</sub> at SCK·CEN. Contribution to the 2<sup>nd</sup> Annual Meeting of the European DisCo project. Köln (Germany), May 27-28.
- [5] Bosbach, D., Cachoir, C., Myllykylä, E., Jegou, C., Cobos, J., Farnan, I., Corkhill, C. (2019). Deliverable D4.1: Model materials experiments: First dissolution results. DisCo project (Grant Agreement: 755443).
- [6] Neck, V. and Kim, J.I. (2001). Solubility and hydrolysis of trivalent actinides. *Radiochim. Acta*, 89, 1-16.

# Dissolution of alpha-doped UO<sub>2</sub> with and without Cr in the presence of corroding Fe, in synthetic and natural groundwater

*Myllykylä, E.*

VTT Technical Research Centre of Finland Ltd,  
Espoo (FI)

---

## 1. Introduction

The objective of this study is to investigate the effect of Cr-doping on the dissolution of  $\alpha$ -doped UO<sub>2</sub> in conditions relevant to final disposal. The idea is to compare the results of these dissolution experiments to the ones conducted with real spent nuclear fuel in the DisCo project and also the ones conducted previously with similar alpha doped simulant materials but either in simulant waters [1-4] or in natural ground waters [5-6] and without Cr-doping. The aim is to understand the matrix dissolution of novel Cr-doped spent fuel in groundwater conditions.

The experiments are conducted under Ar atmosphere of the glove box. The first experiments are conducted with <sup>233</sup>U alpha doped UO<sub>2</sub> fragments, already used in dissolution experiments in previous projects [1-6]. These materials are referred as “old” material herein and they are UO<sub>2</sub> materials with 5% or 10% <sup>233</sup>U alpha doping, simulating the alpha dose of 10,000 years old and 3000 years old spent nuclear fuel, respectively. Similar UO<sub>2</sub>, without alpha doping (0%), has been used a reference. The new pellet materials (UO<sub>2</sub>, Cr-doped UO<sub>2</sub>, <sup>238</sup>Pu-doped UO<sub>2</sub> and Cr/<sup>238</sup>Pu-doped UO<sub>2</sub>) will be prepared and characterized by SCK·CEN in collaboration with Jülich. The doping level of <sup>238</sup>Pu-doped UO<sub>2</sub> pellets, to be fabricated, will correspond to the alpha dose of ~ 10,000 years old nuclear fuel. Fabrication of these materials has been delayed from 2019. The delivery to Finland was arranged in the beginning of June 2020 as the final patch of Pu-doped pellets were ready.

## 2. Methods

### 2.1 Natural groundwaters

These leaching experiments are conducted mainly in natural groundwaters. Some parallel experiments will be conducted also in bicarbonate water with “new” Cr-doped materials. Natural groundwaters have been sampled from the Olkiluoto site, which is the planned site for disposal of spent nuclear fuel in Finland.

In the previous EU project, REDUPP [5-6], three different groundwaters from different depths (fresh, brackish, saline) were used in leaching experiments of UO<sub>2</sub>. This aimed to study possible effects of complex chemical composition of natural groundwater to the dissolution rate of UO<sub>2</sub>. The bigger aim of REDUPP project was to focus on the interactions between solid surface and fluid with different fluorite-type structures similar to UO<sub>2</sub>. In the DisCo project the experiments with <sup>233</sup>U-doped UO<sub>2</sub> are conducted only in brackish OL-KR6, because it showed slight solubility increasing effect with 10% alpha doping

in previous experiments [5-6]. Brackish, high carbonate water does represent currently at the groundwater conditions at the disposal level (app. -400 m). However, this kind of conditions might occur for example in the postglacial situation, if the groundwater layers will be strongly mixed at Olkiluoto site.

ONK-KR15 groundwater has been selected for the leaching experiments of new UO<sub>2</sub> materials fabricated in DisCo project. ONK-KR15 stands for the ONKALO characterization drill core at the depth of -399 m. This groundwater represents groundwater conditions at the disposal level. It has less sulphate and carbonate (0.16 mM) in comparison to OL-KR6 (2.5 mM HCO<sub>3</sub><sup>-</sup>), but relatively low salinity compared to saline waters (see Table 1). ONK-KR15 water resembles the composition of saline OL-KR5 used previously in REDUPP experiments, but ONK-KR15 was selected instead due to unavailability of OL-KR5. It represents groundwater water, which has not been mixed with any other water types. These kind of low carbonate and saline groundwater conditions prevails in disposal sites in Finland and Sweden. Thus, it is relevant to gain information the possible effect of low carbonate in comparison to bicarbonate (1 to 2 mM) concentrations used in many reference waters in DisCo project.

**Table 1:** Compositions for natural groundwaters OL-KR6 (brackish) and ONK-KR15 (saline) to be used in DisCo dissolution experiments. Two columns for OL-KR6 show the slight temporal variation and ONK-KR15 are given as average values from data collected from 2011 to 2018.

	OL-KR6 (2013)	OL-KR6 (2016)	ONK-KR15 (2011-2018)
pH	7.6	7.6	8.0
Ammonium, NH <sub>4</sub> (mg/L)	0.31	0.29	0.025
Bicarbonate, HCO <sub>3</sub> (mg/L)	159	153	9.7
Bromide, Br (mg/L)	12	11	46
Calcium, Ca (mg/L)	540	530	1242
Chloride, Cl (mg/L)	3340	3340	6162
Dissolved Inorganic Carbon (mg/L)	27	31	1.8
Fluoride, F (mg/L)		0.4	1.6
Iron, Fe (total) (mg/L)	0.36	0.28	0.01
Iron, Fe <sup>2+</sup> (mg/L)		0.28	0.015
Magnesium, Mg (mg/L)	151	151	33
Nitrate, NO <sub>3</sub> (mg/L)	0.4	0.4	< 0.04
Nitrite, NO <sub>2</sub> (mg/L)	0.2	0.2	< 0.02
Nitrogen, N <sub>Total</sub> (mg/L)	0.36		0.077
Non Purgeable Organic Carbon (mg/L)	4.6	5.1	3.5
Phosphate, PO <sub>4</sub> (mg/L)		0.2	0.2
Potassium, K (mg/L)	18	18	10
Silicate, SiO <sub>2</sub> (mg/L)	11	12	6.3
Sodium, Na (mg/L)	1460	1460	2392
Strontium, Sr (mg/L)	5.5	5.8	10.2

	OL-KR6 (2013)	OL-KR6 (2016)	ONK-KR15 (2011-2018)
Sulphate, SO <sub>4</sub> (mg/L)	404	406	0.33
Sulphide, S <sub>2</sub> <sup>-</sup> (mg/L)		0.02	0.05
Sulphur, S <sub>Total</sub> (mg/L)	130	130	0.6
Total Dissolved Solids (mg/L)	6101	6088	9913
Carbonate alkalinity, HCl uptake (mmol/L)	0.05	0.05	< 0.05
Total acidity, NaOH uptake (mmol/L)	0.18	0.16	0.05
Total alkalinity, HCl uptake (mmol/L)	2.6	2.5	0.16

OL-KR6 groundwater (from depth 135 m to 137 m) was sampled at the continuous measurement station on the ground in June 2018. The composition of natural water (OL-KR6) has shown slight temporal variation depending on the sampling year. The OL-KR6 groundwater was sampled via valves into the 2 L glass bottles purged with nitrogen gas prior to sampling. Bottles were delivered from Olkiluoto to VTT (Espoo) and imported into the glove box during the same day as the samples were taken. The alkalinity and pH of the groundwater were periodically measured under glove box conditions. Both pH and alkalinity showed slight increase during 300 days equilibration period in the glove box (see Figure 1). This may be the effect of degassing of CO<sub>2</sub> under Ar atmosphere.

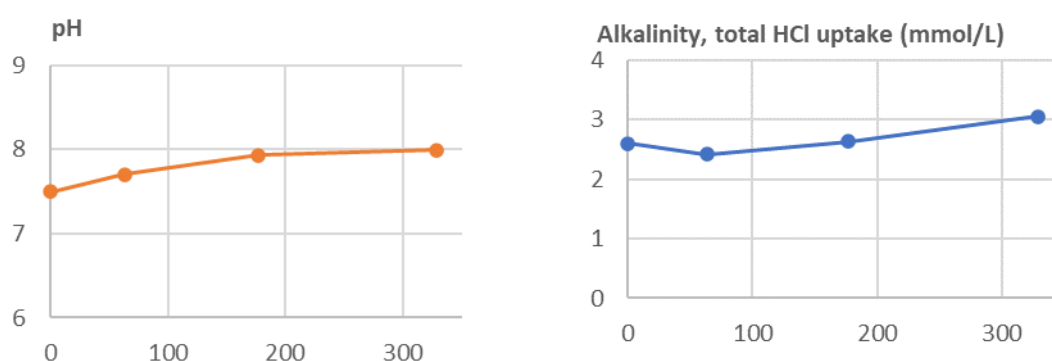


**Figure 1:** Evolution of pH and Alkalinity of OL-KR6 ground water during during 300 days period under glove box conditions.

The elemental concentrations of OL-KR6 are followed during the experiments. In addition, pH will be measured few times and alkalinity in the end of the experiments. The purpose if these measurements is to evaluate the durability and representativeness of OL-KR6 ground water during the experiments.

One liter of the KR-6 groundwater was allowed to equilibrate with iron strips to sweep the natural uranium away from the groundwater before starting the actual dissolution experiments. The initial uranium concentration decreased from  $5 \cdot 10^{-9}$  mol/L to  $1 \cdot 10^{-11}$  mol/L. Due to formation of black precipitates the water was also filtered with syringe and 0.22  $\mu$ m filter prior to leaching experiments.

ONK-KR15 was sampled from underground research facility ONKALO, in Olkiluoto in early April 2020. Some experiments are also conducted with Cr doped material in bicarbonate FIN water

(19 mM NaCl and 1 mM NaHCO<sub>3</sub>), as a reference and to allow for comparability of results of other working groups within the DisCo project.

## 2.2 Leaching experiments

The old samples, <sup>233</sup>U alpha doped UO<sub>2</sub> fragments (see Table 2 and Figure 2), were stored under anaerobic glove box conditions for 4 years. There are parallel samples (2-0 and 1-0, 1-5 and 2-5, 1-10 and 2-10) for 1 g samples and only one sample per doping level with higher mass (~ 3 g). The previous dissolution experiments were carried under saline groundwater and thus, the samples required preparation before experiments by pre-leaching twice with bicarbonate solution before start of the actual experiments in natural groundwater. This removed salts possibly precipitated during the storage period.

**Table 2:** Compositions for 0%, 5% and 10% <sup>233</sup>U doped pellets including the sample masses.

UO <sub>2</sub> phase	[ <sup>233</sup> U] (%)	[ <sup>235</sup> U] (%)	[ <sup>238</sup> U] (%)	<sup>235</sup> U/ <sup>238</sup> U	Samples (g)
Un-doped	0	2.82	97.18	0.029	1, 1, 3 g
5% <sup>233</sup> U-doped 15.7 MBq/g	5.0	4.5	90.5	0.050	1, 1, 3 g
10% <sup>233</sup> U-doped 31.4 MBq/g	10.0	4.5	85.5	0.053	1, 1, 2.5 g



**Figure 2:** The old samples, <sup>233</sup>U alpha doped UO<sub>2</sub> fragments placed in glass saucers inside the test vessels during the bicarbonate pre-leaching without iron.

The experimental system for dissolution tests is described in Figure 3, showing the test vessel with an iron strip leaning to vessel wall, and UO<sub>2</sub> fragments placed into a glass saucer, which functions as a holder for the UO<sub>2</sub> fragments. The iron foil maintains the reducing conditions, producing some H<sub>2</sub>. It also mimics the cast iron insert of the copper canister that will be present next to spent nuclear fuel in the repository.

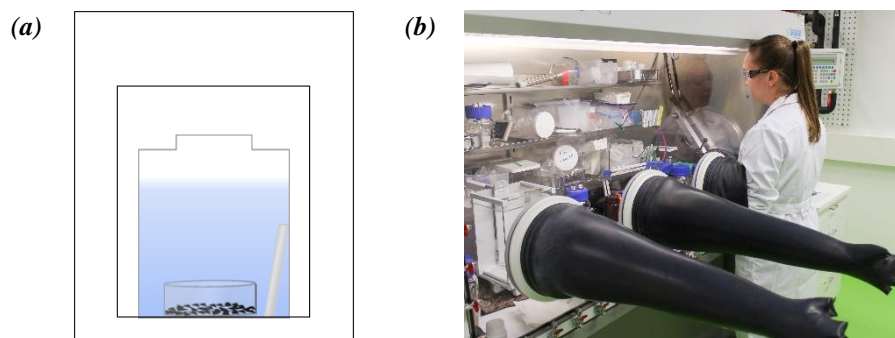


**Figure 3:** Schematic view of closed plastic vessel ( $V = 60$  mL) (a) in which the experiments will be conducted in the anaerobic glove box (b).  $\text{UO}_2$  fragments are placed in the glass saucer and the iron strip is leaning on the vessel wall in leaching media.

The experiments were set-up by adding 40 mL of filtered OL-KR6 groundwater and one piece of iron foil (1.5 cm x 3 cm) into 60 mL polypropylene vessel and this was allowed to equilibrate for 2 days before addition of  $\text{UO}_2$  solids. The iron foils were cut and gently polished from Goodfellow iron foils (100 mm x 100 mm x 0.125 mm, 99.5% Fe). After pre-washing in bicarbonate solution,  $\text{UO}_2$  fragments were rinsed twice with 2 mL of MQ-water, and allowed to dry for a short moment, before weighting them into a clean saucer. The saucer with fragments was placed on the bottom of the test vessel. Prior to the spike of  $^{235}\text{U}$ -rich solution, 168  $\mu\text{L}$  of 0.01 M NaOH was added to neutralize the acid content of the spike. Next, the solution spike  $^{235}\text{U}/^{238}\text{U} \sim 10/1$  was added to give an initial total U concentration of  $3.4 \cdot 10^{-9}$  mol/L and the solution was stirred with the tip of the pipette before closure.

The first samples ( $t = 0$ ) were taken already made before the addition of  $\text{UO}_2$  fragments. The following samples, 1.2 mL, were taken in the time intervals 2 h, 1, 4, 12, 41, 61, 105 and 201 days. The sample volume was compensated with addition of filtered OLK-KR6 groundwater. The samples were acidified with 12  $\mu\text{L}$  of suprapure  $\text{HNO}_3$  (ULTREX II by J.T. Baker). Uranium concentration and isotope ratio  $^{235}\text{U}/^{238}\text{U}$  was measured with sector field ICP-MS (Element 2 by ThermoScientific). The analyses have been run from 1/5 diluted samples with APEX IR sample introduction system, which intensifies the signal of uranium approximately 7 fold in comparison with standard spray chamber with peltier cooling.

At the end of the experiments, the metallic surfaces will be studied with microscopic methods (e.g. SEM, TEM) for identification of the formation of secondary minerals.

### 3. Results and discussion

Figure 4 shows the evolution of measured  $^{238}\text{U}$  concentrations in DisCo leaching experiments with  $\sim 1$  g and  $\sim 3$  g samples in OL-KR6 water with different doping levels (0, 5 or 10% indicated in the second number of the test code). In all experiments, the concentration of  $^{238}\text{U}$  has settled at the level between  $2 \cdot 10^{-11}$  and  $5 \cdot 10^{-11}$  mol/L after 200 days. The 1 g sample, with doping level 5% (1-5) shows slightly lower concentration level compared to other 1 g samples.



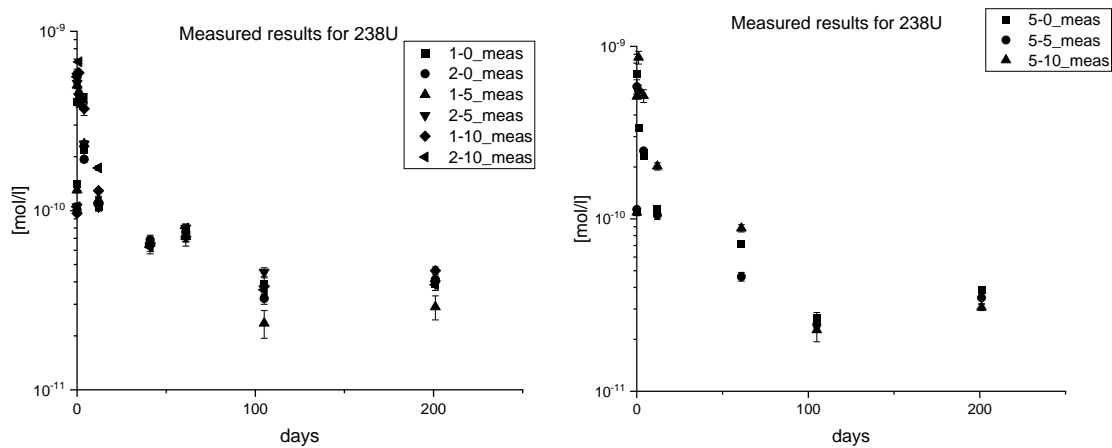


**Figure 4:** Evolution of of  $^{238}\text{U}$  concentrations in these DisCo leaching experiments with ~ 1 g (2-0 and 1-0, 1-5 and 2-5, 1-10 and 2-10) and 3 g (5-0, 5-5-, 5-10) samples in OL KR6 water with different doping levels (0, 5 or 10) during 200 days of the experiment.

In comparison to parallel experiments conducted in REDUPP project [5-6], the concentration of  $^{238}\text{U}$  has settled at slightly higher level with 1 g samples than in REDUPP experiments, even though the magnitude of the difference is small (see Figure 5). In the case of 3 g samples, with higher surface to volume ratio, the concentration of  $^{238}\text{U}$  has settled at lower or same level than in REDUPP experiments (see Figure 6). In these experiments, different doping levels did not show notable difference in the concentration levels.

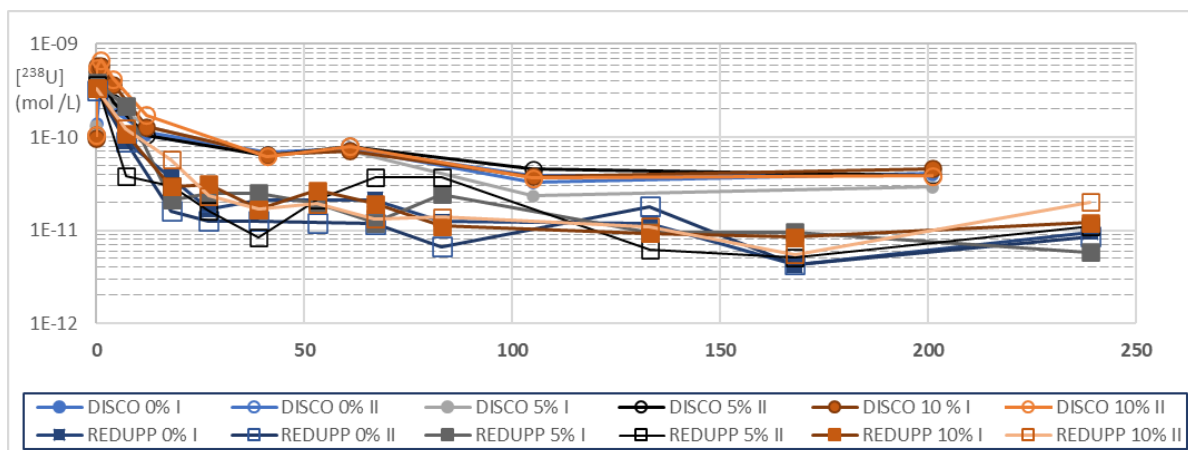


**Figure 5:** Evolution of  $^{238}\text{U}$  concentrations in DisCo leaching experiments with ~ 1 g samples in OL KR6 water with different doping levels during 200 days of the experiment. The results of REDUPP project in same conditions are presented in comparison (I and II stand for parallel experiments e.g. 1-0 and 2-0).

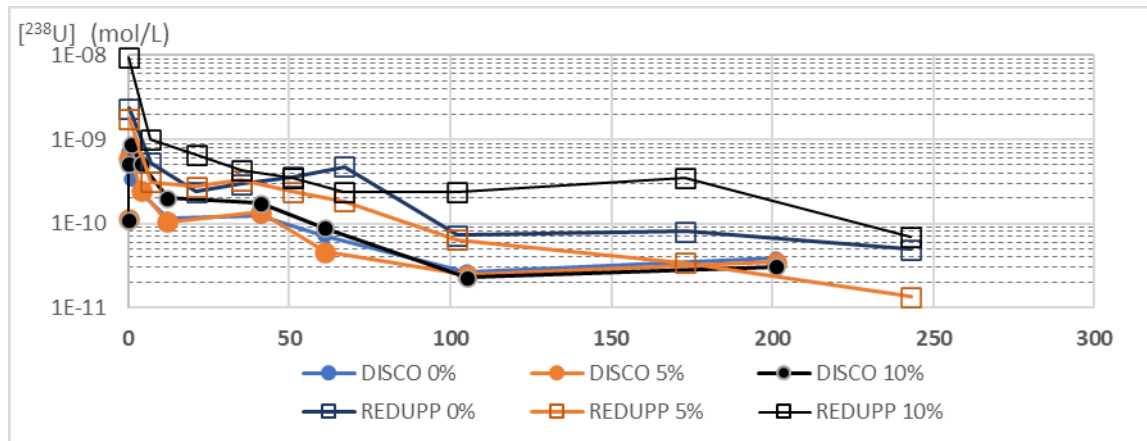


**Figure 6:** Comparison of  $^{238}\text{U}$  concentrations in these DisCo and REDUPP leaching experiments with  $\sim 3$  g samples in OL KR6 water with different doping levels during 250 days of the experiment.

In addition to concentrations, isotopic ratio  $^{235}\text{U}/^{238}\text{U}$  in the aqueous phase was measured from the samples. The initial ratio 7.9 drop below 1 in after 10 days and below 0.1 after 50 days in all experiments as shown in Figure 7. When taking into account the original ratios in solid and aqueous phase and the change and the original concentration in we can use the ratio to calculate the cumulative release from solid phase to solution.

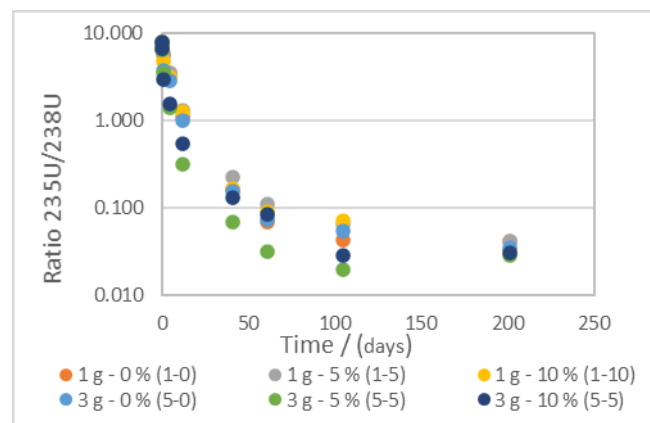


**Figure 7:** Evolution of  $^{235}\text{U}/^{238}\text{U}$  ratios in  $\text{UO}_2$  dissolution experiments conducted in OL-KR6 water.

Figure 8 shows the measured  $^{238}\text{U}$  concentrations (solid) in comparison to ones calculated from original concentrations and the change in isotopic ratio during the experiment. The isotopic dilution method reveals that the cumulative uranium release during the 200 days experiment can be at the magnitude of  $10^{-7}$  mol/L. The calculations tend to produce bigger errors (see Figure 8) as the experimental time extends, because more iteration rounds are needed to calculate the concentrations from initial values at the last sampling point.

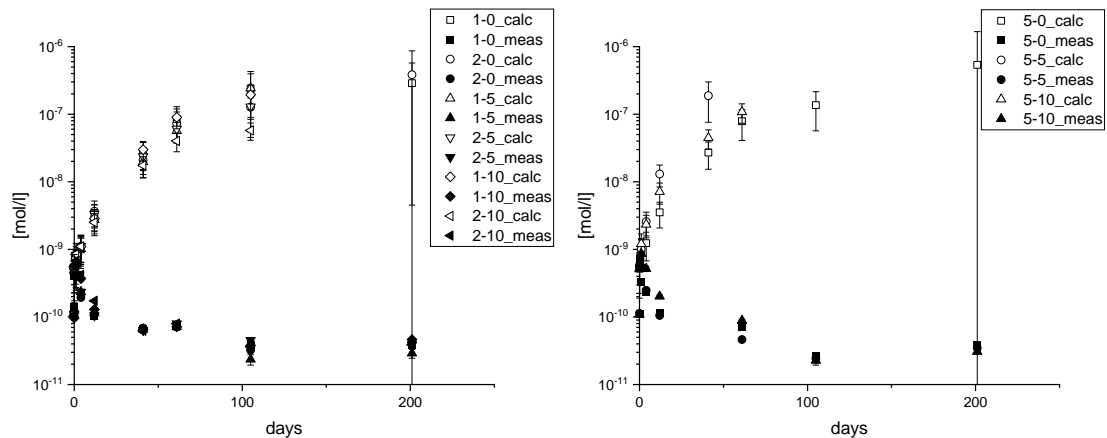


**Figure 8:** Evolution of  $^{238}\text{U}$  measured concentrations (solid) in DisCo leaching experiments with 1 g (left) and  $\sim 3$  g (right) samples in OL KR6 water in comparison to cumulative release (hollow symbols) calculated with isotopic dilution method.

## Conclusions

During the 200 days experiments the solubility of uranium settles between  $2 \cdot 10^{-11}$  and  $5 \cdot 10^{-11}$  mol/L. However, the cumulative release, calculated from isotopic dilution, indicates total release during 200 days has increased above  $1 \cdot 10^{-7}$  mol/L. This describes the amount of total release when dissolution and precipitation/sorption are taking place simultaneously. There are no remarkable differences in measured concentrations between different doping levels. Calculated cumulative concentrations show more scattering, but probably more detailed data analysis is needed to conclude any effects of doping levels as the uncertainties seem to be also larger for calculated concentrations. Thus, clear indication of the effect of doping level could not be observed in OL-KR6 groundwater.

The next experimental series with  $\text{UO}_2$ ,  $\text{UO}_2 + ^{238}\text{Pu}$ -doping,  $\text{UO}_2 + \text{Cr}$  and  $\text{UO}_2 + \text{Cr} + ^{238}\text{Pu}$  will give information, if the Cr-doping will show any effects on the solubility of  $\text{UO}_2$

## Acknowledgement

*The research leading to these results has received funding from the European Commission Horizon 2020 Research and Training Programme of the European Atomic Energy Community (EURATOM) (H2020-NFRP-2016-2017-1) under grant agreement n° 755443 (DisCo project).*

## References

- [1] Ollila, K., Albinsson, Y., Oversby, V., Cowper, M. (2003). Dissolution rates of unirradiated  $\text{UO}_2$ ,  $\text{UO}_2$  doped with  $^{233}\text{U}$ , and spent fuel under normal atmospheric conditions and under reducing conditions using an isotope dilution method. SKB Technical Report, TR-03-13.
- [2] Ollila, K. and Oversby, V. (2004). Measurement of dissolution rates of  $\text{UO}_2$  matrix with the isotope dilution method. MRS Proceedings, 807, 47-52.
- [3] Ollila, K. and Oversby, V. (2005). Dissolution of unirradiated  $\text{UO}_2$  and  $\text{UO}_2$  doped with  $^{233}\text{U}$  under reducing conditions. Posiva Report, 2005-05.

- 
- [4] Ollila, K. (2008). Dissolution of unirradiated UO<sub>2</sub> and UO<sub>2</sub> doped with <sup>233</sup>U in low- and high-ionic strength NaCl under anoxic and reducing conditions. Posiva Working Report, 2008-50.
- [5] Evins, L.Z., Juhola, P., Vähänen, M. (2014). REDUPP Final Report (FP7, agreement no. 269903). Posiva Working Report, 2014-12.
- [6] Ollila, K., Myllykylä, E., Tanhua-Tyrkkö, M., Lavonen, T. (2013). Dissolution rate of alpha-doped UO<sub>2</sub> in natural groundwater. J. Nucl. Mater., 442, 320-325.

# Production and characterisation of $(U_{1-x}Th_x)O_2$ samples to model mixed oxide fuel dissolution

*Perry, E.T., Popel, A.J. and Farnan, I.*

Department of Earth Sciences, University of Cambridge, Cambridge (UK)

---

## 1. Introduction

The objective of this work is to produce homogeneous and inhomogeneous U/Th MOx pellets of the same composition, that can be readily compared with the CEA DisCo study of Pu/U MOx. A first set of pellets were produced before the end of the first reporting period, but had not been fully analysed. This stage of the work, which commenced with the PhD of Emma Perry, builds on that presented last year by attempting to produce more homogenous  $(U/Th)O_2$  samples of a higher density at the target composition (75 mol% U). A simplified oxalate co-precipitation route was used based on a method reported by Altaş et al. [1] for making  $(U_{1-x}Th_x)O_2$  samples. The (U/Th) system serves as an analogue model for the  $(U_{1-x}Pu_x)O_2$  system and was chosen to complement the CEA DisCo study involving the oxidative dissolution of  $(U_{1-x}Pu_x)O_2$  in Callovo-Oxfordian clay water (COx). Following a discrepancy in results obtained at UCAM and CEA on the persistence of peroxide in COx water, methodologies are being developed to better understand the behaviour of peroxide in the dissolution experiments, where there are multiple water components.

## 2. Summary of the results for first batch of pellets

Of the three pellets produced in the first batch last year (B1-P1), one (B1-P1-S1) was characterised using XRD, EDX and SEM.

Using XRD, a lattice parameter for the sintered pellet was found to be 5.514 Å, yielding a nominal pellet composition of  $U_{0.66}Th_{0.34}O_2$  from Vegard's law, however this is unlikely to be a precise description due to the width of the XRD peaks and the fact that Vegard's law is only valid for a true solid solution. If the uranium content is lower than the target 75% due to an incomplete reduction of U(VI) to U(IV) in the solution such that at least some U(VI) remained in solution, then an improvement in the reductive efficiency of U(VI) in the first stage of synthesis could be beneficial.

Figure 1 shows the images produced using an Everhart-Thornley Detector (secondary electrons, SE) and a Circular Backscatter Detector (backscattered electrons, BSE) in high vacuum with an accelerating voltage of 25 kV, a spot size of 4.5 and a dwell time of 3 μs. SE imaging shows open porosity at the surface. This is thought to be due to an estimated sintering temperature of ~1300°C in the atmospherically controlled furnace, this sintering temperature will be increased in future work. In the bottom row of Figure 1, some larger grains can be seen.

The EDX image in Figure 2 shows that there are regions of uneven distribution of uranium and thorium in the sample. At present this is a qualitative observation. An uneven distribution of actinides is characteristic of inhomogeneous mixed oxide uranium plutonium oxide fuel such as that produced by

the MIMAS process. Thus, these samples have some utility in probing this aspect of the oxidative dissolution of mixed actinide oxides under prevailing anoxic conditions. The first stage of sintering is the diffusion of uranium from uranium rich regions so the uneven distribution suggests that the diffusion of uranium was limited. The uranium rich areas probably form from U(VI) after U(IV) Th(IV) precipitate together or due to a differential precipitation rate for U(IV) and Th(IV). An improvement to the first step reduction stage should solve this or alternatively it has been recommended by Claparede et al. [2] that grinding the powders before sintering can result in a smaller composition range.

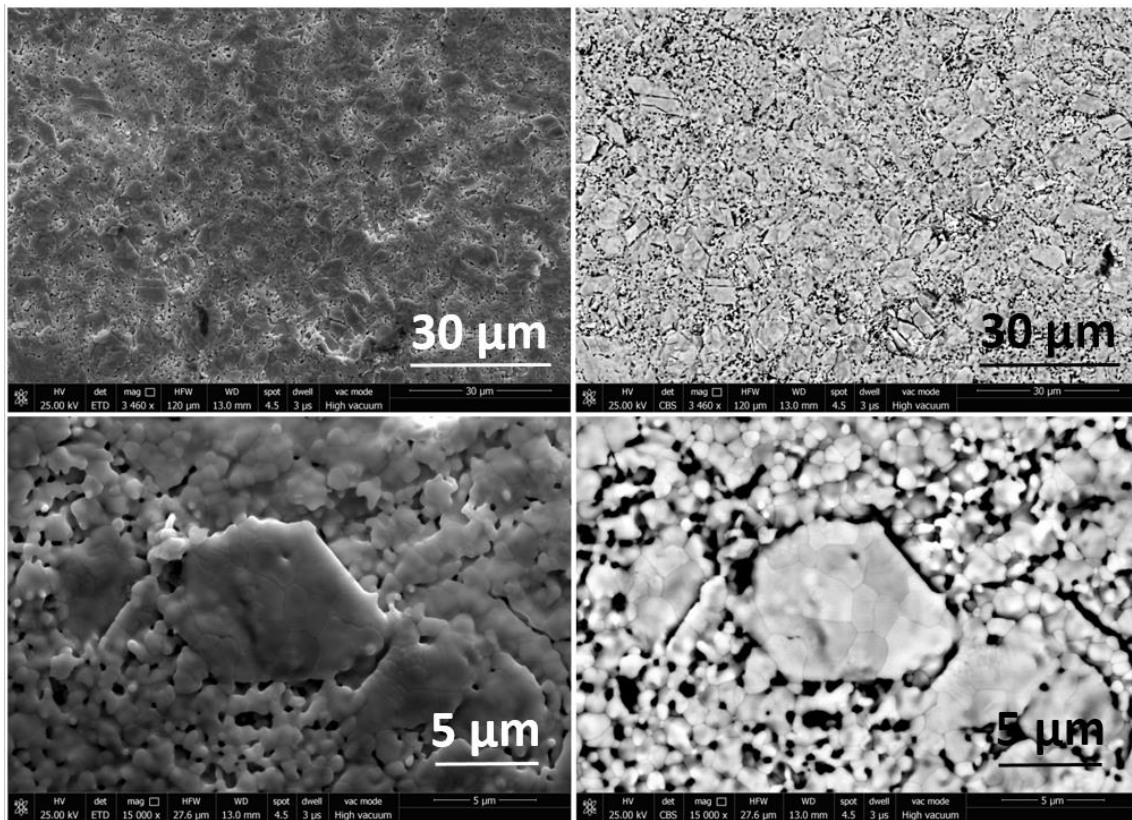


**Figure 1:** SEM images (SE and BSE) of B1-P1-S1 at two different magnifications, 30 μm and 5 μm.

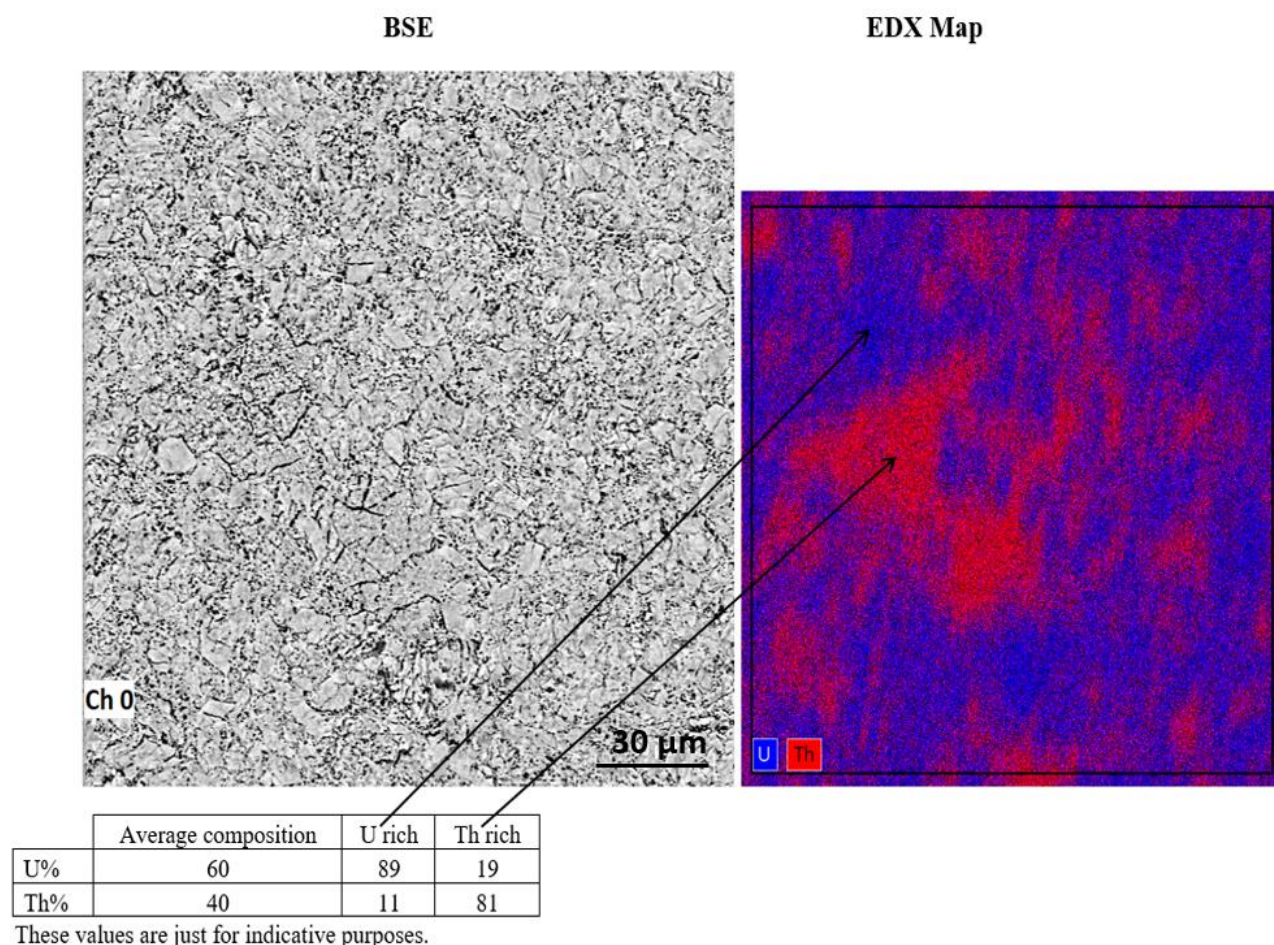


**Figure 2:** BSE and EDX images of B1-P1-S1 at a 30  $\mu\text{m}$  scale.

### 3. Preparation of samples, batch 2

Uranium was supplied in the form of a  $\text{UO}_2(\text{NO}_3)_2 \cdot 6\text{H}_2\text{O}$  salt, where its oxidation state is +6. Since  $\text{U}^{4+}(\text{aq})$  and  $\text{Th}^{4+}(\text{aq})$  have similar solubilities, the key point in preparing  $(\text{U}_{1-x}\text{Th}_x)\text{O}_2$  samples is to reduce  $\text{U}^{6+}(\text{aq})$  to  $\text{U}^{4+}(\text{aq})$  to ensure a congruent co-precipitation with  $\text{Th}^{4+}(\text{aq})$  on addition of oxalic acid. In order to improve the reduction of U(IV) and potentially increase the uranium content of the final pellet, an Adams catalyst as recommended by Sahu et al. [3] was used.

All operations took place in an anoxic glovebox ( $< 0.1$  ppm  $\text{O}_2$ ) with an integrated furnace below the glovebox accessed from the anoxic glovebox. As before, stoichiometric 3:1 uranyl and thorium nitrate solution was prepared under air by dissolving 2.8 g of  $\text{UO}_2(\text{NO}_3)_2 \cdot 6\text{H}_2\text{O}$  and 1.1 g of  $\text{Th}(\text{NO}_3)_4 \cdot 6\text{H}_2\text{O}$  in 5.6 g of deionised Milli-Q (18.2  $\text{M}\Omega \cdot \text{cm}$ ) water to achieve a pellet target composition of  $\text{U}_{0.75}\text{Th}_{0.25}\text{O}_2$ .

0.5 g Adams catalyst (79-83% loading, 75  $\text{m}^2/\text{mg}$  surface area from Sigma Aldrich 459925-1G) was pre-treated in 5.6 mL of 3 M HCl before transfer to the glovebox when it was deaerated using 5%  $\text{H}_2$  / 95% Ar for 5 hours. This solution was added to the uranium thorium nitrate solution and it was bubbled with 5%  $\text{H}_2$  / 95% Ar for 16 hours. Loss due to evaporation was 0.45 g per hour. The catalyst was filtered out. The solution, estimated to have a volume of about 2 mL, remained yellow and no precipitation was observed.



A 200% excess of oxalic acid solution was prepared under ambient air by adding 4.0 g of  $\text{H}_2\text{C}_2\text{O}_4$  to 46.1 g of deionised water. The obtained solution was also deaerated inside the anoxic glove box by bubbling a 5%  $\text{H}_2$  / 95% Ar gas for 3.5 hours. Due to evaporation the weight changed by 1.042 g in this time such that the final solution was 1 mol/L and no precipitate formed.

In the glovebox, the deaerated 1 M oxalic acid solution was added to the prepared U/Th nitrate solution to precipitate a mixed U/Th oxalate. The solution remained yellow, indicating that some uranyl ions were still present in it.

The finely divided solid obtained was filtered and thoroughly washed with deaerated deionised water. It was left to dry on a filter paper in the glove box under anoxic conditions (Ar atmosphere, 0.1 ppm  $\text{O}_2$ ) for a day.

Then, the precipitate was placed into a furnace attached to the Ar atmosphere glove box, where the synthesis took place, to be dried at 70°C. The dried precipitate was decomposed by heating for 3 hours at 530°C and the colour changed from white to dark brown.

## Future Work

Removal of the atmospheric control tube in the glovebox furnace will allow significantly higher temperatures to be obtained while still in an anoxic atmosphere. Together with even with longer sintering times and a second stage of pellet reduction at lower temperature in Ar/ $\text{H}_2$  or  $\text{N}_2$ / $\text{H}_2$  this should allow mixed oxides to be obtained with close to 2.00 stoichiometry, Tan et al (2019) produced  $\text{UO}_{2.01}$  using this method. As a back-up sintering at 1700°C in 5%  $\text{H}_2$  / 95%  $\text{N}_2$  atmosphere in collaboration with the University of Sheffield is possible. Samples will be characterised using XRD, SEM and EDX and annealed at 800°C in a reducing gas mixture at the University of Cambridge before dissolution is studied.

In preparation for the WP4 dissolution study of homogenous and inhomogeneous  $(\text{U}_{1-x}\text{Pu}_x)\text{O}_2$  in COx ground water and  $10^{-4}$  mol/L hydrogen peroxide, we are investigating our previously reported result that there was no loss of peroxide concentration over 14 days when Callovo-Oxfordian groundwaters were introduced to the solution. This potentially contradicts recent results from the CEA group studying unirradiated Pu-MOx. We are developing a methodology to conduct UV/vis spectroscopy of hydrogen peroxide and to carry out direct spectroscopic tests using nuclear magnetic resonance on the same samples. This work aims to explore the performance of a chemical detection method (via the reaction of peroxide to produce a product detected by UV-vis spectroscopy) with more direct measures of peroxide. The presence of iron in solution is known to rapidly decrease peroxide concentration as reported in CEA MOx work presented in WP4.

## Summary

Inhomogeneous samples have been characterised and their dissolution will be studied. In order to increase the homogeneity and potentially the uranium content of the pellets, an improved method of reduction of uranyl ions in the first stage of synthesis has been attempted through use of an Adams catalyst. To minimise the range in composition and the surface porosity the pellets will be sintered for longer times at higher temperatures.



## Acknowledgement

*The research leading to these results has received funding from the European Commission Horizon 2020 Research and Training Programme of the European Atomic Energy Community (EURATOM) (H2020-NFRP-2016-2017-1) under grant agreement n° 755443 (DisCo project). Thanks are given to Giulio I. Lampronti for his help in conducting XRD and SEM study and data analysis. ICO EPSRC Centre for Doctoral Training in Nuclear Energy [Grant EP/L015900/1] for providing a PhD studentship for ETP.*

## References

- [1] Altaş, Y., Eral, M., Tel, H. (1997). Preparation of homogeneous  $(\text{Th}_{0.8}\text{U}_{0.2})\text{O}_2$  pellets via coprecipitation of  $(\text{Th,U})(\text{C}_2\text{O}_4)_2 \cdot n\text{H}_2\text{O}$  powders. *J. Nucl. Mater.*, 249, 46-51.
- [2] Claparede, L., Clavier, N., Mesbah, A., Tocino, F., Szenknect, S., Ravaux, J., Dacheux, N. (2019). Impact of the cationic homogeneity on  $\text{Th}_{0.5}\text{U}_{0.5}\text{O}_2$  densification and chemical durability. *J. Nucl. Mater.*, 514, 368-379.
- [3] Sahu, A., Vincent, T., Shah, J.G., Wattal, P.K. (2014). Reduction of uranium (VI to IV) by hydrogenation using Adams catalyst. *Desalin. Water Treat.*, 52, 426-431.

# Production of unirradiated advanced doped UO<sub>2</sub> fuel for dissolution studies at repository conditions

*Rodríguez-Villagra, N., Fernández, S., Jiménez-Bonales, L., Milena-Pérez, A., Núñez, A., Durán, S., Anta, L., Gutiérrez, L. and Cobos, J.*

CIEMAT, Madrid (ES)

---

## 1. Introduction

Extensive work has been devoted to the conventional UO<sub>2</sub> fuel stability under representative conditions of a Deep Geological Repository (DGR). This research about fuel stability is focused on new promising candidates for improving PCI (Pellet-Cladding Interaction), namely Cr-doped UO<sub>2</sub> (GAIA) and Al-Cr-doped UO<sub>2</sub> (ADOPT); Gd-doped UO<sub>2</sub> was also included, since Gd is a burnable poison and a trivalent rare-earth dopant (RE<sup>III</sup>). The results will be the basis for potential more complex systems which would correspond to real irradiated doped fuels. Previous studies suggest that RE<sup>III</sup> play an important role on UO<sub>2</sub> oxidation [1], revealing that they prevent the complete oxidation to U<sub>3</sub>O<sub>8</sub> [2-3], so in order to better understand the effect of RE<sup>III</sup> dopants, a set of dissolution experiments performed in presence of H<sub>2</sub> is shown. It is well known that HCO<sub>3</sub><sup>-</sup> (one of the key complexing constituents in the groundwater) is highly likely to influence fuel dissolution by enhancing the solubility of U<sup>VI</sup> thus preventing secondary phase formation [4]. Simultaneously, the groundwater-radiation interaction is of interest in DGR because it affects the redox system through several chemical species formation, including H<sub>2</sub>O<sub>2</sub> and H<sub>2</sub> [5]. The presence of reducing species, such as H<sub>2</sub> (anaerobic iron corrosion and radiolytically produced) in combination with H<sub>2</sub>O<sub>2</sub> (the most important radiolytic oxidant) affect the reactivity of UO<sub>2</sub> that could trigger an increase of radionuclides release. H<sub>2</sub> can suppress [6] and H<sub>2</sub>O<sub>2</sub> promotes [7] the oxidative dissolution of the UO<sub>2</sub> surface, therefore both must be considered in a long-term safety assessment.

In order to evaluate the influence of additives (doped fuels) together with H<sub>2</sub> and different leachants on UO<sub>2</sub> matrix stability, dissolution tests were performed in order to acquire further knowledge regarding disposal conditions, within the frame of EC DisCo Project. In this study, UO<sub>2</sub>-based model materials were systematically produced and carefully characterised to understand the effects of the addition of Cr- or Al-oxide into the fuel matrix on SNF dissolution behaviour under repository relevant conditions. Specimens were fabricated by homogenizing stoichiometric proportions of UO<sub>2</sub> with a nominal concentration of 0.06 wt.% Cr<sub>2</sub>O<sub>3</sub>, 0.05 wt.% Cr<sub>2</sub>O<sub>3</sub> - 0.02 wt.% Al<sub>2</sub>O<sub>3</sub> and 4.5 wt.% Gd<sub>2</sub>O<sub>3</sub> over the UO<sub>2</sub> total mass. Prepared samples were characterized using XRD, Raman spectroscopy and SEM-EDX. Dissolution experiments of freshly prepared fuel were conducted in synthetic groundwater solutions without and with HCO<sub>3</sub><sup>-</sup> that could be considered as relevant to those coming from the interaction of water between natural barriers (groundwater) and EBS (Engineering Barrier System). The effect of H<sub>2</sub> was studied by means of leaching experiments of doped-UO<sub>2</sub> pellets under a N<sub>2</sub> / 4.7% H<sub>2</sub> atmosphere. The U and dopants concentration released into the aqueous solution were quantified by ICP-MS. pH and redox were also tracked during the experiments.

## 2. Optimization of sample preparation

During the two first years of the project, the manufacturing method [8] was implemented and samples of  $\text{UO}_2$  - 0.06 wt.%  $\text{Cr}_2\text{O}_3$ ,  $\text{UO}_2$  - 0.05 wt.%  $\text{Cr}_2\text{O}_3$  - 0.02 wt.%  $\text{Al}_2\text{O}_3$  and  $\text{UO}_2$  - 4.5 wt.%  $\text{Gd}_2\text{O}_3$  were obtained consistently and well sintered [9], subsequently dissolution tests were carried out with solid samples prepared in WP2, named Initial Samples (IS) manufactured from the Initial Powder (IP).

The model materials (Cr, Cr/Al and Gd-doped  $\text{UO}_2$ ) were synthesised at CIEMAT within the WP2 of this project. However, improvements on the characteristics of the pellets, focusing on achieving a greater increase in the grain size of the  $\text{UO}_2$  - 0.06 wt.%  $\text{Cr}_2\text{O}_3$ , were pursued along the last year. For this purpose, it was decided to start from a pure material, with the aim of breaking the "memory effect" of the material and the possible structural stresses that its atomic structure presents. In order to achieve this, it was decided to start from a  $\text{UO}_2$  Purified Powder ( $\text{UO}_2$  PP). The  $\text{UO}_2$  purification technique consisted of dissolving the solid waste in  $\text{HNO}_3$  4 M, filtering the resultant solution to eliminate possible solid impurities and then selectively separating the uranium, precipitating it and calcining it (Figure 1).

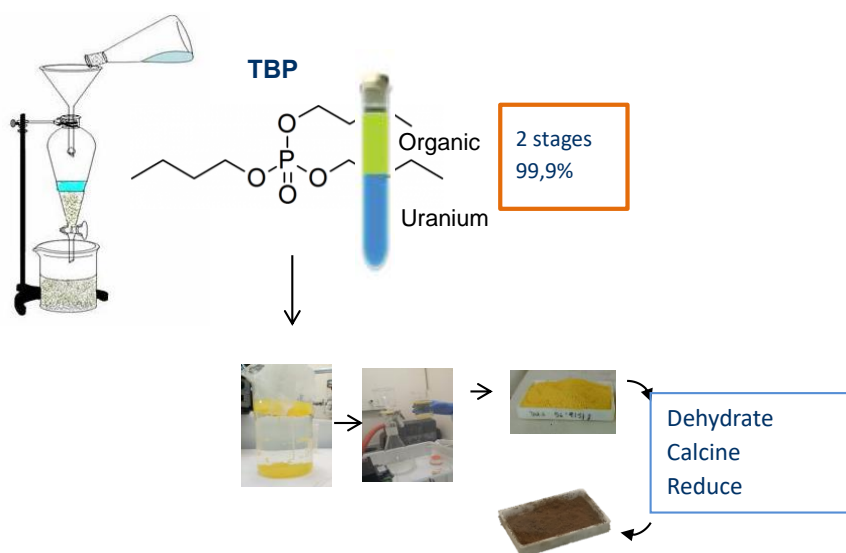


**Figure 1:** Diagram of  $\text{UO}_2$  purification process.

The selective separation of uranium by liquid-liquid extraction process was carried out using tributyl phosphate (TBP), a compound widely used on an industrial scale in the PUREX process [10-12].

In addition, through this process it is possible to optimize the available resources by applying the principles of "circular economy" and at the same time to generate a smaller amount of radioactive waste by purifying and reusing the  $\text{UO}_2$  powder recovered from the waste generated in previous manufacturing processes, such as cutting, grinding and polishing of previously purified material.

X-ray diffractograms of both the  $\text{UO}_2$  Purified Powder and the Initial Powder (PP and IP, respectively) were obtained in order to check the optimal process result. Figure 2 shows that the Full Width at Half Maximum (FWHM) of the diffraction peaks in pattern b) is narrower than pattern a) indicating greater crystallinity than  $\text{UO}_2$  IP and formation of a single and pure phase,  $\text{UO}_2$ .

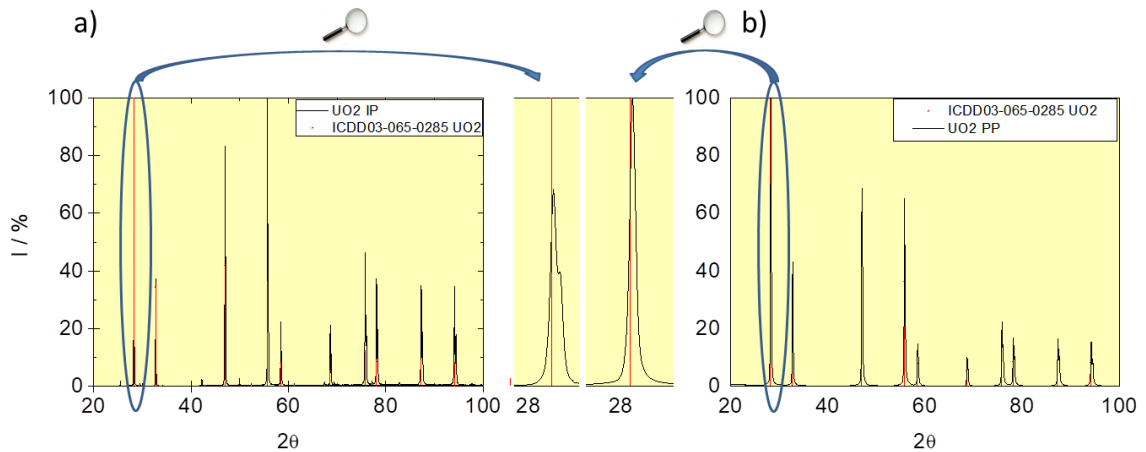


**Figure 2:** XRD pattern of (a) UO<sub>2</sub> initial powder (UO<sub>2</sub> IP) and (b) UO<sub>2</sub> purified powder (UO<sub>2</sub> PP).

From the diffraction peaks measured, a lattice parameter value was obtained by applying the unit cell refinement method. Applying Vegard's equation [13] to determine the state of oxidation, the powder obtained is nearly stoichiometric. Finally, the stoichiometric point will be obtained during the sintering of the monoliths in a reducing atmosphere.

#### Vegard's equation UO<sub>2+x</sub>

$$a_0(\text{Å}) = 5.470 \pm 0.006 - (0.24 \pm 0.08)x, \quad (0 < x < 0.13) \quad \text{Eq. 1}$$

$$a_0 = 0.546632(4) \text{ nm} \rightarrow x = 0.02 \gg \text{UO}_{2.02}$$

On the other hand, a higher Cr<sub>2</sub>O<sub>3</sub> Purity Powder supplied by Alfa - Aesar (Cr<sub>2</sub>O<sub>3</sub> PP) than previous used in the fabrication (IP) was also used in this new batch of UO<sub>2-x</sub> wt.% Cr<sub>2</sub>O<sub>3</sub> samples production. A narrower FWHM of the peaks is also obtained with the Cr<sub>2</sub>O<sub>3</sub> PP, thus demonstrating its higher crystallinity, as can be seen in Figure 3b.

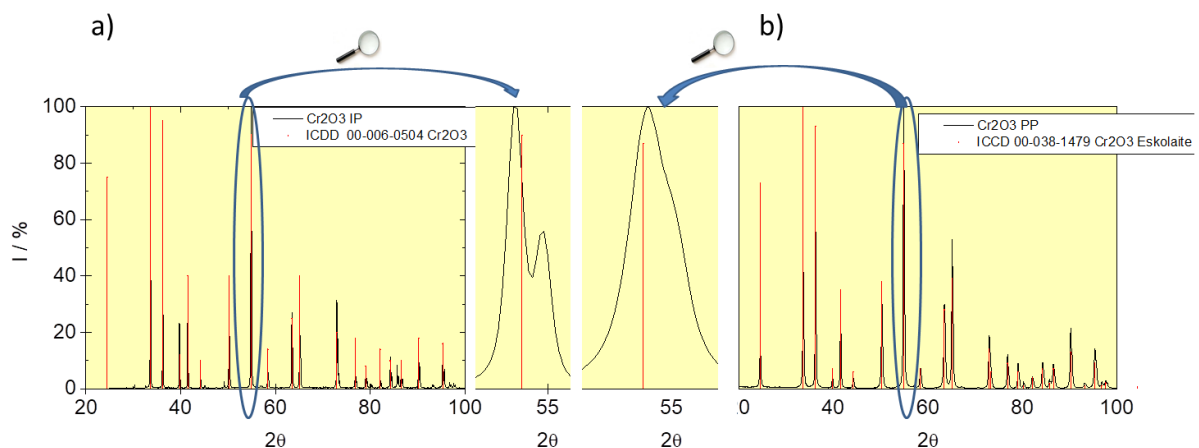


**Figure 3:** XRD pattern of (a) Cr<sub>2</sub>O<sub>3</sub> initial powder (Cr<sub>2</sub>O<sub>3</sub> IP) and (b) Cr<sub>2</sub>O<sub>3</sub> purity powder (Cr<sub>2</sub>O<sub>3</sub> PP).

Regarding particle size distribution, Figure 4 shows how  $\text{UO}_2$  PP have significantly reduced their particle size from  $19.6 \mu\text{m}$  to  $3.68 \mu\text{m}$ . In contrast, the  $\text{Cr}_2\text{O}_3$  PP have a high particle size and larger particle size range, indicating the need to use the mill to reduce it.

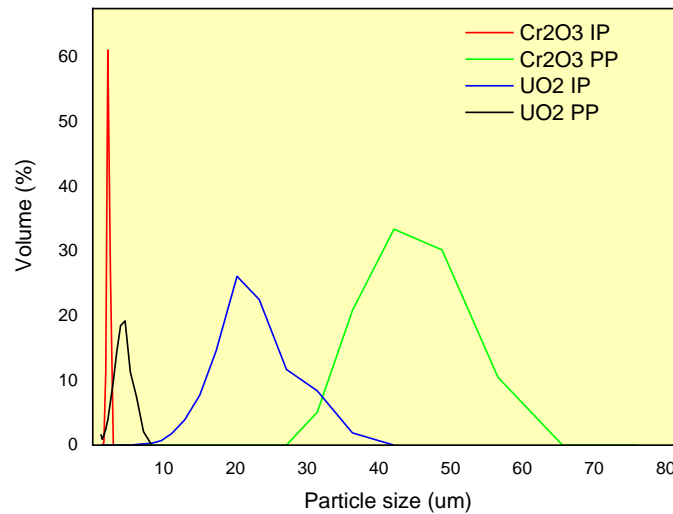


**Figure 4:** Particle size distribution of initial and improved (purified y purity) starting materials  $\text{UO}_2$  and  $\text{Cr}_2\text{O}_3$ .

Table 1 shows a summary of the characterisation (median for a volume distribution of particle size  $D(v,0.5)$ , specific surface area SSA and lattice parameter) of the IP and the PP.

**Table 1:** Raw material characterization.

Sample	Lattice parameter (nm)	SSA (BET) ( $\text{m}^2/\text{g}$ )	$D(v,0.5)$ ( $\mu\text{m}$ )
$\text{UO}_2$ IP	$a = b = c = 0.546920(4)$	$0.95 \pm 0.02$	10.97
$\text{UO}_2$ PP	$a = b = c = 0.546632(4)$	$4.67 \pm 0.04$	3.52 - 3.68
$\text{Cr}_2\text{O}_3$ IP	$a = b = 0.49586(7); c = 1.3592(2)$	$3.47 \pm 0.02$	5.22
$\text{Cr}_2\text{O}_3$ PP	$a = b = 0.495943(5); c = 1.359586(1)$	$16.63 \pm 0.12$	40.52

Once the powders were mixed in the right proportions, the monoliths were obtained by pressing them. They were sintered and by polishing and revealing them they were prepared for characterization. For the time being, we are continuing with this characterization and the interpretation of the data obtained. However, the exact dopant contents of the pellets prepared are not sufficient to test the broad question of how Cr is dissolved in the  $\text{UO}_2$  matrix. More pellets will be prepared to undertake more dissolution tests.

### 3. Autoclave dissolution experiments

To understand the matrix dissolution of modern LWR fuels and in particular the effect of Cr on the dissolution rate of the spent fuel, Cr, Cr/Al and Gd-doped materials have been prepared, within WP2 of this project. These model materials have been exposed to three reference waters: inert system  $\text{NaClO}_4$  at pH 7.2 (PC), bicarbonate water at pH 8.9 (BC) and young cementitious water at pH 13.5 (YCW-Ca)

relevant for geological disposal in 4.7% H<sub>2</sub> / N<sub>2</sub> atmosphere, initially assumed as reducing conditions but unforeseen oxygen intrusion must have occurred due to the unexpectedly high U concentrations found. The role of perchlorate system used as a blank test (without carbonate) is to adjust low ionic strength with a non-complexing agent because of its low reactivity in order to be compared with BC and YCW-Ca systems. The model materials synthesised according to a protocol developed within the WP2 of this project at CIEMAT along the first year of the project, have been used to start the leaching tests in the second trimester of 2018, while the improved fabrication procedure of Cr doped UO<sub>2</sub> will be completed in the second trimester of 2020.

First batch of doped UO<sub>2</sub> disks were leached and once the fabrication of new improved Cr-UO<sub>2</sub> samples will be completed, new leaching tests are foreseen in the first semester 2020. In anticipation of the improved model materials, preparatory leaching experiments were performed at 4.7% H<sub>2</sub> / N<sub>2</sub>. Static dissolution experiments were started in the first semester of 2018 with doped UO<sub>2</sub>, either in inert water (PC: NaClO<sub>4</sub> 20 mM) at pH 7.2, bicarbonate solution (BC: 19 mM NaHCO<sub>3</sub> + 1 mM NaCl) at pH 8.5 and Young Cementitious Water at pH 13.5 (YCW-6). Further details about the simulated water compositions are shown in Table 2 (YCW-Ca light was improved with regard to the last meeting by bettering reagents purity and lowering Ca content, see column referred as YCW-3 at Table 2). All tests were performed in an Ar glove box at room temperature in autoclaves under 7-8 bar 4.7% H<sub>2</sub> / N<sub>2</sub> (inert system without Pt and BC and YCW-Ca with a Pt wire, in which sample disk was suspended). Even though in previous description of experiments, in the 1<sup>st</sup> and 2<sup>nd</sup> Annual Meetings, O<sub>2</sub> concentration in the glove box was reported to be below 2 ppm, a failure of oxygen sensor was identified during the latest experiments (YCW) and hence, real concentration reached was 1000 ppm along all the tests. Stainless steel autoclaves with a PEEK insert were described in previous report [14]. For this dissolution experiments, the pellets were first annealed at 1000°C in reducing conditions. Aliquots of aqueous phase were collected through a sampling valve without opening the reactor, due to the overpressure inside the reactor. Then, autoclaves were refilled with 4.7% H<sub>2</sub> / N<sub>2</sub> up to 8 bar.

Filtered (GHP Acrodisc, PALL, 0.2 µm) and ultrafiltered (Amicon Ultra-4 3k de Millipore, < 2 nm) samples were measured by ICP-MS to quantify dissolved U concentrations. However, for a better measurement of U in solution this filtration procedure was changed from the sixth sampling in YCW-Ca experiments, therefore samples were not-filtered and ultrafiltered. At the end of each experiment, autoclaves were rinsed with 2 M HNO<sub>3</sub> in order to estimate the amount of U sorbed on the system.

**Table 2:** Composition of the synthetic aqueous media.

Conc. (mol/L)	PC-1	BC-1	YCW-3 (YCW-Ca)	YCW-6
Na	$2.18 \cdot 10^{-2}$	$2.1 \cdot 10^{-2}$	$1.35 \cdot 10^{-1}$	$1.3 \cdot 10^{-1}$
Mg	$2.07 \cdot 10^{-6}$	$1.48 \cdot 10^{-6}$	$2 \cdot 10^{-6}$	< LOQ
Al	$3.61 \cdot 10^{-10}$	$3.55 \cdot 10^{-9}$	$5.0 \cdot 10^{-8}$	$4 \cdot 10^{-9}$
K	$2.80 \cdot 10^{-4}$	$1.40 \cdot 10^{-4}$	$3.46 \cdot 10^{-1}$	$3 \cdot 10^{-1}$
Ca	$2.89 \cdot 10^{-6}$	$5.6 \cdot 10^{-6}$	$7.8 \cdot 10^{-4}$	$1.7 \cdot 10^{-4}$
Cr	$1.9 \cdot 10^{-9}$	$4 \cdot 10^{-9}$	$7 \cdot 10^{-8}$	$9.2 \cdot 10^{-8}$

Conc. (mol/L)	PC-1	BC-1	YCW-3 (YCW-Ca)	YCW-6
Mn	$7.0 \cdot 10^{-9}$	$1.9 \cdot 10^{-8}$	$1.6 \cdot 10^{-7}$	$3 \cdot 10^{-8}$
Fe	$3.4 \cdot 10^{-8}$	$9 \cdot 10^{-8}$	$9.3 \cdot 10^{-7}$	$4.2 \cdot 10^{-7}$
Co	$3.9 \cdot 10^{-10}$	$1.43 \cdot 10^{-9}$	$1.8 \cdot 10^{-9}$	< LOQ
Ni	< $1.7 \cdot 10^{-9}$	< $1.7 \cdot 10^{-9}$	< $1.7 \cdot 10^{-9}$	< LOQ
Cu	$2.3 \cdot 10^{-9}$	$1.2 \cdot 10^{-8}$	$2.2 \cdot 10^{-7}$	$9.7 \cdot 10^{-8}$
Cs	$1.9 \cdot 10^{-10}$	$1.38 \cdot 10^{-9}$	$1.7 \cdot 10^{-9}$	$2.3 \cdot 10^{-10}$
Ba	$9.9 \cdot 10^{-9}$	$1.8 \cdot 10^{-8}$	$1.4 \cdot 10^{-7}$	$1.9 \cdot 10^{-8}$
Ce	$7.1 \cdot 10^{-12}$	$1 \cdot 10^{-10}$	< $7 \cdot 10^{-12}$	< LOQ
Gd	$9 \cdot 10^{-12}$	$8 \cdot 10^{-11}$	< $6 \cdot 10^{-12}$	< LOQ
Pb	$5.7 \cdot 10^{-10}$	$5.3 \cdot 10^{-9}$	$4.0 \cdot 10^{-8}$	$1.5 \cdot 10^{-8}$
Th	< $4.3 \cdot 10^{-12}$	< $4.3 \cdot 10^{-12}$	< $4.3 \cdot 10^{-12}$	< LOQ
U	$1.2 \cdot 10^{-10}$	$3.6 \cdot 10^{-9}$	$5.9 \cdot 10^{-9}$	< LOQ
Cl <sup>-</sup>	$1.0 \cdot 10^{-4}$	$1.1 \cdot 10^{-3}$	$3.9 \cdot 10^{-4}$	$1.5 \cdot 10^{-8}$
SO <sub>4</sub> <sup>2-</sup>	-	$3.3 \cdot 10^{-5}$	$2.5 \cdot 10^{-4}$	$1.9 \cdot 10^{-3}$
pH	$7.2 \pm 0.1$	$8.9 \pm 0.1$	$13.5 \pm 0.1$	$13.5 \pm 0.1$

Figures 5 illustrate the U released vs. time for dissolution of a) UO<sub>2</sub> - 0.06 wt.% Cr<sub>2</sub>O<sub>3</sub>, b) UO<sub>2</sub> - 0.05 wt.% Cr<sub>2</sub>O<sub>3</sub> - 0.02 wt.% Al<sub>2</sub>O<sub>3</sub>, and c) UO<sub>2</sub> - 4.5 wt.% Gd<sub>2</sub>O<sub>3</sub>, respectively. Based on the first series of tests, H<sub>2</sub> atmosphere (pH<sub>2</sub> = 0.37 ± 1 bar) was not capable to maintain system reducing conditions, as it is suggested from data. Filled symbols correspond to filtered (or not-filtered) and empty symbols to ultrafiltered samples quantified by ICP-MS. The U concentration in the solutions reached plateau levels in PC and YCW-6, but not in BC.

At pH = 7.2 (PC) the filtered U concentration remains close to 10<sup>-9</sup> M for the three doped UO<sub>2</sub> samples over the whole test duration (~ 140 d), close to the solubility limit of 10<sup>-8</sup> - 10<sup>-9</sup> M [15]. At pH 8.9 (BC), higher U concentrations are quantified compared to those at 7.2 (~ 10<sup>-6</sup> M for Cr-doped UO<sub>2</sub>, ~ 10<sup>-7</sup> M for Cr/Al-doped UO<sub>2</sub> and ~ 10<sup>-8</sup> M for Gd-doped UO<sub>2</sub>). The trend of U concentration in solution shows that there is a slight increase in dissolution with time for the Cr-doped UO<sub>2</sub> in BC with no plateau when compared with PC or YCW-6 media. This could be caused by oxidation/dissolution of the pellet surface, promoted by the complexing agent HCO<sub>3</sub><sup>-</sup>. Nevertheless, as it was suggested by USFD in [14] more analysis for longer time periods is required. At pH = 13.5, U concentrations are similar to those in the tests in BC, despite the highest HCO<sub>3</sub><sup>-</sup>/CO<sub>3</sub><sup>2-</sup> concentration measured in YCW-6 (0.45 M) and for both, no differences were found between filtered/not-filtered and ultrafiltered samples. Ollila [16] pointed out the redox sensitivity of the U solubility at strongly alkaline pH like cement pore water conditions. It suggests that the measured Eh (YCW-6) in these experiments in the range of -9 to -40 mV could be enough to increase the U concentrations even if in BC the Eh has been found to be higher (70-138 mV).

We can confirm with the current data that U is extremely sensitive to oxidative dissolution at high pH (13.5). The almost negligible differences between filtered/not-filtered and ultrafiltered samples are considered as an indication that there was no colloids formation for any of the experiments.

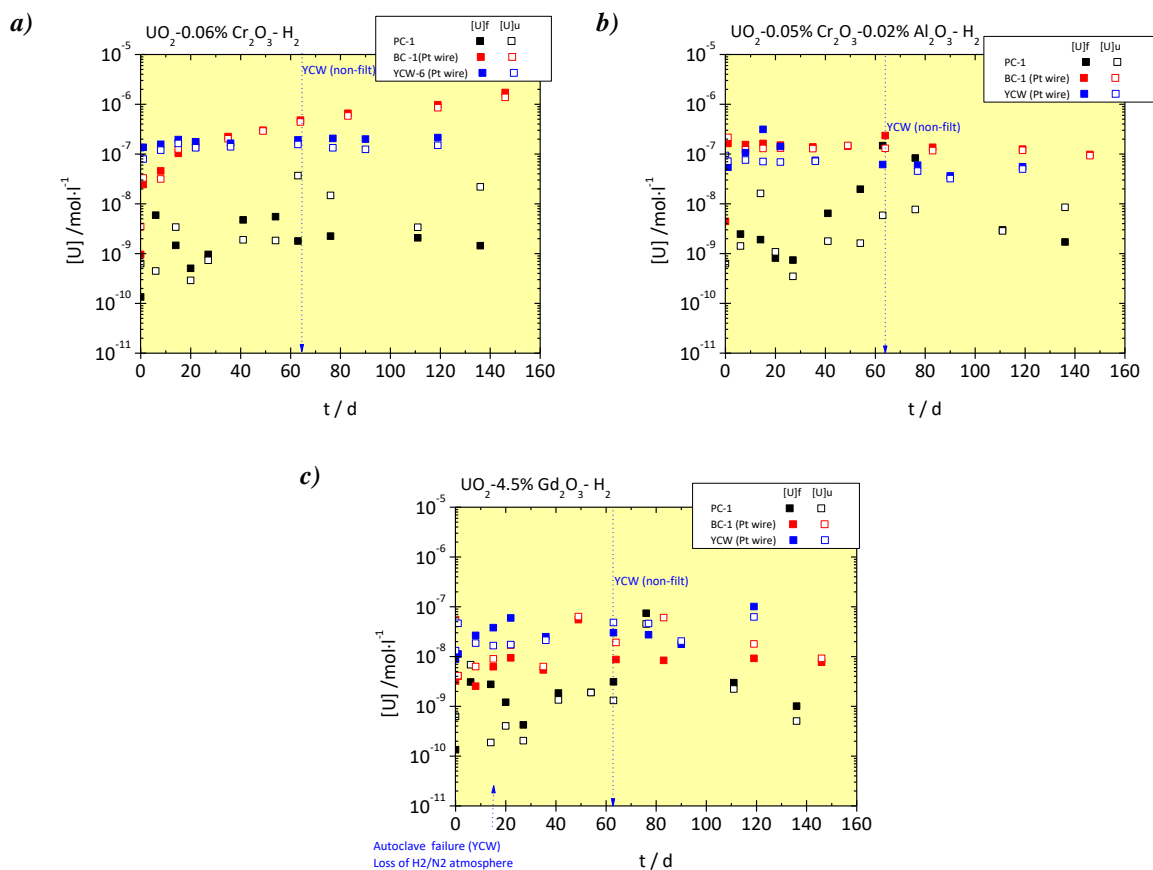


**Figure 5:** U concentration measured for the first test series of (a)  $\text{UO}_2$  - 0.06 wt.%  $\text{Cr}_2\text{O}_3$ , (b)  $\text{UO}_2$  - 0.05 wt.%  $\text{Cr}_2\text{O}_3$  - 0.02 wt.%  $\text{Al}_2\text{O}_3$  and (c)  $\text{UO}_2$  - 4.5 wt.%  $\text{Gd}_2\text{O}_3$  in 0.02 M  $\text{NaClO}_4$  (pH = 7.2), 0.019 M  $\text{NaHCO}_3$  (pH = 8.9, Pt wire) and YCW-6 (pH = 13.5, Pt wire) in autoclave experiments ( $p\text{H}_2 = 0.37 \pm 1$  bar) at  $22 \pm 3^\circ\text{C}$ . Filled symbols represent filtered (or not-filtered) and empty symbols are ultrafiltered.

The normalised dissolution rates of U ( $R_L(\text{U})$  in  $\text{g}/\text{m}^2\cdot\text{d}$ ) as a function of time were calculated from the concentrations of dissolved U, the geometric surface area, the U mass fraction in the solid sample and the initial mass of sample. Generally, the normalized dissolution rate profile decreased vs. time, as shown in Figure 6 for samples a)  $\text{UO}_2$  - 0.06 wt.%  $\text{Cr}_2\text{O}_3$ , b)  $\text{UO}_2$  - 0.05 wt.%  $\text{Cr}_2\text{O}_3$  - 0.02 wt.%  $\text{Al}_2\text{O}_3$ , and c)  $\text{UO}_2$  - 4.5 wt.%  $\text{Gd}_2\text{O}_3$ .



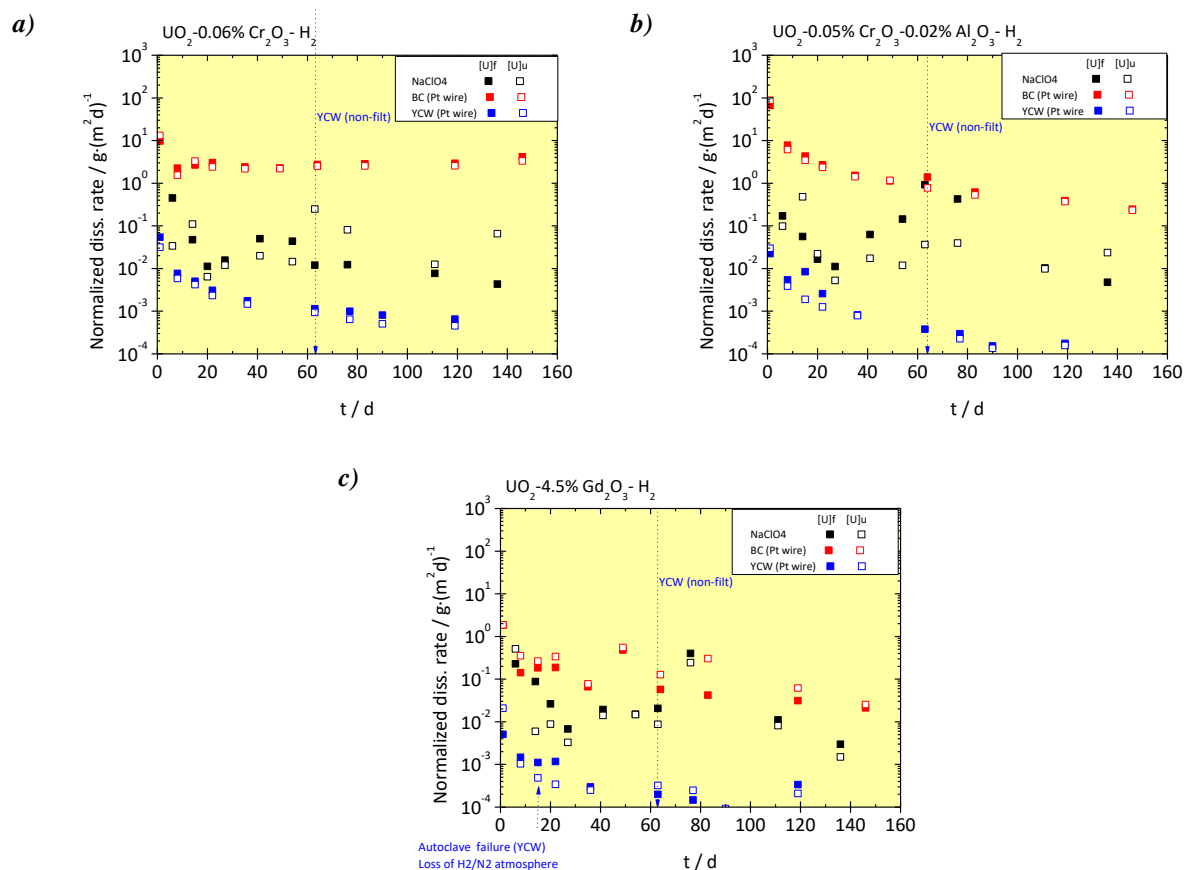


**Figure 6:**  $R_L(U)$  for the first test series of (a)  $UO_2 - 0.06 \text{ wt.}\% Cr_2O_3$ , (b)  $UO_2 - 0.05 \text{ wt.}\% Cr_2O_3 - 0.02 \text{ wt.}\% Al_2O_3$  and (c)  $UO_2 - 4.5 \text{ wt.}\% Gd_2O_3$  in 0.02 M NaClO<sub>4</sub> (pH = 7.2), 0.019 M NaHCO<sub>3</sub> (pH = 8.9, Pt wire) and YCW-6 (pH = 13.5, Pt wire) in autoclave experiments ( $p_{H_2} = 0.37 \pm 1 \text{ bar}$ ) at  $22 \pm 3^\circ\text{C}$ . Filled symbols represent filtered (or not-filtered) and empty symbols are ultrafiltered.

For the sake of simplicity, even though  $R_L(U)$  values have been plotted in  $\text{g}/\text{m}^2 \cdot \text{d}$  as other colleagues in the project, all of them has been re-calculated in  $\text{mol}/\text{m}^2 \cdot \text{d}$  for comparison to literature data.

In PC solution (pH = 7.2), the initial/final dissolution rates were found to be  $2 \cdot 10^{-3}$  to  $3 \cdot 10^{-5} \text{ mol}/\text{m}^2 \cdot \text{d}$  for Cr-doped  $UO_2$  pellet,  $7 \cdot 10^{-4}$  to  $3 \cdot 10^{-5} \text{ mol}/\text{m}^2 \cdot \text{d}$  for the Cr/Al-doped  $UO_2$  and  $1 \cdot 10^{-3}$  to  $3 \cdot 10^{-5} \text{ mol}/\text{m}^2 \cdot \text{d}$  for the Gd-doped  $UO_2$ . Taking into account the low geometric surface area, the final U dissolution rates for the shown pellets are quite similar, it seems that the dopant has no significant effect on the dissolution rates of these  $UO_2$ -based materials, although Gd- $UO_2$  that has been found to have the lowest value.

In BC solution (pH = 8.9), normalised dissolution rates were significantly higher, as the bicarbonate concentration was higher than other values used in literature. In this media the initial/final dissolution rates were found to be  $4 \cdot 10^{-2}$  to  $2 \cdot 10^{-2} \text{ mol}/\text{m}^2 \cdot \text{d}$  for Cr-doped  $UO_2$  pellet,  $3 \cdot 10^{-1}$  to  $1 \cdot 10^{-3} \text{ mol}/\text{m}^2 \cdot \text{d}$  for the Cr/Al-doped  $UO_2$  and  $8 \cdot 10^{-3}$  to  $9 \cdot 10^{-5} \text{ mol}/\text{m}^2 \cdot \text{d}$  for the Gd-doped  $UO_2$ . The obtained data are far from those obtained by Gimenez et al. [17] for unirradiated  $UO_2$  in flow through reactors using  $[HCO_3^-] 10^{-3} \text{ M}$ . The mentioned authors of the flow through experiments reported a dissolution rate of U of  $9 \cdot 10^{-6} \text{ mol}/\text{m}^2 \cdot \text{d}$ .

In YCW-6 solution (pH = 13.5), normalised dissolution rates were significantly higher as the bicarbonate concentration was higher than other values used in literature. In this media the initial/final dissolution rates were found to be  $2 \cdot 10^{-4}$  to  $3 \cdot 10^{-6}$  mol/m<sup>2</sup>·d for Cr-doped UO<sub>2</sub> pellet,  $9 \cdot 10^{-5}$  to  $7 \cdot 10^{-7}$  mol/m<sup>2</sup>·d for the Cr/Al-doped UO<sub>2</sub> and  $2 \cdot 10^{-5}$  to  $9 \cdot 10^{-7}$  mol/m<sup>2</sup>·d for the Gd-doped UO<sub>2</sub>.

SEM, XRD and Raman measurements on pellets after the dissolution experiments are in progress and will complement the picture of data obtained. In addition, more studies of the dissolution as a function of dopant concentration are essential to predict this effect at long-term behaviour.

## Acknowledgement

*The research leading to these results has received funding from the European Commission Horizon 2020 Research and Training Programme of the European Atomic Energy Community (EURATOM) (H2020-NFRP-2016-2017-1) under grant agreement n° 755443 (DisCo project).*

## References

- [1] Curti, E., Miron, G.D., Kulik, D.A. (2019). Development and application of a solid solution model for Cr doped UO<sub>2</sub> fuel. Deliverable D1.15: 2<sup>nd</sup> Annual Workshop Proceedings. DisCo project (Grant Agreement: 755443).
- [2] Kim, J.-G., Ha, Y.-K., Park, S.-D., Jee, K.-Y., Kim, W.-H. (2001). Effect of a trivalent dopant, Gd<sup>3+</sup>, on the oxidation of uranium dioxide. *J. Nucl. Mater.*, 297(3), 327-331.
- [3] Olds, T.A., Karcher, S.E., Kriegsman, K.W., Guo, X., McCloy, J.S. (2020). Oxidation and anion lattice defect signatures of hypostoichiometric lanthanide-doped UO<sub>2</sub>. *J. Nucl. Mater.*, 530, 151959.
- [4] Hossain, M.M., Ekeroth, E., Jonsson, M. (2006). Effects of HCO<sub>3</sub><sup>-</sup> on the kinetics of UO<sub>2</sub> oxidation by H<sub>2</sub>O<sub>2</sub>. *J. Nucl. Mater.*, 358(2-3), 202-208.
- [5] Dzaugis, M.E., Spivack, A.J., D'Hondt, S. (2015). A quantitative model of water radiolysis and chemical production rates near radionuclide-containing solids. *Radiat. Phys. Chem.*, 115, 127-134.
- [6] Carbol, P., Cobos-Sabate, J., Glatz, J.-P., Ronchi, C., Rondinella, V., Wegen, D.H., Wiss, T., Loida, A., Metz, V., Kienzler, B., Spahiu, K., Grambow, B., Quiñones, J., Martínez Esparza, A. (2005). The effect of dissolved hydrogen on the dissolution of <sup>233</sup>U doped UO<sub>2</sub>(s), high burnup spent fuel and MOX fuel. SKB Technical Report, TR-05-09.
- [7] Lousada, C.M., Trummer, M., Jonsson, M. (2013). Reactivity of H<sub>2</sub>O<sub>2</sub> towards different UO<sub>2</sub>-based materials: The relative impact of radiolysis products revisited. *J. Nucl. Mater.*, 434(1-3), 434-439.
- [8] Fernandez, S., Nieto, M.I., Cobos, J., Moreno, R. (2016). CeO<sub>2</sub> pellet fabrication as spent fuel matrix analogue. *J. Eur. Ceram. Soc.*, 36, 3505-3512.
- [9] Cobos, J., Rodríguez-Villagra, N., Fernández, S., Gutierrez, L., Bonales, L.J., Durán, S., Anta, L. (2018). Ongoing CIEMAT activities on fabrication and stability studies of doped UO<sub>2</sub> in the frame of the DisCo project: sample characterization, experimental set-up and first results. D2.1: 2<sup>nd</sup> Annual Meeting Proceedings. DisCo project (Grant Agreement: 755443).
- [10] Madic, C. (2000). Overview of the hydrometallurgical and pyrometallurgical processes studied worldwide for the partitioning of high active nuclear wastes. Proceedings of OCDE-NEA 6<sup>th</sup> Information Exchange Meeting on P&T.
- [11] Mathur, J., Murali, M.S., Nash, K.L. (2001). Actinide partitioning - a review. *Solvent Extr. Ion Exch.*, 19(3), 357-390.

- 
- [12] Baetslé, L.H., Wakabayashi, T., Sakurai, S. (1999). Status and assessment report on actinide and fission product partitioning and transmutation. OECD/NEA Paris, France.
- [13] Rousseau, G., Desgranges, L., Charlot, F., Millot, N., Nièpce, J.C., Vladivieso, F., Baldinozzi, G., Bérrar, J.F. (2006). A detailed study of  $\text{UO}_2$  to  $\text{U}_3\text{O}_8$  oxidation phases and the associated rate-limiting steps. *J. Nucl. Mater.*, 355, 10-20.
- [14] Bosbach, D., Cachoir, C., Myllykylä, E., Jegou, C., Cobos, J., Farnan, I., Corkhill, C. (2019). Deliverable D4.1: Model materials experiments: First dissolution results. DisCo project (Grant Agreement: 755443).
- [15] Yajima, T., Kawamura, Y., Ueta, S. (1995). Uranium(IV) solubility and hydrolysis constants under reduced conditions. *MRS Proceedings*, 353, 1137-1142.
- [16] Ollila, K. (2008). Solubility of  $\text{UO}_2$  in the high pH range in 0.01 to 0.1 M NaCl solution under reducing conditions. POSIVA Working Report, 2008-75.
- [17] Gimenez, J., Clarens, F., Casa, I., Rovira, M., de Pablo, J., Bruno, J. (2005). Oxidation and dissolution of  $\text{UO}_2$  in bicarbonate media: Implications for the spent nuclear fuel oxidative dissolution mechanism. *J. Nucl. Mater.*, 345(2-3), 232-238.

# Assessment of long-term durability of Cr<sub>2</sub>O<sub>3</sub> doped UO<sub>2</sub>

*Smith, H., Cordara, T., Mohun, R., Stennett, M.C., Hyatt, N.C. and Corkhill, C.L.*

Immobilisation Science Laboratory, Department of  
Materials Science and Engineering, The University  
of Sheffield, Sheffield (UK)

---

## 1. Introduction

Adaptation of the microstructure of uranium dioxide nuclear fuel has been achieved through doping with additives such as chromium dioxide. The addition of Cr<sub>2</sub>O<sub>3</sub> to the UO<sub>2</sub> matrix results in an enlarged grain size when compared standard UO<sub>2</sub>. Such alteration in grain size has been proven beneficial to in reactor performance, for example, fuel swelling and pellet cladding interactions are reduced, allowing for longer dwell times and general improvement in fuel efficiency [1-4]. The current option for management of post-operation spent fuel is direct disposal in an engineered geological disposal facility (GDF). This will consist of a multi-barrier containment system, designed for the retention of radionuclides and mitigation of radioactive material reaching the biosphere. In the event of failed container conditions, groundwater is expected to reach spent fuel and facilitate corrosion processes. The behaviour of UO<sub>2</sub> in this environment is well established [5], however, the development of Cr<sub>2</sub>O<sub>3</sub> doped fuels has led to a number of studies investigating the incorporation mechanism of Cr into the UO<sub>2</sub> matrix revealing apparent changes in the crystal chemistry [6-9]. As such, the aim of this work is to investigate the dissolution behaviour of a range of Cr<sub>2</sub>O<sub>3</sub> doped UO<sub>2</sub> materials in conditions relevant to geological disposal and begin to understand this behaviour in terms of the direct effects Cr-doping has to UO<sub>2</sub> such as grain size, defect chemistry and oxidation state.

## 2. Experimental methodology

### 2.1 Sample synthesis and preparation

A suite of Cr<sub>2</sub>O<sub>3</sub> doped UO<sub>2</sub> samples were prepared via a wet synthesis route using uranium (VI) nitrate hexahydrate and chromium (III) nitrate nonahydrate in solution. Precipitation of a U/Cr precursor was achieved by adding ammonium hydroxide until a pH of 8-10 was reached. The recovered precursor was converted to the oxide by calcination in a reducing atmosphere (5% H<sub>2</sub> : 95% N<sub>2</sub>) for 4h at 750°C. Powders were then homogenised at 35 Hz for 15 mins and pressed into 6 mm pellets using a uniaxial press. Sintering at 1700°C for 8 h in a reducing atmosphere (5% H<sub>2</sub> : 95% N<sub>2</sub>) produced dense pellets of UO<sub>2</sub> doped with 0, 100, 600, 1200, 1800 and 2400 ppm Cr. Sintered pellets were polished to 1 µm finish and annealed at 1500°C for 4-6 h in a reducing atmosphere.

### 2.2 Characterisation

Geometric densities of sintered pellets were calculated from average geometry and mass measurements, which were used to determine the specific surface area used in dissolution experiments. The microstructures of the Cr-doped UO<sub>2</sub> samples were characterised via Scanning Electron Microscopy (SEM) using a Hitachi TM3030 SEM operating with an accelerating voltage of 15 kV, images were then

used to determine grain size as a function of Cr content. Confirmation of  $\text{UO}_2$  single phase was carried out using X-ray diffraction (XRD) using a Bruker D2 Phase diffractometer utilizing a  $\text{Cu K}\alpha$  source. Investigation of defect formation due to Cr-doping was carried out using Raman spectroscopy; a Renishaw inVia Reflex confocal spectrometer equipped with a Leica DM2500 microscope and a 514 nm (green) argon excitation laser with 1800 lines/mm grating was used for a spectral acquisition between 200 and  $750\text{ cm}^{-1}$ . X-ray absorption spectroscopy was carried out on Cr-doped samples, plus a suite of Cr standards of known oxidation state and coordination environment at Diamond Light Source (UK), Beamline B18. Cr- K-edge XANES (5989 eV) were collected in fluorescence mode.

### 2.3 Durability investigation

Long-term durability experiments were set up using sintered pellets of each Cr-doped concentration, submerged in 50 mL of sodium chloride / bicarbonate solution (19 mM  $\text{NaCl}$  + 1 mM  $\text{NaHCO}_3$ ) at  $25^\circ\text{C}$ . At specific time points, an aliquot of the solution was removed for analysis by Inductively Coupled Plasma-Mass Spectroscopy (ICP-MS, Thermofisher RQ) and fresh solution replaced. The normalised mass loss ( $N_L$ ) of U and Cr was determined using concentration data to calculate an elemental mass loss ( $M(\text{U})$ ) and normalising to the geometric specific surface area ( $S$ ) and the mass fraction of U ( $f(\text{U})$ ) in the sample, according to Eq. 1. Samples were taken at day 1, 3, 7, 14, 21 then weekly up to day 98 and then bi-weekly for the duration of the experiment. Data is shown for analysis performed up to 120 days. The average pH of the leachate for the duration of the experiment was  $7.88 \pm 0.01$ .

$$N_L(\text{U}) = \frac{M(\text{U})}{f(\text{U}) \times S} \quad \text{Eq. 1}$$

## 3. Results and discussion

Initial evaluation of the normalised mass loss of U as a function of dopant concentration showed that durability increased with increasing Cr content (Figure 1a). Similarly, an overall reduction in dissolution rate of U was observed (Figure 1b). These data indicate that as the concentration of Cr in  $\text{UO}_2$  is increased from 0 to 2400 ppm, less U is released into solution.

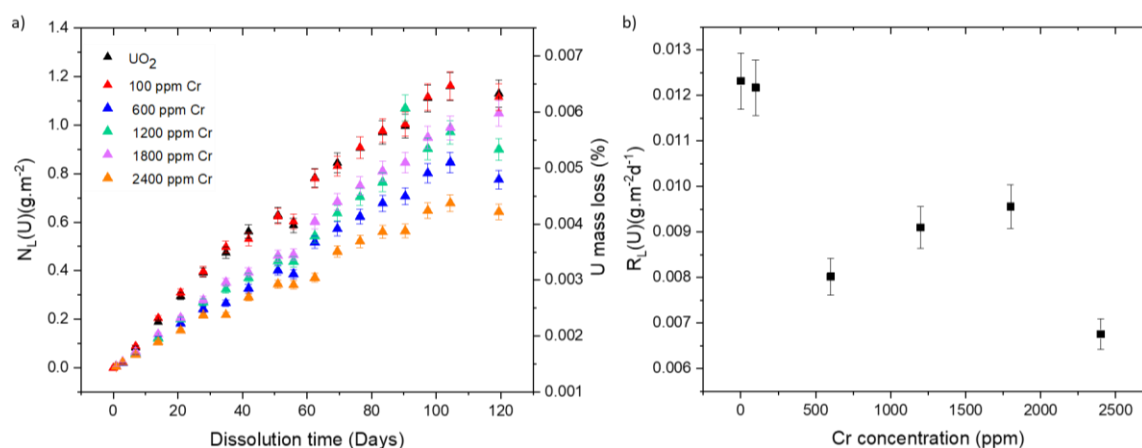


**Figure 1:** (a) Normalised U mass loss ( $\text{g m}^{-2}$ ) and (b) rate of U dissolution ( $\text{g m}^{-2} \text{d}^{-1}$ ) from  $\text{Cr}_2\text{O}_3$ -doped  $\text{UO}_2$  over a 120-day period of dissolution in 19 mM  $\text{NaCl}$  + 1 mM  $\text{NaHCO}_3$  at  $25^\circ\text{C}$ , as a function of  $\text{Cr}_2\text{O}_3$  content.

The relationship between Cr-doping content and dissolution behaviour can be dependent on a number of influencing factors; the first is an increased grain size, induced from Cr doping. It is understood that dissolution occurs preferentially at grain boundaries [10] so as the number of grain boundaries is decreased, the dissolution rate should decrease. However, the change in grain size measured for the samples (grain sizes between 10 and 15  $\mu\text{m}$ ) was not significant enough to observe any relationship with dissolution rate (Figure 2). Further development of the sample fabrication method is required to achieve a large difference in grain size, so that the relationship between grain size and dissolution rate can be ascertained.

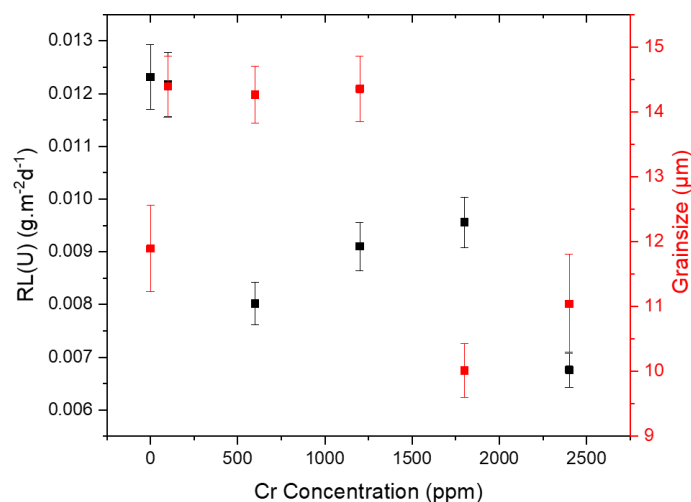


**Figure 2:** Rate of U loss ( $\text{g}/\text{m}^2\cdot\text{d}$ ) compared to average grain size ( $\mu\text{m}$ ), as a function of  $\text{Cr}_2\text{O}_3$  content.

The second factor affecting  $\text{UO}_2$  dissolution is defect formation in the  $\text{UO}_2$  crystal structure. Understanding the type of defects formed upon doping gives an indication of the incorporation mechanism of Cr in  $\text{UO}_2$ . Oxygen interstitials ( $\text{O}_i$ ) are incorporated into the lattice due to oxidation of  $\text{UO}_2$  to hyperstoichiometric  $\text{UO}_{2+x}$ , however, it has been considered that Cr can incorporate into such interstitial sites leading to increased concentration of cation vacancies, allowing greater U diffusion and increased grain size. Alternatively, oxygen vacancies ( $\text{O}_v$ ) are formed due to the charge compensation mechanism employed when  $\text{Cr}^{3+}$  substitutes for  $\text{U}^{4+}$  [6,8,11]. In this case, grain growth is attributed to Cr precipitates forming a second peritectic phase upon sintering [12].

The contribution of both  $\text{O}_v$  and  $\text{O}_i$  can be interpreted through Raman spectroscopy (Figure 3a) where the first band ( $\text{T}_{2g}$ ) at  $445\text{ cm}^{-1}$  is characteristic of  $\text{UO}_2$  and the second band (LO) at  $\sim 550\text{ cm}^{-1}$  indicates defects in the crystal structure. Deconvolution of the LO peak (Figure 3a, inset) can separate the contributions and identify the type of defects present. When the intensity ratio of the defect band to  $\text{T}_{2g}$  is considered, the concentration of defects is increased as a function of  $\text{Cr}_2\text{O}_3$  content in doped  $\text{UO}_2$  (Figure 3b). The concentration of oxygen interstitials remains constant; this is an artefact of hyperstoichiometric  $\text{UO}_{2+x}$  (constant in all samples) whereas the contribution from oxygen vacancies gradually increases with increased  $\text{Cr}_2\text{O}_3$ . This supports the incorporation of  $\text{Cr}^{3+}$  interstitially, however determination of the U oxidation state, via U M-edge XANES analysis will further confirm this.

The dissolution of  $\text{UO}_2$  is a two-stage process beginning with the oxidation of  $\text{UO}_2$  to soluble  $\text{UO}_2^{2+}$ . It would, therefore, be reasonable to assume that an increase in  $\text{O}_v$ , due to doping, would increase the availability of O to incorporate into the crystal structure and increased the rate of dissolution. However,

when the defect contribution as a function of  $\text{Cr}_2\text{O}_3$  dopant concentration is compared to the rate of U dissolution, the opposite relationship is observed (Figure 4). An explanation for this is given in recent investigation of Gd-doped  $\text{UO}_2$  where it was suggested that a higher dopant concentrations,  $\text{O}_v$  clusters form, reducing the availability to incorporate O [13-15].

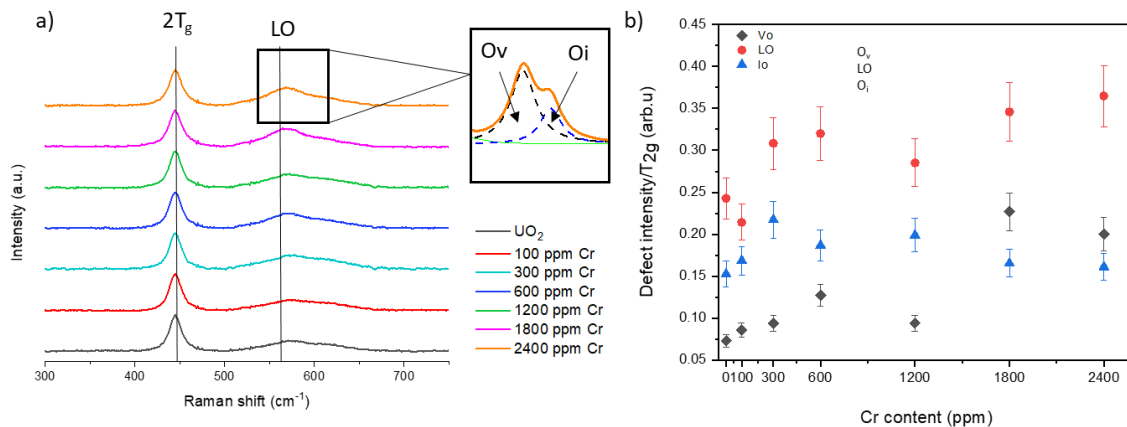


**Figure 3:** (a) Raman spectroscopy of  $\text{Cr}_2\text{O}_3$  doped  $\text{UO}_2$  as a function of Cr content showing the  $T_{2g}$  band and LO defect band with the deconvolution of the LO defect band into contributions from Oxygen interstitials and vacancies (inset) and (b) overall defect intensity (red ●) of  $\text{Cr}_2\text{O}_3$  doped  $\text{UO}_2$  (a.u.) as a function of  $\text{Cr}_2\text{O}_3$  content showing the contribution from  $\text{O}_v$  (black ◆) and  $\text{O}_i$  (blue ▲).

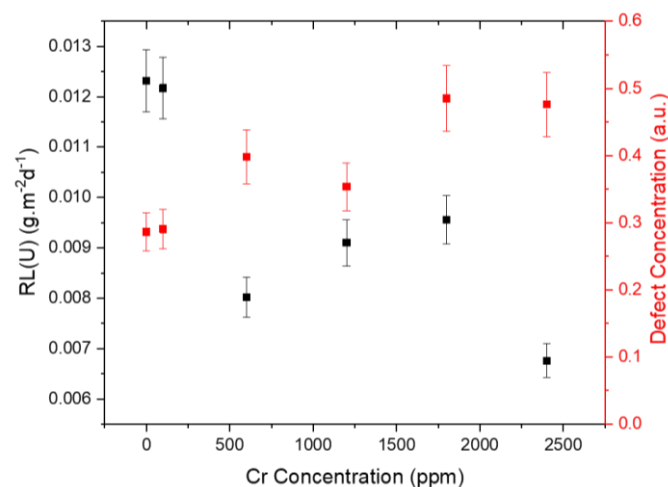


**Figure 4:** Rate of U loss ( $\text{g}/\text{m}^2\cdot\text{d}$ ) compared to defect concentration (a.u.), as a function of  $\text{Cr}_2\text{O}_3$  content.

The oxidation state of Cr in the  $\text{UO}_2$  matrix can support the theories discussed in relation to defect concentration. Estimation of the oxidation state of Cr in the doped  $\text{UO}_2$  samples was deduced via linear regression of the white line positions of Cr-doped  $\text{UO}_2$  compared to that of the standards of known Cr oxidation state (Figure 5). It was revealed that above 300 ppm doped  $\text{UO}_2$ , Cr is present as  $\text{Cr}^{3+}$ , consistent with a substitution mechanism. However, at 300 ppm Cr, the oxidation state appeared to be an intermediate between  $\text{Cr}^{3+}$  and  $\text{Cr}^0$  suggesting more than one oxidation state is present at low dopant concentrations. This potentially correlates to the dissolution rate of U (Figure 1b), which was higher for the lowest concentrations of Cr-doping.

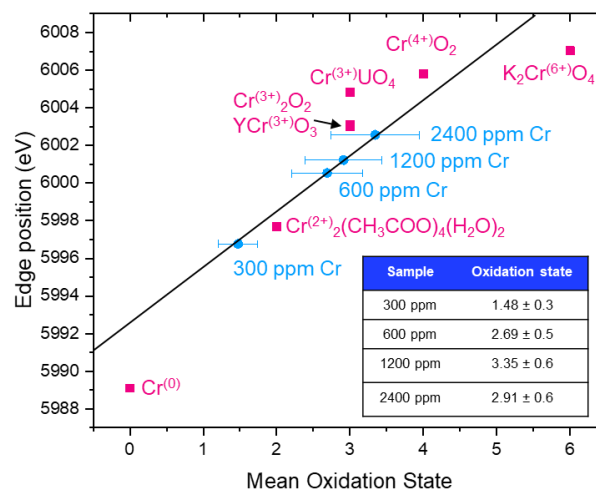


**Figure 5:** Linear regression of mean oxidation state present in  $\text{Cr}_2\text{O}_3$  doped  $\text{UO}_2$  (blue ●) compared to standards of known oxidation state (pink ■).

## Conclusions and future work

The dissolution behaviour of  $\text{Cr}_2\text{O}_3$  doped  $\text{UO}_2$  has been investigated by determination of the normalised mass loss of U as a function of Cr content; initial results suggest increased durability with  $\text{Cr}_2\text{O}_3$  content up to 2400 ppm Cr. The results have been evaluated in relation to grain size, defect concentration and Cr oxidation state, revealing the potential influence of  $\text{O}_v$  formation on the observed dissolution behaviour in that clustering could inhibit the dissolution of the  $\text{UO}_2$  matrix. Future work will include determination of the distribution of Cr within the matrix through EPMA and analysis of the U oxidation state in all samples by U M-edge XANES. Durability investigations are ongoing with additional experiments performed at 40°C and 60°C in the same solution, which will be used to evaluate the kinetics of dissolution. Experiments will also be performed in an oxygen-deficient environment to understand doped  $\text{UO}_2$  dissolution under anoxic conditions.

## Acknowledgement

*The research leading to these results has received funding from the European Commission Horizon 2020 Research and Training Programme of the European Atomic Energy Community (EURATOM) (H2020-NFRP-2016-2017-1) under grant agreement n° 755443 (DisCo project).*

## References

- [1] Peres, V., Favregeon, L., Andrieu, M., Palussire, J.C., Baland, J., Delafoy, C., Pijolat, M. (2012). High-temperature chromium volatilization from  $\text{Cr}_2\text{O}_3$  powder and  $\text{Cr}_2\text{O}_3$ -doped  $\text{UO}_2$  pellets in reducing atmospheres. *J. Nucl. Mater.*, 423, 93-101.
- [2] Arborelius, J., Backman, K., Hallstadius, L., Limbäck, M., Nilsson, J., Rebensdorff, B., Zhou, G., Kitano, K., Löfström, R., Rönnerberg, G. (2006). Advanced doped  $\text{UO}_2$  pellets in LWR applications. *J. Nucl. Sci. Technol.*, 43(9), 967-976.
- [3] Che, Y., Pastore, G., Hales, J., Shirvan, K. (2018). Modeling of  $\text{Cr}_2\text{O}_3$ -doped  $\text{UO}_2$  as a near-term accident tolerant fuel for LWRs using the BISON code. *Nucl. Eng. Des.*, 337, 271-278.



- 
- [4] Massih, A. (2014). Effects of additives on uranium dioxide fuel behaviour. Swedish Radiation Safety Authority, 74.
- [5] Shoesmith, D.W. (2000). Fuel corrosion processes under waste disposal conditions. *J. Nucl. Mater.*, 282, 1-31.
- [6] Leenaers, A., De Tollenaere, L., Delafoy, C., Van den Berghe, S. (2003). On the solubility of chromium sesquioxide in uranium dioxide fuel. *J. Nucl. Mater.*, 317, 62-68.
- [7] Bourgeois, L., Dehaut, P., Lemaignan, C., Hammou, A. (2001). Factors governing microstructure development of Cr<sub>2</sub>O<sub>3</sub>-doped UO<sub>2</sub> during sintering. *J. Nucl. Mater.*, 297, 313-326.
- [8] Cooper, D.A., Stanek, M.W.D., Anderson, C.R. (2018). The role of dopant charge state on defect chemistry and grain growth of doped UO<sub>2</sub>. *Acta Mater.*, 150, 403-413.
- [9] Guo, Z., Ngayam-happy, R., Krack, M., Pautz, A. (2017). Atomic-scale effects of chromium-doping on defect behaviour in uranium dioxide fuel. *J. Nucl. Mater.*, 488, 160-172.
- [10] Corkhill, C.L., Myllykylä, E., Bailey, D.J., Thornber, S.M., Qi, J., Maldonado, P., Stennett, M.C., Hamilton, A., Hyatt, N.C. (2014). Contribution of energetically reactive surface features to the dissolution of CeO<sub>2</sub> and ThO<sub>2</sub> analogues for spent nuclear fuel microstructures. *ACS Appl. Mater. Interfaces.*, 6, 12279-12289.
- [11] Cardinals, T., Govers, K., Vos, B., Van Den Berghe, S., Verwerft, M., De Tollenaere, L., Maier, G., Delafoy, C. (2012). Chromia doped UO<sub>2</sub> fuel: Investigation of the lattice parameter. *J. Nucl. Mater.*, 424, 252-260.
- [12] Cardinaels, T., Hertog, J., Vos, B., De Tollenaere, L., Delafoy, C., Verwerft, M. (2012). Dopant solubility and lattice contraction in gadolinia and gadolinia-chromia doped UO<sub>2</sub> fuels. *J. Nucl. Mater.*, 424, 289-300.
- [13] Razdan, M. and Shoesmith, D.W. (2014). Influence of trivalent-dopants on the structural and electrochemical properties of uranium dioxide (UO<sub>2</sub>). *J. Electrochem. Soc.*, 161, H105-H113.
- [14] Razdan, M. and Shoesmith, D.W. (2014). The electrochemical reactivity of 6.0 wt% Gd-Doped UO<sub>2</sub> in aqueous carbonate/bicarbonate solutions. *J. Electrochem. Soc.*, 161, H225-H234.
- [15] Liu, N., Kim, J., Lee, J., Youn, Y., Kim, J., Kim, J., Noël, J.J., Shoesmith, D.W. (2017). Influence of Gd doping on the structure and electrochemical behavior fo UO<sub>2</sub>. *Electrochim. Acta*, 247, 496-504.

# Spent fuel matrix alteration 1D model integrating water radiolysis and reactive solute transport – model calibration and validation

*Riba, O., Coene, E., Silva, O. and Duro, L.*

Amphos 21, Barcelona (ES)

---

## Abstract

A 1D reactive transport model has been implemented in iCP (interface COMSOL Multiphysics - PhreeqC) to assess the corrosion of Spent Fuel (SF) matrix, considered as  $\text{UO}_2(\text{am,hyd})$  with Pd as representative element of the epsilon particles, and assumed to be a homogeneous material. The model couples: i) the generation of water radiolysis species by alpha and beta radiation considering a complete radiolysis system with kinetic reactions involving:  $\text{H}^+$ ,  $\text{OH}^-$ ,  $\text{O}_2$ ,  $\text{H}_2\text{O}_2$ ,  $\text{H}_2$ ,  $\text{HO}_2^-$ ,  $\text{HO}_2^\cdot$ ,  $\text{O}^\cdot$ ,  $\text{O}^-$ ,  $\text{O}_2^-$ ,  $\text{H}^\cdot$ ,  $\cdot\text{OH}$  and  $\text{e}^-$ , ii) the processes occurring at the SF surface: oxidation of  $\text{UO}_2(\text{am,hyd})$  and subsequent dissolution or reduction of the oxidized fuel by activated  $\text{H}_2$ , and iii) corrosion of  $\text{Fe}(\text{s})$  in oxic and anoxic conditions. Processes i) were implemented in COMSOL and processes ii) and iii) were implemented in PHREEQC with their kinetic constants being calibrated with existing experimental data. The model was compared to new experimental data demonstrating its ability to reproduce independent data not used in its calibration

## 1. Introduction and objectives

The safety assessment of deep geological disposal of used nuclear fuel (spent fuel, SF) requires a fundamental understanding of the processes controlling fuel alteration and the release of radionuclides into the geosphere. The spent fuel is a very complex system and, as shown in Figure 1, different interrelated processes control its alteration. It is important to remark that not only oxidized uranium can be released in the solution, but also non-oxidized uranium can be predominant under reducing conditions.

Improved models implemented in software such as COMSOL [1-3], MATLAB [4], and HYTEC [5] have allowed to include the most relevant processes of the system by introducing some simplifications. These simplifications were mainly applied to the chemistry and to the radiolytic scheme. In the latter, simplifications consist of, for instance, considering only the production of  $\text{H}_2\text{O}_2$  and  $\text{H}_2$  instead of the complete radiolysis scheme. Radiolysis and chemical complexation/dissolution reactions occur at very different time scales, often with rates differing by more than 6 orders of magnitude. Uranium (the main element of the fuel) and the iron of the steel-container and metallic insert have a complex chemistry. This complexity and the difference in time scales represent an important modelling challenge.

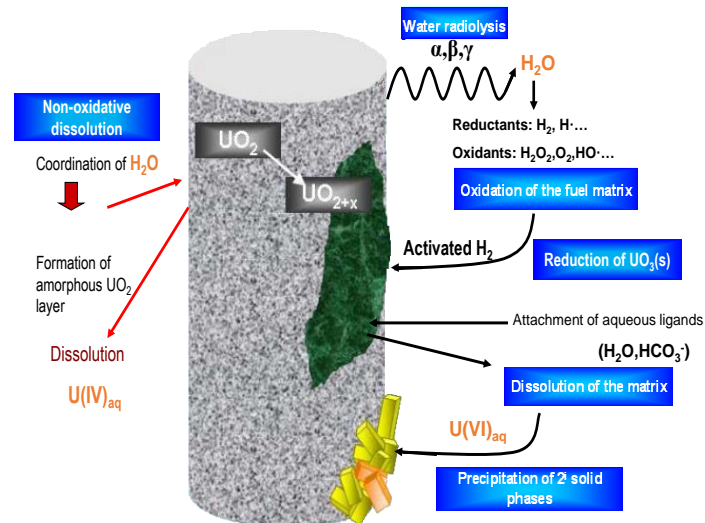


**Figure 1:** Processes involved in the spent fuel matrix alteration.

During the first two years of the DisCo project, the main work has been:

- i. to implement the spent fuel matrix alteration model in the reactive transport tool iCP [6] (interface coupling COMSOL Multiphysics [7] and PhreeqC [8]) which integrates the complete water radiolysis system and its effect on the  $\text{UO}_2(\text{am,hyd})$  alteration under container conditions.
- ii. to calibrate the kinetic constants with existing experimental data and to develop a 1D reactive transport model.

The efforts of the third year of the project have been focussed on:

- i. testing the capabilities of the model by simulating new experimental data generated in the framework of DisCo project.
- ii. improvement of the 1D reactive transport model by: (a) including  $\text{Fe}(\text{s})$  to simulate the corrosion of the canister, and (b) considering the spent fuel matrix as a porous medium, which limits diffusion of  $\text{Fe}$  into and  $\text{U}$  out of the matrix and constitutes a more realistic representation of SF alteration.

The above tasks and achievements are in line with Amphos 21 objectives included in the DisCo proposal and fully accomplish the study described in Task 2: Assessment of the behaviour of the fuel under the conditions developed inside the canister, as discussed with experimentalists. This includes a discussion on the effect that different types of metallic dopants ( $\text{Cr}_2\text{O}_3$ ,  $\text{Al}_2\text{O}_3$ ,  $\text{Gd}_2\text{O}_3$ ) can have on the SF response to the environment conditions.

The next year of the project will be mainly focused in developing the conceptual model described in Task 1: To develop a conceptual geochemical model that accounts for the impact of platinumoid metal alloy particles (epsilon metals) on SF dissolution under highly reducing conditions and in the presence of hydrogen. Under these conditions, in finely divided form and well dispersed into the  $\text{UO}_2$  matrix, and if the partial pressure of hydrogen ( $P_{\text{H}_2}$ ) is high enough, elements of the platinum group (Tc, Ru, Rh, Pd, Ir, Pt,...) are expected to behave as catalyst and to reduce  $\text{U}(\text{VI})$  into  $\text{U}(\text{IV})$ .

## 2. Modelling approach

The method coupling water radiolysis, aqueous chemistry and solute transport used to simulate the dissolution of SF inside a failed waste container is described in detail in Riba et al. (2020) [9]. Figure 2 shows a scheme of the two-way coupling approach used in iCP to integrate the different processes involved in the SF alteration. Notice that the processes concerning the SF alteration (from 1 to 6) refers to the interconnected processes outlined in Figure 1.

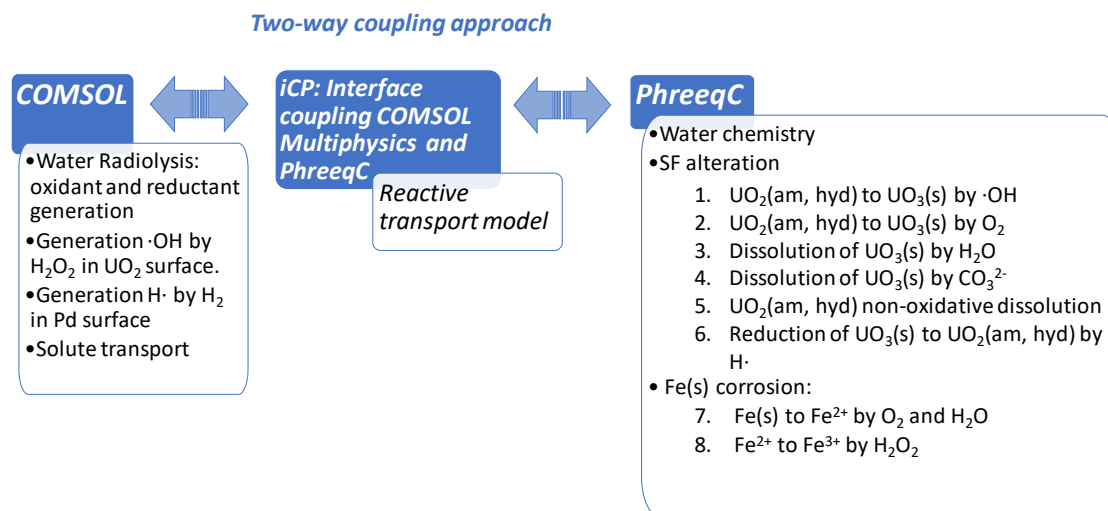


**Figure 2:** Integration in iCP of the different processes involved in the SF alteration.

As indicated in Figure 2, the generation of oxidants and reductants by water radiolysis with alpha/beta radiation is implemented in COMSOL. This considers the radiolytic scheme and yields of primary products in the chemical stage (processes occurring at time  $> 10^{-6}$  s) from Kelm and Bohnert (2004) [10] and Eriksen et al. (2008) [11] (see appendix A) as in Cera et al. (2006) [12]. The generation of ·OH by the decomposition reaction of H<sub>2</sub>O<sub>2</sub> on the UO<sub>2</sub>(am,hyd) surface [13] and the generation of H· by activation of H<sub>2</sub> on the Pd surface [14] are also implemented in COMSOL.

The generation of the above-mentioned products, calculated with an ordinary differential equation (ODE) solver, was coupled with the solute transport equation (Eq. 1) through a source term.

$$\phi \frac{\partial c_i}{\partial t} + \nabla(-D_e \nabla c_i) = S_i + \sum_j R_{ij} \quad \text{Eq. 1}$$

where  $\phi$  (-) is the porosity,  $c_i$  (mol/kg<sub>w</sub>) the aqueous concentration of species  $i$ ,  $D_e$  (m<sup>2</sup>/s) the effective diffusion coefficient,  $S_i$  (mol/kg<sub>w</sub>·s) the source term of species  $i$  and  $R_{ij}$  the reaction term between species  $i$  and  $j$ .

The chemical reaction terms  $R_{ij}$  are calculated in PhreeqC and include all the processes specified in Figure 1. The thermodynamic database used in the modelling is ThermoChimie version 9b0 [15].

### 3. Calibration of the kinetic constants

Processes 1) to 6) presented in Figure 2 occur on the SF matrix. Calibration of their kinetic constants has been performed with the experimental data described by Cera et al. (2006) [16], also used in the MICADO project [17]. The kinetic value corresponding to the dissolution of  $\text{UO}_2(\text{am,hyd})$  to  $\text{U}(\text{IV})(\text{aq})$  defined as non-oxidative dissolution (process 5 in Figure 2) was taken from Bruno et al. (1991) [18].

Iron corrosion by  $\text{H}_2\text{O}$  and  $\text{O}_2$  has been included in the model (process 7 in Figure 2). It is worth noting that Odorowski (2015) [5] specifies the need of introducing a reaction accounting for the oxidation of  $\text{Fe}(\text{s})$  under reducing conditions apart from the process of consumption of  $\text{O}_2$  by  $\text{Fe}(\text{s})$ . First, the kinetic constant for iron oxidation in anoxic conditions was set to  $6.6 \mu\text{m}/\text{y}$  in accordance with the literature under reducing conditions [19-21]. Secondly, the kinetic constant for iron oxidation with  $\text{O}_2$  was adjusted to experimental data generated in the REDUPP European project [22] on  $\text{UO}_2$  dissolution in natural groundwater in the presence of a corroding metallic iron strip. The adjusted kinetic constant corresponds to a rate value of  $20 \mu\text{m}/\text{y}$ , which is in agreement with the values found in the literature for iron corrosion under oxidizing conditions [19] (see Figure 3 in [9]). The above kinetic rate value is one order of magnitude higher than the one used by Odorowski et al. (2017) [23] also in the DisCo project. Thus, the present simulations allow to explore a less conservative scenario, respect to the conditions studied in [23]. Finally, the kinetic constant for process 8 in Figure 2) was taken from Wu et al. (2014) [3].

### 4. Results

After calibrating the kinetic constants, a 1D reactive transport model was implemented under reducing conditions considering a SF matrix with a homogeneous chemical composition of  $\text{UO}_2$  ( $\text{UO}_2$  containing 1 atom% of Pd, as representative element of the epsilon particles, behaving as catalyst for the activation of  $\text{H}_2$ ).

A uniform alpha dose rate of  $2.86 \cdot 10^{-2} \text{ Gy}/\text{s}$  affecting the first  $13 \mu\text{m}$  in water adjacent to the SF surface was assumed in the 1D simulations. This uniform alpha dose rate is equivalent to a non-uniform exponential distribution of dose rate affecting  $35 \mu\text{m}$  in water adjacent to the SF surface, in the sense that both produce the same total dose rate [1]. The aqueous solution considered has  $\text{pH} = 9$  and an initial concentration of  $[\text{Fe}] = 1 \cdot 10^{-9} \text{ M}$ . The production and recombination reactions of the species generated by  $\alpha$ -water radiolysis are limited to the SF and the first  $13 \mu\text{m}$  adjacent to it, whereas solute diffusion is considered in the full geometry. The right boundary allows for out-diffusion with a prescribed concentration for all solutes. A 1D model was implemented to study the influence of Fe. In this model, the  $\text{UO}_2(\text{am,hyd})$  is considered as a non-porous media and the domain length is 1 mm. The results of the simulations are presented in section 4.1 Another 1D model was implemented to explore the response of the geochemical system when the  $\text{UO}_2(\text{am,hyd})$  is assumed to be a porous medium and Fe is present in the system. In this case, the domain extension is 6 mm and the results are presented in section 4.2.

#### ***4.1 1D reactive transport model with $\text{UO}_2(\text{am,hyd})$ as a non-porous medium***

The following two 1D simulations were run to quantify the effect of Fe on the alteration of spent fuel matrix:

- i. **Simulation without Fe(s)**, where the model considers three sub-domains: SF surface zone (1  $\mu\text{m}$ ),  $\alpha$ -radiation zone in the water very close to the SF surface (13  $\mu\text{m}$ ) and a diffusion zone being considered in the full geometry (1 mm).
- ii. **Simulation with Fe(s)**, where the model considers four sub-domains: the same three domains described in simulation without Fe, plus a steel surface zone (1  $\mu\text{m}$ ), which composition correspond to 99% of Fe.

To compare with existing simulations, the models consider the same parameters and geometry as in Wu et al. (2012) [1]. For that reason, the extension of the domain was assumed to be 1 mm (Figure 3). The concentration at the right boundary is prescribed to zero for all species except for Fe in the second simulation. Both models include a non-porous SF matrix surface at the left boundary. This surface is closed to solute transport but interacts chemically with water in the Spent Fuel matrix surface zone (see Figure 3). Porosity is set to 1 in the whole model resulting in an effective diffusion coefficient of  $10^{-9} \text{ m}^2/\text{s}$  for all species.

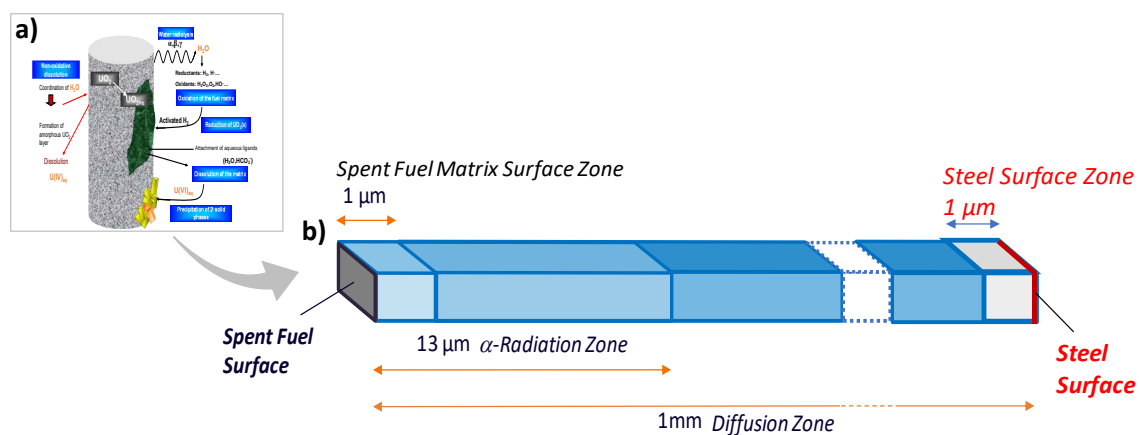


**Figure 3:** (a) Interrelated processes occurring controlling the alteration of the spent fuel matrix. (b) Geometry (not to scale) considered in the 1D models with  $\text{UO}_2(\text{am,hyd})$  as a non-porous medium to simulate the processes occurring in the spent fuel matrix surface described in Figure 3a.

The calculated concentrations of the species generated by water radiolysis ( $\text{H}_2\text{O}_2$ ,  $\text{O}_2(\text{aq})$ ,  $\text{H}_2(\text{aq})$ ,  $\text{H}\cdot$ ,  $\cdot\text{OH}$ ,  $\text{e}^-$ ,  $\text{HO}_2^-$ ,  $\text{O}\cdot$ ,  $\text{O}\cdot$ ,  $\text{HO}_2^-$  and  $\text{O}_2^-$ ) reached steady state very rapidly (in 4 hours). On the other hand, the concentration of uranium increases progressively, reaching a quasi-steady state after 36.5 days.

The concentrations of  $\text{H}_2\text{O}_2$ ,  $\text{O}_2(\text{aq})$ ,  $\text{H}_2(\text{aq})$  and U as a function of the distance from the SF surface at 36.5 days are shown in Figure 4a (for the simulation without Fe) and Figure 4b (for the simulation with Fe). It is observed that  $\text{H}_2\text{O}_2$ ,  $\text{O}_2(\text{aq})$ ,  $\text{H}_2(\text{aq})$  stabilized at the same concentrations in both cases. Nonetheless, the total uranium concentration is  $\sim 10^{-9} \text{ M}$  in the absence of Fe and it is mainly in the oxidized form U(VI) ( $\sim 80\%$  of total uranium). This is consistent with the fact that the redox pair U(IV)/U(VI) controls the  $\text{Eh} = -0.2 \text{ V}$  at  $\text{pH} = 9$  (see Figure 4c). However, for the simulation with Fe(s), the uranium in solution predominates in its reduced form. This is associated to an  $\text{Eh} = -0.4 \text{ V}$  at  $\text{pH} = 9$ , controlled by the redox pair  $\text{Fe}^{2+}/\text{magnetite}$ , with  $[\text{Fe}]_{\text{total}} = 10^{-8} \text{ M}$ , as shown in Figure 4c.

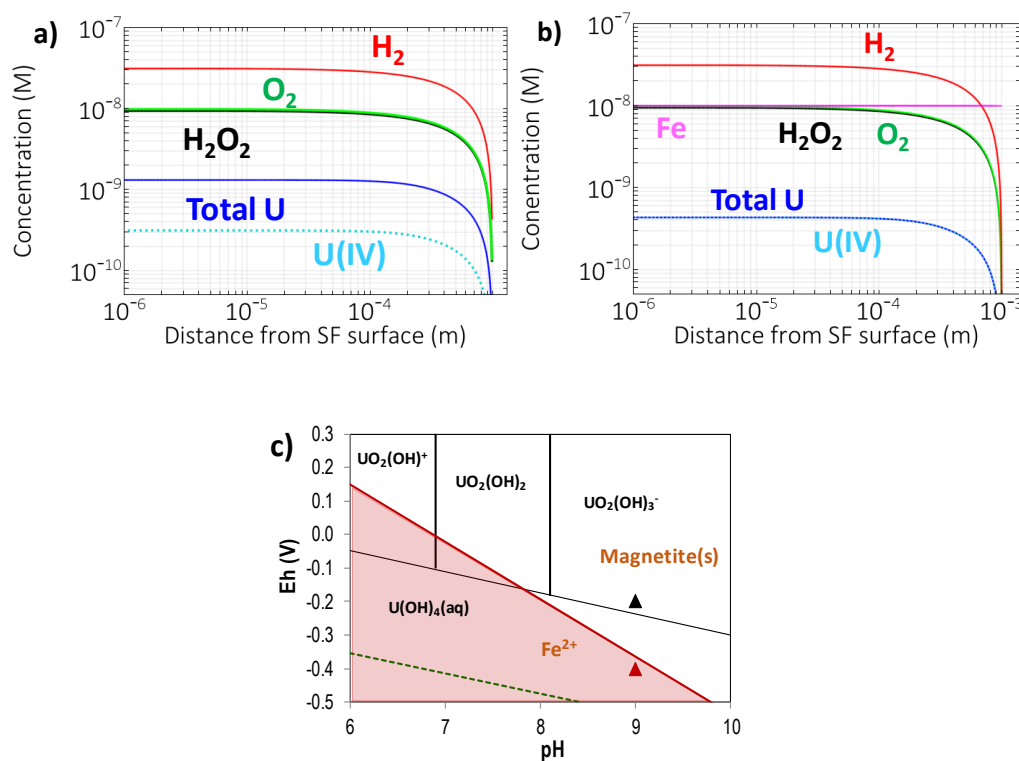


**Figure 4:** Simulated  $H_2O_2$ ,  $O_2(aq)$ ,  $H_2(aq)$ , total U and U(IV) concentration profiles after 36.5 days (a) without and (b) with Fe(s). (c) Uranium and iron predominance diagram at  $[U] = 10$  nM and  $[Fe] = 10$  nM; the symbols resulted from the Eh and pH determined in 1D simulation without Fe(s) (in black) and with Fe(s) (in red).

The obtained results are comparable with the concentrations simulated in Wu et al. (2014) [3], calculated under the same alpha dose rate and radiation range in water. The concentrations of  $H_2(aq)$ ,  $H_2O_2$  and U are very similar in both models. However, the  $O_2(aq)$  concentration is almost two orders of magnitude higher in the present model than in [3]. Our kinetic constants were calibrated against experimental data from Cera et al. (2006) and this gives confidence to the results obtained in this work. The difference between the  $O_2$  concentrations in Wu et al. (2014) [3] and those in the present model can be attributed to the different radiolytic schemes and the different reaction rates or processes considered in the SF matrix by each model. The  $UO_2(am,hyd)$  dissolution rate determined from the present model without Fe(s) is  $2 \cdot 10^{-6} \text{ y}^{-1}$  ( $1.2 \text{ pmol/m}^2 \cdot \text{s}$ ) which is in the range of the values considered in safety assessments ( $10^{-7} \text{ y}^{-1}$ , with maximum =  $10^{-6} \text{ y}^{-1}$  and minimum =  $10^{-8} \text{ y}^{-1}$ ) [24-29]. The above occurs when the inhibiting (protecting) effect of  $H_2$  on the long-term dissolution of SF matrix is considered. Including iron in the model reduced the corrosion rate down to  $10^{-6} \text{ y}^{-1}$  ( $0.6 \text{ pmol/m}^2 \cdot \text{s}$ ). This limited effect of Fe on the alteration of the SF matrix alteration may be due to the small surface area of the steel considered in the model. However, it should be noted that Wu et al. (2014) [3] showed that when the  $Fe^{2+}$  concentration in the bulk solution increased from 0 to  $10^{-8} \text{ M}$ , the diffusive flux of  $UO_2^{2+}$  decreased only from 0.6 to  $0.5 \text{ pmol/m}^2 \cdot \text{s}$ . This is associated to a reduction in the SF dissolution rate of only 20%, which is in the same order of magnitude than the reduction predicted with the present simulations. 1D reactive transport model with  $UO_2(am,hyd)$  as a porous medium.

In order to quantify the effect of porosity on the dissolution of the spent fuel matrix, a new 1D simulation with the system domain shown in Figure 5 was performed considering a porous  $UO_2(am,hyd)$ . The porosity is set at 0.15, value estimated by considering a density of  $8.93 \text{ g/cm}^3$  for  $UO_2$  pellet [30] (including porosity) and a grain density of  $10.52 \text{ g/cm}^3$  [31]. The estimated porosity is equivalent to a

specific surface area of  $21.3 \text{ m}^2/\text{mL}$  (in comparison with  $1 \text{ m}^2/\text{mL}$  used in the simulations described in section 4.1). As shown in Figure 5, the model considers four sub-domains: a porous SF zone (5 mm), an  $\alpha$ -radiation zone in the water very close to the SF surface ( $13 \text{ }\mu\text{m}$ ), a diffusion zone (6 mm) and a steel surface zone ( $1 \text{ }\mu\text{m}$ ). The steel surface zone is assumed to be pure water (porosity = 1) in contact with a steel surface.

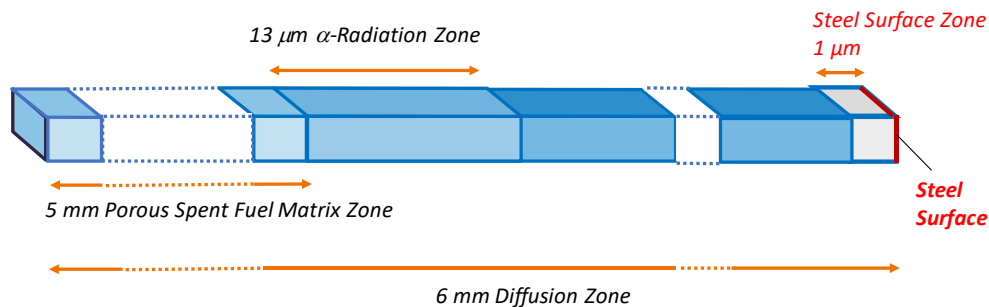


**Figure 5.** Geometry (not to scale) considered in the 1D models that consider a porous spent fuel matrix.

Figure 6a presents the evolution of total U and U(IV) aqueous concentration profiles. The simulated U concentration agrees with precipitation of schoepite ( $\text{UO}_2(\text{OH})_2(\text{beta})$ ) inside the pellet (seen in Figure 6b) limiting the uranium in solution to  $[\text{U}] = 5 \cdot 10^{-7} \text{ M}$  at  $E_h = -0.16 \text{ V}$  [15]. Inside the SF and close to the interface with the free aqueous phase, the uranium decreases sharply with  $[\text{U}] = 6 \cdot 10^{-8} \text{ M}$  at the surface after 34 days. A front of U(VI)(aq) starts forming in the free aqueous phase at the interface with the  $\text{UO}_2(\text{am,hyd})$  surface, being significant at 3 days. This front increases and moves away from the  $\text{UO}_2(\text{am,hyd})$  surface until it reaches a steady state after 29 days at a maximum distance of  $\sim 500$  microns away from the SF pellet surface. Nearby the Fe(s) surface (right boundary), the total uranium in solution is U(IV)(aq) in equilibrium with  $\text{UO}_2(\text{am,hyd})$  and the  $E_h = -0.4 \text{ V}$ . Note that the existence of this oxidized U(VI)(aq) front might be conditioned by the small size of the steel surface.

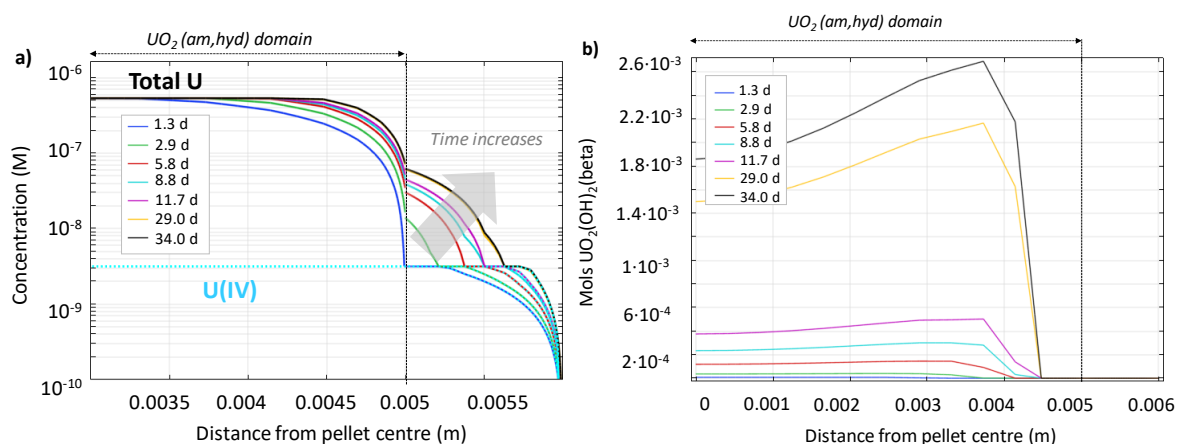


**Figure 6.** Modelling results considering a 5 mm porous matrix of SF. (a) Total U (solid lines) and U(IV) (dotted lines) concentration profiles at different simulation times. (b) Moles of schoepite at different simulation times.

The calculated corrosion rate is  $9 \cdot 10^{-7} \text{ y}^{-1}$  when considering the  $\text{UO}_2(\text{am,hyd})$  as a porous medium, in agreement with the model discussed in section 4.1 when a steel surface zone is considered.



## 4.2 Simulation of experimental data generated in DisCo project

The present model has been applied to simulate standard  $\text{UO}_2$  spent fuel leaching experiments performed by Studsvik Nuclear AB in the framework of DisCo WP3. As described in Fidalgo et al. (2020) [32], the fuel was irradiated in a commercial boiling water reactor to a local burnup of  $\sim 51.7$  MWd/kg<sub>U</sub>. Fuel fragments, after a washing step to attempt to wash away any pre-oxidized phases formed during air storage in cell, were leached in simplified groundwater (consisting of 10 mM NaCl and 2 mM  $\text{NaHCO}_3$  and stabilizing a pH = 8.2). An autoclave pressurized up to 55 bar of  $\text{H}_2$  was used (no replenishment of gas due to pressure loss during the experiment was performed to avoid air intrusion in the system). Figure 7 shows the evolution of the experimental concentrations of  $^{237}\text{Np}$  (a),  $^{99}\text{Tc}$  (b),  $^{239}\text{Pu}$  (c),  $^{100}\text{Mo}$  (d) and Figure 8a the concentration of  $^{238}\text{U}$ , represented as symbols. As discussed in Fidalgo et al. (2020) surprisingly high concentration of Pu is found, which continue to increase after 432 days of leaching, probably due to the existence of pre-oxidized phases. Another interesting observation is that other sensitive redox elements such as  $^{99}\text{Tc}$  and  $^{100}\text{Mo}$  are not only one order of magnitude higher than expected but also steadily increasing with time [32].

When applying the spent fuel matrix alteration model to simulate the above experiment, the following calculations and considerations were made:

- i. The dose rate was calculated for the  $\text{UO}_2$  spent fuel fragments from the radioisotopes inventory detailed in FIRST-Nuclides European project [33] to determine the temporal evolution of oxidants and reductants.
- ii. Specific surface area is a parameter often affected by uncertainties. However, some test simulations showed that it is not a very sensitive parameter and an increase of 50% in the specific surface area does not change the results significantly. The rates for the oxidation processes, 1) and 2) in Figure 2, were implemented considering a specific surface of  $4.6 \text{ cm}^2/\text{g}$  (calculated considering a roughness of 3 and an average of two surface area values calculated assuming: i) the fragments have a cubic geometry, and ii) fragments have a sphere geometry).
- iii. The selected equilibrium phases to limit the solubility of  $^{237}\text{Np}$ ,  $^{99}\text{Tc}$ ,  $^{239}\text{Pu}$ , and  $^{100}\text{Mo}$  are  $\text{NpO}_2 \cdot 2\text{H}_2\text{O}(\text{am})$ ,  $\text{TcO}_2 \cdot 1.6\text{H}_2\text{O}$ ,  $\text{PuO}_2(\text{coll})$  and  $\text{MoO}_2(\text{s})$ , respectively. The dashed lines shown in Figure 7 represent the equilibrium concentration of these phases calculated with the equilibrium constants from [15]. The selection of the most likely limiting phases was made by considering that the system is approaching a steady state and taking the concentrations after 400 days as a reference.

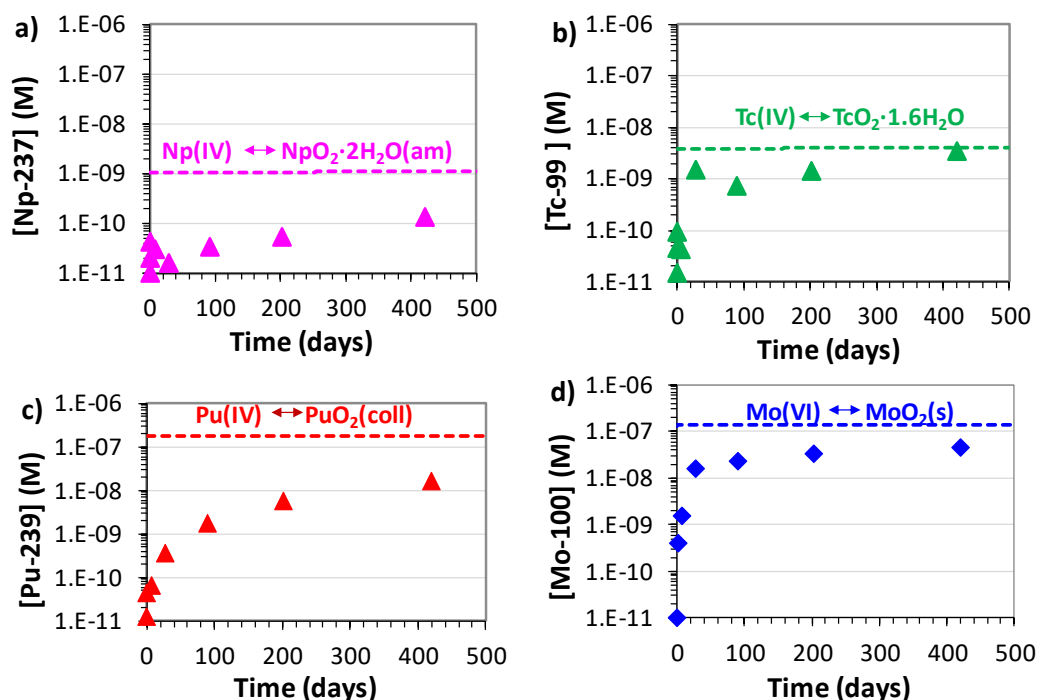


**Figure 7:** Autoclave concentrations of (a)  $^{237}\text{Np}$ , (b)  $^{99}\text{Tc}$ , (c)  $^{239}\text{Pu}$  and (d)  $^{100}\text{Mo}$  as function of time from Fidalgo et al. (2020) [32], represented as symbols. The equilibrium concentrations of each element considering as limiting phases  $\text{NpO}_2 \cdot 2\text{H}_2\text{O}(\text{am})$ ,  $\text{TcO}_2 \cdot 1.6\text{H}_2\text{O}$ ,  $\text{PuO}_2(\text{coll})$  and  $\text{MoO}_2(\text{s})$ , respectively, are represented by dashed lines.

Under the simulated conditions described above, the Eh stabilizes at -0.3 V. As indicated in Figure 8c, it seems that the redox pair  $\text{MoO}_4^{2-}/\text{MoO}_2$  is controlling the Eh of the system.

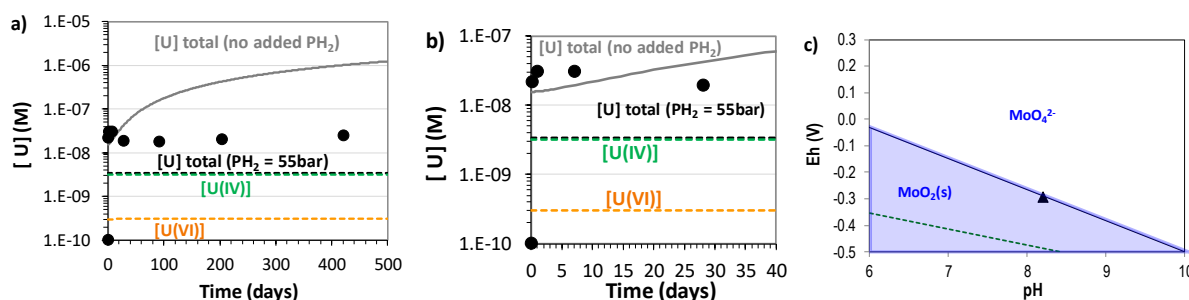


**Figure 8:** (a) Autoclave concentrations of  $^{238}\text{U}$  as function of time from Fidalgo et al. (2020) [32], represented as symbols. Simulated concentrations are represented by dashed lines for total U (black), U(IV) (green) and U(VI) (orange) at  $P_{\text{H}_2} = 55$  bar and as solid grey line for no added  $\text{H}_2(\text{g})$ . (b) Zoom in of Figure (8a) to show the short time evolution of [U]. (c) Molybdenum predominance diagram  $[\text{Mo}]_{\text{total}} = 1 \cdot 10^{-7}$  M, the symbol corresponds to the Eh and pH determined with the model.

Figure 8a and Figure 8b present the uranium in solution determined experimentally by Fidalgo et al. [32], represented as symbols, the same figures also present the uranium concentration determined with the model considering  $P_{\text{H}_2} = 55$  bar (dashed lines) and with the model with no added  $\text{H}_2$  pressure, with only the hydrogen generated by radiolysis (grey solid line). The experimental uranium concentration increases during the first day reaching a maximum concentration of  $\sim 3 \cdot 10^{-8}$  M, as shown in Figure 8b, being in agreement with the model with no added  $P_{\text{H}_2}$ . Subsequently, the experimental [U] decreases slightly until  $\sim 2 \cdot 10^{-8}$  M and from 100 days it increases again at a very slow rate reaching a concentration

of  $3\text{-}4\cdot 10^{-8}$  M after 421 days, one order of magnitude higher than the solubility of amorphous  $\text{UO}_2(\text{am,hyd})$  (see Figure 8a). At reaction times  $> 30$  days, the simulation with no added  $\text{P}_{\text{H}_2}$  indicates linear increase of [U], reaching values of  $\sim 10^{-6}$  M at 400 days. On the other hand, the model considering  $\text{P}_{\text{H}_2} = 55$  bar results in total [U] =  $4\cdot 10^{-9}$  M with 8% of this total uranium present as the oxidized form, therefore, the simulated uranium is predominantly [U(IV)(aq)] in equilibrium with  $\text{UO}_2(\text{am,hyd})$ . The simulated uranium concentration is about one order of magnitude lower than the experimental values ( $3\text{-}4\cdot 10^{-8}$  M after 421 days) supporting the hypothesis of Fidalgo et al. [32] that pre-oxidized phases, presumably formed during humid storage of the spent fuel, have conditioned the release of the uranium in solution.

## Conclusions and future work

During this third year, the project has been devoted to improve the model developed during the two first years by including: i) metallic Fe corrosion, and ii) considering SF as a porous medium in a 1D reactive transport model. Also, the simulation of experimental data generated in the WP3 of DisCo project allowed to compare to new experimental data demonstrating the ability of the model to reproduce independent data. This promoted the collaboration between modellers and experimentalists of the DisCo project.

The implementation and development of the present SF alteration model allows to assess the behaviour of spent fuel under the conditions developed inside the canister (tackling Task 2 of the DisCo project as detailed in section 1).

Two activities are planned for the last year of the project:

- i. extending the reactive transport model to a 1D axi-symmetrical geometry for the spent fuel domain.
- ii. developing a conceptual geochemical model that accounts for the impact of platinoid metal alloy particles (epsilon metals) on SF dissolution under highly reducing conditions with hydrogen.

On the other hand, numerical results from the DisCo project concerning the effect of the dopants on the new types of fuels (ADOPT fuel: Advanced Doped Pellet Technology) supports the experimental evidence that there is no significant effect of Cr-doping on the fuel oxygen potential [32,34]. Therefore, taking into account that no major differences are found in the behaviour between standard  $\text{UO}_2$  and ADOPT spent fuel, the present model applies to the assessment of the behaviour of the fuel under the conditions developed inside the canister, in both types of fuel: standard  $\text{UO}_2$  and ADOPT spent fuel.

## Acknowledgement

*Thanks to Dr. Alexandre Barreiro Fidalgo who kindly provide us with the required information for modelling the dissolution experiments of  $\text{UO}_2$  spent fuel, set up in Studsvik Nuclear AB.*

*The research leading to these results has received funding from the European Commission Horizon 2020 Research and Training Programme of the European Atomic Energy Community (EURATOM) (H2020-NFRP-2016-2017-1) under grant agreement n° 755443 (DisCo project).*

## References

- [1] Wu, L., Beauregard, Y., Qin, Z., Rohani, S., Shoesmith, D.W. (2012). A model for the influence of steel corrosion products on nuclear fuel corrosion under permanent disposal conditions. *Corros. Sci.*, 61, 83-91.
- [2] Wu, L., Liu, N., Qin, Z., Shoesmith, D.W. (2014). Modeling the radiolytic corrosion of fractured nuclear fuel under permanent disposal conditions. *J. Electrochem. Soc.*, 161(8), E3259-E3266.
- [3] Wu, L., Qin, Z., Shoesmith, D.W. (2014). An improved model for the corrosion of used nuclear fuel inside a failed waste container under permanent disposal conditions. *Corros. Sci.*, 84, 85-95.
- [4] Jerden, J.L., Frey, K., Ebert, W. (2015). A multiphase interfacial model for the dissolution of spent nuclear fuel. *J. Nucl. Mater.*, 462, 135-146.
- [5] Odorowski, M. (2015). Etude de l'altération de la matrice (U,Pu)O<sub>2</sub> du combustible irradié en conditions de stockage géologique: Approche expérimentale et modélisation géochimique. Doctoral Thesis.
- [6] Nardi, A., Idiart, A., Trinchero, P., de Vries, L.M., Molinero, J. (2014). Interface COMSOL-PHREEQC (iCP), an efficient numerical framework for the solution of coupled multiphysics and geochemistry. *Comput. Geosci.*, 69, 10-21.
- [7] COMSOL Multiphysics, <https://www.comsol.com/>.
- [8] Parkhurst, D.L. and Appelo, C.A.J. (2013). Description of input and examples for PHREEQC version 3—A computer program for speciation, batch-reaction, one-dimensional transport, and inverse geochemical calculations. U.S. Geological Survey Techniques and Methods, book 6, chap. A43, 497 p.
- [9] Riba, O., Coene, E., Silva, O., Duro, L. (2018). Integrated spent fuel alteration model. Method and first results. Deliverable D1.10: 1<sup>st</sup> Annual Meeting Proceedings. DisCo project (Grant Agreement: 755443).
- [10] Kelm, M. and Bohnert, E. (2004). A kinetic model for the radiolysis of chloride brine, its sensitivity against model parameters and a comparison with experiments. *Forschungszentrum Karlsruhe, FZKA 6977*.
- [11] Eriksen, T.E., Jonsson, M., Merino, J. (2008). Modelling of time resolved and long contact time dissolution studies of spent nuclear fuel in 10 mM carbonate solution—a comparison between two different models and experimental data. *J. Nucl. Mater.*, 375(3), 331-339.
- [12] Christensen, H., Sunder, S., Shoesmith, D.W. (1994). Oxidation of nuclear fuel (UO<sub>2</sub>) by the products of water radiolysis: development of a kinetic model. *J. Alloys Compd.*, 213, 93-99.
- [13] Merino, J., Cera, E., Bruno, J., Quinones, J., Casas, I., Clarens, F., Giménez, J., de Pablo, J., Rovira, M., Martínez-Esparza, A. (2005). Radiolytic modelling of spent fuel oxidative dissolution mechanism. Calibration against UO<sub>2</sub> dynamic leaching experiments. *J. Nucl. Mater.*, 346(1), 40-47.
- [14] Trummer, M., Nilsson, S., Jonsson, M. (2008). On the effects of fission product noble metal inclusions on the kinetics of radiation induced dissolution of spent nuclear fuel. *J. Nucl. Mater.*, 378(1), 55-59.
- [15] ThermoChimie Database version 9b0. Andra thermodynamic database for performance assessment. <https://www.thermochimie-tdb.com/pages/version.php>.
- [16] Cera, E., Bruno, J., Duro, L., Eriksen, T. (2006). Experimental determination and chemical modelling of radiolytic processes at the spent fuel/water interface. SKB Technical Report, TR-06-07.
- [17] Bruno, J., Merino, J., Tamayo, A., Ferry, C., Quiñones, J., Iglesias, E., Rodríguez Villagra, N., Nieto, J.M., Martínez-Esparza, A., Loida, A., Metz, V., Jonsson, M., Ekeröth, E., Grambow, B. (2005). MICADO project EURATOM specific programme for research and training on nuclear energy. FINAL D3.1 Deliverable: Application of models to selected datasets, NUWASTE-2005/6-3.2.1.1-2.

- [18] Bruno, J., Casas, I., Puigdomènech, I. (1991). The kinetics of dissolution of  $\text{UO}_2$  under reducing conditions and the influence of an oxidized surface layer ( $\text{UO}_{2+x}$ ): Application of a continuous flow-through reactor. *Geochim. Cosmochim. Acta*, 55(3), 647-658.
- [19] Féron, D., Crusset, D., Gras, J.M. (2008). Corrosion issues in nuclear waste disposal. *J. Nucl. Mater.*, 379(1-3), 16-23.
- [20] ANDRA (2005). Andra Référentiel matériaux. Tome 4 la corrosion des matériaux métalliques. Andra.
- [21] Smart, N.R. and Hoch, A.R. (2010). A survey of steel and Zircaloy corrosion data for use in the SMOGG gas generation model. Serco Report, SA/ENV-0841, Issue 3.
- [22] Evins, L.Z., Juhola, P., Vähänen, M. (Eds.) (2014). REDUPP Final Report. POSIVA report, 2014-12.1.
- [23] Odorowski, M., Jégou, Ch., de Windt, L., Broudic, V., Jouan, G., Peugeot, S., Martin, Ch. (2017). Effect of metallic iron on the oxidative dissolution of  $\text{UO}_2$  doped with a radioactive alpha emitter in synthetic Callovian-Oxfordian groundwater. *Geochim. Cosmochim. Acta*, 219, 1-21.
- [24] Martínez Esparza, A., Cuñado, M.A., Gago, J.A., Quiñones, J., Iglesias, E., Cobos, J., González de la Huebra, A., Cera, E., Merino, J., Bruno, J., de Pablo, J., Casas, I., Clarens, F., Giménez, J. (2005). Development of a Matrix Alteration Model (MAM). ENRESA, PT-01-2005.
- [25] SKB (2010). Data report for safety assessment SR-Site. SKB Technical Report, TR-10-52.
- [26] POSIVA (2013). Safety case for the disposal of spent nuclear fuel at Olkiluoto - Models and data for the repository system 2012. POSIVA Report, 2013-01.
- [27] Johnson, L. (2014). A model for radionuclide release from spent  $\text{UO}_2$  and MOX fuel. Nagra Report, NAB 13-37.
- [28] NWMO (2015). Technical program for long-term management of Canada's used nuclear fuel – Annual Report 2014. NWMO Technical Report, TR-2015-01.
- [29] JAEA (2015). Preliminary assessment of geological disposal system for spent fuel in Japan - First progress report on direct disposal. JAEA-Research, 2015-016.
- [30] Cobos, J., Rodríguez-Villagra, N., Fernández, S., Gutierrez, L., Bonales, L.J., Durán, S., Anta, L. (2019). Ongoing CIEMAT activities on fabrication and stability studies of doped  $\text{UO}_2$  in the frame of the DisCo project: sample characterization, experimental set-up and first results. *In*: Evins, L.Z, Valls, A., Duro, L. (Eds.) Deliverable D1.15: 2<sup>nd</sup> Annual Meeting Proceedings. DisCo project (Grant Agreement: 755443).
- [31] Arborelius, J., Backman, K., Hallstadius, L., Limbäck, M., Nilsson, J., Rebensdorff, B., Zhou, G., Löfström, R., Röennberg, G. (2006). Advanced doped  $\text{UO}_2$  pellets in LWR applications. *J. Nucl. Sci. Technol.*, 43(9), 967-976.
- [32] Fidalgo, A.B., Roth, O., Puranen, A., Evins, L.Z., Spahiu, K. (2020). Aqueous leaching of ADOPT and standard  $\text{UO}_2$  spent nuclear fuel under  $\text{H}_2$  atmosphere. *MRS Advances*, 5(3-4), 167-175.
- [33] Roth, O., Puranen, A., Askeljung, C., Cui, D. (2014). Selection of materials and characterization of samples used in spent fuel leaching and laser ablation studies. *In*: Kienzler, B., Metz, V., Duro, L., Valls, A. (2014). Final (3<sup>rd</sup>) Annual Workshop Proceedings. FIRST-Nuclides project (Contract Number: 295722).
- [34] Curti, E., Miron, G.D., Kulik, D.A. (2019). Development and application of a solid solution model for Cr-doped  $\text{UO}_2$  fuel. *In*: Evins, L.Z, Valls, A., Duro, L. (Eds.) Deliverable D1.15: 2<sup>nd</sup> Annual Meeting Proceedings. DisCo project (Grant Agreement: 755443).

## Appendix A

### *Kinetic reaction scheme<sup>1</sup> for water radiolysis [10]*

Reactions	$M^{-1} \cdot s^{-1}$ or $s^{-1}$	Reactions	$M^{-1} \cdot s^{-1}$ or $s^{-1}$
$H_2O \rightarrow H^+ + OH^-$	$k = 2.60 \cdot 10^{-5}$	$H + O_2^- \rightarrow HO_2^-$	$k = 2.00 \cdot 10^{10}$
$H^+ + OH^- \rightarrow H_2O$	$k = 1.43 \cdot 10^{11}$	$H + HO_2 \rightarrow H_2O_2$	$k = 8.50 \cdot 10^9$
$H_2O_2 \rightarrow H^+ + HO_2^-$	$k = 3.56 \cdot 10^{-2}$	$H + H_2O_2 \rightarrow H_2O + OH$	$k = 4.20 \cdot 10^7$
$H^+ + HO_2^- \rightarrow H_2O_2$	$k = 2.00 \cdot 10^{10}$	$H + O_2 \rightarrow HO_2$	$k = 2.10 \cdot 10^{10}$
$E^- + H_2O \rightarrow H + OH^-$	$k = 1.90 \cdot 10^1$	$HO_2 + HO_2 \rightarrow H_2O_2 + O_2$	$k = 8.40 \cdot 10^5$
$H + OH^- \rightarrow E^- + H_2O$	$k = 2.20 \cdot 10^7$	$HO_2 + O_2^- \rightarrow O_2 + HO_2^-$	$k = 9.60 \cdot 10^7$
$OH + OH^- \rightarrow H_2O + O^-$	$k = 1.30 \cdot 10^{10}$	$OH + O^- \rightarrow HO_2^-$	$k = 1.80 \cdot 10^0$
$O^- + H_2O \rightarrow OH + OH^-$	$k = 1.80 \cdot 10^6$	$O + O \rightarrow O_2$	$k = 1.00 \cdot 10^9$
$HO_2 \rightarrow H + O_2^-$	$k = 8.00 \cdot 10^5$	$H_2O_2 \rightarrow H_2O + O$	$k = 3.80 \cdot 10^{-4}$
$H + O_2^- \rightarrow HO_2$	$k = 5.00 \cdot 10^{10}$		
$E^- + H^+ \rightarrow H$	$k = 2.30 \cdot 10^{10}$		
$E^- + E^- \rightarrow H_2 + OH^- + OH^-$	$k = 5.50 \cdot 10^9$		
$E^- + H \rightarrow H_2 + OH^-$	$k = 2.50 \cdot 10^{10}$		
$E^- + O_2^- \rightarrow HO_2^- + OH^-$	$k = 1.30 \cdot 10^{10}$		
$E^- + HO_2 \rightarrow HO_2^-$	$k = 2.00 \cdot 10^{10}$		
$E^- + H_2O_2 \rightarrow OH + OH^-$	$k = 1.10 \cdot 10^{10}$		
$E^- + O_2 \rightarrow O_2^-$	$k = 1.90 \cdot 10^{10}$		
$E^- + HO_2^- \rightarrow O^- + OH^-$	$k = 3.50 \cdot 10^9$		
$OH + OH \rightarrow H_2O_2$	$k = 5.50 \cdot 10^9$		
$OH + E^- \rightarrow OH^-$	$k = 3.00 \cdot 10^{10}$		
$OH + H \rightarrow H_2O$	$k = 7.90 \cdot 10^9$		
$OH + HO_2 \rightarrow H_2O + O_2$	$k = 6.60 \cdot 10^9$		
$OH + O_2^- \rightarrow O_2 + OH^-$	$k = 1.00 \cdot 10^{10}$		
$OH + H_2O_2 \rightarrow HO_2 + H_2O$	$k = 2.70 \cdot 10^7$		
$OH + H_2 \rightarrow H + H_2O$	$k = 3.40 \cdot 10^7$		
$OH + HO_2^- \rightarrow HO_2 + OH^-$	$k = 7.50 \cdot 10^9$		
$H + H \rightarrow H_2$	$k = 7.80 \cdot 10^9$		

<sup>1</sup> The kinetic constant for the decomposition reaction of  $H_2O_2$ :  $H_2O_2 \rightarrow O + H_2O$  is  $k = 10^{-3} s^{-1}$  [10,12]. As described in Christensen et al. (1994) [12] this rate constant value was set as arbitrary. In the present work, it has been adjusted with the experimental data from Cera et al. (2006) [16] to  $3.8 \cdot 10^{-4} s^{-1}$ .

***Yields of primary products (mol/L x 10<sup>7</sup>) formed on radiolysis of water***

<b><i>Species</i></b>	<b><i>Alpha [11]</i></b>	<b><i>Beta [12]</i></b>
G(H <sub>2</sub> O <sub>2</sub> )	= 0.98	= 0.74
G(HO <sub>2</sub> )	= 0.22	= 0.00
G(H <sub>2</sub> )	= 1.30	= 0.45
G(H)	= 0.21	= 0.60
G(E <sup>-</sup> )	= 0.06	= 2.80
G(OH)	= 0.25	= 2.80
G(OH <sup>-</sup> )	= 0.00	= 0.00
G(H <sup>+</sup> )	= 0.06	= 2.80
G(H <sub>2</sub> O)	= -2.65	= -4.30

# Full reactive transport model of $U_{0.73}Pu_{0.27}O_2$ experimental leaching in synthetic clay groundwater with metallic iron

*De Windt, L.<sup>1</sup>, Kerleguer, V.<sup>1,2</sup>, Jégou, C.<sup>2</sup>, Goblet, P.<sup>1</sup>, Martin, C.<sup>3</sup> and Tocino, F.<sup>4</sup>*

<sup>1</sup> ARMINES/MINES ParisTech, Centre de Géosciences, Fontainebleau (FR)

<sup>2</sup> CEA/DEN/DE2D/SEVT/LMPA, Marcoule, Bagnol sur Cèze (FR)

<sup>3</sup> Andra, Châtenay-Malabry (FR)

<sup>4</sup> EDF R&D, Moret-sur-Loing (FR)

---

## 1. Introduction

The direct disposal of irradiated MOx (mixed plutonium and uranium oxide) fuels in deep geological repositories is a major societal issue in several European countries. The alteration rate of the spent MOx fuel matrix under disposal conditions is a critical issue for the long-term release of radionuclides. The alpha activity of spent fuels may locally disrupt the reducing conditions by inducing alpha radiolysis of the surrounding water (provided that the alpha radiolysis is above a threshold of activity [1]), and thus producing oxidizing species like hydrogen peroxide ( $H_2O_2$ ) that have the capability to strongly enhance the dissolution of the oxide matrix. With this respect, the alpha-activity of MOx is relatively high but the chemical resistance upon oxidation of Pu-enriched agglomerates, specifically found in MOx fuels, is expected to play a beneficial role [2]. In this context, it is well known that the presence of redox active species like hydrogen may scavenge oxidizing species responsible for the radiolytic dissolution of spent fuel (e.g. [3]). Whether iron may also counteract the water radiolysis effects has been studied more recently (e.g. [4,5]). In particular, there is a need to understand the behaviour of the spent fuel in truly reducing conditions imposed by the corrosion of iron structures in the proximity of the spent fuel matrix (e.g. carbon steel overpacks).

These two key questions on MOx behaviour in the disposal environment (i.e. the stabilization effect of Pu content and the scavenging process of metallic iron) are investigated in the DisCo project by a tight collaboration between experimental contribution (WP4) and modelling work (WP5) on the leaching of homogeneous unirradiated MOx pellets (24 wt.% Pu,  $U_{0.73}Pu_{0.27}O_2$ ) in synthetic claystone porewater in contact with a coupon (foil) of metallic iron. Modelling is also performed in a preliminary step on the leaching of the homogeneous MOx pellets in carbonated water to better investigate the effect of plutonium on the dissolution kinetics and mechanisms. The pore water of reference is the one of the Callovo-Oxfordian (COx) clay formation (the composition is detailed in [5]) This formation has been selected for the deep repository of radioactive waste by the French national radioactive waste management agency (ANDRA). It is worth noting that the geologic disposal of spent MOx fuels is still an open option in France (vs. reprocessing).



## 2. Summary of the first two-year results and tasks of the third-year project

With respect to MOx leaching in carbonate water, the first two years of the DisCo project led to a consistent model of the kinetic processes ( $\text{H}_2\text{O}_2$  production and disproportionation, oxidative dissolution), the release of uranium controlled by  $\text{UO}_2 \cdot n\text{H}_2\text{O}$ , and the release of plutonium controlled by the precipitation of an amorphous  $\text{Pu}(\text{OH})_4$  altered layer [6]. The plutonium content increased  $\text{H}_2\text{O}_2$  disproportionation and made  $\text{U}_{0.73}\text{Pu}_{0.27}\text{O}_2$  more resistant than  $\text{UO}_2$  towards leaching.

With respect to MOx leaching in clay porewater in presence of an iron foil, the first two years of the DisCo project provided a consistent but preliminary model coupling the kinetics of  $\text{H}_2\text{O}_2$  production by radiolysis, the kinetics of Fe(II) release in solution by metallic iron corrosion, the kinetics of Fe(II)/ $\text{H}_2\text{O}_2$  interaction, the oxidative and reducing kinetics of MOx leaching and the release of uranium and plutonium [6]. The scavenging effect of Fe(II) on MOx oxidative radiolytic products, inhibiting dissolution, was possibly demonstrated on the basis of the aqueous chemistry during the first 100 days but required to be finalized.

During the third year of the DisCo project:

- The first task undertaken has been the writing (in particular the modelling section) and the publication of a peer-reviewed paper “The mechanisms of alteration of a homogeneous  $\text{U}_{0.73}\text{Pu}_{0.27}\text{O}_2$  MOx fuel under alpha radiolysis of water” in the Journal of Nuclear Materials in collaboration with CEA, ANDRA and EDF [7].
- The second task has dealt with the completion of the reactive transport model of  $\text{U}_{0.73}\text{Pu}_{0.27}\text{O}_2$  experimental leaching in synthetic clay groundwater with metallic iron, thanks to the new results acquired by CEA in WP4 over more than one year. The postmortem characterizations of the solid phases have been especially valuable.
- In last and third task, the simulation grid and the input file of HYTEC have been adapted as a preliminary step to apply the model to the configuration of a disposal cell of MOX fuels.

## 3. Modelling approach

### 3.1 Reactive transport model and databases

CHESS is a stand-alone geochemical code identical to the geochemical module of reactive transport code HYTEC [8]. CHESS simulates the chemistry of complex aqueous systems, including minerals, organics, colloids and gases. Thermodynamic equilibrium and kinetic controls can be both considered in CHESS. The diffusive transport of a reactive species  $i$  is coupled to chemistry in HYTEC based on sequential iterative coupling scheme. The thermodynamic database ThermoChimie [9] was used for all the simulations. With respect to the aqueous species, molecular hydrogen  $\text{H}_2(\text{aq})$  produced by both by water radiolysis and the anoxic corrosion of iron was fully decoupled (kinetic inhibition) from the redox reactions in the modelling, e.g. it could not reduce  $\text{H}_2\text{O}_2$  or U(VI) in solution. The disproportionation of  $\text{H}_2\text{O}_2(\text{aq})$  into  $\text{H}_2\text{O}$  and  $\text{O}_2(\text{aq})$  was under kinetic control only.

### 3.2 Key geochemical reactions and their kinetics

#### H<sub>2</sub>O<sub>2</sub> production and disproportionation

Under alpha irradiation, the most important species to be considered regarding the dissolution of U<sub>0.73</sub>Pu<sub>0.27</sub>O<sub>2</sub> is H<sub>2</sub>O<sub>2</sub>. The hydrogen peroxide production rate law by water radiolysis at the vicinity of the MOX pellet was:

$$\frac{d[H_2O_2(aq)]}{dt} = (k^{prod}) A_v \quad \text{Eq.1}$$

where A<sub>v</sub> is the volumetric surface area of the pellet in m<sup>2</sup>/L. The constant k<sup>prod</sup> normalized to the surface pellet was calculated from alpha dose rate and alpha primary yield. Only the alpha emitters present in a 12 μm thick surface layer contribute to irradiating the solution and, therefore, to producing H<sub>2</sub>O<sub>2</sub> (see [5] for more details on the calculation assumptions).

The disproportionation reaction, H<sub>2</sub>O<sub>2</sub> → H<sub>2</sub>O + 0.5 O<sub>2</sub>, was modelled with a first-order rate on H<sub>2</sub>O<sub>2</sub>:

$$\frac{d[H_2O_2(aq)]}{dt} = (-k^{disprop} [H_2O_2(aq)]) A_v \quad \text{Eq. 2}$$

whose rate constant k<sup>disprop</sup> was estimated from the leaching experiment in carbonated water under argon ([O<sub>2</sub>] < 1 vppm) [7].

#### Dissolution of the homogeneous MOX

The oxidative dissolution rate law of the U<sub>0.73</sub>Pu<sub>0.27</sub>O<sub>2</sub> matrix was:

$$\frac{d[U_{0.73}Pu_{0.27}O_2]}{dt} = (-k^{oxid} [H_2O_2(aq)]) A_v \quad \text{Eq. 3}$$

whose rate constant k<sup>oxid</sup> was fitted from the leaching experiment in carbonated water under argon ([O<sub>2</sub>] < 1 vppm) [7].

The dissolution rate law of the U<sub>0.73</sub>Pu<sub>0.27</sub>O<sub>2</sub> matrix under reducing conditions was:

$$\frac{d[U_{0.73}Pu_{0.27}O_2]}{dt} = (-k^{red}) A_v \quad \text{Eq. 4}$$

whose rate constant k<sup>red</sup> was fitted from the leaching experiment in COx water with iron (PhD thesis of Valentin Kerleguer, to be published).

#### Anoxic corrosion of metallic iron

The kinetics of the reaction Fe(0) + 2 H<sub>2</sub>O → Fe<sup>2+</sup> + 2 OH<sup>-</sup> + H<sub>2</sub> was:

$$\frac{d[Fe(0)]}{dt} = -k^{corr} A_v \quad \text{Eq. 5}$$

where A<sub>v,Fe</sub> is the volumetric surface of the iron foils and the intrinsic kinetic rate constant k<sup>corr</sup> was taken from the literature [5]. More details on all those kinetic laws can be found in the deliverable D5.3 [6].

## 4. Results and discussion

### 4.1 Corrosion products of the iron foil

The corrosion of the iron foil releases ferrous iron ions into the synthetic COx solution (Figure 1d). A fraction of them precipitates as the carbonated corrosion product siderite (Figure 1f), the remaining fraction diffuses from the foil throughout the cell solution. Figure 1b shows that the model predicted a slight increase in pH locally around the iron foil, because its anoxic corrosion liberates hydroxide ions (Eq. 5). This local increase in pH shifts the carbonate equilibria and explains the precipitation of the carbonated minerals siderite  $\text{FeCO}_3$ . It is worth noting that chukanovite ( $\text{Fe}_2\text{CO}_3\text{OH}_2$ ) has been found experimentally but, from a thermodynamic point of view, chukanovite is in a metastable state vs siderite.

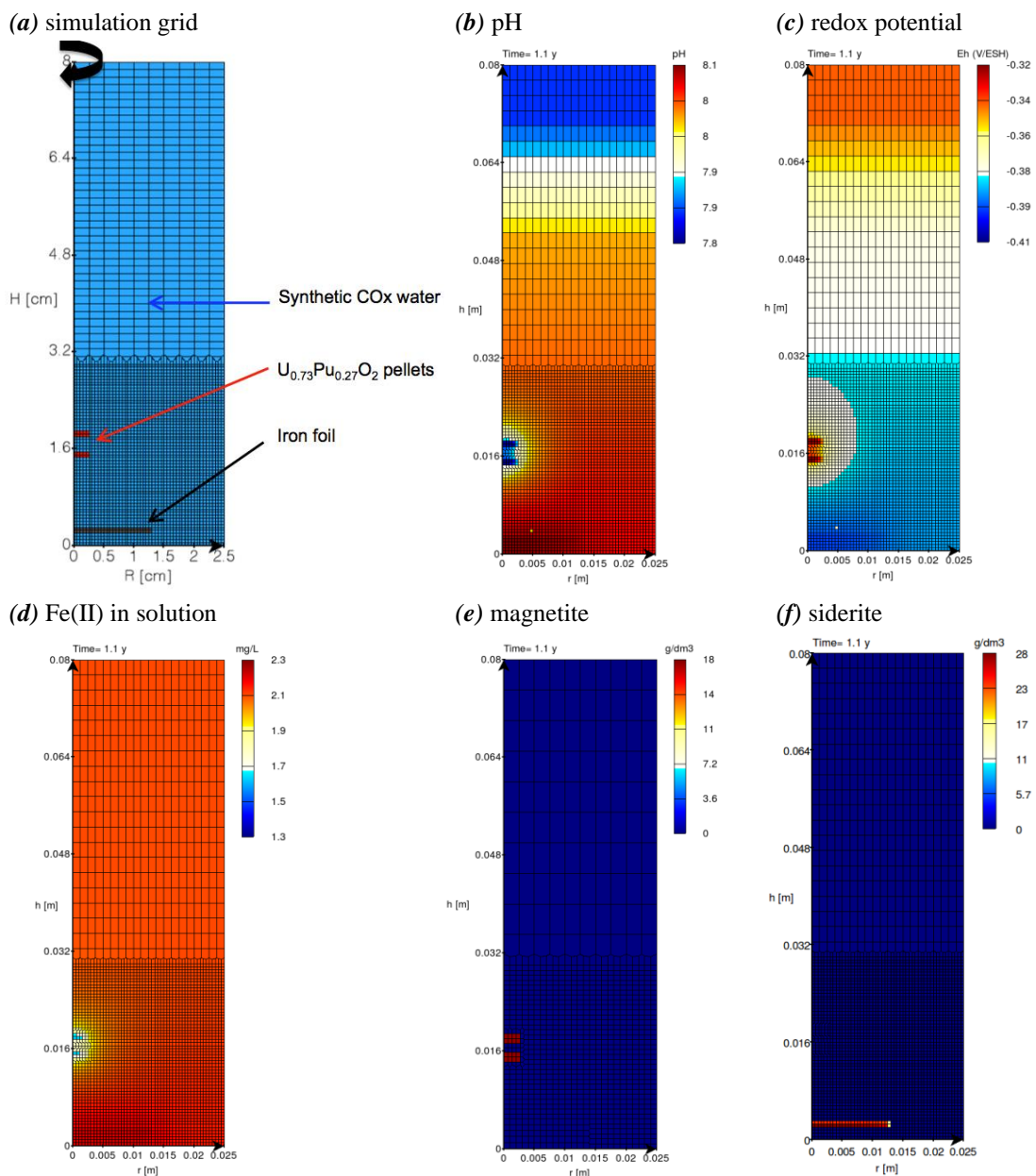


**Figure 1:** (a) Simulation grid of the cylindrical leaching cell including the MOx pellets, the COx synthetic water and the precorroded metallic iron foil; modelling after 400 days of (b,c,d) solution chemistry, (e) precipitation of magnetite on the MOX pellets and (f) siderite on the iron foil.

## 4.2 Scavenging effect of Fe(II) vs H<sub>2</sub>O<sub>2</sub>

The complete consumption of hydrogen peroxide by aqueous ferrous iron can be expressed as the following mass balance equation (Eq. 6).



The decrease of Fe(II) concentration in the solution in contact with the MOX pellets (Figure 1d) is due its redox reaction with hydrogen peroxide (leading to the full depletion of H<sub>2</sub>O<sub>2</sub>). This reaction produces Fe(III) in solution (Eq. 6) which precipitates as magnetite (Fe(III)<sub>2</sub>Fe(II)O<sub>4</sub>) on the pellet surface (Figure 1e). It is in agreement with the precipitation of magnetite observed in the WP4 experiment. It is worth mentioning that goethite precipitated in a previous study on the leaching of alpha-doped UO<sub>2</sub> pellets under similar experimental conditions [5]. As shown in Figure 2, the shift from goethite towards magnetite is probably due to the fact that the pH of the leaching solution is slightly more alkaline in the present experiments (pH 8 instead of pH 7).

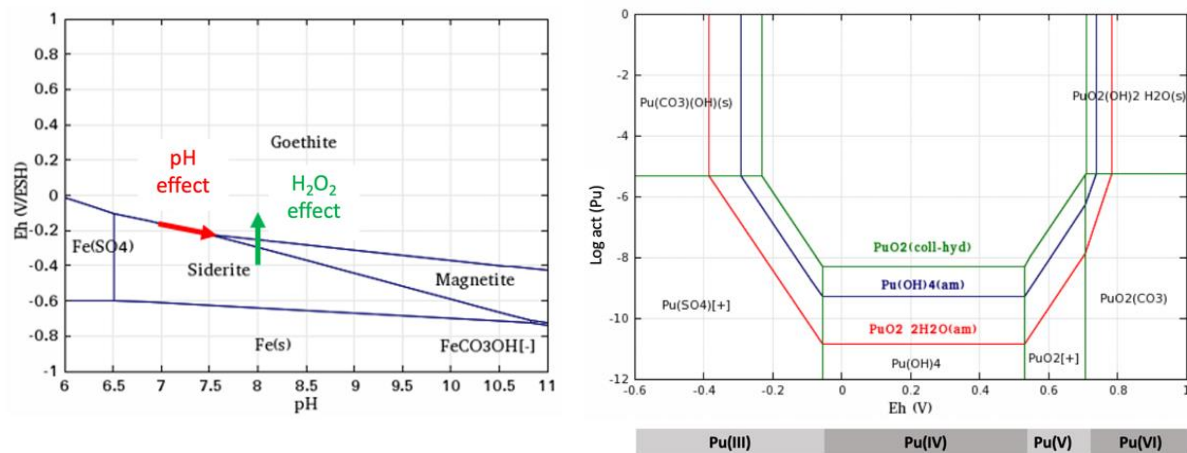


**Figure 2:** Speciation diagram calculated with the ThermoChimie database for the CO<sub>x</sub> porewater: corrosion products of iron vs. pH (left), and successive redox states of plutonium vs. Eh in at pH 8 (right).

## 4.3 Uranium and plutonium releases

In agreement with the WP4 results, the calculated dissolved concentration of uranium remains low over one year (Figure 3). In the model, the uranium solubility is controlled by the precipitation of the amorphous solid UO<sub>2</sub>·nH<sub>2</sub>O onto the surface pellets. The release of plutonium (Figure 3) is well captured by the model provided that the secondary amorphous Pu(OH)<sub>4</sub> precipitates. The formation of Pu(OH)<sub>4</sub> is only possible if the redox potential was less reducing in the experiment than calculated in the modelling (which is likely), otherwise Pu(OH)<sub>3</sub> shall precipitate as shown by the speciation diagram of Figure 2. A sensitivity analysis has been done on the solubility product of Pu(OH)<sub>3</sub> (whose solubility product varies over one order of magnitude in the literature), but the calculated aqueous concentration and the location of the Pu precipitates were never in agreement with the experimental observations with Pu(OH)<sub>3</sub>.

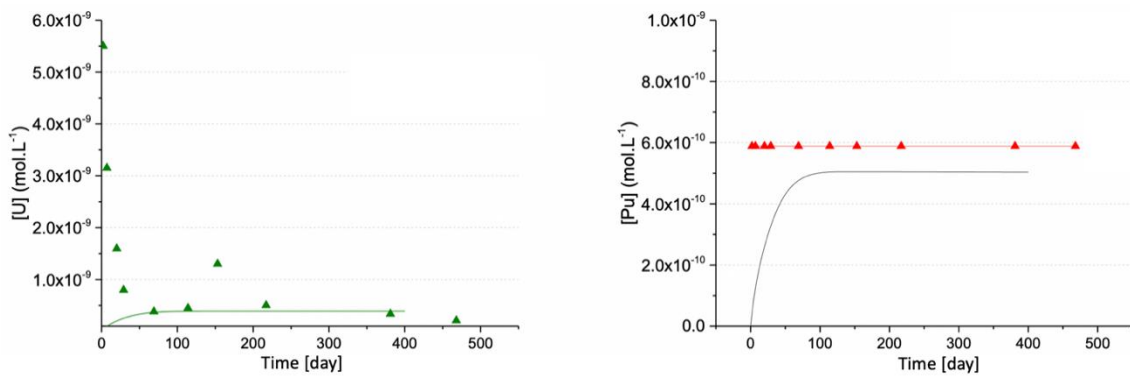


**Figure 3:** Experimental and calculated evolution with time of uranium (left) and plutonium (right) concentrations in the leaching cell.

### Conclusions and perspectives

The present reactive transport model fully couples the interconnected key geochemical reactions, schematically represented in Figure 4. The model simulates reasonably well, over more than 1 year, the experimental evolution of the aqueous chemistry, the degree of alteration of the homogeneous MOx matrix, the corrosion of the iron, the location of the redox front and the subsequent precipitation of magnetite. The redox front (Eq. 6) is located right at the surface pellet in the present study due to the more significant diffusion of Fe(II) dissolved species compared to the H<sub>2</sub>O<sub>2</sub> production. The coupled geochemical scheme, the mineralogical secondary products, the kinetics, as well as the actinide concentrations, are very close to the results already obtained for alpha-doped UO<sub>2</sub> (a proxy for UOx fuel matrix). Under oxidative conditions, the higher content of Pu decreases the alteration of the matrix compared to UO<sub>2</sub>. Under strongly reducing conditions, the possibility of promoting the alteration of the MOx matrix by reducing Pu(IV) into the more soluble Pu(III) state should be further investigated.

In the last year of the DisCo project, the knowledge gained from this reactive transport modelling at the laboratory scale will serve as a basis for a simplified mass balance simulation (e.g. between radiolytic H<sub>2</sub>O<sub>2</sub> and iron scavenging) at the scale of a disposal cell of spent MOX fuel. The simulation grid and the input file of HYTEC have been adapted as a preliminary step to apply the model to a transversal section of the cell made of one single MOX assembly inserted in a carbon steel overpack. In this modelling set up, the overpack is directly placed in a carbon steel liner within the COx host rock. Several types of metallic iron corrosion products (siderite, magnetite, iron-silicates...) and, therefore, various concentration limits of dissolved Fe(II), could be considered in the modelling.

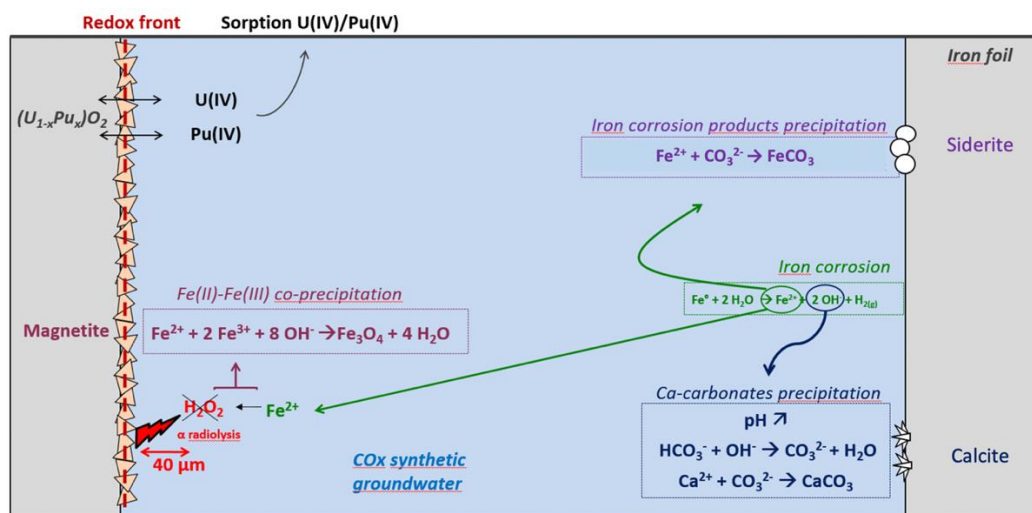


**Figure 4:** Coupled reactions taken into account in the modelling of MOX alteration in synthetic CO<sub>x</sub> porewater in the presence of metallic iron.

## Acknowledgement

The careful review by two EUG members are gratefully acknowledged.

The research leading to these results has received funding from the European Commission Horizon 2020 Research and Training Programme of the European Atomic Energy Community (EURATOM) (H2020-NFRP-2016-2017-1) under grant agreement n° 755443 (DisCo project).

## References

- [1] Poinssot, C., Ferry, C., Lovera, P., Jegou, C., Gras, J.-M. (2005). Spent fuel radionuclide source term model for assessing spent fuel performance in geological disposal. Part II: Matrix alteration model and global performance. *J. Nucl. Mater.*, 346, 66-77.
- [2] Odorowski, M., Jégou, C., De Windt, L., Broudic, V., Peugot, S., Magnin, M., Tribet, M., Martin, C. (2016). Oxidative dissolution of unirradiated Mimas MOX fuel (U/Pu oxides) in carbonate water under oxic and anoxic conditions. *J. Nucl. Mater.*, 468, 17-25.
- [3] Spahiu, K., Cui, D.Q., Lundstrom, M. (2004). The fate of radiolytic oxidants during spent fuel leaching in the presence of dissolved near field hydrogen. *Radiochim. Acta*, 92, 625-629.
- [4] Amme, M., Pehrman, R., Deutsch, R., Roth, O., Jonsson, M. (2012). Combined effects of Fe(II) and oxidizing radiolysis products on UO<sub>2</sub> and PuO<sub>2</sub> dissolution in a system containing solid UO<sub>2</sub> and PuO<sub>2</sub>. *J. Nucl. Mater.*, 430, 1-5.
- [5] Odorowski, M., Jegou, C., De Windt, L., Broudic, V., Jouan, G., Peugot, S., Martin, C. (2017). Effect of metallic iron on the oxidative dissolution of UO<sub>2</sub> doped with a radioactive alpha emitter. *Geochim. Cosmochim. Acta*, 219, 1-21.
- [6] De Windt, L., Goblet, P., Kerleguer, V., Jégou, C. (2019). Progress on the modelling of the homogeneous U<sub>0.73</sub>Pu<sub>0.27</sub>O<sub>2</sub> alteration as a simulant of MOX fuel matrices in an underground disposal cell. Deliverable D5.3. DisCo project (Grant Agreement: 755443).

- [7] Kerleguer, V., Jegou, C., De Windt, L., Broudic, V., Jouan, G., Miro, S., Tocino, F., Martin, C. (2020). The mechanisms of alteration of a homogeneous  $U_{0.73}Pu_{0.27}O_2$  MOX fuel under alpha radiolysis of water. *J. Nucl. Mater.*, 529, 151920.
- [8] van der Lee, J., De Windt, L., Lagneau, V., Goblet, P. (2003). Module-oriented modeling of reactive transport with HYTEC. *Comput. Geosci.*, 29, 265-275.
- [9] Giffaut, E., Grive, M., Blanc, P., Vieillard, P., Colas, E., Gailhanou, H., Gaboreau, S., Marty, N., Made, B., Duro, L. (2014). Andra thermodynamic database for performance assessment: ThermoChimie. *Appl. Geochem.*, 49, 225-236.

# Thermodynamic modelling of oxygen potential for Cr-doped and conventional UO<sub>2</sub> fuel as a function of temperature and burnup

*Curti, E. and Kulik, D.A.*

Paul Scherrer Institut, Laboratory for Waste Management (LES), Villigen (CH)

---

## Abstract

In the framework of WP5, thermodynamic calculations were carried out at PSI in order to assess the influence of Cr-doping on the fuel oxygen potential. Exceedingly high oxygen potentials could lead to detrimental effects under repository conditions, such as enhanced UO<sub>2</sub> matrix dissolution and increased solubility of redox sensitive nuclides (e.g. Pu, Np, Mo). After developing a ternary three-sites solid solution model for Cr-doped hyperstoichiometric urania (years 1 and 2 of this project), efforts in the past year were focused on expanding the UO<sub>2</sub> solid solution model by including end-members of soluble radionuclides (lanthanides, minor actinides and Pu). As far as possible, mixing parameters were determined by fitting experimental data. Moreover, two new ideal solid solutions were introduced: a binary (Ba,Sr)ZrO<sub>3</sub> phase (grey phase) and a quinary (Mo, Ru, Pd, Tc, Rh) metallic phase ( $\epsilon$ -particles). After these implementations, the oxygen potentials of high burnup fuel (60 GWd/t<sub>IHM</sub>) were calculated to be about 5-10 kJ/mol higher than in the previous calculations, but still identical for Cr-doped and non-doped fuels and within the range of experimental values. Zircaloy oxidation at the inner side of the cladding was estimated to potentially reduce oxygen potentials by up to 40-60 kJ/mol. Finally, we computed the evolution of oxygen potential as a function of burnup. The results indicate initially low, rapidly increasing oxygen potentials, reaching a limiting curve in the Ellingham diagram at burnups  $\geq 42$  GWd/t<sub>IHM</sub>. The oxygen potentials calculated for Cr-doped fuel were found to be higher than for conventional fuel only in the very initial burning stages, otherwise no or negligible differences are found. These results indicate that Cr-doping should not affect the oxidation state of the fuel. Therefore, no adverse effect on fuel dissolution, and radionuclide release is expected. This is confirmed by first results of leach experiments on Al/Cr-doped ADOPT fuel carried out in the context of DisCo.

## 1. Implementation of solid solutions and model fuel compositions

### *1.1 Extension of the thermodynamic solid solution model for Cr-doped UO<sub>2</sub> fuel*

In the previous two project years, a ternary three-sites solid solution was developed to describe mixing between Cr(III), U(IV) and U(V) end-members in UO<sub>2</sub>. The mixing parameters of this solid solution could be determined by fitting against appropriate experimental data [1]. Fuel oxygen potential calculations were then carried out assuming equilibrium with the mentioned solid solution and a number of stoichiometric (i.e. single-component) minor phases to represent the behaviour of fission products and actinides. It is however known that many fission products and actinides produced during fuel irradiation are soluble in UO<sub>2</sub> or other minor fuel solids [2]. Lanthanides and minor actinides dissolve



in the cationic sites of the  $\text{UO}_2$  lattice leading to a homogeneous distribution within the matrix, while elements like Ru, Mo, Tc, Rh and Pd are incompatible with the  $\text{UO}_2$  lattice. They form discrete intermetallic solid solution phases known as “ $\epsilon$ -particles” or “white inclusions”. Moreover, fission products such as Ba, Sr and Zr mix as separate oxide solid solutions known with the generic term “grey phase”. In the following section, we explain how such multicomponent phases were implemented in our thermodynamic fuel model. Contrary to Cr(III) we were not able to determine the parameters defining reciprocal interactions among mixing moieties due to limited experimental data for calibration. Thus, for both the “ $\epsilon$ -particles” and “grey” solid solution phases, we assumed ideal mixing.

In the case of the  $\text{UO}_2$  solid solution, it was however possible to calibrate the mixing properties for Nd(III) and La(III) against experimental data. Figure 1 illustrates the procedure adopted to determine adequate end-members and interaction parameters for Nd(III) in  $\text{UO}_2$ . A first attempt to fit the oxygen potential data of Une and Oguma [3] using the end-members  $\text{Nd}_2\text{O}_3$ ,  $(\text{UO}_2)_2$ ,  $(\text{UO}_{2.25})_2$  proved to be unsuccessful, since it was not possible to find interaction parameter values capable of reproducing the typical sigmoidal shape centred on  $\text{O}/\text{M} = 2.00$  of the experimental oxygen potential curve. An unsatisfactory “best fit”, obtained by setting the U(IV)-Nd(III) interaction coefficient to a value of +20 kJ/mol, is shown as dashed line in Figure 1. The misfit is a clear indication that additional end-members are needed to correctly describe the  $\text{Nd}_x\text{U}_{1-x}\text{O}_{2\pm y}$  solid solution. In order to shift the dashed curve in Figure 1 to the right, so that O/M ratios only barely below an O/M ratio of 2.00 are obtained, one needs to assume a substitution mechanism that keeps more oxygen in the  $\text{UO}_2$  lattice. Such a mechanism is e.g. the coupled substitution  $\text{Nd}^{3+} + \text{U}^{5+} \rightarrow 2 \text{U}^{4+}$ , which does not involve formation of vacancies in the oxygen sublattice and thus does not reduce the O/M ratio. Thermodynamically, this substitution can be rationalized as an additional end-member with stoichiometry  $\text{Nd}^{\text{III}}\text{U}^{\text{V}}\text{O}_4$ , to be added to the aforementioned three.

This implementation allowed us to generate the continuous curve shown in Figure 1, which reproduces satisfactorily the experimental data. The curve was obtained by fitting the Gibbs energy of formation for  $\text{Nd}^{\text{III}}\text{U}^{\text{V}}\text{O}_4$ , while setting the U(IV)-Nd(III) interaction coefficient to zero. A determination of the interaction coefficient was not possible, because no phase with stoichiometry  $\text{Nd}^{\text{III}}\text{U}^{\text{V}}\text{O}_4$  is known, thus experimentally derived formation properties are not available for this end-member (contrary to the other three). An analogous procedure (not shown) was applied to calibrate the solid solution properties of the  $\text{La}^{\text{III}}\text{U}^{\text{V}}\text{O}_4$  end-member against oxygen potential data of  $\text{La}_x\text{U}_{1-x}\text{O}_{2\pm y}$ .

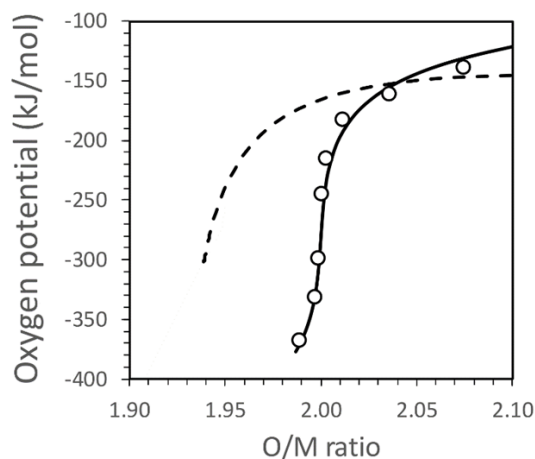


**Figure 1:** Best fits of oxygen potential data from Une and Uguma [3] for  $\text{Nd}_x\text{U}_{1-x}\text{O}_{2\pm y}$  ( $x = 0.14$ ) measured at 1500 °C, using a ternary (dashed line) and a quaternary solid solution (continuous line).

The mixing properties of other lanthanides and actinides in  $UO_2$  were then estimated by chemical analogy. This finally resulted in a solid solution comprising 19 end-members ( $Am_2O_3$ ,  $AmUO_4$ ,  $Ce_2O_3$ ,  $CeUO_4$ ,  $(CeO_2)_2$ ,  $Cm_2O_3$ ,  $CmUO_4$ ,  $Cr_2O_3$ ,  $La_2O_3$ ,  $LaUO_4$ ,  $Nd_2O_3$ ,  $NdUO_4$ ,  $(NpO_2)_2$ ,  $(NpO_{2.5})_2$ ,  $Pu_2O_3$ ,  $PuUO_4$ ,  $(PuO_2)_2$ ,  $(UO_2)_2$ ,  $(UO_{2.25})_2$ ) in which mixing of 15 species over three distinct sites is allowed ( $Am^{3+}$ ,  $Ce^{3+}$ ,  $Ce^{4+}$ ,  $Cm^{3+}$ ,  $Cr^{3+}$ ,  $La^{3+}$ ,  $Nd^{3+}$ ,  $Np^{4+}$ ,  $Np^{5+}$ ,  $Pu^{3+}$ ,  $Pu^{4+}$ ,  $U^{4+}$  and  $U^{5+}$  in the cationic sublattice;  $O^{2-}$  and vacancies in the interstitial and anionic sublattices). For the implementation of the solid solutions in the GEM-Selektor code [4] with the HERACLES database [5], we resorted (as was done previously) to Berman's sublattice model [6]. A more detailed account of the thermodynamic model implementation will be given in the final report of the DisCo project.

## 1.2 Model fuel compositions

Table 1 shows the elemental compositions of the model fuels considered in this study (without cladding), along with a complete list of phases considered in the equilibrium calculations. Two sets of fuel inventories are given in two variants, one for non-doped (conventional)  $UO_2$  fuel (A, B), the other for fuel doped with 1 mol% Cr(III) oxide (C, D). Inventories A and C refer to fuel 2 years after download; inventories B and D to fuel at download time.

**Table 1:** Model inventories for conventional and Cr-doped  $UO_2$  fuels with 60  $GWd/t_{HM}$  average burnup (in mol% with respect to initial U). The rightmost column indicates model phases into which a given element may enter at equilibrium. Multicomponent phases (solid solutions and gas) are typed in italics.

	non-doped		Cr-doped		Phases
	A	B	C	D	
Cr	0.00	0.00	1.00	1.00	$UO_2$ / Cr / $Cr_2O_3$ / $CeCrO_3$
U	92.32	92.61	91.40	91.68	$UO_2$
Am	0.05	0.04	0.05	0.04	$UO_2$
Ba	0.25	0.24	0.25	0.23	$(Ba,Sr)ZrO_3$ / $BaMoO_4$
Ce	0.36	0.39	0.36	0.39	$UO_2$ / $CeCrO_3$
Cm	0.02	0.02	0.02	0.02	$UO_2$
Cs	0.42	0.43	0.42	0.42	$Cs_2MoO_4$
I	0.04	0.04	0.04	0.04	RbI / <i>gas</i>
Kr	0.09	0.09	0.09	0.09	<i>gas</i>
La	0.40	0.39	0.40	0.39	$UO_2$
Mo	0.75	0.70	0.75	0.69	$\epsilon$ -phase / $MoO_2$ / $BaMoO_4$ / $Cs_2MoO_4$
Nd	0.81	0.73	0.80	0.73	$UO_2$
Np	0.09	0.10	0.09	0.09	$UO_2$
Pd	0.36	0.32	0.35	0.31	$\epsilon$ -phase
Pu	1.26	1.20	1.24	1.19	$UO_2$
Rb	0.08	0.08	0.08	0.08	$\epsilon$ -phase / RbI / $Rb_2O$ / <i>gas</i>
Rh	0.08	0.07	0.08	0.07	$\epsilon$ -phase

	non-doped		Cr-doped		Phases
	A	B	C	D	
Ru	0.50	0.52	0.50	0.52	$\varepsilon$ -phase / RuSe <sub>2</sub> / RuTe <sub>2</sub>
Se	0.01	0.01	0.01	0.01	RuSe <sub>2</sub> / gas
Sr	0.19	0.20	0.19	0.20	(Ba,Sr)ZrO <sub>3</sub>
Tc	0.16	0.16	0.16	0.16	$\varepsilon$ -phase
Te	0.09	0.05	0.09	0.05	RuTe <sub>2</sub> / gas
Xe	0.85	0.83	0.84	0.82	gas
Zr	0.80	0.78	0.79	0.78	ZrO <sub>2</sub> / (Ba,Sr)ZrO <sub>3</sub>

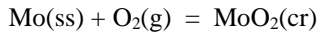
Compositions A and C were derived from the inventory given in Table XV by Ferry et al. [7] for 2 years old PWR spent fuel with a burnup of 60 GWd/t<sub>IHM</sub>. Compositions B and D were obtained from own calculations with the webKORIGEN++ code, available at the Nucleonica site [8], and represent non-aged 60 GWd/t<sub>IHM</sub> fuels (i.e. at download time). The small differences between the two sets indicate that compositional changes due to decay in the very first years after download are minor and can presumably be neglected.

## 2. Results of thermodynamic calculations

### 2.1 Oxygen potentials of 60 GWd/t<sub>IHM</sub> conventional and Cr-doped fuels

Figure 2 summarizes the results of oxygen potential calculations in the temperature range 400°C -1400°C for Cr-doped fuel with 60 GWd/t<sub>IHM</sub> burnup (composition C in Table 1). The red line labelled “3ss” shows oxygen potentials predicted assuming equilibration with the three optimized solid solutions discussed in section 1.1 (UO<sub>2</sub>,  $\varepsilon$ -phase, simplified grey phase). It represents the currently best-refined thermodynamic fuel model. An analogous calculation based on the equivalent inventory for non-doped fuel (composition A in Table 2.1) yielded identical oxygen potentials at all temperatures. This confirms the provisional conclusion drawn in the preceding deliverable D5.2 [9] that Cr-doping should have no effect on the fuel oxygen potential, at least at high burnup. The oxygen potentials calculated with the former incomplete solid solution model [9] were however 10-20 kJ/mol lower and coincided with the green broken oxygen potential line in Figure 2 (labelled “ps”), calculated assuming equilibration only among pure stoichiometric phases (i.e. without any solid solution). In the latter calculations pure metallic Mo and pure Mo(IV) oxide were predicted to coexist at all temperatures, thus constraining the oxygen potential exactly along the Mo-MoO<sub>2</sub> equilibrium line (also shown in Figure 2).

The higher potentials obtained with the updated “3ss” model can be explained with the dilution effect introduced by treating metallic Mo as a component of the  $\varepsilon$ -particles solid solution, rather than as a pure phase. The activity of Mo is no longer unit and is lowered to its mole fraction in the ideal (Mo, Ru, Tc, Rh, Pd) solid solution. The effect is illustrated by the equilibrium relations for the reaction among Mo in the metallic solid solution, gaseous oxygen and pure Mo(IV) oxide:



$$K = \frac{a_{\text{MoO}_2(\text{cr})}}{p_{\text{O}_2} a_{\text{Mo(ss)}}} = \frac{1}{p_{\text{O}_2} x_{\text{Mo}}} \rightarrow p_{\text{O}_2} = \frac{1}{K x_{\text{Mo}}} \rightarrow \Delta \bar{G}_{\text{O}_2} \equiv RT \ln(p_{\text{O}_2}) = -RT(\ln K + \ln x_{\text{Mo}})$$

where  $K$  is the temperature-specific equilibrium constant,  $a_i$  are activities,  $R$  the gas constant,  $T$  is the absolute temperature and  $x_{\text{Mo}}$  is the mole fraction of Mo in the  $\epsilon$ -phase. Because  $x_{\text{Mo}} < 1$  in a solid solution, the term  $\ln x_{\text{Mo}}$  is always negative. It thus decreases with increasing dilution, causing a shift toward higher oxygen potentials.

The third calculation in Figure 2 (red broken line labelled “3ss + zox”) shows the potential effect of including zirconium oxidation at the internal side of the cladding. Such a process must lead to a decrease of the oxygen potential, as oxygen is consumed by the reaction  $\text{Zr} + \text{O}_2 = \text{ZrO}_2$ . To simulate it, formation of a 10  $\mu\text{m}$  thick  $\text{ZrO}_2$  layer from metallic Zr was assumed, which is, according to available experimental data [10,11] about the maximum possible corrosion depth due to internal clad oxidation. The implementation in GEM-Selektor was achieved simply by adding to the input fuel composition C an amount of metallic Zr corresponding to a 10  $\mu\text{m}$  ring of material at the inner side of a typical cladding sheet. As shown in Figure 2, including Zircaloy oxidation could well lead to a considerable decrease in oxygen potential (by up to 40-60 kJ/mol).

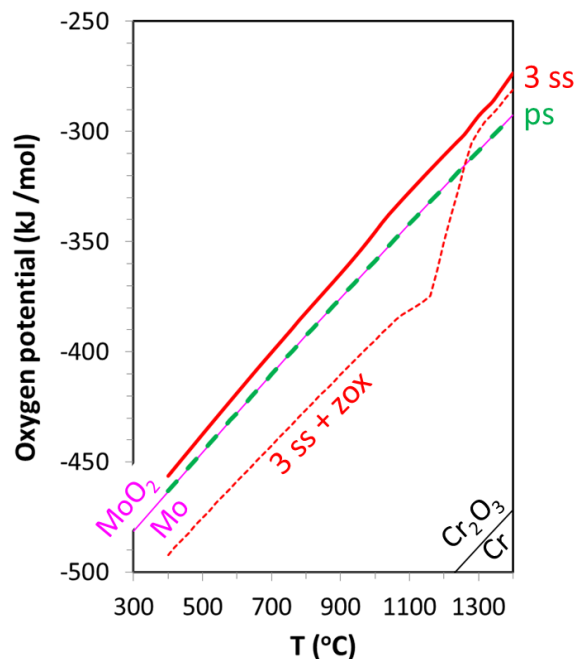


**Figure 2:** Summary plot showing three oxygen potential calculations for Cr-doped fuel composition C, using different phase selections and assumptions (see text for explanations).

## 2.2 Evolution of oxygen potential with irradiation progress

The previous calculations all refer to fuels with a high burnup of 60  $\text{Gwd}/t_{\text{IHM}}$ . In the next set of calculations, we trace the evolution of the oxygen potential with increasing burnup, both for conventional and Cr-doped fuels, however neglecting the possible influence of Zircaloy oxidation. To this aim, we first computed model inventories for conventional  $\text{UO}_2$  fuels of different burnups (1, 23, 42, 53 and 60  $\text{Gwd}/t_{\text{IHM}}$ ) from WebKORIGEN++ calculations [8], corresponding to 11 days and 1.2,

2.5, 3.6, 4.8 years of operation in a PWR, assuming in total five 292-days burning cycles and 73 days intervals for maintenance and reloading. The compositions of Cr-doped fuels were then determined by adding 0.5 mol%  $\text{Cr}_2\text{O}_3$  (1 mol% total Cr) to the corresponding conventional fuel composition and reducing proportionally the amounts of  $\text{UO}_2$  and fission products.

Figure 3 shows the resulting Ellingham diagram, leaving out for the sake of clarity the calculations at 42 and 53  $\text{GWd/t}_{\text{HM}}$ . The shaded fields delimit regions of measured oxygen potentials for non-doped fuels of 13-58 [12-13], and 101  $\text{GWd/t}_{\text{HM}}$  burnup [14].

The results indicate very low oxygen potentials in the initial stages of irradiation. With increasing burnup, they enter the regions defined by experimentally determined oxygen potentials and progressively increase up to values exceeding the pure Mo – pure  $\text{MoO}_2$  buffer line. At 1  $\text{GWd/t}_{\text{HM}}$  the oxygen potentials of doped and non-doped fuel are almost identical up to 1180°C, then the two curves diverge at higher temperatures. The potential of the non-doped fuel further decreases while the potential of the Cr-doped fuel increases exactly along the Cr-Cr $_2\text{O}_3$  buffer line. Inspection of the results shows that in the latter calculation, Cr(III) is partially reduced to metallic Cr at  $T \geq 1180^\circ\text{C}$ . Therefore, since both pure  $\text{Cr}_2\text{O}_3$  and pure Cr metal coexist at equilibrium (besides the Cr-bearing  $\text{UO}_2$  solid solution), the fuel oxygen potential must follow the corresponding buffer line. At low temperatures (400°C - 700°C) the oxygen potential of both conventional and Cr-doped fuel is controlled by the  $\text{O}_2$  consuming reaction  $\text{Cs}_2\text{ZrO}_3(\text{cr}) + \text{Mo}(\text{ss}) + 3/2 \text{O}_2(\text{g}) \rightarrow \text{ZrO}_2(\text{cr}) + \text{Cs}_2\text{MoO}_4(\text{cr})$ .

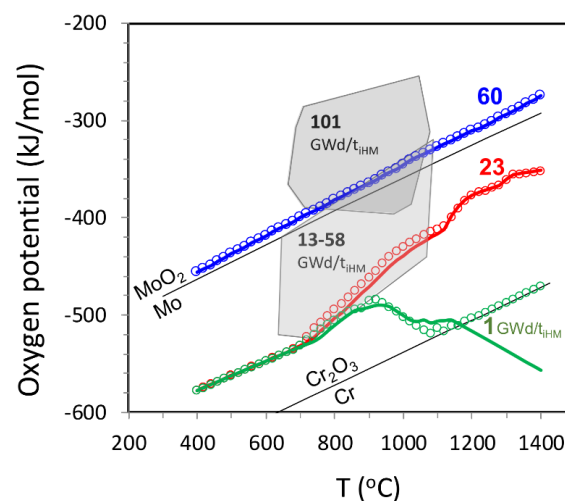


**Figure 3:** Calculated evolution of oxygen potential for conventional and Cr-doped  $\text{UO}_2$  fuel with increasing burnup. The grey fields delimit values of published experimental data for non-doped  $\text{UO}_2$  fuels with burnups of 13-58  $\text{GWd/t}_{\text{HM}}$  [12-13] and 101  $\text{GWd/t}_{\text{HM}}$  [14]. Coloured lines indicate oxygen potentials for non-doped  $\text{UO}_2$  fuel, calculated at the specified burnup. Circles show corresponding calculations for Cr-doped fuel. The oxygen potentials of Mo-Mo $\text{O}_2$  and Cr-Cr $_2\text{O}_3$  pure metal/oxide pairs are shown as black lines.

At 23  $\text{GWd/t}_{\text{HM}}$  and up to 700°C the oxygen potential curves of Cr-doped and non-doped fuel coincide and are identical to those obtained at 1  $\text{GWd/t}_{\text{HM}}$  because of the previously mentioned buffering equilibrium among  $\text{Cs}_2\text{ZrO}_3(\text{cr})$ ,  $\text{Mo}(\text{ss})$ ,  $\text{ZrO}_2(\text{cr})$  and  $\text{Cs}_2\text{MoO}_4(\text{cr})$ . Contrary to the calculation for 1  $\text{GWd/t}_{\text{HM}}$ , however, the amount of metallic molybdenum present in the fuel is now sufficient to avoid consumption of the Cs molybdate phase. Therefore, metallic  $\text{Mo}^0$  and  $\text{Mo}^{6+}$  coexist further at higher temperatures, preventing the decrease in oxygen potential predicted in the 1  $\text{GWd/t}_{\text{HM}}$  calculation.

The oxygen potentials computed for non-doped and Cr-doped fuel with burnups of 42 (not shown), 53 (not shown) and 60 GWd/t<sub>IHM</sub> were found to coincide over the whole temperature range. These results indicate that the oxygen potential of both types of fuel is well buffered at high burnups. The calculated values exceed the potentials of the pure Mo – pure MoO<sub>2</sub> buffer by about 5-20 kJ/mol. As previously discussed, this effect is a consequence of the dilution of Mo in the  $\epsilon$ -particles solid solution.

Finally, the oxygen potential curves shown in Figure 3 for 60 GWd/t<sub>IHM</sub> fuels at download time (compositions B and D in Table 1) are found to be identical to the red continuous curve in Figure 2, referring to 60 GWd/t<sub>IHM</sub> fuel two years after download (compositions A and B). This coincidence implies that oxygen potentials in irradiated LWR fuels are rather insensitive to variations in fuel compositions induced by few years of decay. Therefore, the results presented in this study should be applicable to a large variety of irradiated LWR fuels.

## Conclusions

The major conclusion from this modelling study is that Cr-doping should have no significant effect on oxygen potential and stoichiometry of UO<sub>2</sub> fuels irradiated in light water reactors. Therefore, undesired in-pile effects such as enhanced diffusivity of radionuclides, a reduction of fuel thermal conductivity during neutron irradiation, or increased Zircaloy oxidation at the inner side of the cladding, are unlikely. Moreover, since the oxidation state of the fuel will not be affected by Cr-doping, increased matrix dissolution and oxidation of redox-sensitive radionuclides to water-soluble species are not expected to occur under repository conditions.

The comparison of oxygen potential calculations obtained with a refined thermodynamic model including three solid solutions (UO<sub>2</sub>,  $\epsilon$ -particles and simplified grey phase) with those obtained by a simpler model in which only stoichiometric solids are equilibrated, reveals that the fuel oxygen potential is sensitive to the activity of Mo in the metallic inclusions ( $\epsilon$ -particles). With increasing molybdenum dilution in the  $\epsilon$ -particle phase, higher oxygen potentials result. The calculated increase is noticeable but marginal when compared with the range of experimental oxygen potentials. Surprisingly, replacing stoichiometric oxides with a complex non-ideal UO<sub>2</sub> solid solution has only a minor effect on the oxygen potential.

Calculations as a function of irradiation progress indicate low initial oxygen potentials (less than -500 kJ/mol at a burnup of 1 GWd/t<sub>IHM</sub>), with significant differences between Cr-doped and non-doped fuel at high temperature. At burnups exceeding about 20 GWd/t<sub>IHM</sub> the calculated oxygen potentials overlap the region defined by the range of experimental data. Only minor differences between Cr-doped and non-doped fuel are computed. At higher burnups ( $\geq 42$  GWd/t<sub>IHM</sub>) the calculated oxygen potentials of Cr-doped and non-doped fuels are identical and converge to values about 5-20 kJ/mol above the line defined by the pure Mo-MoO<sub>2</sub> buffer. Finally, calculations carried out to estimate the effect of zirconium alloy oxidation at the internal side of the cladding, indicate that this process may considerably reduce the oxygen potential (by 40-60 kJ/mol).

## Acknowledgement

The research leading to these results has received funding from the European Commission Horizon 2020 Research and Training Programme of the European Atomic Energy Community (EURATOM) (H2020-NFRP-2016-2017-1) under grant agreement n° 755443 (DisCo project).

## References

- [1] Curti, E., Miron, G.D., Kulik, D.A. (2019). Preliminary thermodynamic calculations for WP5, Task 1. Deliverable D1.10: 1<sup>st</sup> Annual Meeting Proceedings. DisCo project (Grant Agreement: 755443).
- [2] Kleykamp, H. (1985). The chemical state of the fission products in oxide fuels. *J. Nucl. Mater.*, 131, 221-246.
- [3] Une, K. and Oguma, M. (1983). Oxygen potentials of (U,Nd)O<sub>2±x</sub> solid solutions in the temperature range 1000-1500°C. *J. Nucl. Mater.*, 118, 189-194.
- [4] Wagner, Th., Kulik, D.A., Hingerl, F.F., Dmytrieva, S.V. (2012). GEM-Selektor geochemical modeling package: TSolMod library and data interface for multicomponent phase models. *Can. Mineral.*, 50, 1173-1195.
- [5] GEMS specific HERACLES v.0.2. database for U, TRU and FP speciation, <https://www.psi.ch/en/heracles/gems-specific-heracles-database> (accessed 30 January 2020).
- [6] Berman, R.G. and Brown, T.H. (1984). A thermodynamic model for multicomponent melts, with application to the system CaO-Al<sub>2</sub>O<sub>3</sub>-SiO<sub>2</sub>. *Geochim. Cosmochim. Acta*, 48, 661-678.
- [7] Ferry, C., Poinssot, Ch., Broudic, V., Cappelaere, Ch., Desgranges, L., Garcia, Ph., Jégou, C., Lovera, P., Marimbeau, P., Piron, J.-P., Poulesquen, A., Roudil, D. (2004). Synthesis on the long term spent fuel evolution. CEA Report, CEA-R-6084.
- [8] Nucleonica, <https://nucleonica.com/index.aspx> (Accessed 24 January 2020).
- [9] Curti, E. and Kulik, D.A. (2019). Defect chemistry and thermodynamics of Cr-doped UO<sub>2</sub> fuels: Model development and applications. Deliverable 5.2: Solid phase: Description of models, review of critical thermodynamic data and first test calculations. Progress report on Task 1. DisCo project (Grant Agreement: 755443).
- [10] Déhaut, Ph. (2000). Le combustible nucléaire et son état physico-chimique à la sortie des réacteurs. CEA Report, CEA-R-5923.
- [11] Ciszak, C. (2017). Etude de l'accrochage pastille/gaine des crayons combustibles des réacteurs à eau pressurisée. Ph.D. Thesis, Université Bourgogne-Franche-Comté, France.
- [12] Matzke, Hj. (1995). Oxygen potential measurements in high burnup LWR UO<sub>2</sub> fuel. *J. Nucl. Mater.*, 223, 1-5.
- [13] Une, K., Tominaga, Y., Kashibe, S. (1991). Oxygen potentials and lattice parameter of irradiated BWR fuels. *J. Nucl. Sci. Technol.*, 28(5), 409-417.
- [14] Walker, C.T., Rondinella, V.V., Papaioannou, D., Van Winckel, S., Goll, W., Manzel, R. (2005). On the oxidation state of UO<sub>2</sub> nuclear fuel at a burn-up of around 100 MWd/kg<sub>HM</sub>. *J. Nucl. Mater.*, 345, 192-205.

---

# **EUG Feedback**

---



## Summary of Feedback from the End User Group

The members of the End User Group (EUG) had their third meeting during the last day of the third DisCo annual meeting, in parallel with the General Assembly. Present at the EUG meeting were representatives of the following WMO's: ANDRA (Christelle Martin), ENRESA (Miguel Cuñado Peralta), Nagra (Lukas Martin), RWM (Rosemary Hibberd), Posiva (Barbara Pastina) and SKB (Kastriot Spahiu). Furthermore, representatives of the following 5 regulators were also present at the EUG meeting: BASE (former BfE, Christoph Borkel), CSN (Carlos Javier Diez), ENSI (Eduard Feldbaumer), FANC (Kevin Govers), and SSM (Jinsong Liu). The meeting was led by Roberto Gaggiano (ONDRAF/NIRAS), who is the EUG representative and was also present at the ExCom meeting on the first day of the workshop.

Due to the Covid-19, the 3<sup>rd</sup> Annual Meeting was held by videoconference. In spite of this, the meeting was organised in a very efficient way. Having such a large annual meeting via videoconference seemed to be very challenging; however, the meeting efficiency and the communication was not compromised:

- The presenters respected the scheduled presentation time;
- The Q&A sessions were efficiently organized by means of both oral questions after the presentations and questions via chat.

According to the EUG, the DisCo project is very well progressing. Most scientific contributions are on track. In particular, a very good progress is observed for the tests which were started at the beginning of the project. However, some issues and delays are identified within the project:

- The batch of UO<sub>2</sub> pellets (Pu-and Cr-doped) are ready to be used for tests at VTT. However, since only one year of project is left, the EUG is worried that the tests at VTT will not be performed on time;
- The severe delay of the work at JRC, already noticed last year, was not recovered this year. Currently the tests at JRC are foreseen to start during the summer 2020 or (pessimistically) by the end of the year. The EUG is worried that the experiments will not be finished by the end of the project;
- The EUG suggests improving the progress of the work at UCAM (some difficulties in the synthesis of the material were already noticed last year).

Considering that the DisCo project also aims at disseminating knowledge, the EUG can only insist on exchanging good practices with partners and perhaps conduct staff exchanges to get the expertise. The EUG encourages the researchers to contact other DisCo partners who can help with the synthesis of the material since only one year of project is left.

The S&T contributions were sent to the EUG members in advance of the workshop. As clarified last year, one of the roles of the EUG is to advise the participants of the project and see if the needs and expectations of the EUG are achieved/satisfied. The interaction with the EUG allows checking whether the project provides the answers to the questions/needs of the EUG and makes sure that the work remains within the initially set scope of the project. This year the EUG has sent the first input on the S&T contributions before the annual meeting so that the presenters could take this input into account in the presentations. The EUG appreciates the effort of the presenters in answering to the questions and remarks of the EUG during the presentations. The EUG feels the importance of a good follow up of the progress of the project and would like to follow the same review procedure for the next annual meeting:

- Early deadline for the submission of the contribution;

- First feedback based on the contributions before the annual meeting (1-2 weeks in advance).

Since the next annual meeting will be the last one of the DisCo project, the EUG recognizes the importance of focusing on scientific presentations of the completed work. However, the EUG is interested in having also a clear view on the performed activities. An equilibrium between activity reporting and scientific input should be found and the interconnections among the different WPs should be evidenced. According to the EUG, the WP leaders should be given more time during the 4<sup>th</sup> annual meeting in order to provide a broad overview of the WPs. The EUG suggests that the WP leaders meet the group some time before the annual meeting with the aim of discussing the overall results of the different WPs. The EUG expects that the results provided in the S&T contributions will be put into perspective by the WPs leaders next year, being the end of the project.

In case the DisCo meeting is delayed, due to the current Covid-19 situation and the consequent impact on the scientific activities, the EUG suggests having an intermediate meeting before the final project meeting.

Moreover, the EUG suggests the possibility to attend the next annual meeting remotely, which would be beneficial for some EUG members.

The entire EUG looks forward to the next annual meeting in Barcelona (in May 2021) and wishes to thank the ExCom and all the beneficiaries for their excellent work done so far. The EUG is also grateful to Alba Valls and Amphos 21 for the organization and the technical support of this meeting.